

BIOCHEMISTRY IN BACTERIOFERRITIN

by

Uthaiwan Suttisansanee

A thesis

presented to the University of Waterloo

in fulfillment of the

thesis requirement for the degree of

Master of Science

in

Chemistry

Waterloo, Ontario, Canada, 2006

© Uthaiwan Suttisansanee 2006

I hereby declare that I am the sole author of this thesis. This is a true copy of the thesis, including any required final revisions, as accepted by my examiners.

I understand that my thesis may be made electronically available to the public.

ABSTRACT

Bacterioferritin, an iron storage protein having a 24-subunit (α_{24}) quaternary structure, was used as a model for the study of host-guest interactions and guest encapsulation, making use of its spherical cage-like structure. A hexahistidine-affinity tag fused to the C-terminus of each bacterioferritin subunit was constructed. The C-terminus of each subunit points toward the inside of the cavity, while the N-terminus is exposed on the surface of the protein. The hexaHistag was able to form strong interactions with a nickel-nitrilotriacetic acid linked dye molecule (guest) and this interaction was used in attempts to develop a principle to control guest molecule encapsulation within the spherical cavity of the 24-mer bacterioferritin protein molecule. The procedure involved (1) subunit dissociation under acidic pH, (2) affinity controlled dye-Histag binding with exposed C-terminal (His)₆ residues and (3) reassociation of the subunits at neutral pH. The encapsulation conditions involving step 1 and 3 were studied preliminarily using laser light scattering to measure size (hydrodynamic radius) of the protein particle with apoferritin as a model system as it resembles the size and structure of bacterioferritin. In order to encapsulate guest molecules, the emptied shell of bacterioferritin was generated by site-directed mutagenesis resulting in ferroxidase- as well as heme-free bacterioferritin mutants (E18A/M52L/E94A), and these mutants were used to examine protein stability before conducting encapsulation experiments. However, wild-type bacterioferritin possessed highest stability in maintaining its multisubunit structure; hence, it was used for the encapsulation studies. It was found that 100% bacterioferritin with His₆-tag at the C-terminus, and a combination of 60% bacterioferritin with His₆-tag at the C-terminus and 40% bacterioferritin without His₆-tag at the C-terminus yielded similar amounts of encapsulated

guest molecules. This suggested that all hexahistidine at the C-terminus were not equally available for dye molecule binding.

ACKNOWLEDGEMENTS

I would like to extend my sincere thank to Dr. John Honek, my supervisor, for giving me the opportunity to work on this project. His advice, guidance, patience, and time are very appreciated.

I also would like to thank Dr. Elisabeth Daub for her advice on protein engineering, Dr. Zhending Su for his advice on mass spectroscopy, and Liz Gargatsoungias for information on bacterioferritin.

I would like to give special thanks to the Meiering Lab for providing access to their Nanosizer ZS instrument, to Peter Stathopoulos for sharing his knowledge of laser light scattering, to the Palmer Lab for providing a PTI Fluorometer, and to Shenhui Lang for her advice on fluorescence measurement.

I also wish to acknowledge the Thai Government, Thailand for financial support during my graduate studies.

I am grateful to Nicole Sukdeo, Pei Hang, and Paula Walasek for their expertise and their patience in teaching me how the lab works. I also would like to thank Christine Hand, Danish Khan, and Kadia Mullings for their support and encouragement. I cannot say anything else except “you guys are the best”.

I would like to thank my family, Sacorn, Jewhiang, Rossukon, and Sasirada for their understanding and support. I am lucky that I was born in this family. I also would like to thank Platong for the courage and caring.

In addition, I would like to thank my housemate, Ming Bao, for her cooking during a past year.

TABLE OF CONTENTS

	Page
ABSTRACT	iii
ACKNOWLEDGEMENTS	v
TABLE OF CONTENTS	vi
LIST OF TABLES	x
LIST OF FIGURES	xiii
LIST OF ABBREVIATIONS	xxv
 CHAPTER 1: INTRODUCTION	
1.1: Bacterial Iron Homeostasis	1
1.1.1: Role of Iron in Living Organisms.....	1
1.1.2: Iron Transporters.....	3
1.1.3: Iron Storage Proteins and Their Applications.....	8
1.1.4: Regulatory Role of Iron.....	23
1.2: <i>Escherichia coli</i> Bacterioferritin	25
1.2.1: Discovery of Bacterioferritin.....	25
1.2.2: Overall Structure.....	26
1.2.3: Heme Binding Site.....	31
1.2.4: Iron Core Formation.....	34
1.3: Nanotechnology and Encapsulation	40
1.3.1: The Host.....	40
1.3.2: The Guest.....	49
1.3.3: Linkage.....	51
1.3.4: Applications of Encapsulation Processes.....	56
1.4: Possible Aspects for Bacterioferritin Encapsulation	57
1.5: Summary of Experimental Objectives Achieved	64

CHAPTER 2: CONDITIONAL TESTS FOR DISSOCIATION AND REASSOCIATION OF APOFERRITIN SUBUNITS USING LIGHT SCATTERING TECHNIQUES

2.1: Literature Research on Dissociation and Reassociation of Horse Spleen Apoferritin	66
2.2: Reagents, Materials, and Equipment	72
2.3: Experimental Protocols	73
2.4: Results and Discussion	76
2.4.1: Effect of Protein Concentration.....	76
2.4.2: Effect of pH.....	78
2.4.3: Effect of Electrolytes.....	79
2.4.4: Effect of Glycerol.....	80
2.4.5: Effect of Incubation Time on Dissociation.....	81
2.4.6: Effect of Reassembly Time.....	82
2.5: Conclusions	83

CHAPTER 3: OVEREXPRESSION AND PURIFICATION OF FERROXIDASE CENTER- AND HEME-FREE BACTERIOFERRITIN

3.1: Literature Research on the Ferroxidase Center- and Heme-free Bacterioferritin	85
3.2: Reagents, Materials, and Equipment	87
3.3: Experimental Protocols	90
3.3.1: Protocols for Control Experiments.....	90
3.3.2: Protein Engineering.....	93
3.3.3: Protein Expression, Induction, and Purification.....	97
3.4: Results and Discussion	101
3.4.1: Control Experiments on Protein Stability Conditions.....	101
3.4.2: Cloning of Wild-type and Bacterioferritin Mutants.....	107
3.4.3: Overexpression and Purification of Wild-type and Bacterioferritin Mutants..	108
3.4.4: Protein Stability of Wild-type and Bacterioferritin Mutants.....	113
3.5: Conclusions	120

CHAPTER 4: OVEREXPRESSION, PURIFICATION, AND ENCAPSULATION PROPERTIES OF C-TERMINAL HIS₆-TAGGED BACTERIOFERRITIN

4.1: Literature Research on C-terminal Extension and Encapsulation of Bacterioferritin	121
4.2: Reagents, Materials, and Equipment	125
4.3: Experimental Protocols	125
4.3.1: Protein Engineering.....	125
4.3.2: Protein Expression, Induction, and Purification	127
4.3.3: Identification of Dye Molecule.....	128
4.3.4: Preparation for Encapsulation Experiments	134
4.3.5: Determination of the Fluorescence Quenching.....	141
4.3.6: Measurement of Heme Groups Incorporated in Bacterioferritin	142
4.3.7: Determination of the Presence of Iron Atoms in Bacterioferritin	143
4.3.8: Determination of the Number of Dye Molecules Encapsulated into Bacterioferritin.....	143
4.4: Results and Discussion	144
4.4.1: DNA Cloning and Protein Purification.....	144
4.4.2: Dye Identification.....	146
4.4.3: Optimum Conditions for Encapsulation of Bacterioferritin.....	152
4.4.4: Control Experiments for Encapsulation by Bacterioferritin.....	168
4.4.5: Fluorescence Quenching of the Dye Encapsulated Bacterioferritin.....	177
4.4.6: Heme-incorporated Encapsulated Bacterioferritin.....	178
4.4.7: Iron Storage in Bacterioferritin	179
4.4.8: Dye Molecules Encapsulated in Bacterioferritin	179
4.5: Conclusions	180

CHAPTER 5: SUMMARY AND FUTURE WORK

5.1: Summary	183
5.2: Future Work	185

REFERENCES	187
-------------------------	-----

Appendix 1: Flow Chart for QuikChange[®] Site-directed Mutagenesis PCR	203
Appendix 2: Flow Chart for Site-directed Mutagenesis of bFT-E94A	204
Appendix 3: Flow Chart for Protein Purification	205

Appendix 4: Sequencing Results for Wild-type and Variants of Bacterioferritin.....	206
Appendix 5: Mass Spectrometric Results.....	217
Appendix 6: Spectrophotometric Results for Wild-type and Variants of Bacterioferritin.....	227
Appendix 7: Gel Filtration Chromatographic Results (Superose 6) of Wild-type and Variants of Bacterioferritin.....	232
Appendix 8: Calculation of Extinction Coefficient for Dye Molecules in Pro-Q[®] Sapphire 365 Oligohistidine Gel Stain.....	249
Appendix 9: Calculation of Heme Groups Present in Bacterioferritin	254
Appendix 10: Calculation of Encapsulated Dye inside Protein Cavity.....	255
Appendix 11: Metal Analysis of Pro-Q[®] Sapphire 365 Oligohistidine Gel Stain.....	257
Appendix 12: Metal Analysis of Iron Ions Incorporated in 24-subunit Bacterioferritin	259

LIST OF TABLES

	Page
CHAPTER 1	
Table 1.1: Cellular effects of ferritin-like proteins in select bacteria.....	20
Table 1.2: Matrices and elution conditions for various affinity tags used in protein purification.....	53
Table 1.3: Sequence and size of affinity tags.....	54
Table 1.4: Comparison of affinity tag technologies.....	55
CHAPTER 3	
Table 3.1: The forward and reverse primers used to generate each mutation by site-directed mutagenesis.....	96
Table 3.2: PCR recipe for bFT variants except bFT-E94A derived from QuikChange [®] Site-Directed Mutagenesis Instruction Manual from Stratagene.....	96
Table 3.3: PCR Programming protocols for QuikChange [®] Site-Directed Mutagenesis method.....	97
Table 3.4: The molecular weight of each eluted peak of Superose 6 gel filtration chromatography varies under different salt concentrations.....	104
Table 3.5: The calculated molecular weight of each eluted peak from gel filtration chromatography (Superose 6) of 3.35 mg/mL bFT-WT in 20 mM Tris-OH (pH 8.0) and 100 mM NaCl calculated using the Bio-Rad protein standard.....	112
Table 3.6: A summary of the protein structure, 24-subunit and smaller subunits (dimer and monomer), of wild-type bFT compared with bFT variants.....	119
CHAPTER 4	
Table 4.1: The forward and reverse primers used to generate bFT-WT with a <i>Nde</i> I cutting site at the 5' end and a <i>Xho</i> I cutting site at the 3' end.....	127

Table 4.2:	PCR conditions for generating a bFT-WT construct with a <i>NdeI</i> cutting site at the 5' end and a <i>XhoI</i> cutting site at the 3' end.....	127
Table 4.3:	PCR Programming sets for generating the bFT-WT construct with a <i>NdeI</i> cutting site at the 5' end and a <i>XhoI</i> cutting site at the 3' end.....	127
Table 4.4:	The protein concentrations of the Histag protein that encapsulated dye molecules at various periods encapsulating time were calculated after dialysis overnight.....	157
Table 4.5:	The protein concentrations of Histag/WT mixtures calculated after dialysis overnight.....	160
Table 4.6:	The protein concentrations of Histag protein and the combination of Histag/WT mixture calculated after dialysis overnight with and without an additional 5 hours of dialysis time.....	165

APPENDIX 7

Table A7.1:	The table shows the molecular weight of standard protein and eluted volumes in duplicate, which used for plotting standard protein curve.....	233
Table A7.2:	The table shows the molecular weight, the Stokes radius, the average elution volumes, the sedimentation coefficient, and the sedimentation coefficient times Stokes radius of protein standards	235
Table A7.3:	The calculated molecular weight of eluted Superose 6 fractions of bFT-WT.....	238
Table A7.4:	The calculated molecular weight of eluted Superose 6 fractions of bFT-E18A.....	239
Table A7.5:	The calculated molecular weight of eluted Superose 6 fractions of bFT-M52L.....	240
Table A7.6:	The calculated molecular weight of eluted Superose 6 fractions of bFT-E94A.....	241
Table A7.7:	The calculated molecular weight of eluted Superose 6 fractions of bFT-E18A/M52L.....	242
Table A7.8:	The calculated molecular weight of eluted Superose 6 fractions of bFT-M52L/E94A.....	243

Table A7.9: The calculated molecular weight of eluted Superose 6 fractions of bFT-E18A/E94A.....	244
Table A7.10: The calculated molecular weight of eluted Superose 6 fractions of bFT-E18A/M52L/E94A.....	246
Table A7.11: The calculated molecular weight of eluted Superose 6 fractions of bFT with His ₆ -tag at the C-terminus.....	247

APPENDIX 8

Table A8.1: Collected data for emission intensity and excitation intensity of the series of different dye stain dilutions.....	252
Table A8.2: Collected data for optical densities of the series of different dye stain dilutions.....	253

APPENDIX 9

Table A9.1: The table represents the number of heme groups incorporated in various bFT samples.....	254
--	-----

APPENDIX 10

Table A10.1: The table shows data for the calculation of encapsulated dye molecules in 100% Histag and the combination of 60/40:Histag/WT proteins.....	256
--	-----

APPENDIX 11

Table A11.1: ALS Laboratory Group Analytical Report for metal analysis results representing the metal detection in Pro-Q [®] sapphire 365 oligohistidine gel stain and metal-free water (a control sample)	258
--	-----

APPENDIX 12

Table A12.1: ALS Laboratory Group Analytical Report for metal analysis results representing the metal detection in 24-subunit bFT with His ₆ -tag at the C-terminus (two trials sample) and dialysis buffer (a control sample).....	260
---	-----

LIST OF FIGURES

	Page
CHAPTER 1	
Figure 1.1: Schematic representation of siderophore-mediated iron uptake in bacteria..	5
Figure 1.2: Schematic representation of ferrous iron uptake by Feo system in <i>E. coli</i> ...	7
Figure 1.3: The schematic presentations of overall structure and one subunit of <i>Listeria Dps</i>	10
Figure 1.4: The iron binding residues of <i>Listeria Dps</i>	10
Figure 1.5: The overall structure of <i>Trichoplusia Ni</i> secreted FT and one subunit structure of human mitochondria FT.....	14
Figure 1.6: The di-iron binding site of the human FT H-chain.....	14
Figure 1.7: The multiple alignment of horse spleen ferritin (H-chain and L-chain) sequences and <i>E. coli</i> bacterioferritin sequence	18
Figure 1.8: The chemical structures of protoporphyrin IX and coproporphyrin III.....	19
Figure 1.9: Roles of Fur and RyhB in mediating Fe-dependent gene regulation in <i>E. coli</i>	24
Figure 1.10: The amino acid sequence of <i>E. coli</i> bFT.....	26
Figure 1.11: Single crystals and the electron micrograph of <i>E. coli</i> bFT	28
Figure 1.12: The space-filled and half-the-sphere structures of <i>E. coli</i> bFT.....	29
Figure 1.13: The cross eyed stereo view of a 12-subunit <i>E. coli</i> bFT represents the heme binding groups and the C-terminal end.....	29
Figure 1.14: The ribbon diagram of two neighboring subunits of <i>E. coli</i> bFT showing heme-binding site and ferroxidase center.....	30
Figure 1.15: The ribbon diagram of two neighboring subunits of <i>E. coli</i> bFT representing the residues involved in intersubunit stability	30
Figure 1.16: The ribbon diagram of four subunits of <i>E. coli</i> bFT showing the residues involve in intersubunit and intrasubunit stability.....	31

Figure 1.17:	The schematic representation of the bFT heme-binding site.....	33
Figure 1.18:	The ribbon diagram of two neighboring subunit of <i>E. coli</i> bFT showing the two propionate groups of heme, two iron atoms, L loops, and the C-terminus.....	34
Figure 1.19:	The residues forming ferroxidase center of <i>E. coli</i> bFT are located helices A-D.....	36
Figure 1.20:	The space-filled structure of six subunits of <i>E. coli</i> bFT creating a 3-fold channel and a zoom-in ribbon structure representing the residues that form the channel.....	37
Figure 1.21:	The space-filled structure of eight subunits <i>E. coli</i> bFT creating 4-fold channel and a zoom-in ribbon structure representing the residues that form the channel.....	37
Figure 1.22:	A schematic diagram representing the encapsulation of Prussian-blue in FT.....	43
Figure 1.23:	A schematic diagram representing the GroEL-CdS nanoparticle complexes.....	43
Figure 1.24:	The space-filling structure representing interior of small heat shock protein from <i>Methanococcus jannaschii</i> that viewed along 3-fold axis and 4-fold axis.....	44
Figure 1.25:	The cTEM of vault particles and half-a-capsid images representing the inner and outer structure.....	44
Figure 1.26:	The cTEM represents structural images of the closed and opened conformation of CMV.....	46
Figure 1.27:	A schematic diagram representing the encapsulation of CCMV particle.....	46
Figure 1.28:	The cTEM image of DMPC/Chol liposomes before and after drug loading.....	47
Figure 1.29:	The structures representing various sizes and shapes of synthesized organic particles, which are Cram's carcerand, bis(glycouril) macrocycle, softball-like glycouril derivative, a dimerization of (<i>R</i>)-2-bromo-3-methylbutyric acid, and pyrogallol[4]arene.....	48
Figure 1.30:	The diagram represents the host opening for guests exchanged by flap opening.....	50

Figure 1.31:	The diagram represents the dissociation of one subunit host to allow the exit of guest molecule.....	50
Figure 1.32:	The schematic diagram represents the example of a bFT encapsulation using His-tag affinity binding at the C-terminus that interacts with a nickel nitrilotriacetic acid-modified guest.....	59
Figure 1.33:	The schematic diagram represents a fusion protein approach to encapsulate guest molecules in bFT cavity, which is utilized by a guest gene that is attached to the 3' end of the bFT gene with an appropriate linker oligonucleotide in between.....	61
Figure 1.34:	The image represents the possible encapsulation of a guest molecule inside bFT cavity by the interaction of a guest containing a Cys residue and heme-iron atom of bFT forming five-coordinate sulfur donor-ligated ferrous heme adducts.....	62
Figure 1.35:	The schematic diagram represents possible encapsulated method by using a covalent site chain heme propionate-guest interaction.....	63
Figure 1.36:	The diagram showing the encapsulation processes of bFT, which involves dissociation of 24-subunit cluster, binding with guest molecules, and reassociation with encapsulated guest molecules inside protein cavity.....	65

CHAPTER 2

Figure 2.1:	The scattered light on the detector shows constructive and destructive phase.....	71
Figure 2.2:	The relationship between diffusion speed and size of small particles and large particles.....	71
Figure 2.3:	The size distribution by intensity plot of 0.2 mg/mL apoFT (pH 7.0) shows the intensity of apoFT that was incubated at room temperature overnight, the intensity of apoFT that was incubated for 5 min, and the intensity of filtered apoFT that was also incubated for 5 min.....	78
Figure 2.4:	The plot of pH of protein solution (HCl addition) versus average size of apoFT (1.0 mg/mL) as determined by DLS shows a rapid decrease in average hydrodynamic diameter of the protein as pH decreases from 3.0 to 1.5.....	79
Figure 2.5:	The size distribution by intensity plot of apoFT (0.7 mg/mL) with salt control (pH 7.0).....	80

Figure 2.6:	The size distribution by intensity plot represents the effects of glycerol on protein stability.....	81
Figure 2.7:	The size distribution by intensity plot represents the effects of declustering time.....	82
Figure 2.8:	The size distribution by intensity plot represents the effects of reassembly time.....	83

CHAPTER 3

Figure 3.1:	Superose 6 gel filtration chromatograms of 1.35 mg/mL apoFT in buffer containing 20 mM Tris-OH (pH 8.0) and either 100 mM, or 150 mM, or 200 mM NaCl show two peaks of eluted protein, which are marked as peak 1 and peak 2.....	103
Figure 3.2:	Normalized Superose 6 gel filtration chromatograms of apoFT in 20 mM Tris-OH (pH 8.0) containing 100, 150, or 200 mM NaCl.....	104
Figure 3.3:	The normalized Superose 6 gel filtration chromatograms of 3.35 mg/mL bFT-WT in buffer containing 20 mM Tris-OH (pH 8.0) and either 100 mM KCl or 100 mM NaCl	105
Figure 3.4:	The normalized Superose 6 gel filtration chromatograms of 0.34 (blue), 0.68, and 1.35 mg/mL apoFT in buffer containing 20 mM Tris-OH (pH 8.0) and 100 mM NaCl represents the overlap of different intensity of 24-subunit peaks and the formation of self-associated clusters at higher protein concentrations.....	106
Figure 3.5:	The normalized Superose 6 gel filtration chromatograms of 1.35 mg/mL bFT-WT and 3.35 mg/mL bFT-WT in 20 mM Tris-OH (pH 8.0) and 100 mM NaCl show the overlap peaks of the 24-subunit cluster.....	106
Figure 3.6:	The normalized Superose 6 gel filtration chromatograms of 3.35 mg/mL bFT-WT in buffer containing 100 mM NaCl and either 20 mM Tris-OH (pH 8.0) or 20 mM Tris-OH (pH 7.0)	107
Figure 3.7:	The 1% agarose gel illustrates the digestion of bFT-WT and bFT-E18A/E94A with <i>BsmI</i> and <i>HindIII</i>	108
Figure 3.8:	SDS PAGE gel of the protein purification of bFT-E18A by heat denaturation and ammonium sulfate precipitation.....	111
Figure 3.9:	The Superose 6 chromatogram of 3.35 mg/mL bFT-WT in 20 mM Tris-OH (pH 8.0) and 100 mM NaCl.....	111

Figure 3.10:	SDS PAGE results of Superose 6 eluted peaks of 3.35 mg/mL bFT-WT in 20 mM Tris-OH (pH 8.0) and 100 mM NaCl.....	112
Figure 3.11:	The UV-visible spectrum of peak 6 bFT-WT from Superose 6 (peak 6 in Figure 3.9) scanned from 300-600 nm shows that there is no absorption at 418 nm wavelength (corresponding to Soret band of the oxidized heme moiety), which indicated the presence of heme in this fraction.....	113
Figure 3.12:	The UV spectrum of peak 6 bFT-WT from Superose 6 (peak 6 in Figure 3.9) scanned from 220-300 nm shows an intense peak at ~260 nm and small peak at 280 nm.....	113
Figure 3.13:	The normalized Superose 6 chromatograms of 3.35 mg/mL bFT-WT and 1.35 mg/mL bFT-E18A in 20 mM Tris-OH (pH 8.0) and 100 mM NaCl showing the overlap of 24-subunit, dimer, and monomer peaks.....	115
Figure 3.14:	The normalized Superose 6 chromatograms of 3.35 mg/mL bFT-WT and 1.35 mg/mL bFT-M52L in 20 mM Tris-OH (pH 8.0) and 100 mM NaCl showing the overlap of 24-subunit and dimer peaks.....	116
Figure 3.15:	The normalized Superose 6 chromatograms of 3.35 mg/mL bFT-WT and 1.35 mg/mL bFT-E94A in 20 mM Tris-OH (pH 8.0) and 100 mM NaCl showing the overlap of 24-subunit and dimer peaks.....	116
Figure 3.16:	The normalized Superose 6 chromatograms of 3.35 mg/mL bFT-WT and 1.35 mg/mL bFT-E18A/M52L in 20 mM Tris-OH (pH 8.0) and 100 mM NaCl showing the overlap of 24- and monomer peaks.....	116
Figure 3.17:	The normalized Superose 6 chromatograms of 3.35 mg/mL bFT-WT and 1.35 mg/mL bFT-E18A/E94A in 20 mM Tris-OH (pH 8.0) and 100 mM NaCl showing the overlap of 24-mer and monomer peaks. The variant might contain a 12-mer peak.....	117
Figure 3.18:	The normalized Superose 6 chromatograms of 3.35 mg/mL bFT-WT and 1.35 mg/mL bFT-M52L/E94A in 20 mM Tris-OH (pH 8.0) and 100 mM NaCl showing the overlap of a dimer peak.....	117
Figure 3.19:	The normalized Superose 6 chromatograms of 3.35 mg/mL bFT-WT and 3.35 mg/mL bFT-E18A/M52L/E94A in 20 mM Tris-OH (pH 8.0) and 100 mM NaCl showing the overlap of 24-subunit, dimer, and monomer peaks.....	117
Figure 3.20:	The normalized Superose 6 chromatograms of 3.35 mg/mL bFT-E18A/M52L/E94A and 0.40 mg/mL 2-subunit peak of bFT-E18A/M52L/E94A in 20 mM Tris-OH (pH 8.0) and 100 mM NaCl showing the overlap of the dimer peak.....	118

Figure 3.21: The normalized Superose 6 chromatograms of 1.012 mg/mL 24-mer peak and 5.892 mg/mL bFT-E18A/M52L/E94A in 20 mM Tris-OH (pH 8.0) and 100 mM NaCl show the overlap of 24-mer peak.....118

Figure 3.22: The ribbon structure of *E. coli* bFT showing Glu18 and Glu94, which are facing the inner core and locating at the outer helices.....119

CHAPTER 4

Figure 4.1: The schematic representation of encapsulation processes in bFT.....124

Figure 4.2: The excitation spectrum scanning from 300-400 nm with the fixed emission wavelength at 440 nm and the emission spectrum scanning from 400-550 nm with the fixed excitation wavelength at 345 nm of Pro-Q[®] sapphire 365 oligohistidine gel stain using a fluorometer..... 129

Figure 4.3: The UV-visible spectrum of Pro-Q[®] sapphire 365 oligohistidine gel stain scanned from 300-550 nm showing the highest absorption at 345 nm..... 130

Figure 4.4: A summary showing the encapsulating protocols, where buffer A is 10 mM PIPES (pH 2.0) solution containing 150 mM NaCl and 10% glycerol and buffer B is 10 mM PIPES (pH 8.0) solution containing 100 mM NaCl..... 136

Figure 4.5: The 1% agarose gel representing PCR products of bFT-WT with *NdeI* cutting site at the N-terminus and *XhoI* cutting site at the C-terminus..... 145

Figure 4.6: SDS PAGE of protein purification of bFT with His₆-tag at the C-terminus by heat denaturation and ammonium sulfate precipitation..... 145

Figure 4.7: The structure of coumarin, 7-amino-3-(1-carboxy-1-(bis(carboxymethyl)amino)-5-(acetylamino))pentyl-4-methylcoumarin-6-sulfonic acid, and Alexa Fluoro 350 carboxylic acid..... 149

Figure 4.8: The electrospray mass spectrum of commercial PIPES..... 150

Figure 4.9: The electrospray mass spectrum of dye molecules in Pro-Q[®] sapphire 365 oligohistidine gel stain..... 151

Figure 4.10: The emission spectrums scanned between wavelengths 400-550 nm with the fixed excitation at 345 nm of the native dye molecules in Pro-Q[®] sapphire 365 oligohistidine gel stain (PIPES buffer pH 7.0), the diluted dye molecules in 6 M Gdn-HCl solution, PIPES buffer, and 6 M Gdn-HCl solution showing maximum fluorescence intensity at 440 nm..... 152

Figure 4.11:	The emission spectrums scanned between wavelengths 400-550 nm with the fixed excitation at 345 nm of the 24-mer Histag protein, non-specific dye binding Histag protein, Histag protein after 30, 60, and 90 min declustering time showing maximum fluorescence intensity at 440 nm.....	154
Figure 4.12:	The Superose 6 gel filtration chromatograms of 24-mer Histag protein, non-specific dye binding Histag protein, Histag protein with encapsulated dye after 30 min declustering time, Histag protein with encapsulated dye after 60 min declustering time, Histag protein with encapsulated dye after 90 min declustering time.....	155
Figure 4.13:	The size distribution by intensity plot of 24-subunit Histag protein, Histag protein with encapsulated dye after 30 min, 60 min, and 90 min declustering time.....	156
Figure 4.14:	The emission spectrums scanned between wavelengths 400-550 nm with the fixed excitation wavelength at 345 nm of bFT with His ₆ -tag at the C-terminus with encapsulated dye with 1, 2, and 3 hours encapsulation time showing maximum fluorescence intensity at 440 nm.....	157
Figure 4.15:	The Superose 6 gel filtration chromatograms of 24-mer Histag protein, Histag protein after encapsulated with dye molecules for 1 hour, 2 hours, and 3 hours.....	158
Figure 4.16:	The size distribution by intensity plot of 24-mer Histag protein, Histag protein after encapsulated with dye molecules for 1 hour, 2 hours, and 3 hours.....	158
Figure 4.17:	The emission spectrums scanned between wavelengths 400-550 nm with the fixed excitation at 345 nm of Histag protein with encapsulated dye, WT protein, and the various combinations of Histag/WT mixture showing maximum fluorescence intensity at 440 nm.....	160
Figure 4.18:	The Superose 6 gel filtration chromatograms of 24-mer WT protein, 24-mer Histag protein, 100/0:Histag/WT mixture, and 60/40:Histag/WT mixture	161
Figure 4.19:	The size distribution by intensity plot of 24-mer Histag protein, 24-mer WT protein, 100/0:Histag/WT mixture with encapsulated dye, and 60/40:Histag/WT mixture with encapsulated dye	161
Figure 4.20:	The emission spectrums scanned between wavelengths 400-550 nm with the fixed excitation wavelength at 345 nm of 0.15 and 0.45 mg/mL WT protein with encapsulated dye showing maximum fluorescence intensity at 440 nm.....	162

Figure 4.21:	The Superose 6 gel filtration chromatograms of 24-mer WT protein, 0.15 mg/mL and 0.45 mg/mL WT protein with encapsulated dye.....	163
Figure 4.22:	The size distribution by intensity plot of 24-mer WT, 0.15 mg/mL and 0.45 mg/mL WT protein with encapsulated dye.....	163
Figure 4.23:	The emission spectrums scanned between wavelengths 400-550 nm with the fixed excitation wavelength at 345 nm of 0.23 mg/mL of Histag protein with encapsulated dye and 60/40:Histag/WT mixture before and after an additional 5 hours of dialysis time showing maximum fluorescence intensity at 440 nm.....	165
Figure 4.24:	The Superose 6 gel filtration chromatograms of 24-mer Histag protein, 24-mer WT protein, 100/0:Histag/WT mixture with encapsulated dye, and 100/0:Histag/WT mixture with an additional 5 hours of dialysis time..	166
Figure 4.25:	The Superose 6 gel filtration chromatograms of 60/40:Histag/WT mixture with encapsulated dye, 60/40:Histag/WT mixture with an additional 5 hours of dialysis time, 60/40:Histag/WT mixture with an additional 5 hours of dialysis time without adjusting protein concentration.....	167
Figure 4.26:	The size distribution by intensity plot of 24-mer Histag protein, 100/0:Histag/WT mixture with encapsulated dye, 100/0:Histag/WT mixture with an additional 5 hours of dialysis time, and 100/0:Histag/WT mixture with an additional 5 hours of dialysis time without adjusting protein concentration	167
Figure 4.27:	The size distribution by intensity plot of 24-mer Histag protein, 60/40:Histag/WT mixture with encapsulated dye, 60/40:Histag/WT mixture with an additional 5 hours of dialysis time, 60/40:Histag/WT mixture with an additional 5 hours of dialysis time without adjusting protein concentration	168
Figure 4.28:	The emission spectrums scanned between wavelengths 400-550 nm with the fixed excitation wavelength at 345 nm of 24-mer WT protein, WT protein with encapsulated dye, and WT protein with encapsulated dye and with an additional 5 hours of dialysis time showing maximum fluorescence intensity at 440 nm.....	169
Figure 4.29:	The Superose 6 gel filtration chromatograms of 24-mer WT protein, WT protein with encapsulated dye after dialysis overnight, and WT protein with encapsulated dye and with an additional 5 hours of dialysis time.....	170
Figure 4.30:	The size distribution by intensity plot of 24-mer WT protein, WT protein with encapsulated dye, and WT protein with encapsulated dye and with an additional 5 hours of dialysis time.....	170

Figure 4.31:	The emission spectrums scanned between wavelengths 400-550 nm with the fixed excitation wavelength at 345 nm of 24-mer Histag protein, 24-mer WT protein, non-specific dye binding Histag protein before and after an additional 5 hours of dialysis time, and non-specific dye binding WT protein before and after an additional 5 hours of dialysis time showing maximum fluorescence intensity at 440 nm.....	172
Figure 4.32:	The Superose 6 gel filtration chromatograms of 24-mer Histag protein, 24-mer WT protein, non-specific dye binding Histag protein before and after an additional 5 hours of dialysis time, and non-specific dye binding WT protein before and after an additional 5 hours of dialysis time.....	173
Figure 4.33:	The size distribution by intensity plot of 24-mer WT protein, non-specific dye binding WT protein with an additional 5 hours of dialysis time, and non-specific dye binding WT protein without an additional 5 hours of dialysis time	174
Figure 4.34:	The size distribution by intensity plot of 24-mer Histag protein, non-specific dye binding Histag protein with an additional 5 hours of dialysis time, and non-specific dye binding Histag protein without an additional 5 hours of dialysis time.....	174
Figure 4.35:	The Superose 6 gel filtration chromatograms of 24-mer Histag protein, 24-mer WT protein, non-encapsulated Histag protein, non-encapsulated WT protein, and non-encapsulated 60/40:Histag/WT mixture	175
Figure 4.36:	The Superose 6 gel filtration chromatograms of non-encapsulated Histag protein, non-encapsulated WT protein, and non-encapsulated 60/40:Histag/WT mixture. All non-specific dye binding and proteins with encapsulated dye were dialyzed overnight followed by change of dialysis buffer and then dialyzed for an additional 5 hours	176
Figure 4.37:	The size distribution by intensity plot of 24-mer Histag protein, non-encapsulated Histag protein, non-encapsulated WT protein, and non-encapsulated 60/40:Histag/WT mixture. All non-specific dye binding and proteins with encapsulated dye were dialyzed overnight.....	176
Figure 4.38:	The size distribution by intensity plot of 24-mer Histag protein, non-encapsulated Histag protein, non-encapsulated WT protein, and non-encapsulated 60/40:Histag/WT mixture All non-specific dye binding and proteins with encapsulated dye were dialyzed overnight followed by change of dialysis buffer and then dialyzed for an additional 5 hours....	177

Figure 4.39:	The emission spectrums scanned between wavelengths 400-550 nm with the fixed excitation at 345 nm of the 60/40:Histag/WT mixture with encapsulated dye, the denatured 60/40:Histag/WT mixture with encapsulated dye (with 6 M Gdn-HCl solution), denatured 24-mer Histag protein (with 6 M Gdn-HCl), and 6 M Gdn-HCl solution showing maximum fluorescence intensity at 440 nm.....	178
Figure 4.40:	Structural modeling of the 24-mer His-tag bFT	182

APPENDIX 5

Figure A5.1:	The electrospray mass spectrums of wild-type bFT	218
Figure A5.2:	The electrospray mass spectrums of bFT-E18A	219
Figure A5.3:	The electrospray mass spectrums of bFT-M52L	220
Figure A5.4:	The electrospray mass spectrums of bFT-E94A	221
Figure A5.5:	The electrospray mass spectrums of bFT-E18A/M52L	222
Figure A5.6:	The electrospray mass spectrums of bFT-E18A/E94A	223
Figure A5.7:	The electrospray mass spectrums of bFT-M52L/E94A	224
Figure A5.8:	The electrospray mass spectrums of bFT-E18A/M52L/E94A	225
Figure A5.9:	The electrospray mass spectrums of bFT with His ₆ -tag at the C-terminus	226

APPENDIX 6

Figure A6.1:	The spectrophotometric chromatogram of bFT-WT with zoom in view at 525 and 560 nm	227
Figure A6.2:	The comparison of spectrophotometric chromatograms between wild-type bFT and bFT-E18A	228
Figure A6.3:	The comparison of spectrophotometric chromatograms between wild-type bFT and bFT-M52L	228
Figure A6.4:	The comparison of spectrophotometric chromatograms between wild-type bFT and bFT-E94A	229

Figure A6.5: The comparison of spectrophotometric chromatograms between wild-type bFT and bFT-E18A/M52L.....	229
Figure A6.6: The comparison of spectrophotometric chromatograms between wild-type bFT and bFT-M52L/E94A	230
Figure A6.7: The comparison of spectrophotometric chromatograms between wild-type bFT and bFT-E18A/E94A	230
Figure A6.8: The comparison of spectrophotometric chromatograms between wild-type bFT and bFT-E18A/M52L/E94A	231

APPENDIX 7

Figure A7.1: The Superose 6 gel filtration chromatogram of Bio-Rad standard protein...	232
Figure A7.2: The Superose 6 gel filtration chromatogram of Blue Dextran	233
Figure A7.3: The Bio-Rad protein standard curve used for molecular weight calculation of protein samples.....	232
Figure A7.4: The plot of Stokes radius versus elution volumes of protein standards showing the linear equation that is used for the calculation of Stokes radius of apoFT	236
Figure A7.5: The plot of molecular weights versus Stokes radius times sedimentation coefficients of protein standards showing the linear equation that is related to the Stokes-Einstein and Svedberg equations and is used for the calculation of the molecular weight for 24-subunit apoFT.....	236
Figure A7.6: The Superose 6 gel filtration chromatogram of bFT-WT.....	237
Figure A7.7: The SDS PAGE results of Superose 6 eluted fractions of bFT-WT.	238
Figure A7.8: The Superose 6 gel filtration chromatogram of bFT-E18A	239
Figure A7.9: The SDS PAGE results of Superose 6 eluted fractions of bFT-E18A.....	239
Figure A7.10: The Superose 6 gel filtration chromatogram of bFT-M52L	240
Figure A7.11: The SDS PAGE results of Superose 6 eluted peaks of bFT-M52L.	240
Figure A7.12: The Superose 6 gel filtration chromatogram of bFT-E94A	241
Figure A7.13: The SDS PAGE results of Superose 6 eluted fractions of bFT-E94A.....	241

Figure A7.14: The Superose 6 gel filtration chromatogram of bFT-E18A/M52L	242
Figure A7.15: The SDS PAGE results of Superose 6 eluted fractions of bFT-E18A/M52L.	242
Figure A7.16: The Superose 6 gel filtration chromatogram of bFT-M52L/E94A	243
Figure A7.17: The SDS PAGE results of Superose 6 eluted fractions of bFT-M52L/E94A.....	243
Figure A7.18: The Superose 6 gel filtration chromatogram of bFT-E18A/E94A	244
Figure A7.19: The SDS PAGE results of Superose 6 eluted peaks of bFT-E18A/E94A...	245
Figure A7.20: The Superose 6 chromatogram of bFT-E18A/M52L/E94A	245
Figure A7.21: The SDS PAGE results of Superose 6 eluted fractions of bFT-E18A/M52L/E94A.	246
Figure A7.22: The Superose 6 gel filtration chromatogram of bFT with His ₆ -tag at the C-terminus	247
Figure A7.23: The SDS PAGE results of Superose 6 eluted fractions of bFT-WT with His ₆ -tag at the C-terminus.....	248

APPENDIX 8

Figure A8.1: The emission spectrums scanned between wavelengths 400-550 nm of dye series show maximum fluorescent intensity at 440 nm.....	250
Figure A8.2: The excitation spectrums scanned between wavelengths 300-400 nm of dye series show maximum fluorescent intensity at 345 nm.....	251
Figure A8.3: The plot of fluorescent intensity of emission wavelength 440 nm and excitation wavelength at 345 nm versus % dye concentration.....	252
Figure A8.4: The plots of fluorescent intensity of excitation wavelength at 345 nm versus dye concentration compared with that of optical density versus dye concentration showing the slopes of the trend lines that represent extinction coefficient of Pro-Q [®] sapphire 365 oligohistidine gel stain.....	253

LIST OF ABBREVIATIONS

Å	angstrom
ABC	ATP binding cassette
Amp	ampicillin
APDs	avalanche photodiodes
apoFT _{HS}	horse spleen apoferritin
ATD	antitubercular drug
ATP	adenosine triphosphate
bp	base pair(s)
bFT	bacterioferritin
bFT-WT	wild-type bacterioferritin
BSA	bovine serum albumin
C-terminus	carboxylic acid-terminus
Carb	carbinicillin
CBP	calmodulin-binding peptide
CCMV	Cowpea chlorotic mottle virus
CD	circular dichroism
CdS	cadmium(II) sulfide
CH ₃ CO ₂ H	acetic acid
Chol	cholesterol
Cl ⁻	chloride ion
CM	cytosolic membrane
Co ²⁺ -CMA	cobalt(II)-carboxymethylaspartate

Co ₃ O ₄	cobalt oxide
Co(O)OH	cobalt oxyhydroxide
CPK	Corey, Pauling, Kulin
cTEM	cryo-transmission electron microscopy
CYD	covalent yet dissociable NorpD peptide
Cu ²⁺	copper ion
Da	Dalton
ddH ₂ O	distilled deionized water
DLS	dynamic light scattering
DMPC	1,2-dimyristoyl- <i>sn</i> -glycero-3-phosphocholine
DNA	deoxyribonucleic acid
dNTP	deoxynucleotide triphosphate
Dps	DNA-binding protein
DSPC	1,2-distearoyl- <i>sn</i> -glycero-3-phosphocholine
DTT	dithiothreitol
EDTA	ethylenediamine tetraacetic acid
EGTA	Ethylenebis(oxyethylenitrilo) tetraacetic acid
e.p.r.	electron paramagnetic resonance
Eq	equation
EXAFS	extended X-ray absorption fine structure
Fe ²⁺	ferrous iron
Fe ³⁺	ferric iron
Fe-S	iron-sulfur

FPLC [®]	fast peptide and protein liquid chromatography
FT	ferritin
Fur	ferric uptake regulator
g	gram
Gdn-HCl	guanidinium hydrochloride
GFP	green fluorescent protein
GSH	glutathione
GST	glutathione S-transferase
GTP	guanosine triphosphate
H ₂	dihydrogen
HAT	histidine affinity tag
H-chain	heavy chain
HCl	hydrochloride
Histag	bacterioferritin with hexahistidine at the C-terminus
HO [•]	hydroxyl radical
H ₂ O ₂	hydrogen peroxide
HPC	heavy chain of protein C
hr	hour
Hsp	heat shock protein
ICP-MS	Inductively Coupled Plasma Mass Spectrometry
IPTG	isopropyl-β-D-thiogalactopyranoside
kb	kilobase pair(s)
kDa	kiloDalton

KSHV	Kaposi's sarcoma-associated herpes virus
L	liter
L-chain	light chain
LB	Luria Bertani media
LLS	laser light scattering
M	molar
\mathcal{M}_1	unfolded subunit
M_{24}	native tetracosamer of bacterioferritin
Mab	monoclonal antibody
MBP	maltose-binding protein
M-chain	medium chain
MDa	megaDalton
mg	milligram
μg	microgram
M_i	assembly intermediates of bacterioferritin with <i>i</i> subunits
min	minute
mL	milliliter
μL	microliter
mM	millimolar
μm	micrometer
μmol	micromole
Mn^{2+}	manganese ion
MPa	megapascal

mRNA	messenger ribonucleic acid
ms	millisecond
MS	mass spectrometry
mW	milliWatt
MW	molecular weight
MWM	molecular weight marker
N ₂	dinitrogen
N/A	not available
Na ⁺	sodium ion
NaCl	sodium chloride
NaHCO ₃	sodium bicarbonate
NaN ₃	sodium azide
NaOH	sodium hydroxide
Na ₂ SO ₄	sodium sulfate
ng	nanogram
(NH ₄) ₂ SO ₄	ammonium sulfate
Ni ²⁺ -NTA	nickel nitrilotriacetic acid
n.i.r.-m.c.d.	near infrared magnetic circular dichroism
ng	nanogram
nm	nanometer
nM	nanomolar
N-terminus	amino-terminus
PCR	polymerase chain reaction

PIPES	1,4-piperazinebis(ethanesulfonic acid)
PLG	poly(DL-lactide-co-glycolide)
pmol	picamol
Pt	platinum
O ₂	dioxygen
O ₂ ⁻	superoxide
OD	optical density
OM	outer membrane
PCR	polymerase chain reaction
pI	isoelectric point
PIPES	1,4-Piperazinebis(ethanesulfonic acid)
Q-TOF	quadrupole time of flight
RNA	ribonucleic acid
rpm	revolutions per minute
ROS	reactive oxygen species
s	second
SBP	streptavidin binding protein
SDS PAGE	sodium dodecyl sulfate polyacrylamide gel electrophoresis
SLNs	solid lipid nanoparticles
sRNA	small ribonucleic acid
STR	Strep-Tactin
<i>t</i> _{1/2}	half life time
TBE	Tris-borate-EDTA buffer

TCA	trichloroacetic acid
T _m	melting temperature
TMV	tobacco mosaic virus
Tris-OH	2-amino-2-(hydroxymethyl)-1, 3-propanedial-hydroxide
V	volt
v/v	volume by volume
WT	wild type bacterioferritin
w/v	weight by volume

Note: The standard three letter and one letter amino acid codes as well as the one letter DNA base codes have been used throughout this report.

CHAPTER 1: INTRODUCTION

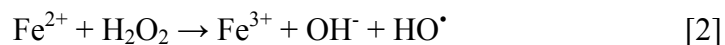
1.1: Bacterial Iron Homeostasis

1.1.1: Role of Iron in Living Organisms

Iron is the fourth most abundant metal in the earth's crust and is essential to virtually all organisms (Köster, 2001). It participates in many major biological processes such as photosynthesis, N₂ fixation, methanogenesis, H₂ production and consumption, respiration, the tricarboxylic acid cycle, oxygen transport, gene regulation, and DNA biosynthesis (Andrews *et al.*, 2003; Massé and Arguin, 2005). It is also an extremely versatile prosthetic component for incorporation into proteins as a biocatalyst or electron carrier (Smith, 2004). It mainly exists in one of two readily interconvertible redox states: the reduced Fe²⁺ ferrous form and the oxidized Fe³⁺ ferric form. However, oxidation of the ferrous ion pool to the ferric form creates two problems. Firstly, iron can be extremely toxic from the reaction of Fe(II) and dioxygen yielding the production of intermediate reactive oxygen species. Therefore, it is important for cells to find suitable systems for managing cellular iron. Secondly, Fe(III) has poor solubility under aerobic conditions at neutral pH. This prevents its use as a readily bioavailable iron source, because storage of non-soluble Fe(III) is needed to be converted to soluble Fe(II) before use in living organisms.

Oxidative stress is a universal phenomenon experienced by both aerobic and anaerobic organisms. The cellular stress is caused by intracellular reactive oxygen species (ROS) that can generate a mixture of superoxide (O[•]₂) and hydrogen peroxide (H₂O₂) as products (Smith, 2004). From this mixture, superoxide can react with a ferric iron (Fe³⁺) yielding soluble ferrous iron (Fe²⁺) and dioxygen (O₂) (Eq. 1). Then, hydrogen peroxide, a powerful oxidant, is

able to react with free ferrous iron generating damaging hydroxyl radicals (HO[•]) through the Fenton reaction (Eq. 2). The combination of these two reactions is called the Haber-Weiss reaction (Wiedenheft *et al.*, 2005; Andrews *et al.*, 2003) (Eq. 3).



Hydroxyl radicals can induce lipid peroxidation, DNA strand breaks, and degradation of various biomolecules (Andrews, 1998; Harrison and Arosio, 1996). In order to avoid deprivation or over-abundance of iron, bacteria and eukaryotes have developed a tight regulatory system to keep this metal within a narrow concentration range.

There are five strategies to regulate iron. Firstly, high affinity iron transporters enable iron to be scavenged in various forms from the organism's environment. Secondly, intracellular iron is stored and released depending on the limitation of external supplies. Thirdly, employment of redox stress resistance systems such as degradation of iron-induced reactive oxygen species and repair of redox stress-induced damage determine the amount of iron in cells. In addition, iron consumption is controlled by down-regulating the expression of iron-containing proteins under iron-restricted conditions. Lastly, iron responsive regulatory systems coordinate the expression of the above iron homeostatic machinery according to iron availability (Andrews *et al.*, 2003).

1.1.2: Iron Transporters

There are at least five systems that can secrete extracellular iron to the cytoplasm. These include siderophore-based iron acquisition, ferrous iron transport, ferric reduction, metal-type ATP binding cassette transporters, low-affinity iron transport, and iron acquisition by pathogens.

Siderophore-based Iron Acquisition

There are three ways to solubilize ferric oxides including lowering the external pH to render ferric iron more soluble, reducing ferric iron to the relatively soluble ferrous form, and employing ferric ion chelators as solubilizing agents (Guerinot, 1994). In the last case, extracellular Fe^{3+} can be secreted and solubilized by high affinity extracellular ferric chelators, called siderophores, prior to transport (Wandersman and Delepelaire, 2004). Gram-negative bacteria take up iron-siderophore complexes via specific outer membrane (OM) receptors (such as Cir, FecA, FepA, FhuA, FhuE, and Fiu in *Escherichia coli* K12), which are driven by the cytosolic membrane (CM) potential (Andrews *et al.*, 2003) (Figure 1.1A). Other sources of iron such as ferric citrate, heme, lactoferrin, and transferrin are also recognized by siderophores (Köster, 2001; Bullen *et al.*, 1978). These iron-siderophore complexes are transported across the OM by the energy-transducing TonB-ExbB-ExbD system, because they are too large to diffuse through the channels. Then, periplasmic binding proteins shuttle ferri-siderophores from the OM receptors to ATP binding cassette transporters (FecBCDE, FepBCDEFG, and FhuBCD) that deliver ferri-siderophores to the cytosol, where the complexes are likely dissociated by reduction to the soluble form of iron (Fe^{2+}) and sequestered into iron-utilizing proteins (Litwin and Calderwood, 1993). Gram-positive bacteria lacking an OM require

neither OM receptors nor the TonB-ExbB-ExbD system to allow ferri-siderophores to traverse their CM (Figure 1.1B). The protein-dependent ATP binding cassette permeases found in Gram-negative species are also employed in Gram-positive organisms. These binding proteins are generally lipoproteins tethered to the external surface of the CM.

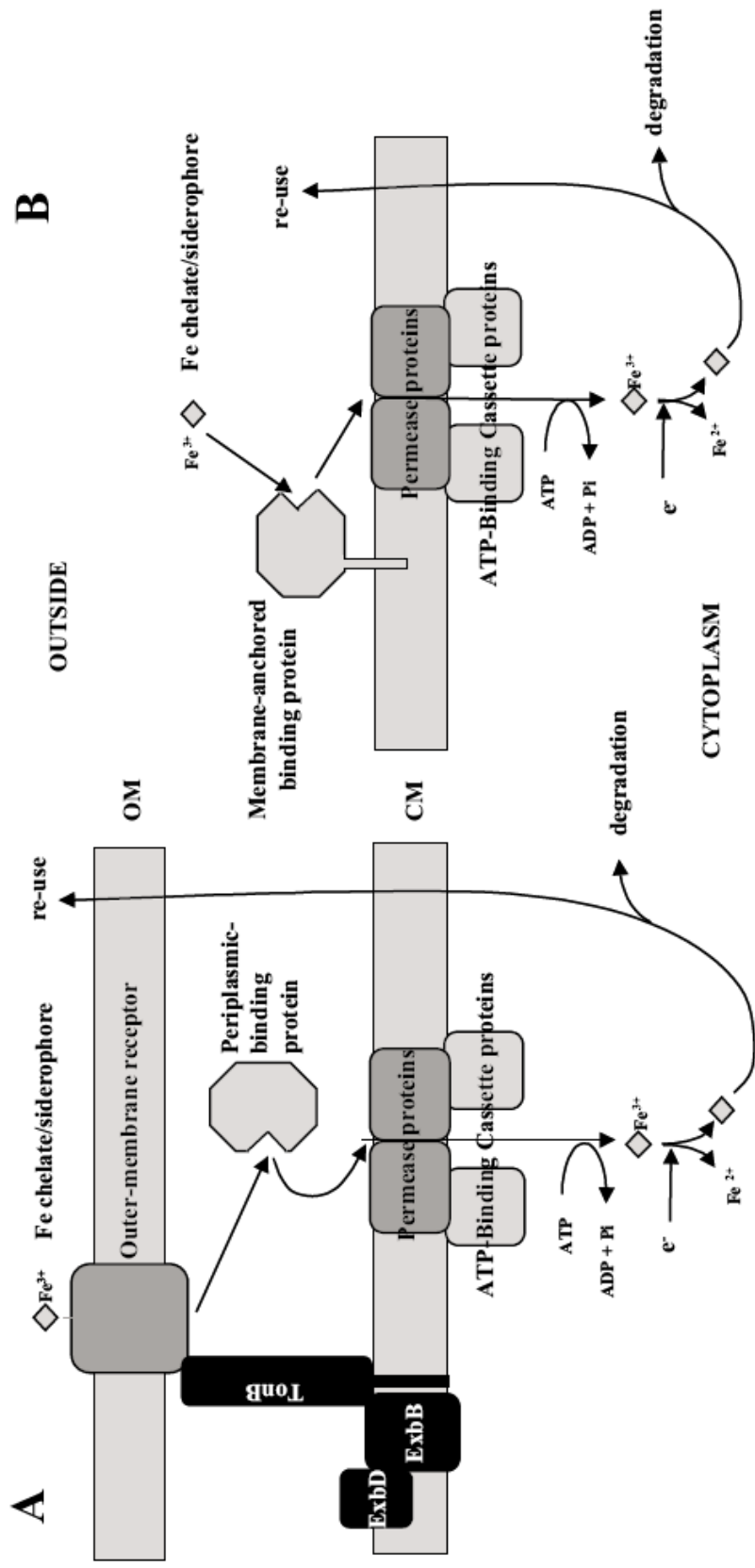


Figure 1.1: Schematic representation of siderophore-mediated iron uptake in Gram-negative (A) and Gram-positive (B) bacteria (Andrews *et al.*, 2003).

Ferrous Iron Transport and Ferric Reduction

This system traverses ferrous iron via Feo, the protein encoded by anaerobically induced iron-repressed *feoAB* genes (Kammler *et al.*, 1993). This iron transport system consists of three types of proteins; FeoA, FeoB, and FeoC (Cartron *et al.*, 2006). FeoA is a small, soluble SH3-domain protein consisting of 75-amino acid, while FeoB consists of 773 amino acid residues. The FeoB N-terminus possesses G protein functionality (Marlovits *et al.*, 2002). It also has a C-terminal integral inner-membrane domain, which forms two motifs (gates) locating in the CM allowing Fe^{2+} to pass through from the OM and periplasm (Figure 1.2). In order for Fe^{2+} to go across the CM, it needs an ATP/GTP-driven active transport process for FeoA, which is required for maximum FeoB activity (Kammler *et al.*, 1993). FeoC consists of 78 residues and functions as an iron-sulfur ([Fe-S])-dependent transcriptional repressor (Cartron *et al.*, 2006). The hydrophilic FeoC is only associated with γ -proteobacterial Feo systems.

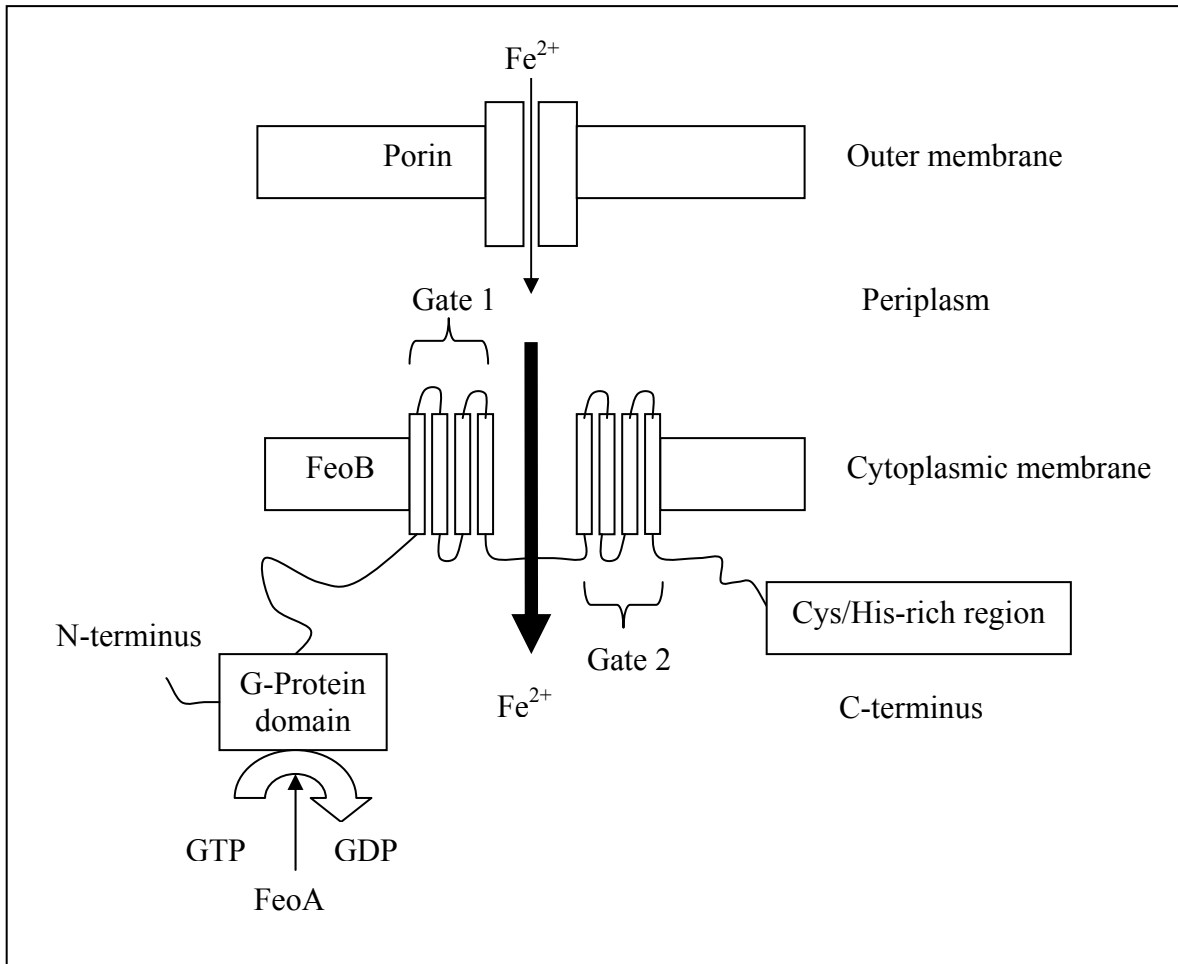


Figure 1.2: Schematic representation of ferrous iron uptake by Feo system in *E. coli* (the Figure is derived from Cartron *et al.*, 2006).

Metal-type ATP binding cassette transporters

Under anaerobic conditions, ferric iron can be transported without involving any chelators. Another type of bacterial iron transporter is the metal-type ATP binding cassette (ABC) systems that is specific to iron but does not necessarily require OM receptors or siderophores (Köster, 2001). The ferric iron is delivered into the periplasm via receptor mediated Ton complex-formation.

Low-affinity Iron Transport

Low affinity transport may be non-biological (i.e. iron binding to the cell surface) since in the absence of the high-affinity Feo system, this modality of uptake does not facilitate normal growth even in the presence of high iron concentrations (Velayudhan *et al.*, 2000).

Iron Acquisition by Pathogens

The problems that bacteria face in acquiring sufficient iron from their surroundings are particularly pronounced for pathogens. Pathogens often use low environmental iron levels as a signal for the induction of virulence genes (Litwin and Calderwood, 1993). Pathogens are able to counter the iron restriction imposed by their hosts through the use of siderophores (Andrews *et al.*, 2003).

1.1.3: Iron Storage Proteins and Their Applications

Iron storage proteins are widely distributed among prokaryotes, archaea, high- and low-G+C gram-positive bacteria, cyanobacteria, *Bacteroides*, *Thermotogales*, and all four subdivisions of the *Proteobacteria*, suggesting that the facility to store iron is an important general requirement of prokaryotes (Abdul-Tehrani *et al.*, 1999). Iron is presented within the cells of living organisms either in iron-containing protein and enzyme complexes or in iron-storage proteins. It can be incorporated in protein molecules in heme-containing forms. These heme-iron atoms bind to sulfur in various types of [Fe-S] clusters, in mixed-metal centers (e.g. containing nickel), as di-iron, or as mononuclear iron centers. Three types of iron storage proteins are recognized in bacteria including the smaller DNA-binding protein from starved cells that is unique to prokaryotes, the archetypal ferritins found in eukaryotes, and the heme-

containing bacterioferritins found only in eubacteria (Smith, 2004). Although the three types of iron storage proteins belong to distinct evolutionary lineages, they are distantly related to each other in term of structural and functional similarities (Andrews *et al.*, 1991b). Iron storage proteins take up iron in the soluble ferrous form, but iron is deposited in the central cavity in the oxidized and less soluble ferric form.

DNA-binding Protein

DNA-binding protein from starved cells (Dps) is an approximately spherical multisubunit protein consisting of 12 identical subunits with a total molecular weight (MW) of ~240 kDa. The protein can store up to 500 iron atoms within the central cavity (Zhao *et al.*, 2002) (Figure 1.3a). The outer shell diameter is ~10 nm and the interior diameter is ~5 nm (Wiedenheft *et al.*, 2005). The secondary structure of Dps shows that each subunit is folded into a four-helix bundle (A-D) (Figure 1.3b). The ferroxidase center is located at the interface of two-fold symmetry-related subunits such that the iron ligands are contributed by both symmetry-related monomers (12-subunit). The X-ray crystal structure of *Listeria* Dps (previously known as *Listeria* ferritin) showed that the ferroxidase center contains one bound iron coordinated by Glu62 and Asp58 from one subunit, a His31 from the symmetry-related subunit, and a water molecule that is located 3 Å from the iron atom, forming a hydrogen bond with His43 from the same monomer (Ilari *et al.*, 2005; Ilari *et al.*, 2000) (Figure 1.4). The residues involved in iron binding at this site are well conserved in Dps proteins.

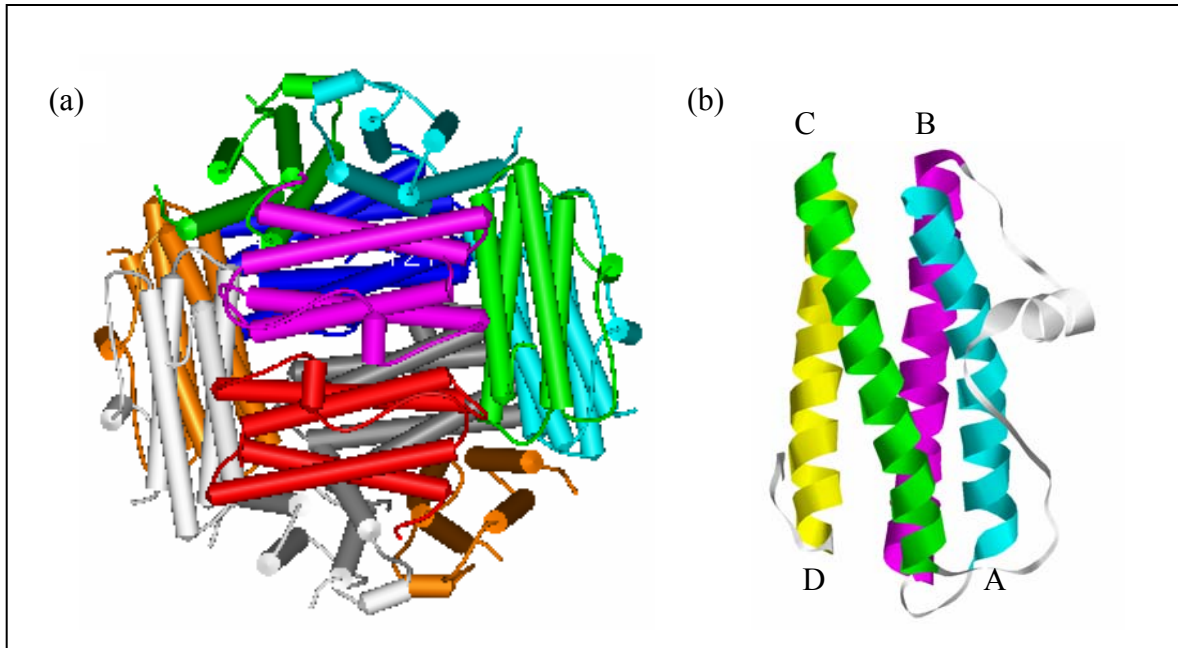


Figure 1.3: The schematic presents (a) the overall structure of *Listeria Dps* and (b) its secondary structure of one subunit, which consists of helix A (blue), helix B (purple), helix C (green), and helix D (yellow) (PDB entry 1QGH) (Ilari *et al.*, 2000). Each color in (a) represents one subunit, while each color in (b) represents helices and loops.

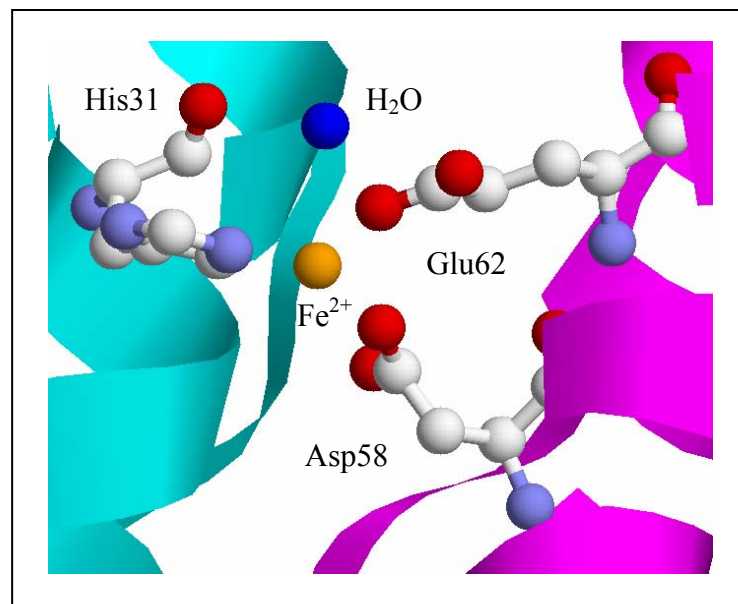


Figure 1.4: The iron binding residues (CPK ball and stick display) of *Listeria Dps* are His31, Asp58, Glu62, and a water molecule (blue) with iron atom (yellow) (PDB entry 1QGH) (Ilari *et al.*, 2000).

Listeria Dps sequesters iron in three different reaction phases: iron binding to the ferroxidase centers, oxidation by dissolved oxygen, and mineralization to form a microcrystalline structure (Su *et al.*, 2005). The overall process of iron deposition and detoxification by *Listeria* Dps is described by the following equations.

For ferroxidation,

- 1) Fe^{2+} binding to each of the 12 sites of *LiDps*: $\text{Fe}^{2+} + \text{Dps}^Z \rightarrow [(\text{Fe}^{2+})\text{-Dps}]^{Z+1} + \text{H}^+$
- 2) Fe^{2+} oxidation/hydrolysis: $[(\text{Fe}^{2+})\text{-Dps}]^{Z+1} + \text{Fe}^{2+} + \text{H}_2\text{O}_2 \rightarrow [(\text{Fe}^{3+})_2(\text{O})_2\text{-Dps}]^{Z+1} + 2\text{H}^+$.

For mineralization,

- 1) Fe^{2+} oxidation/hydrolysis: $2\text{Fe}^{2+} + \text{H}_2\text{O}_2 + 2\text{H}_2\text{O} \rightarrow 2\text{Fe}(\text{O})\text{OH}_{(\text{core})} + 4\text{H}^+$.

From the mineralization, it has been shown that H_2O_2 , an efficient oxidant, is rapidly used in the ferroxidase center of Dps, which simultaneously eliminates the two components of the Fenton reaction ($\text{Fe}(\text{II})$ and H_2O_2) that contribute hydroxide radicals. Upon site-directed mutation of the iron binding site in *L. innocua* Dps, it was found that this iron storage protein is mainly required for hydrogen peroxide detoxification and not for iron uptake (Ilari *et al.*, 2005).

Ferritin

Ferritins (FTs) are found in organisms as diverse as bacteria, fungi, plants and vertebrates. Their wide distribution among living species implies a fundamental and ancient role in iron metabolism. The structure of FT, which has been widely studied, is a 24-identical subunit protein with a molecular weight of ~480 kDa and forms a rhombic dodecahedral

protein shell that encloses up to 4500 iron atoms in an oxide/hydroxide/phosphate core (Harrison and Arosio 1996; Theil, 1987; Stillman *et al.*, 2001; Liu and Theil, 2005) (Figure 1.5a). The outside diameter of the protein is 12–13 nm and the internal cavity diameter is 7–8 nm. Each subunit consists of a four-helix bundle (A-D) and a fifth shorter helix (E) (Figure 1.5b) forming a cylinder that packs in a hollow shell of 432 (cubic) symmetry. Mammalian FT consists of H- and L-chains (heavy- and light-chains, respectively), which are encoded on different chromosomes. These H- and L-chains consist of 182 and 174 amino acids, respectively and share approximately 54% amino acid homology. This protein shell has eight hydrophilic channels along its three-fold axes, six hydrophobic channels along its four-fold axes, 12 grooved structures on its interior along two-fold axes, and an intrasubunit ferroxidase site located between the four helices of the H subunits. Each H-chain subunit has a ferroxidase center formed by seven amino acid residues, while the L-chain confers nucleation sites for iron binding (Chasteen, 1998; Harrison *et al.*, 1998). The FT ferroxidase center contains di-iron binding sites called site A, which uses nitrogen from a histidine residue and carboxyl group from acid residues as iron coordinating ligands, and site B where the metal is coordinated only by means of carboxyl group (Treffry *et al.*, 1997) (Figure 1.6). The bound iron atoms are separated by 3 Å but are connected by an oxo-bridge of a carboxyl group. The residues at this site are highly conserved and act as ligands for the binding of two ferrous ions, the first step in the iron uptake process. The bound ferrous ion pair is subsequently oxidized by O₂ which results in the formation of an oxo-bridged di-ferric intermediate. The ferric iron thus forms and migrates to the central cavity where either a ferrihydrite core is formed, or an amorphous ferric phosphate core builds up, depending on whether phosphate is present (as is the case *in vivo*) (Mann *et al.*, 1987). It was also found that the rate of Fe(II) oxidation was maximal for

additions of two Fe(II) atoms/subunit, and modification of site A ligands results in slow iron binding and slow oxidation, while modification at site B does not prevent Fe(II) binding at site A but greatly reduces the oxidation rate (Treffry *et al.*, 1997). Iron uptake is more efficient in the presence of L/H heteropolymers of mammalian FT than with either of the homopolymers. The H-chain facilitates ferric ion formation, and the L-chain facilitates the mineralization of ferric ion in the cavity. In general, H-rich FTs are characteristic of brain and heart tissues having low iron content when compared with that of L-rich FTs, which are found in typical iron-storage organs such as liver and spleen (Carrondo, 2003). Amphibian red cells contain three types of chain, H, L and M (medium), which can form heteropolymers. When iron is needed by the cell, stored iron can be mobilized from FT by reduction of the ferric ion in the core. This is followed by chelation of Fe(II) and removal of the ferrous ion. FT can serve as a source of iron for “housekeeping” purposes, including acting as a source of iron for enzymatic active sites, other protein prosthetic groups (i.e. [Fe-S] cluster), and as a mechanism to detoxify excess intracellular iron to prevent oxidative damage.

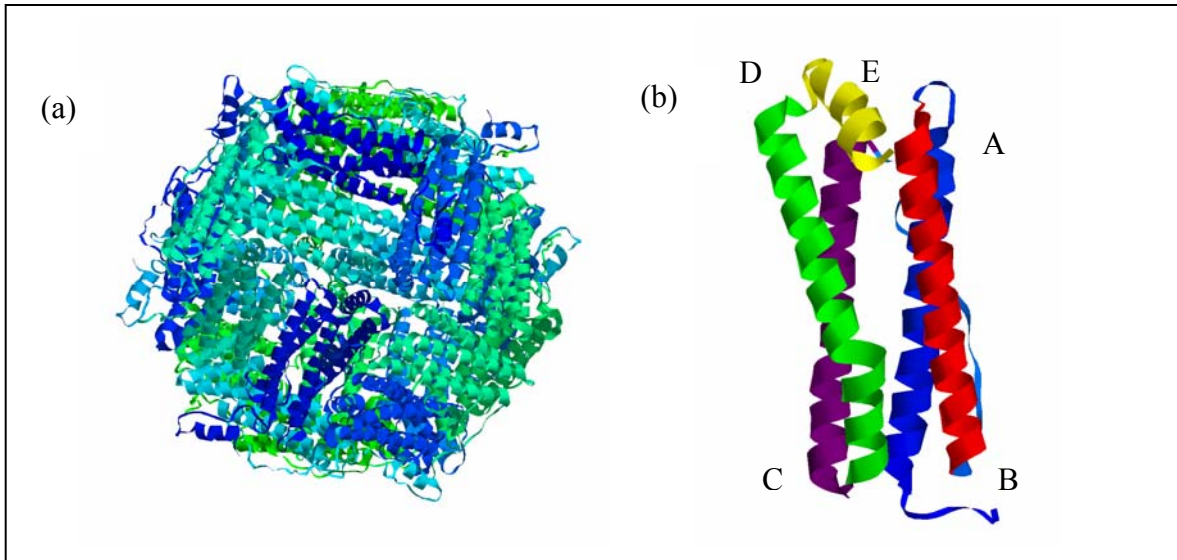


Figure 1.5: The ribbon diagrams represent the overall structures of *Trichoplusia Ni* secreted FT (PDB entry 1Z60) (Hamburger *et al.*, 2005) (a) and one subunit structure of human mitochondria FT, which shows helix A (blue), helix B (red), helix C (purple), helix D (green), and helix E (yellow) (PDB entry 1R03) (Langlois d'Estaintot *et al.*, 2004) (b).

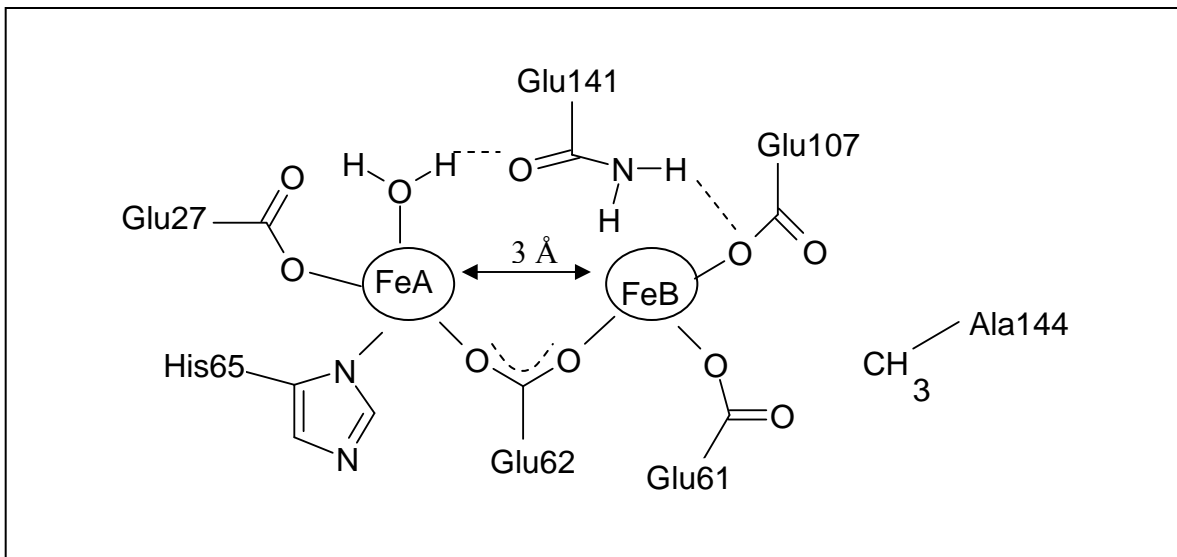


Figure 1.6: The di-iron binding site of the human FT (H-chain) contains Glu27, Tyr34, Glu61, Glu62, His65, Glu107, and Glu141 as iron binding residues (adapted from Treffry *et al.*, 1997).

Bacterioferritin

The iron-storage protein bacterioferritin (bFT) has been isolated from many organisms i.e. *Desulfovibrio desulfuricans* (Romão *et al.*, 2000b), *Escherichia coli* (Yariv *et al.*, 1981), and *Helicobacter pylori* (Evans Jr. *et al.*, 1995). It was found that the production of hydroxyl radicals from the *in vitro* oxidation of ferrous ion by H₂O₂ was greatly decreased when bFT was present, and this process did not lead to the production of a hydroxyl radical as occurs in the Fenton reaction (Bou-Abdallah *et al.*, 2002). In this thesis, *Escherichia coli* bFT will be focused upon and discussed in more detail in the introduction to the *Escherichia coli* bacterioferritin section.

Unlike mammalian or bacterial FT, bFT contains a cytochrome *b* component (heme group) (Yariv *et al.*, 1981). In early studies, there was some evidence indicating that bFT forms a protein family that was distinct from FT. In a study of *Azotobacter chroococcum* bFT, it was found that antibodies directed against bFT did not cross-react with human and horse FT, but partially cross reacted with plant FT purified from lentil seeds (phytoferritin) (Chen and Crichton, 1982). Similar results were found based on research of the immunological properties of *Escherichia coli*, *Pseudomonas aeruginosa*, and *Azotobacter vinelandii* bFT when compared with FT from plants and animals (Andrews *et al.*, 1991a). Besides, the prediction of preliminary structure based on N-terminal amino acid analysis combined with chemical modification of *Escherichia coli* bFT showed no homology between FT and bFT (Tsugita and Yariv, 1985). Despite their low sequence similarity (~23% identity between *Escherichia coli* bFT and horse spleen FT amino acid residues) (Figure 1.7), the complete sequence of *Escherichia coli* bFT, the conservation of ferroxidase centre residues, and X-ray crystallographic results do indicate evolutionary relatedness between bFT and FT. Both

proteins are similar in molecular weight, subunit weight, amino acid composition, isoelectric point (pI), size, and shape (Andrews *et al.*, 1989b; Andrews *et al.*, 1991b; Lawson *et al.*, 1991; Frolow *et al.*, 1994; Dautant *et al.*, 1998). Sequence alignment and model-building studies have also shown that FT and bFT have similar subunit conformations and quaternary structure (Grossman *et al.*, 1992; Cheesman *et al.*, 1993). X-ray crystallography of bFT has also been studied recently for *Azotobacter vinelandii* (Liu *et al.*, 2004), *Desulfovibrio desulfuricans* (Macedo *et al.*, 2003), *Escherichia coli* (Frolow *et al.*, 1994; Dautant *et al.*, 1998), and *Rhodobacter capsulatus* (Cobessi *et al.*, 2002) to gain more knowledge of bFT structural and functional properties.

While *E. coli* bFT is the most frequently investigated study case currently, bFT from *A. vinelandii* had been studied previously and focused on structural and magnetic properties of the iron core (Stiefel and Watt, 1979; Mann *et al.*, 1987). It was found that *A. vinelandii* bFT consists of two non-identical subunits (Harker and Wullstein, 1985) similar to bFTs from *P. aeruginosa* and *P. putida* (Moore *et al.*, 1986; al-Massad *et al.*, 1992; Miller *et al.*, 2000), while most bFTs from other bacteria such as *E. coli* consist of only one type of subunit.

The maximum number of heme groups (heme IX) that can bind in each organism is varied. There are normally 12 heme groups per 24 subunits in bFT from *A. vinelandii* (Stiefel and Watt, 1979) and *E. coli* (Smith *et al.*, 1988; Yariv *et al.*, 1981). These proteins will not bind additional heme (Smith *et al.*, 1989). However, it has also been found that there are 5-9 hemes per 24 subunits in *P. aeruginosa* (Moore *et al.*, 1986) with the maximum binding of 24 heme groups per 24 subunits (Kadir and Moore, 1990). The difference in maximum heme binding suggests different protein shell configurations. This may result from half-of-sites reactivity of *A. vinelandii* bFT with negative cooperativity preventing heme binding at 12 sites

(Moore *et al.*, 1992a). It was also found that not all bFTs contain heme IX (Figure 1.8). The bFT in *D. desulfuricans* contains heme III (Figure 1.8) (Romão *et al.*, 2000a; Coelho *et al.*, 2001).

```

H-chain FT      ATGACGACCGCGTTCCCTCGCAGGTGCGCCAGAACTACCACCAGGAC-TCGGAGGCCGC
L-chain FT      ATGA-----GCTCCC-----AGATTGTCAGAAATTAT-TCTACTGAAAGTGGAGGCCGC
bFT            ATGA--AAGGTGATACT-----AAAGTTATA---AATTATCTCAACAAA-CTGTTGG--GA
                ***          * * *          * *          * * * * *          * * * *
H-chain FT      CATCAACC-GTCAGA-TCAACCTGGAGCTCCACGCCTCC-TATGTGTACCTGTCC---AT
L-chain FT      CGTCAACC-GCCTGG-TCAACCTGTACCTGCGGGCCTCC-TACACCTACCTCTCT---CT
bFT            AATGAGCTTGTGCGCAATCAATCAGTACTTTC-----TCCATGCCCGAATGTTTAAAAACT
                * * * * *          * * * * *          * * * * *          * * * * *
H-chain FT      GTCTTTCTATTTTGATCGCGATGATGTGGCTTTGAAGAACTT-TGCCAAATATTTTCTTC
L-chain FT      GGGCTTCTATTTTCGACCGCGACGATGTGGCTCTGGAGGGCGTATGCCAC-----TTCTTC
bFT            GGGGT-----CTCAAACGTCTCAATGA---TGTGGAG----TAT-----C
                * *          * * * *          * * *          * * * *          * *          *
H-chain FT      ACCAATCTCATG-AGGAGAGG---GAACATGCTGAGAACT-GATGAAG--CTGCAGAAC
L-chain FT      CGCGAGTTGGCGGAGGAGAAGCGCGAGGGTGCCGAGCGTCT-CTTGAAG--ATGCAAAAC
bFT            ATGAATCCATTG-ATGAGATG---AAACACGCCGATCGTTATATTGAGCGCATTTCTTTT
                *          * * * * *          *          * * * *          * * *          * *
H-chain FT      CAACGAGGTGGCCG-GATCTTCC-----TT-CAGGACATCAAGAAACCAGACCAGGATGAC
L-chain FT      CAGCGCGGCGGCCGCGTCT-CT----TC-CAGGACTTGCAGAAGCCGTCCCAGGATGAA
bFT            CTGGAAGG-----TCTTCCAAACTTACAGGACCTGGGCAAACCTG-AACA-----
                *          **          * * * *          * * * * *          * * *          **
H-chain FT      TGGGAGAATGGGCTGAAGGCAATGGAGTGTGCATT-ACACTTGGAAAAAAATGTGAATGA
L-chain FT      TGGGGTACAACCCAGACGCCATGAAAGCCGCCAT-TGTCCTGGAGAAGAGCCTGAACCA
bFT            TTGGTGAAGATGTTGA-GGAAATG----CTGCGTTCTGATCTGGCACTTGAGCTGGAT--
                * * * *          * * * *          * * *          * * *          * * *
H-chain FT      GTCACTATTGGAAGTGCACA---AACTGGCCACTGACAAAAATGACCCCACTTGTGTGA
L-chain FT      GGCCCTTTTGGATCTGCATG---CCCTGGGTTCTGCCCAGGCAGACCCCACTCTCTGTGA
bFT            GCGCGGAA-GAATTTGCGTGAGGCAATTGGTTATGCCGATAGCGT-----TCA-TGA
                * * *          * * * *          * *          * * * *          *          * * *
H-chain FT      CTTCTCGAGACTCATTACCTGAATGAGCAGGTGAAAGC---CATCAAAGAATTGGGTGA
L-chain FT      CTTCTTGGAGAGCCACTTCTTAGACGAGGAGGTGAAACT---CATCAAGAAGATGGGCGA
bFT            TTACGTC---AGCCGCG-----ATATGATGATA-GAAATTTTGCCTGATGAAGAAGG----
                * * *          * *          * * *          * * *          * * *          * *
H-chain FT      CCACGT-AACCAACCTGCGCAGGATGGG----GGCCCCGAATCTGG-CATGGCAGAGTA
L-chain FT      CCATCT-GACCAACATCCAGAGGCTCGT----TGGCTCCAAGCTGG-GCTGGGCGAGTA
bFT            CCATATCGACTGGCTGGAAACGGAACCTTGATCTGATTCAGAAGATGGGCTGCAAAATTA
                ***          * * *          *          *          * * * *          * *          * *
H-chain FT      TCTCTTTGACAAGCACACCCTGGGAGAGTGTGACGAGAGCTAA
L-chain FT      TCTCTTTGAAAGGCTCACTCTC-AA--GC---ACGA---CTAA
bFT            TCTG-----CAAGCACAGA-TCC-----GCGAAGAAGGTTGA
                ***          * * * *          *          * * *          * *

```

Figure 1.7: The multiple alignment of horse spleen ferritin (H-chain) sequence (Orino *et al.*, 2005), horse spleen ferritin (L-chain) sequence (Takeda *et al.*, 1993), and *E. coli* bacterioferritin sequence (Andrews *et al.*, 1989b) using CLUSTAL FORMAT for T-COFFEE online program (<http://www.tcoffee.org>) (Notredame *et al.*, 2000).

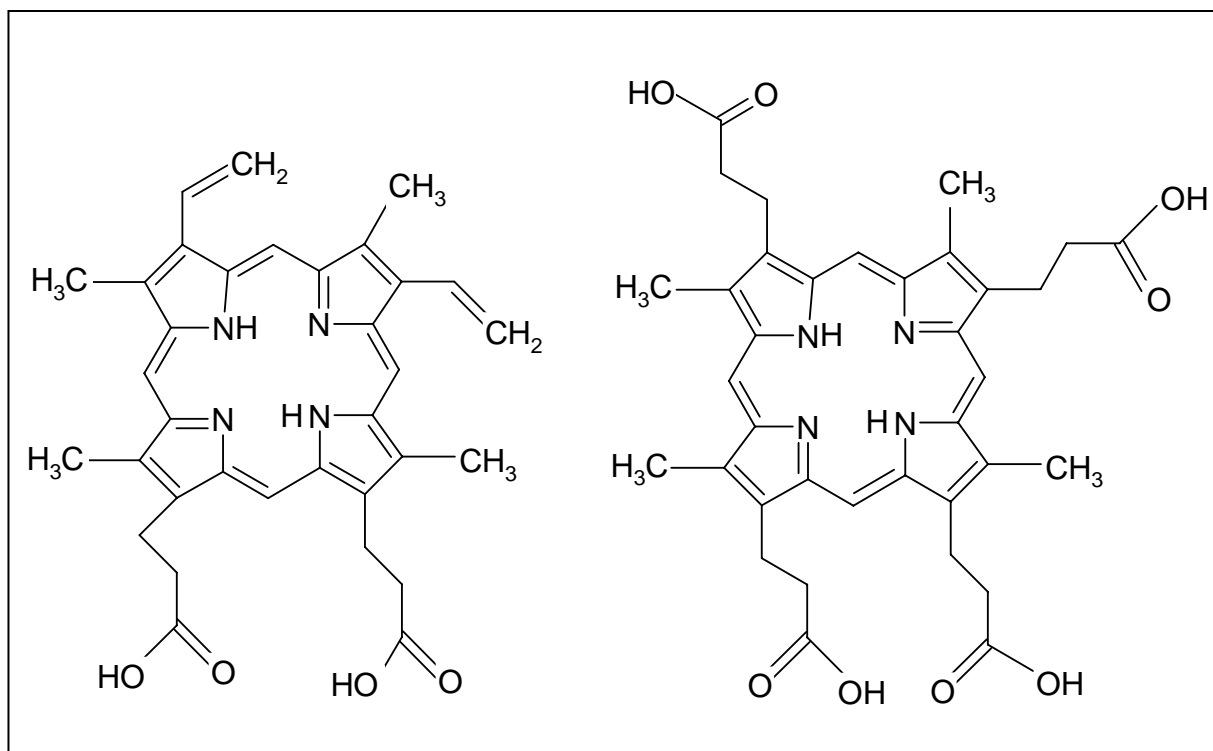


Figure 1.8: The chemical structures of protoporphyrin IX (left) and coproporphyrin III (right) (Romão *et al.*, 2000a).

Applications of Iron Storage Proteins

In several species, the utilization of mutants lacking the ability to synthesize FT-like proteins has yielded information concerning the potential role that these biomolecules play in bacteria. The data obtained by utilizing mutants indicate that the cellular effect of the bacterial FT-like proteins is not consistent, differing from species to species (Table 1.1). These proteins have multifaceted functions. Dps, for example, does not always bind DNA as protective co-crystalline Dps-DNA complexes. In addition, bacterial FT or bFT do not always protect the organism against oxidative stress, nor do these compounds necessarily serve as a source of iron during iron deprivation. In a few cases, FT-like proteins serve to protect the bacterial cells against iron overload.

Table 1.1: Cellular effects of ferritin-like proteins in select bacteria (Smith, 2004)

Bacterial species	Bacterioferritin	Bacterial ferritin	Dodecameric ferritin (Dps-like)
<i>Agrobacterium tumifaciens</i>			<ol style="list-style-type: none"> 1. Binds iron 2. Does not bind DNA 3. Protects against H₂O₂
<i>Bacillus anthracis</i>			<ol style="list-style-type: none"> 1. Binds iron 2. Does not binds DNA 3. Protects against iron overload
<i>Brucella melitensis</i>	<ol style="list-style-type: none"> 1. Binds iron 2. Does not protect against paraquat or H₂O₂ in human hosts 3. Induces a Th-1 immune response in human hosts 		
<i>Campylobacter jejuni</i>		<ol style="list-style-type: none"> 1. Binds iron 2. Serves as an iron source 3. Protects against paraquat and H₂O₂ 	<ol style="list-style-type: none"> 1. Binds iron 2. Does not bind DNA 3. Protects against H₂O₂
<i>Escherichia coli</i>	<ol style="list-style-type: none"> 1. Binds iron 	<ol style="list-style-type: none"> 1. Binds iron 2. Serves as an iron source 3. Does not protect against oxidative stress compounds 	<ol style="list-style-type: none"> 1. Binds iron 2. Binds DNA 3. Protects against H₂O₂ 4. Protects DNA against cleavage by H₂O₂:Fe²⁺

Table 1.1: Cellular effects of ferritin-like proteins in select bacteria (Smith, 2004) (cont.)

Bacterial species	Bacterioferritin	Bacterial ferritin	Dodecameric ferritin (Dps-like)
<i>Helicobacter pylori</i>	<ol style="list-style-type: none"> 1. Binds iron 2. Serves as an iron source 3. Protects against H₂O₂ and paraquat 	<ol style="list-style-type: none"> 1. Binds iron 2. Protects against Fe²⁺, Cu²⁺, and Mn²⁺ overload 3. Does not serve as an iron source 4. Does not protect against paraquat 5. Necessary for colonization of gastric mucosa 	<ol style="list-style-type: none"> 1. Binds iron 2. Binds DNA 3. Activates neutrophils and monocytes 4. Protects against oxygen toxicity 5. Protection against hydroperoxides or paraquat (controversial)
<i>Mycobacterium smegmatis</i>			<ol style="list-style-type: none"> 1. Binds iron 2. Binds DNA 3. Protects DNA from H₂O₂:Fe²⁺ and DNaseI cleavage
<i>Neisseria gonorrhoeae</i>	<ol style="list-style-type: none"> 1. Binds iron 2. Serves as an iron source 3. Protects against H₂O₂ and paraquat 		
<i>Porphyromonas gingivalis</i>		<ol style="list-style-type: none"> 1. Binds iron 2. Serves as an iron source 3. Does not protect against H₂O₂ or cumene hydroperoxide 	<ol style="list-style-type: none"> 1. Binds iron 2. Binds DNA 3. Protects against H₂O₂ 4. Does not appear to protect DNA against DNA inhibitors 5. Does not serve as a source of iron 6. Necessary for viability of bacteria in tissue culture cells

Table 1.1: Cellular effects of ferritin-like proteins in select bacteria (Smith, 2004) (cont.)

Bacterial species	Bacterioferritin	Bacterial ferritin	Dodecameric ferritin (Dps-like)
<i>Pseudomonas aeruginosa</i>	<ol style="list-style-type: none"> 1. Binds iron 2. Protects against H₂O₂ 3. Necessary for maximum catalase-A activity 		
<i>Pseudomonas putida</i>	<ol style="list-style-type: none"> 1. Binds iron 2. Does not serve as an iron source 3. Not necessary for catalase-A activity 4. Not necessary for plant root colonization 		
<i>Streptococcus mutans</i>			<ol style="list-style-type: none"> 1. Binds iron 2. Does not bind DNA 3. Protects against O₂ and H₂O₂
<i>Streptococcus suis</i>			<ol style="list-style-type: none"> 1. Binds iron 2. Does not bind DNA 3. Protects against H₂O₂

1.1.4: Regulatory Role of Iron

The product of the *fur* gene, the Fur protein (ferric uptake regulator), acts as an intracellular iron regulator (Andrews *et al.*, 2003; Massé and Arguin, 2005) (Figure 1.9). After intracellular iron has reached acceptable levels, the activated Fur protein (with ferrous ion) binds to the promoters of most iron acquisition genes and represses their transcription. The Fur-Fe²⁺ complex normally binds between the -35 and -10 sites at the promoters of the *fur* genes. Fur-binding sites were originally found to conform to a 19-bp palindromic consensus sequence known as the ‘iron box’ or ‘Fur box’: 5’-GATAATGAT-3’ (Escolar *et al.*, 1998), while an alternative consensus sequence 5’-TGATAATNATTATCA-3’ has also been proposed lately (Baichoo and Helmann, 2002). The Fur-Fe²⁺ complex also activates the genes for bacterial FT and/or bFT synthesis leading to the removal of excess and potentially harmful ferrous ions from the cytosol, where Fe²⁺ is oxidized to Fe³⁺ and is stored in the protein core (Ratledge and Dover, 2000). Besides, Fur also represses a small sRNA named RyhB, which facilitates degradation of the mRNAs responsible for the synthesis of several iron-utilizing proteins (*sdhCDAB*, *acnA*, *fumA*, *ftnA*, *bfr*, and *sodB*) and positively regulated by Fur (Massé and Gottesman, 2002). RyhB found in *E. coli* (PrrF1 and PrrF2 in *P. aeruginosa* or Cth2 in *S. cerevisiae*) actively stimulates degradation of its mRNA targets by recruiting the RNA degradosome, a complex formed of RNaseE, polynucleotide phosphorylase, enolase and an RNA helicase (Massé and Gottesman, 2002; Wilderman *et al.*, 2004; Puig *et al.*, 2005). RNaseE degrades both RyhB and the mRNA simultaneously once they have paired. This coupled degradation provides an intrinsic mechanism to shut down RyhB. Indeed, when RyhB expression is stopped under iron-replete conditions, the sRNA level drops because of rapid turnover. Destruction of RhyB quickly restores the expression of iron-using proteins, which

sequester iron as soon as it becomes available. In contrast, under conditions of iron deprivation, Fur inactivation enables expression of iron-acquisition genes and RhyB, which represses iron-using proteins. There are several advantages that are intrinsic to the mechanism of sRNAs. The sRNAs do not require new protein synthesis and, thus, activity is fast and efficient in terms of cellular energy use. Although several sRNAs alter translation or stability of their mRNA targets, they do not stop their transcription; therefore, when the sRNA disappears, mRNA expression swiftly resumes. Besides, sRNAs such as RyhB can be quickly turned off when their expression is specifically shut down.

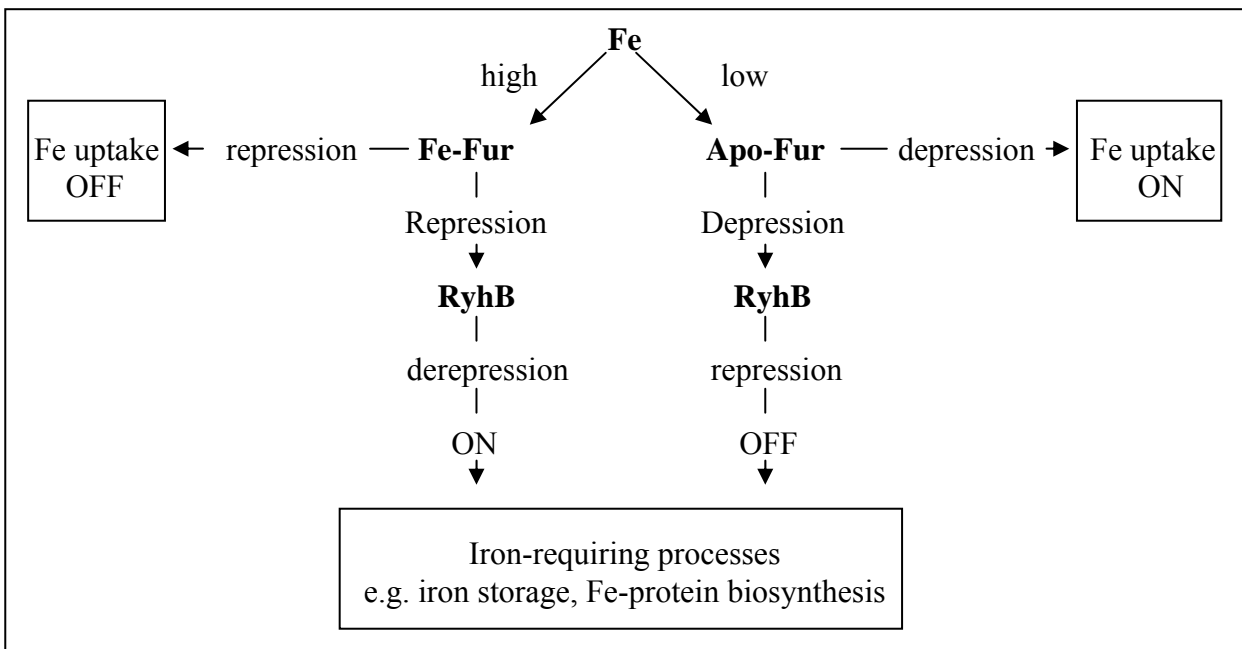


Figure 1.9: Roles of Fur and RyhB in mediating Fe-dependent gene regulation in *E. coli* (Andrews *et al.*, 2003). Fur regulates the cellular iron uptake of the cell and *ryhB* gene expression, and RyhB modulates the sequestration of the metal by protein.

1.2: Escherichia coli Bacterioferritin

1.2.1: Discovery of Bacterioferritin

Bacterioferritin was first isolated from *E. coli* whole cells based on its optical spectrum and was named cytochrome *b₁* (Keilin, 1934; Keilin and Harpley, 1941). Later this cytochrome *b₁* was isolated as a pure protein and was found to have similar optical properties as cytochrome *b₅₅₇* based on its three optical bands for the heme group (Deeb and Hager, 1964). It was also found that the pI of this protein is 4.6 (Bartsch *et al.*, 1971). In 1973, the protein isolated from *A. vinelandii* had been found to be a FT-like protein, which contained heme, and thus was classified as a haemoprotein (Bulen *et al.*, 1973). Later, a transmission electron micrograph showed that this haemoprotein with cytochrome *b₅₅₇*-like properties resembled FT in quaternary character (Stiefel and Watt, 1979). It was found that *E. coli* FT-like haemoprotein had absorption maxima at 417, 530, and 560 nm (Soret, β -, and α -bands, respectively), which were contributed by protohaem IX that was not present in FT (Yariv *et al.*, 1981). From this discovery, the FT-like haemoproteins of bacteria were called bacterioferritin to distinguish this protein from FT (Yariv *et al.*, 1981; Chen and Crichton, 1982). The redox potential, sodium dodecylsulfate polyacrylamide gel electrophoresis results (size), and X-ray crystallographic data also suggested the identity of bFT and cytochrome *b₁* (Yariv, 1983; Smith *et al.*, 1988). The partial sequence was first found by chemical modification and amino acid analysis (Tsugita and Yariv, 1985). The complete sequence of *E. coli* –K12 bFT (Figure 1.10) was derived from the nucleotide sequence of the cloned gene, in which it was comprised of 158 amino acid residues with a subunit MW of 18,495 Da (Andrews *et al.*, 1989b).

1	mkgdtkviny	lnkllgnelv	ainqyflhar	mfknwglkrl	ndveyhesid	emkhadryie
61	rilfleglpn	lqdlgklnig	edveemlrds	laleldgakn	lreaigyads	vhdysrdmm
121	ieilrdeegh	idwleteldl	iqkmglqnyl	qaqireeg		

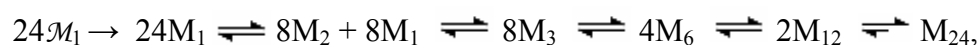
Figure 1.10: Amino acid sequence of *E. coli* bFT (Andrews *et al.*, 1989b).

Escherichia coli contains at least four genes that may be involved in iron storage: *bfd* that encodes the 64-residue [2Fe-2S]-containing bacterioferritin-associated ferredoxin (Bfd), *bfr* that encodes bacterioferritin, *ftnA* which encodes a ferritin (FtnA), and *ftnB* that encodes a ferritin-like protein (FtnB) (Izuhara *et al.*, 1991; Abdul-Tehrani *et al.*, 1999). Only Bfd, FtnA, and bFT have been characterized. Whether FtnB functions as an iron storage protein is uncertain because its primary structure suggests that it lacks an active ferroxidase center (Abdul-Tehrani *et al.*, 1999). FtnA takes up iron approximately three-fold more rapidly than does bFT *in vitro*, but bFT appears to accumulate more iron per molecule than FtnA *in vivo* (Andrews *et al.*, 1993; Hudson *et al.*, 1993). Thus, it has been speculated that FtnA and bFT play roles in short- and long-term iron storage, respectively, like the mammalian H- and L-subunit-rich FTs (Andrews *et al.*, 1993).

1.2.2: Overall Structure

Before the X-ray structure of bFT was determined, there were several studies on predicting its structure. First in 1981, a single crystal of *E. coli* bFT (Figure 1.11a) and its X-ray precession photographs suggested a 432 point-group symmetry and the formation of 24 identical subunits (Yariv *et al.*, 1981). The transmission electron micrograph showed an inner core of 6 nm diameter and an outer shell of 9.5 nm diameter (Figure 1.11b) (Yariv *et al.*, 1981). The primary structure determined by amino acid analysis combined with chemical

modification and partial sequence analysis suggested that the formation of 24 subunits was from one kind of polypeptide chain (Tsugita and Yariv, 1985). After the determination of its complete amino acid sequence, its secondary structure was predicted to possess a high α -helical content consistent with a 4-helix-bundle conformation (Figure 1.12), and a tetracosamer bFT contained 12 heme moieties (Andrews *et al.*, 1989a). The study of self-assembly had shown that the formation of tetracosamer possibly involved structural intermediates as follows (Gerl and Jaenicke, 1988),



where \mathcal{M}_1 is an unfolded subunit, M_i is assembly intermediates with i subunits, and M_{24} is native tetracosamer. Once the X-ray crystallographic data of four crystals was achieved, it indicated that the molecule had a diameter in the range of 119 to 128 Å (Smith *et al.*, 1989). Later, structural comparisons between bFT and a related protein cytochrome *c* (Moore, 1991), structural modeling by X-ray precession photographs of the tetragonal crystals (Smith, 1991), structural prediction by sequence alignments (Grossman *et al.*, 1992), model-building studies (Cheesman *et al.*, 1993), and low resolution X-ray crystallography (Frolova *et al.*, 1993) confirmed the size and shape of bFT. However, when the X-ray crystallographic results with higher resolution were finally achieved (Frolova *et al.*, 1994; Dautant *et al.*, 1998), it was shown that bFT is a slightly distorted spherical shell with an inner cavity diameter of ~80 Å (8 nm) and an outer diameter of 120 Å (12 nm) (Figure 1.12). When bFT forms a cage-like structure, the C-terminus of each subunit is pointing towards the core, while the N-terminus is pointing outward (Figure 1.13). The monomeric *E. coli* bFT contains A (Thr5-Trp35), B (Lys38-Phe64), C (Val83-Val111), D (Tyr114-Met144) helices, which form the usual square left-handed bundle, and helix E (Leu146-Gln151) at the C-terminus that lies almost

perpendicular (78°) to the bundle axis (Figure 1.14). Each heme is bound in a pocket formed by the interface between a pair of symmetry-related subunits, while the di-metal binding sites are located inside a monomer. AB is antiparallel to the CD helices with loop L (Leu65-Asp82) connecting helix B and C. The connection between the L loop and helix C adopts a random coil conformation. Helix E provides stable interactions at four-fold symmetry axes. Two-subunit is stabilized by four hydrogen bonds between O and N atoms of the amide of Gln72 on one monomer and N (Leu77) and O (Gly75) of another parallel monomer, respectively (Figure 1.15a). The inner surface has a salt-bridge between Arg30 and Asp56, and Glu60, although Glu60 is not conserved in all bFTs (Figure 1.16b). Additional intersubunit stability is two salt-bridges that are formed by Glu128 and Glu135 with Arg61 and N-terminal amine of the perpendicular subunit, respectively (Figure 1.16). The amino acid Glu128 also forms a salt bridge with Arg102 of the same subunit linking the C and D helices (Figure 1.16). While, the interaction between intersubunits is hydrophobic, the inner surface of the sphere is hydrophilic from residues contributed by the B and D helices.

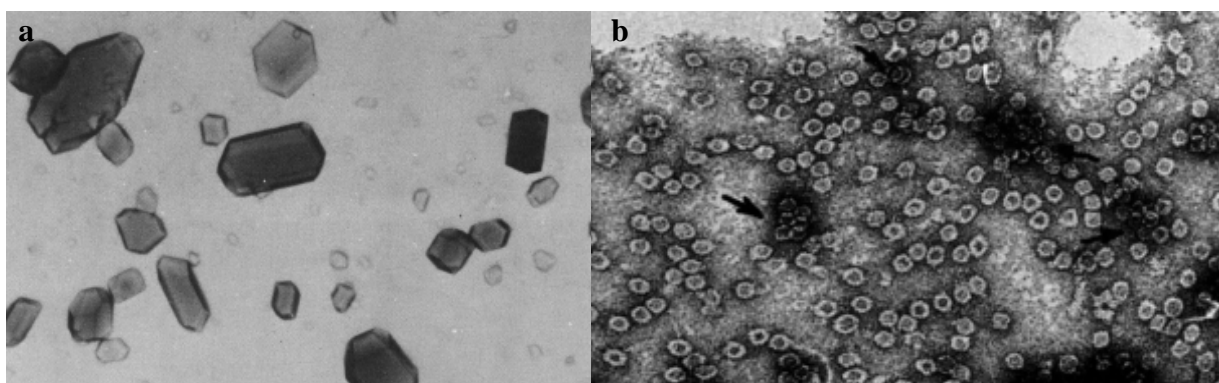


Figure 1.11: Single crystals (a) and the electron micrograph of *E. coli* bFT (b) (adapted from Yariv *et al.*, 1981). The arrow indicates regular packing of the particles.

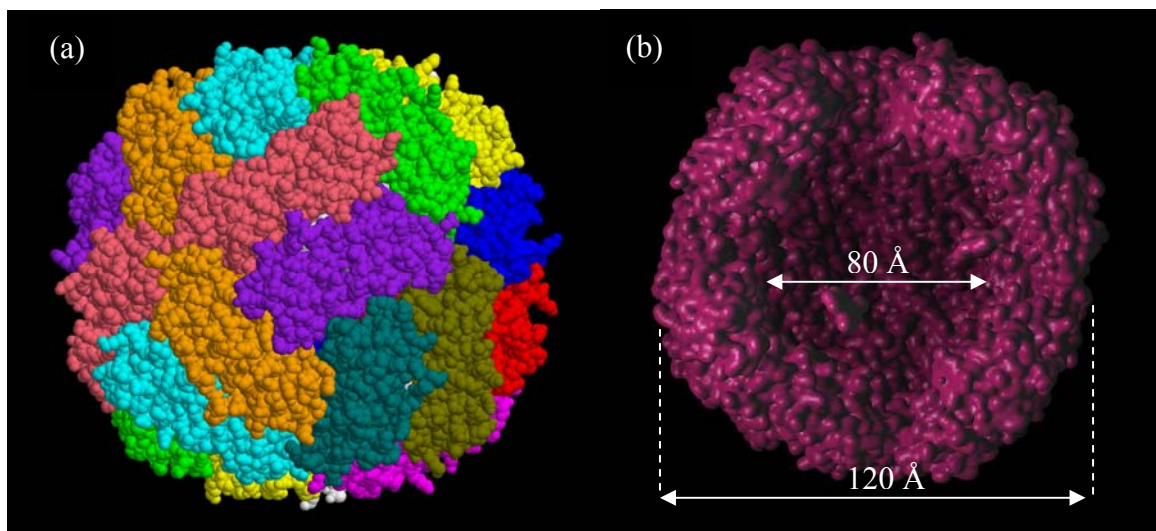


Figure 1.12: The space-filled structure of *E. coli* bFT where each color represents one subunit (a) and half-the-sphere structure that shows the size of the outer surface and the inner cavity (b) (PDB entry 1BCF) (Frolow *et al.*, 1994).

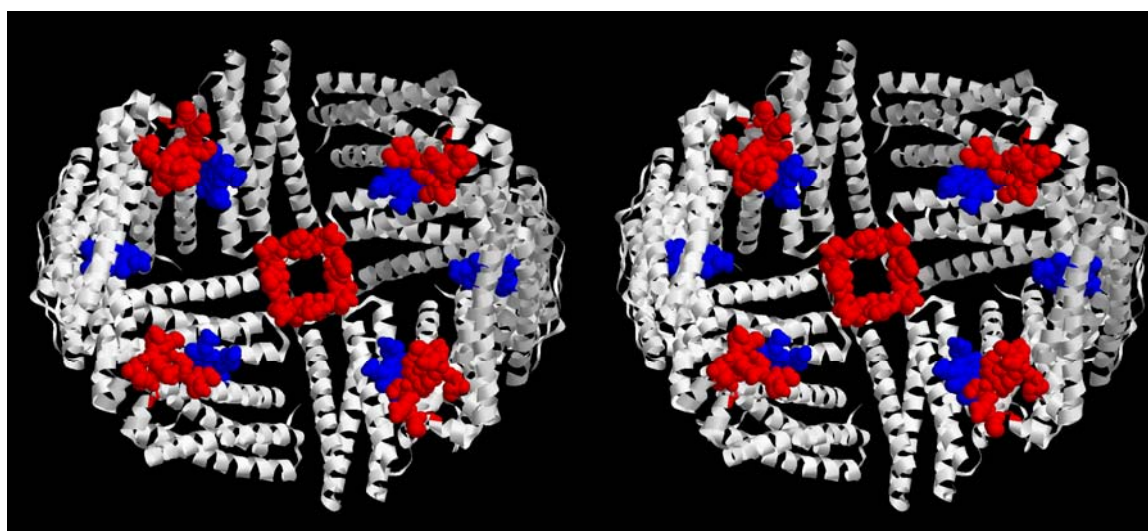


Figure 1.13: The cross eyed stereo view of a 12-subunit *E. coli* bFT represents the heme binding groups (blue) and the C-terminal end (red) that are pointing toward the cavity. The intact bFT is a 24-subunit that forms a completed spherical structure (PDB entry 1BCF) (Frolow *et al.*, 1994).

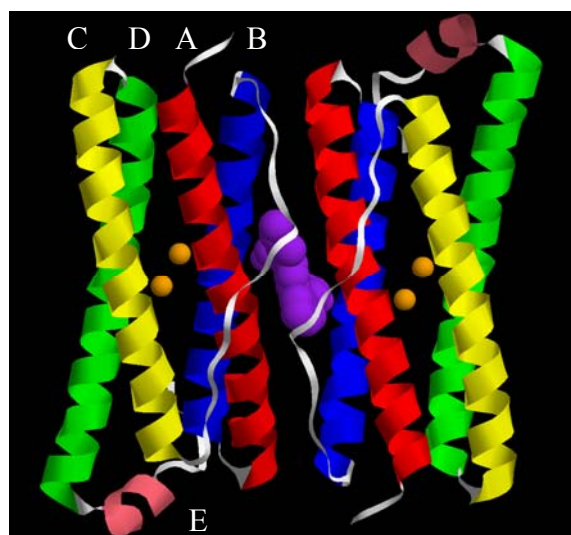


Figure 1.14: The ribbon diagram of two neighboring subunit of *E. coli* bFT showing the heme-binding site and ferroxidase center, where the heme group is colored in purple and two iron atoms are colored in orange. The helices in each subunit are labeled as A (red), B (blue), C (yellow), D (green), and E (pink) (PDB entry 1BCF) (Frolova *et al.*, 1994).

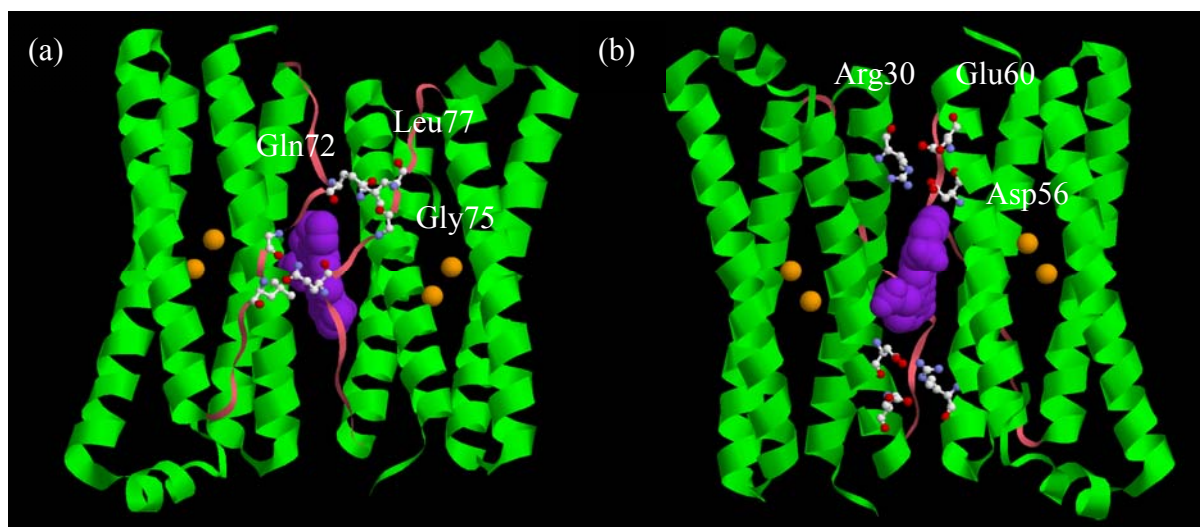


Figure 1.15: The ribbon diagram of two neighboring subunits of *E. coli* bFT (green) representing the residues (CPK ball and stick display) involved in intersubunit stability of two subunits of the *E. coli* bFT on (a) the outer surface and (b) the inner surface (PDB entry 1BCF) (Frolova *et al.*, 1994). The L loop is colored as pink, the heme group is colored as purple, and two iron atoms are colored as orange.

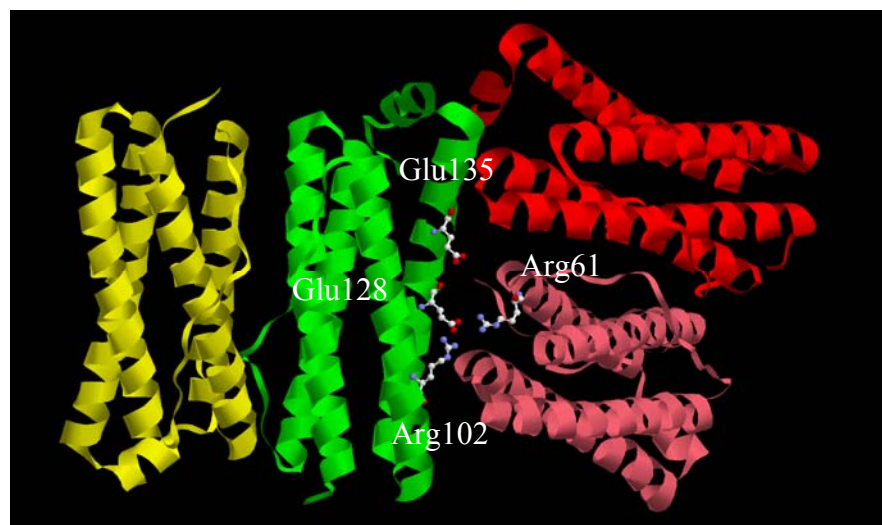


Figure 1.16: The ribbon diagram of four subunits of *E. coli* bFT showing the residues involved in intersubunit and intrasubunit stability (CPK ball and stick display), which are Arg61, Arg102, Glu128, and Glu135 (PDB entry 1BCF) (Frolow *et al.*, 1994).

1.2.3: Heme Binding Site

The absorption of the heme group was first observed when studying the isolated haemoprotein from *A. vinelandii* (Bulen *et al.*, 1973). The heme was found to be intrinsically bound (Stiefel and Watt, 1979). Electron paramagnetic resonance (e.p.r.) and near infrared magnetic circular dichroism (n.i.r.-m.c.d.) experiments combined with additional experiments using extended X-ray absorption fine structure (EXAFS) suggested a bis-methionine axial ligation of heme in *P. aeruginosa* and *A. vinelandii* bFT (Cheesman *et al.*, 1990; Cheesman *et al.*, 1992; George *et al.*, 1993). Based on preliminary modeling (Andrews *et al.*, 1991b) and e.p.r. and m.c.d. spectra combined with molecular modeling of the *E. coli* bFT (Moore *et al.*, 1992a; Cheesman *et al.*, 1993), two potential heme-binding sites were found; site I was an intra-subunit near the outer molecular surface with heme-iron ligands Met31 and Met86 (1 heme per 1 subunit), and site II was an inter-subunit near the cavity surface with ligands Met52 and Met52' from dyad-related neighbors (1 heme per 2 subunits). However, at that time, these

results did not have strongly supporting evidence because neither of these residues is absolutely conserved in the bFT family. Subsequently, multiple sequence alignments suggested that site I was a heme-binding pocket (Grossman *et al.*, 1992), however, low resolution crystallographic structural studies suggested that site II might be a heme site (Frolow *et al.*, 1993). Once the X-ray structure of the *E. coli* bFT was achieved (Frolow *et al.*, 1994; Dautant *et al.*, 1998), it was shown that site II was the correct heme site (Figure 1.17). This site has an approximate two fold-symmetry related set of bimetal centers. The iron of protoporphyrin IX has two axial sulfur ligands at 2.35 Å and from the iron with four nitrogen ligands at 1.97 Å. The distances between the heme Fe atom and the two non-heme metal atoms are 14.5 and 12.8 Å. The hydrophobic pocket, which encloses the heme, forms an indentation opening from the surface of the inner cavity and creeping along the hydrophobic interface between two subunits. The pocket is lined with residues Leu19, Ile22, Asn23, and Phe26 (A helix), Tyr45, Ile49, Met52, Lys53, Ala55, and Asp56 (B helix), Leu71 of the L loop, and the equivalent twofold-axis-related residues. The heme molecule is only accessible from the inside of the protein shell, where its two propionate groups protrude into the hydrophilic internal cavity, and is protected against the outside aqueous medium by the two symmetry-related L loops (Figure 1.18). Heme binding also allows some maintenance of the tertiary and quaternary structure, which might explain the limiting stoichiometry of one heme per 2 subunits (Grossman *et al.*, 1992).

The presence of the iron core has been shown to have no detectable effect on the electronic states on the placement of the heme group (Cheesman *et al.*, 1992). Heme-free bFT variants from *E. coli* take up iron *in vitro* at rates indistinguishable from those of the wild-type protein suggesting that heme is not required for iron uptake (Andrews *et al.*, 1995; Dautant *et*

al., 1998). This is reasonable because the heme iron does not undergo redox cycling when Fe(II) and dioxygen are the substrates for the iron loading of bFT. However, based on mutagenesis studies on the heme-binding site (Andrews *et al.*, 1995) and the study of heme binding to horse spleen FT (Kadir *et al.*, 1992), it has been found that the amount of iron incorporated into heme-free bFT *in vivo* is approximately four times higher than that of the wild-type bFT, which indicates that the heme group is involved in mediating release of iron from bFT by facilitating reduction of the iron core. In addition, it is also found that heme binding does not lead to dissociation of the 24-subunit in bFT (Kadir *et al.*, 1992).

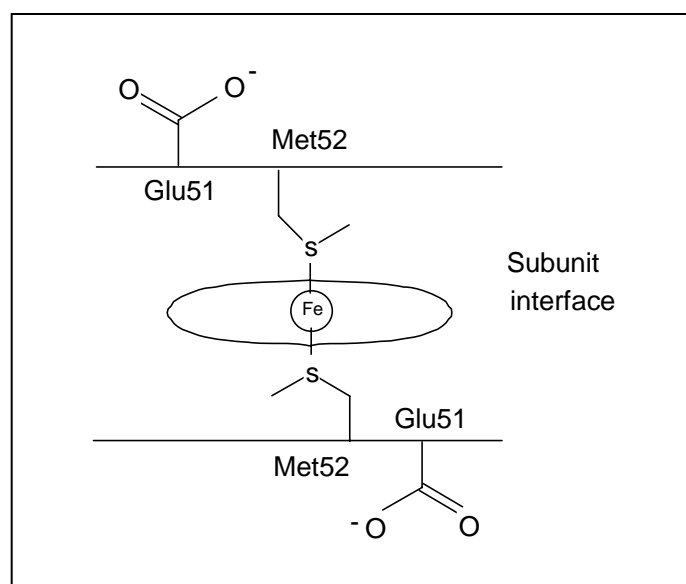


Figure 1.17: The schematic representation of the bFT heme-binding site, which lies between a two neighboring subunits interface shows the interaction of Met52 and Met52' with the heme-iron atom. These two Met residues are close to the Glu51 residue of the ferroxidase center (adapted from Keech *et al.*, 1997)

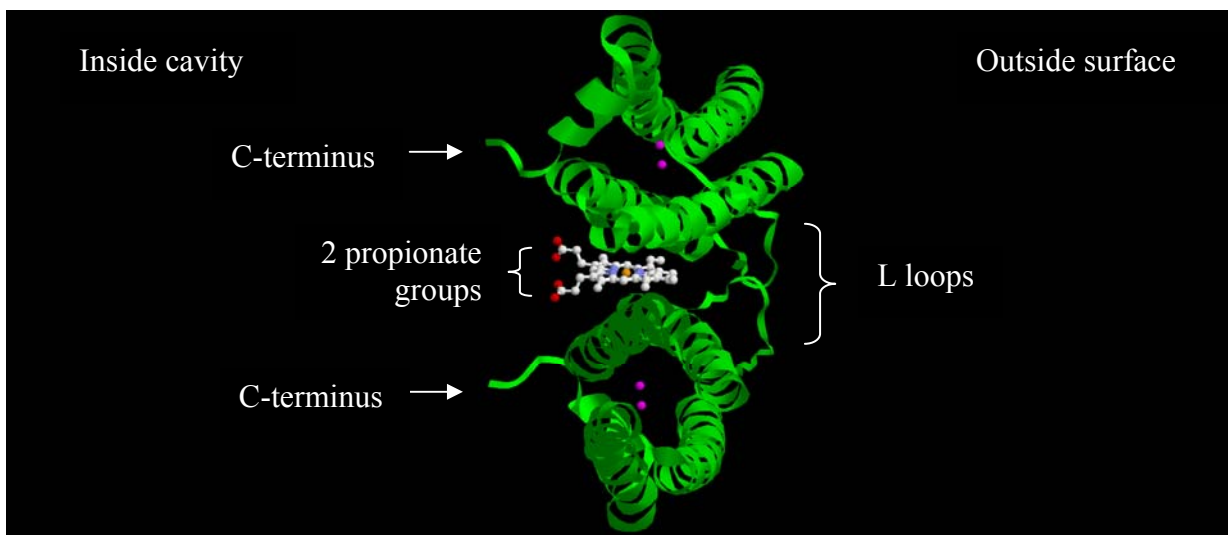


Figure 1.18: The ribbon diagram of two neighboring subunits of *E. coli* bFT (green) showing the two propionate groups of heme (CPK ball and stick display) that lies between this interface, two iron atoms (purple dots) at the ferroxidase center, L loops that protect the heme group from the aqueous medium, and the C-terminal end pointing toward the protein cavity (PDB entry 1BCF) (Frolow *et al.*, 1994).

1.2.4: Iron Core Formation

Studies of the iron core in bFT analyzed by Mössbauer spectroscopy (Matzanke *et al.*, 1989) in combination with e.p.r. and m.c.d. spectroscopies (Cheesman *et al.*, 1992) have shown some features of the core forms (magnetic ordering, anisotropy, and etc.) that differ from the iron core of FT. Sequence alignment (Grossman *et al.*, 1992), molecular modeling (Cheesman *et al.*, 1993), site-directed mutagenesis (Le Brun *et al.*, 1995), and predictions of the di-iron carboxylate protein based on structures and sequences of the related proteins (Nordlund and Eklund, 1995) have shown two potential iron-binding sites and have identified several iron binding residues. The conserved key amino acid residues in the ferroxidase centers of FT compared to bFT have suggested that bFT possesses a ferroxidase center similar to that of H-chain FTs (Andrews *et al.*, 1991b; Grossman *et al.*, 1992). Site-directed mutagenesis studies (Keech *et al.*, 1997) and X-ray crystallography (Frolow *et al.*, 1994;

Dautant *et al.*, 1998) have shown that the amino acids involved in coordination of the di-iron sites are residues Glu18, Glu51, His54, Glu94, Glu127 and His130, which interact with two non-heme iron atoms that are separated by 4.36 Å (Figure 1.19). Each metal ion is capped by the carboxylate moieties of Glu and His ligands. These two iron atoms are connected by two bridging carboxylate groups. Tyr25 is conserved in bFTs and eukaryotic FTs, where its hydroxyl oxygen atom points towards the metal center (distance of 3.6 Å) and its hydrogen atom appears to stabilize the carboxylic oxygen atom of Glu94. Since the tyrosine allows hyperoxidation of the cluster, this Tyr residue protects the active site and prevents permanent oxidative damage to the protein. The channels in bFT that allow for the entry and exit of Fe(II) include 3-fold (Figure 1.20), 4-fold (Figure 1.21), and major channels. Eight subunits of the bFT create 4-fold channels, while six subunits create 3-fold channels. The eight 3-fold and six 4-fold channels are hydrophilic and connect the inner core with the protein environment. The 3-fold channels are lined with Asp109, Arg117, and Asp118, while the 4-fold channels are extremely hydrophilic with four Asn148 residues on the outer surface of the protein shell and four Gln151 residues bound to a heavy atom on the inner surface. The metal binding site is located on the 4-fold axis, while the major sites of iron transfer into the cavity are predicted to be the 3-fold channels. Since bFT and H-chain FT are similar, it has been suggested that the 3-fold channels are the major sites used by Fe(II) to enter and move to the di-iron sites (Levi *et al.*, 1996). Iron oxidation at the di-iron site produces Fe(III), which returns through the 3-fold channels and into the cavity for the formation of the ferrihydrite mineral core (Treffry *et al.*, 1993). The di-iron center is at the bottom of the iron pore (ferroxidase pore), which is approximately circular in shape with an approximately elliptical wider base. The entrance and dimensions of the pore allow Fe atoms and water to enter and exit freely. Iron atoms can enter

through this pore to form the di-iron site. By electrostatic potential calculations, it has been calculated that the outer entrance is surrounded by positive potential that leads to an electrostatic field that could direct cations towards the channel entrance (Carrondo, 2003). It is likely that Fe atoms may have left the di-iron site to the solvent through the pore; however, under physiological conditions it is also possible that these Fe atoms may be translocated into the inner core via a concerted movement of the hydrophilic residues that lie below the iron position (Carrondo, 2003). The major channel, which differs from 3- and 4-fold channels, extends to the interior of the protein shell and is large enough for the entry of iron to the protein core.

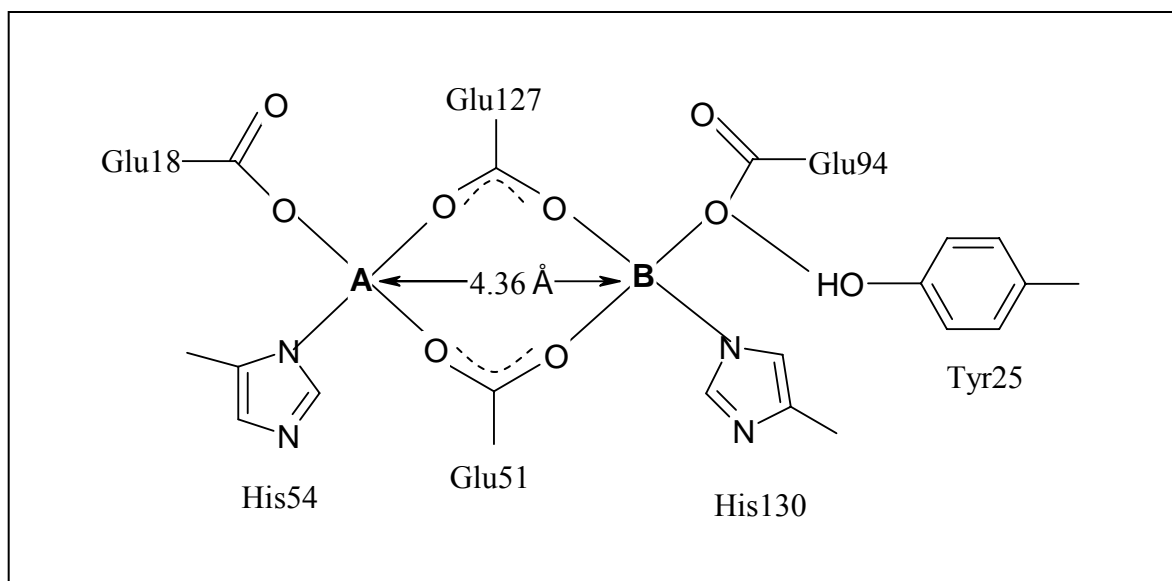


Figure 1.19: The ligands to the ferroxidase center of *E. coli* bFT are located on helices A-D: helix A, Glu18; helix B, Glu51 and His54; helix C, Glu94; and helix D, Glu127 and His130 (adapted from Stillman *et al.*, 2003). A and B are two iron atoms.

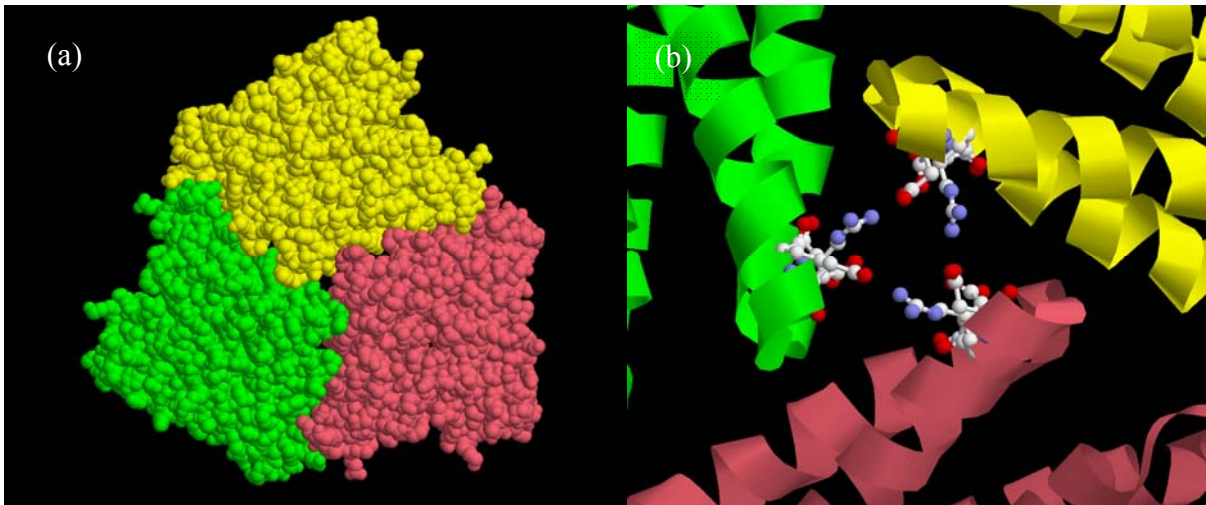


Figure 1.20: The space-filled structure of six subunits of *E. coli* bFT creating a 3-fold channel (a) and a zoom-in ribbon structure representing the residues (CPK ball and stick display) that form the channel (b) (PDB entry 1BCF) (Frolow *et al.*, 1994).

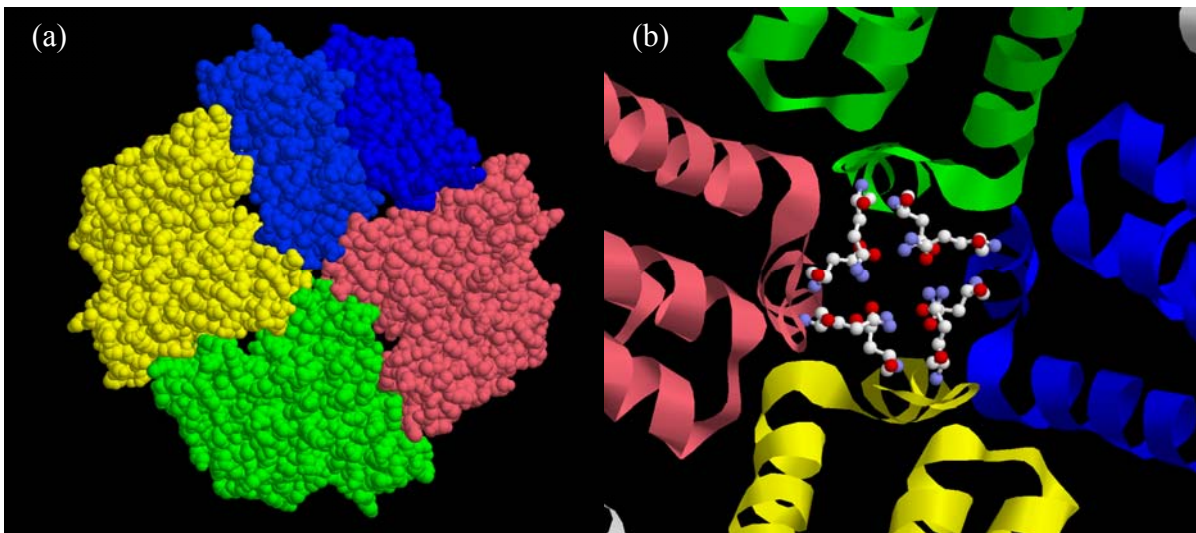


Figure 1.21: The space-filled structure of eight subunits of *E. coli* bFT creating a 4-fold channel (a) and a zoom-in ribbon structure representing the residues (CPK ball and stick display) that form the channel (b) (PDB entry 1BCF) (Frolow *et al.*, 1994).

Iron core formation is dependent upon Fe(II) concentration, pH, and the amount of iron already present in the core (Baaghil *et al.*, 2003). There are three kinetic phases for iron uptake into bFT. First is the binding of two Fe(II) atoms per dinuclear center ($t_{1/2} \sim 50$ ms), second is the rapid oxidation of the Fe(II) ions to Fe(III) in the presence of dioxygen ($t_{1/2} \sim 5$ s), and third is the subsequent core formation ($t_{1/2} \sim 300$ s), which is seen only when more than 50 iron atoms are added to the protein (Le Brun *et al.*, 1993). The effective iron capacity is ~ 2700 irons per cluster (24 subunits) while the theoretical limit is ~ 4500 .

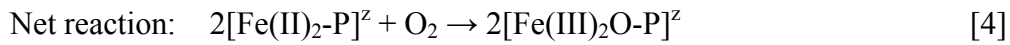
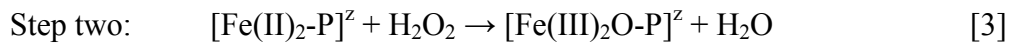
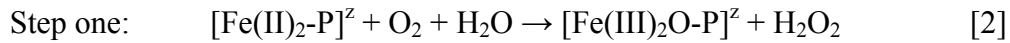
The presence of *E. coli* bFT greatly attenuates the production of hydroxyl radical during Fe(II) oxidation by H_2O_2 , consistent with the ability of bFT to facilitate the pairwise oxidation of Fe(II) by H_2O_2 , thus avoiding single electron reduction products of oxygen and therefore oxidative damage to the protein and cellular components through oxygen radical chemistry (Bou-Abdallah *et al.*, 2002). Once Fe atoms move to the di-iron binding site, there are three main reactions, diferrous binding, ferroxidation, and mineralization that occur to store iron atoms in the protein core and reduce hydroxyl radical formation (Bou-Abdallah *et al.*, 2002; Yang *et al.*, 2000). The first step of two iron atoms binding at the ferroxidase site results in the production of four protons and $[Fe(II)_2-P]^Z$, which represents a diferrous ferroxidase center complex of the protein P with the net charge Z in the diferrous binding reaction (Eq. 1). This di-Fe(II)-protein complex is oxidized in the presence of O_2 and a water molecule to generate Fe(III) and H_2O_2 (Eq. 2). This H_2O_2 is rapidly used in step two of ferroxidation to generate $[Fe(III)_2O-P]^Z$, which represents a μ -oxo-bridged diferric ferroxidase complex, without hydroxyl radical production via Fenton chemistry. This is an indication that the protein is capable of nullifying the toxic combination of Fe(II) and H_2O_2 . H_2O_2 is also an intermediate in the mineralization step and is rapidly consumed to produce Fe(III) (Eq. 5-7).

Then the inner surface will provide a site for Fe(III) binding and facilitate nucleation of the iron core.

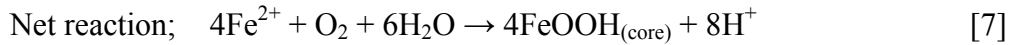
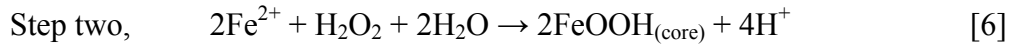
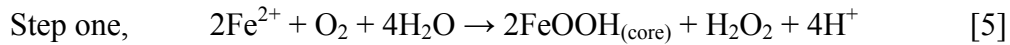
Diferrous binding,



Ferroxidation,



Mineralization,



1.3: Nanotechnology and Encapsulation

Nanotechnology refers to the methodology involved in the creation of functional materials, devices, and systems through control of matter on the nanometer (1 to 100+ nm) length scale (Niemeyer, 2001). This technology allows for construction, using techniques and tools that are being developed today to situate individual atoms and molecules in desired locations.

One of the applications of nanotechnology is the encapsulation of small molecules (guests) by small particles or nanoparticles (host) with several limitations such as size, shape, orientation, and interaction that influence reactions and linkages between guests and host particles. Self-assembled cage-like structures of nanoparticles can be used as constrained environments for the preparation of nanostructured materials and the encapsulation of guest molecules (Conn and Rebek, 1997). These nanoscale containment systems have potential applications in drug delivery, catalysis, and nanoscale circuits (Perkel, 2004).

1.3.1: The Host

Molecular capsules can act as hosts for appropriate guests and bring them into well-defined and controlled nano-environments (Rebek, 2005). There are many kinds of potential hosts including protein cages, viral capsids, polymers, lipid coats, and synthesized organic capsid-like structures. These hosts generally consist of small subunits that self-assemble to form cage-like structures with target substances inside. The interactions between host subunits that hold the complex together include hydrogen bonding, hydrophobic or hydrophilic interactions, which can be disrupted by altering pH, temperature, or using chemical reagents to break bonds. The size, shape, and environment inside these hosts restrict the types of

encapsulated guest molecules. For example, larger hosts permit more complicated arrangements of the guest molecules due to motional freedom from the capsule walls and the possibility of self-interactions.

Protein Cages

Several proteins are capable of acting as hosts for encapsulation. Reported examples have included GroEL, enzymes, heat shock protein (Hsp), vault, and iron storage proteins (Dps, FT, and bFT). Each of them has particular properties (sizes, shapes, and functions) that are suitable for varied and specific applications (Domínguez-Vera and Colacio, 2003; Ishii *et al.*, 2003; Flenniken *et al.*, 2006; Kickhoefer *et al.*, 2005).

Iron storage proteins are the most widely used for encapsulation especially for metal mineralization, and this has included metal clusters of uranium, copper, cobalt, manganese, vanadium, beryllium, cadmium, zinc, nickel, magnesium, iron phosphate, iron arsenate, iron vanadate, and iron molybdate (Hainfeld, 1992; Ensign *et al.*, 2004; Meldrum *et al.*, 1995; Grady *et al.*, 2000; Price and Joshi, 1983; Pead *et al.*, 1995; Douglas and Stark, 2000; Polanams *et al.*, 2005). Larger guest molecules such as Prussian blue, desferrioxamine B complex, and doxorubicin-HCl (anticancer drug) have recently been studied and investigated (Figure 1.22) (Domínguez-Vera and Colacio, 2003; Domínguez-Vera, 2004; Simsek and Kilic, 2005). While most applications are based on FT, few have been developed using Dps and bFT encapsulation, which are typically used only for metal mineralization. It has been found that *L. innocua* Dps could be used as protein cage for two cobalt oxide minerals, Co_3O_4 and $\text{Co}(\text{O})\text{OH}$ (Allen *et al.*, 2003).

GroEL is a chaperonin protein that functions in combination with GroES to refold misfolded proteins. It consists of two supramolecular rings, in which each is comprised of seven subunits of 60 kDa that stack to form a double-decker architecture with a cylindrical cavity of 45 Å in diameter and a wall thickness of 46 Å (Braig *et al.*, 1994). An example of GroEL-utilizing encapsulation is the report of encapsulating cadmium sulfide (CdS) in the protein cavity to allow this semiconductor to have thermal and chemical stability in aqueous media (Ishii *et al.*, 2003). CdS can be released from GroEL cavity by ATP-triggered release and host conformational change (Figure 1.23).

Heat shock proteins (Hsps) possess a chaperone activity similar to GroEL/GroES and form a hollow spherical 24-subunit complex. The complex exhibits octahedral symmetry with an outer diameter of 120 Å and the inner diameter of 65 Å, which resembles those of FT and bFT (Figure 1.24) (Kim *et al.*, 1998). Applications of Hsps have included drug delivery to tumor cells and the formation of a H₂ catalyst inside the Pt-Hsps cavity (Flenniken *et al.*, 2006; Varpness *et al.*, 2005).

Vaults are large proteins formed with 13-MDa ribonucleoprotein particles and having an internal cavity of 5×10^7 Å that can sequester hundreds of proteins (Figure 1.25). Vaults tend to have a hollow, barrel-like structure with two protruding caps and an invaginated waist with overall dimensions of 420 × 420 × 750 Å (Kong *et al.*, 2000). Due to its large structure, the encapsulation of vault particles can accommodate large guests such as green fluorescent protein (GFP) (~28 kDa) and luciferase (~61 kDa) (Kickhoefer *et al.*, 2005).

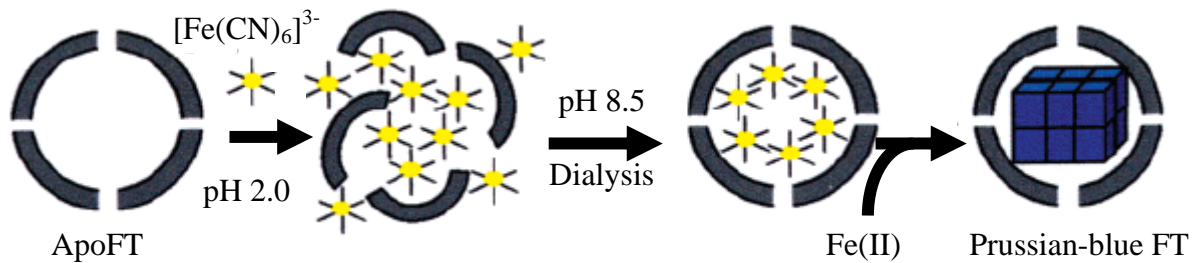


Figure 1.22: A schematic diagram representing the encapsulation of Prussian-blue in FT, which involves declustering of the protein at pH 2.0, encapsulation at pH 8.5, and the formation of a Prussian-blue cluster inside the protein cavity (Domínguez-Vera and Colacio, 2003).

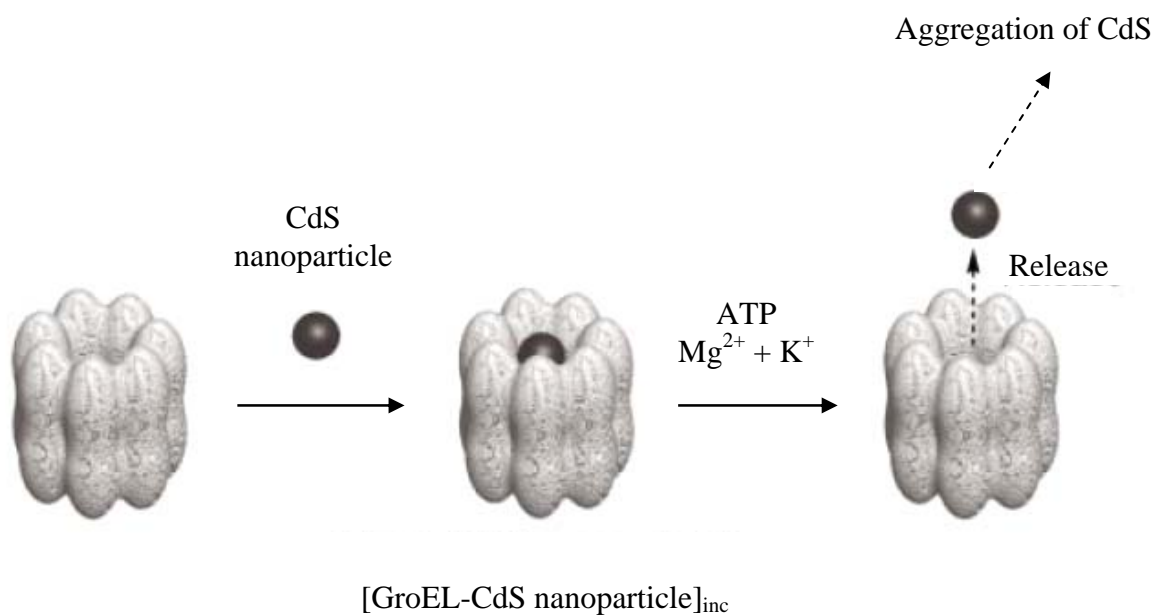
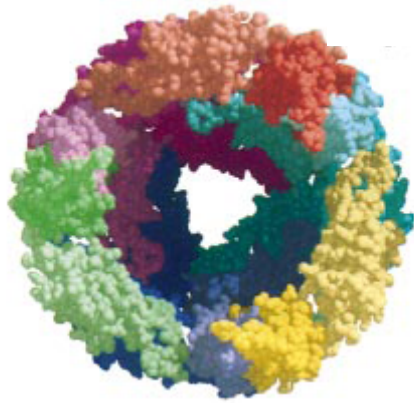


Figure 1.23: A schematic diagram representing the GroEL-CdS nanoparticle complexes, which involves guest released by the action of ATP and a conformational change of the cavity (Ishii *et al.*, 2003).

a



b

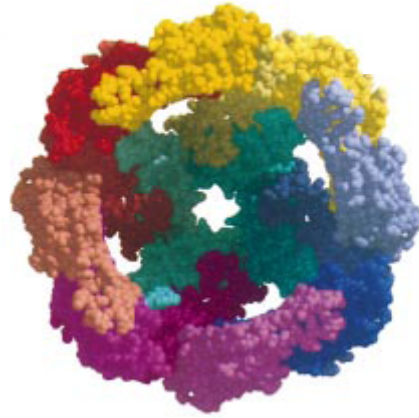
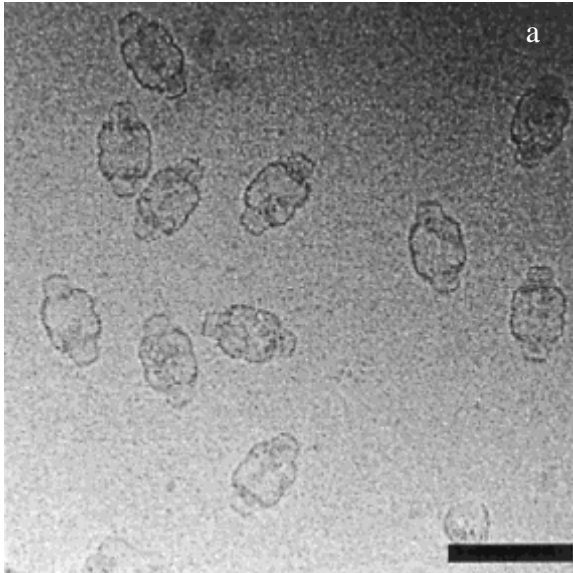


Figure 1.24: The space-filling structure representing the interior of the small heat shock protein from *Methanococcus jannaschii* viewed along 3-fold axis (a) and 4-fold axis (b) (PDB entry 1SHS) (adapted from Kim *et al.*, 1998).



a

b

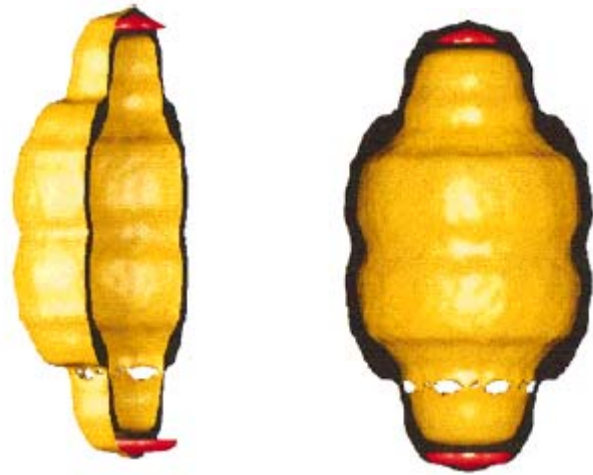


Figure 1.25: Cryo-transmission electron microscopy of vault particles (a) and half-a-capsid images representing the inner and outer structure (b) (Kong *et al.*, 2000). The scale bar corresponds to 1000 Å.

Viral Capsids

Viral capsids serve as proteins for nucleic acid storage and transport. Viruses exist in a range of sizes and shapes. For example, icosahedral structures range in size from 18 to 500 nm and $>2\ \mu\text{m}$ in length for filamentous or rod-shaped viruses. These varieties provide a library of platforms for tailored applications where size, shape, and stability are required. Several viral particles including Cowpea chlorotic mottle virus (CCMV) (Douglas and Young, 1998), tobacco mosaic virus (TMV) (Shenton *et al.*, 1999), MS2 bacteriophage (Anobom *et al.*, 2003), herpes simplex virus (Heymann *et al.*, 2003), polyoma virus-like particles (capsoids) (Abbing *et al.*, 2004), Kaposi's sarcoma-associated herpes virus (KSHV) (Trus *et al.*, 2001), and papillomaviruses (Modis *et al.*, 2002) can be used as constrained reaction vessels for packaging, entrapment of synthetic organics, site-isolated catalysts, and nucleation sites for crystal growth (Douglas and Young, 1998; Douglas and Young, 1999; Abbing *et al.*, 2004).

Most applications are currently based on the CCMV, which includes its chemical modification for multivalent presentation of ligands (Gillitzer *et al.*, 2002), nanoscale building blocks (Wang *et al.*, 2002), use as a viral cage for metal mineralization (Basu *et al.*, 2003), use as a template for chemoselective linkers (Cheung *et al.*, 2003), and as a host-guest encapsulation model (Douglas and Young, 1998). CCMV is an icosahedral virus with a diameter of 30 nm formed by 60 copies of two different types of protein subunits (Liepold *et al.*, 2005). The stability of viral cage is pH dependent, which modulates the opening of 60 separate pores and exposes the interior of the protein cage to the bulk medium. This has also been used to induce the formation of a metal core inside the capsid (Figure 1.26) (Liepold *et al.*, 2005). This mineralization process involved the removal of viral RNA, purification of the

empty viral particle, and selective mineralization of guest molecules within the confines of the virus particle at pH 6.5 (Figure 1.27) (Douglas and Young, 1998).

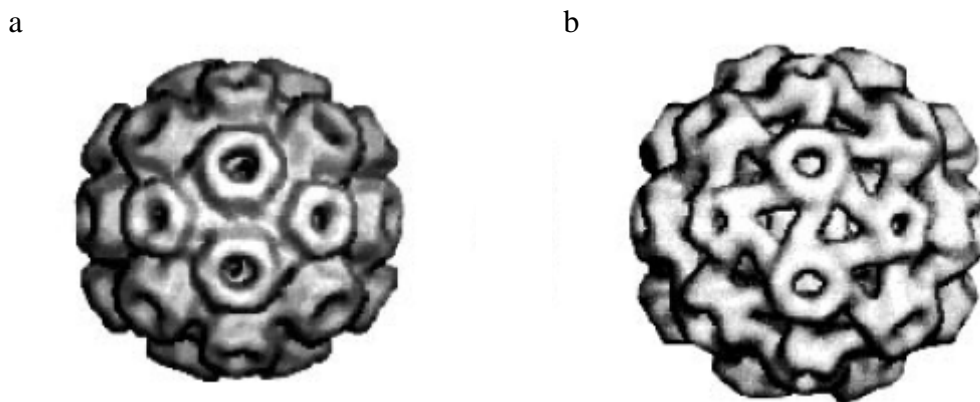


Figure 1.26: Cryo-transmission electron microscopy represents structural images of the closed conformation (a) and opened conformation (b) of CCMV (Douglas and Young, 1998).

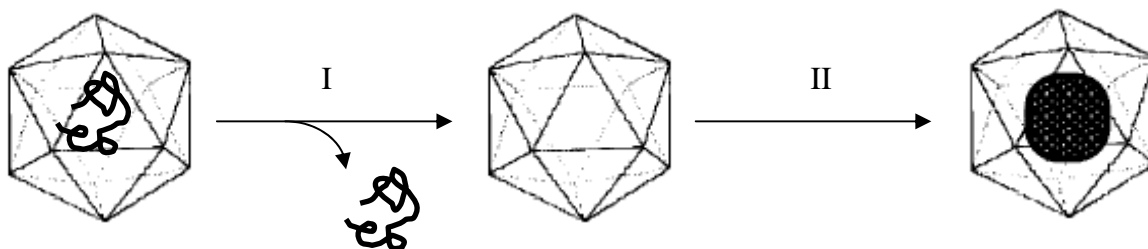


Figure 1.27: A schematic diagram representing the encapsulation of metals inside CCMV particle, a pH dependent process, which involved viral RNA removal to generate empty capsid (step I) and the formation of metal mineralization inside viral coat (step II) (adapted from Douglas and Young, 1998).

Polymers

There are several reported applications on the use of polymer encapsulations. These reports are focused on polymer-based drug delivery. A polymer such as commercially available poly(DL-lactide-co-glycolide) (PLG) is widely used as an antitubercular drug (ATD) carrier (Sharma *et al.*, 2004; Pandey *et al.*, 2003).

Lipid Coats

The applications of lipid coats are generally based on drug delivery systems such as solid lipid nanoparticles (SLNs), which are defined as nanocrystalline suspensions in water prepared from lipids that are solid at room temperature. Examples of guests for these systems have included antitubercular drugs and tobramycin (Pandey *et al.*, 2005; Cavalli *et al.*, 2003). The lipid coated encapsulated drugs can be visualized by cryo-transmission electron microscopy (cTEM) as has been shown for doxorubicin encapsulated in 1,2-dimyristoyl-*sn*-glycero-3-phosphocholine (DMPC)/cholesterol (Chol) and 1,2-distearoyl-*sn*-glycero-3-phosphocholine (DSPC)/Chol liposomes (Figure 1.28) (Abraham *et al.*, 2002). These encapsulations were dependent on lipid composition, pH, and the nature of the crystalline precipitation (Abraham *et al.*, 2002).

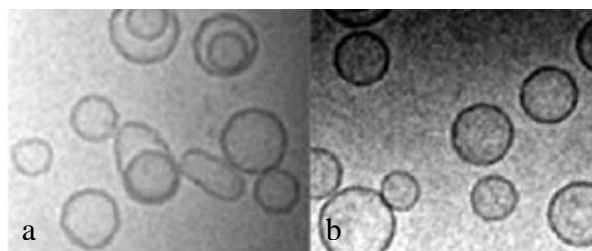


Figure 1.28: Cryo-transmission electron microscopy image of DMPC/Chol liposomes before (a) and after (b) drug loading (Abraham *et al.*, 2002).

Synthesized Organic Capsid-like Structures

Synthetic organic capsids can be varied in size, shape, and chemical functionality depending on the purpose of each particular experiment. Most of them are self-assembling capsules and are a heterogeneous mixture of the synthesized subunits, which can form self-assembled capsules by engaging in reversible non-covalent interaction (Conn and Rebek, 1997). The factors that bring molecular subunits to form a complex are hydrogen bonds,

aromatic π -stacking, polar interactions, and van der Waal's interactions. Some examples of various shapes for these synthetic hosts are Cram's carcerand (American football-like), bis(glycouril) macrocycle (tennis ball-like), a glycouril derivative (softball-like), a dimerization of (*R*)-2-bromo-3-methylbutyric acid (cylindrical capsule), and pyrogallol[4]arene (hexameric cube-like) (Figure 1.29) (Starnes *et al.*, 2001; Stoddart, 1988; Palmer *et al.*, 2005; Palmer and Rebek, 2004; Palmer and Rebek, 2005).

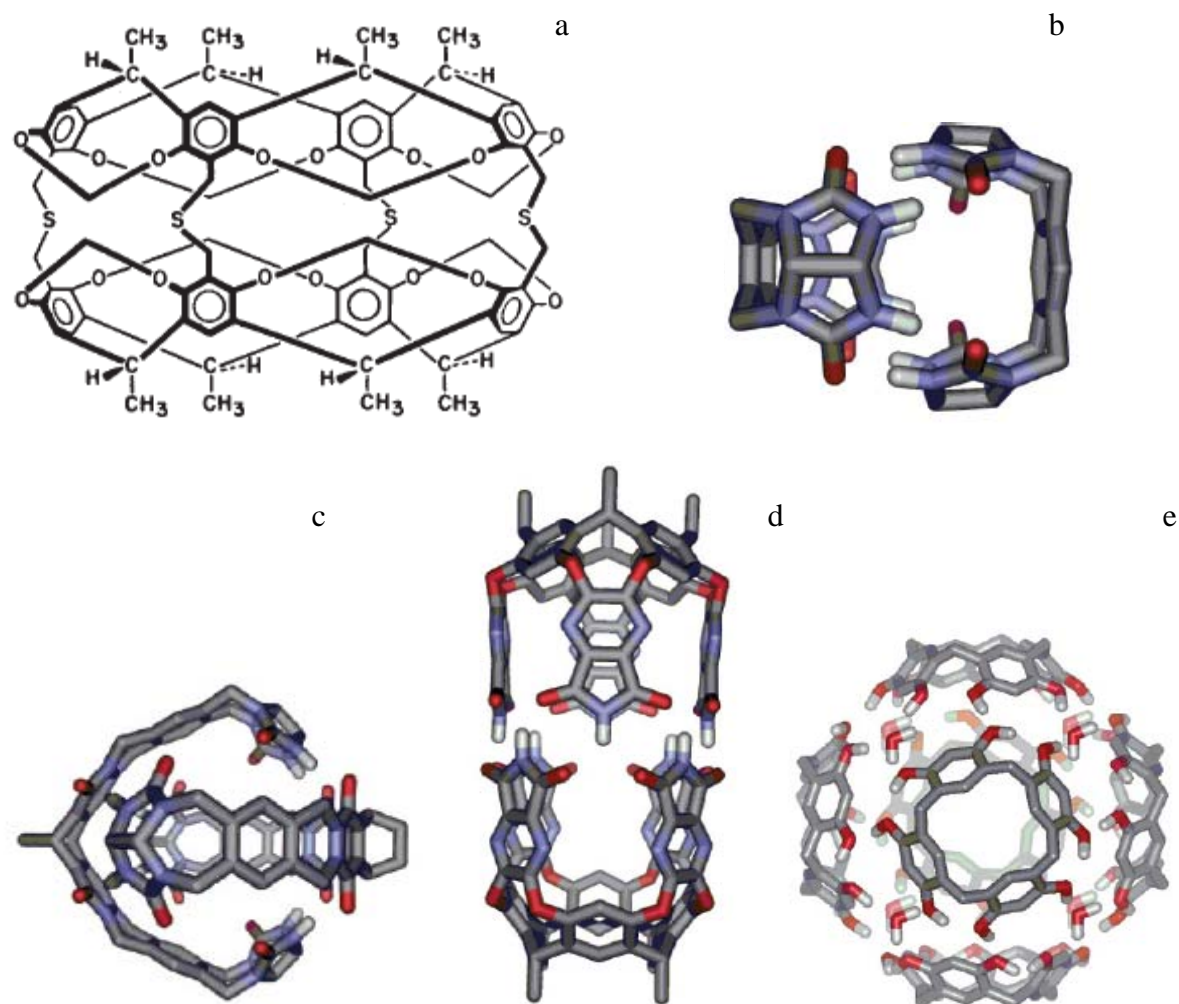


Figure 1.29: The structures representing various sizes and shapes of the synthesized organic particles, which are Cram's carcerand (a), bis(glycouril) macrocycle (b), softball-like glycouril derivative (c), a dimerization of (*R*)-2-bromo-3-methylbutyric acid (d), and pyrogallol[4]arene (e) (Starnes *et al.*, 2001; Stoddart, 1988; Palmer *et al.*, 2005; Palmer and Rebek, 2004; Palmer and Rebek, 2005).

1.3.2: The Guest

There are several types of guests that have been studied in encapsulation experiments such as entrapped metals, small organic compounds, peptides, and proteins. Many factors such as size, shape, number of molecules to be encapsulated, orientation, and interaction within the host particles are pertinent to optimize encapsulation processes. Encapsulated guest molecules become conformationally constrained and their environment is altered in a host cavity, which can lead to higher chemical reaction rates due to orientation effects provided by the host. The immobilization of guest molecules may promote stereoselectivity of a chemical reaction of interest (Palmer *et al.*, 2005).

Generally, guests can enter and exit capsules through the opening and closing of host flaps (Figure 1.30), but smaller guest molecules can exchange simply by diffusion through holes in the host subunits. However, some hosts must undergo complete dissociation to allow guests to enter, which would be followed by reassembly to form the entire intact capsule (Figure 1.31). The arrangement of guest molecules within nanocapsules and the development of methods to control entrapment and manipulation of guests molecules are investigated and remained to be resolved for certain encapsulation systems.

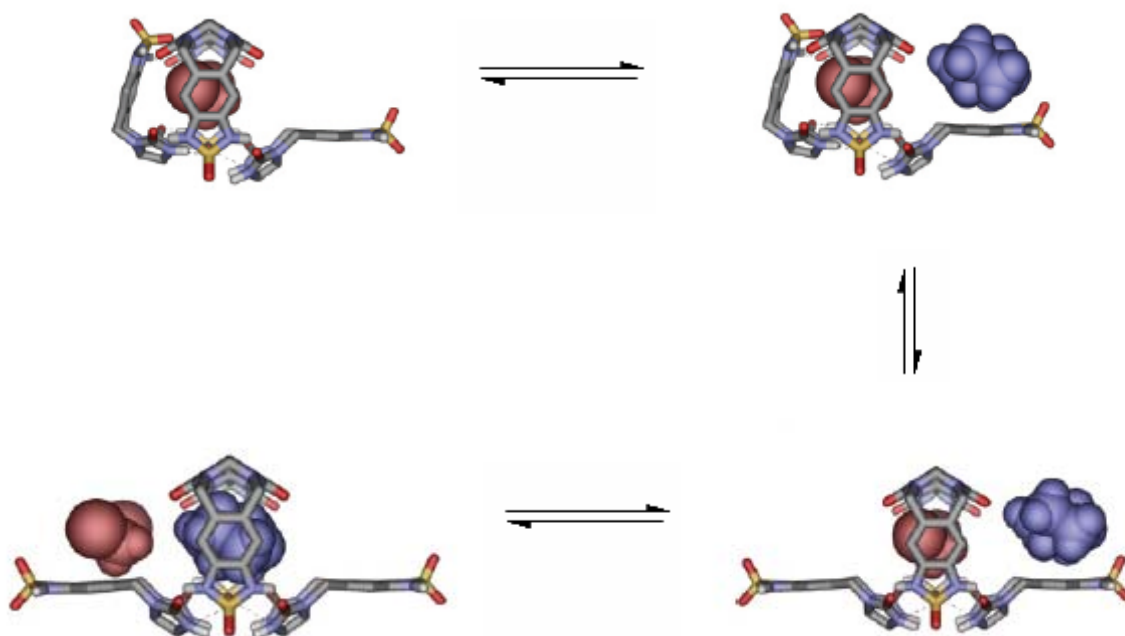


Figure 1.30: The diagram represents the host opening for guests exchange. Initially one flap opens with entrance of the incoming guest, which drives the opening of second flap. The previous guest is ejected with new encapsulation of a new guest molecule (Palmer and Rebek, 2004).

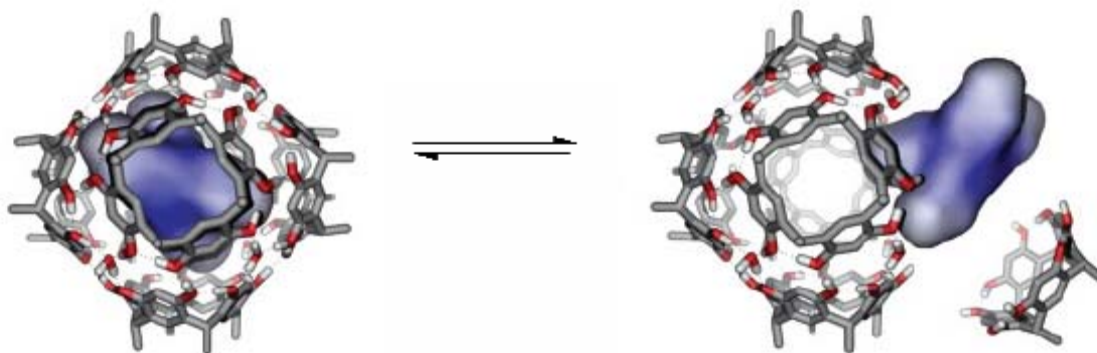


Figure 1.31: The diagram represents the dissociation of one subunit host to allow the exit of a guest molecule (Palmer and Rebek, 2004).

1.3.3: Linkage

There are three important interfaces that can be exploited to allow interaction between host and guest molecules: the exterior, the interior, and the interface between subunits making up the host. The exterior can be chemically modified, so the host particle is targeted to desired binding sites. For example, the anticancer drug, doxorubicin-HCl, has been encapsulated in FT and targeted to cancer cells (Simsek and Kilic, 2005), a viral template TMV has been used for inorganic-organic mineralization (Shenton *et al.*, 1999), and an antibody-antigen outer surface modification has been designed for binding to cell surfaces (Mann *et al.*, 2000). Host extension by addition of constituent subunits can form larger capsules under particular incubation conditions (Naumann *et al.*, 2001), and guest exchange can be promoted by using dissociable subunits or subunits with conformational flexibility that can create an opening of the capsule, which permits entrance and exit of guest molecules (Palmer and Rebek, 2004). Both of these processes involve the manipulation of host subunit (or molecule)-host subunit (or molecule) interactions. In contrast, interaction between the capsule interior (host) and the guest molecule is considered most critical in successful encapsulation techniques.

There are many potential methods for linkage forming between host and guest molecules such as the application of affinity tags (Futaki *et al.*, 2004; Xu *et al.*, 2004), antibody-antigen interactions (Mann *et al.*, 2000), chemical modification (Hooker *et al.*, 2004; Flenniken *et al.*, 2005), DNA directed assembly (Li and Mann, 2004), and protein engineering techniques (Kramer *et al.*, 2004). Affinity tag approaches are interesting and frequently utilized systems in biochemistry to purify proteins from crude extracts. These affinity tags including Arg-tag, calmodulin-binding peptide, cellulose-binding domain, DsbA, c-myc-tag, glutathione S-transferase, FLAG-tag, HAT-tag, His-tag, maltose-binding protein, NusA, S-tag,

SBP-tag, Strep-tag, and thioredoxin (Table 1.2) with various sequences and sizes (Table 1.3) can also be used as tools for host-guest interaction (Terpe, 2003; Li *et al.*, 1999; Lichty *et al.*, 2005). In order to determine suitable affinity tags for each experiment, the size of tags and proteins, their efficiency, cost, availability (source), and eluting agents are important factors to consider (Table 1.4) (Lichty *et al.*, 2005).

Table 1.2: Matrices and elution conditions for various affinity tags used in protein purification (adapted from Terpe, 2003)

Affinity tag	Matrix	Elution condition
Poly-Arg	Cation-exchange resin	NaCl linear gradient from 0 to 400 mM at alkaline pH>8.0
Poly-His	Ni ²⁺ -NTA, Co ²⁺ -CMA (Talon)	Imidazole 20 - 250 mM or low pH
FLAG	Anti-FLAG monoclonal antibody	pH 3.0 or 2 - 5 mM EDTA
Strep-tag II	Strep-Tactin (modified streptavidin)	2.5 mM desthiobiotin
c-myc	Monoclonal antibody	Low pH
S	S-fragment of RNaseA	3 M guanidine thiocyanate, 0.2 M citrate pH 2.0, 3 M magnesium chloride
HAT (natural histidine affinity tag)	Co ²⁺ -CMA (Talon)	150 mM imidazole or low pH
Calmodulin-binding peptide	Calmodulin	EGTA or EGTA with 1 M NaCl
Cellulose-binding domain	Cellulose	Family I: guanidine HCl or urea > 4 M, Family II/III: ethylene glycol
Streptavidin binding protein (SBP)	Streptavidin	2 mM biotin
Chitin-binding domain	Chitin	Fused with intein: 30 - 50 mM dithiothreitol, β-mercaptoethanol or cysteine
Glutathione S-transferase	Glutathione	5 - 10 mM reduced glutathione
Maltose-binding protein	Cross-linked amylose	10 mM maltose

Table 1.3: Sequence and size of affinity tags (Terpe, 2003)

Tag	Residues	Sequence	Size (kDa)
Poly-Arg	5-6 (usually 5)	RRRRR	0.80
Poly-His	2-10 (usually 6)	HHHHH	0.84
FLAG	8	DYKDDDDK	1.01
Strep-tag II	8	WSHPQFEK	1.06
c-myc	11	EQKLISEEDL	1.20
S-	15	KETAAKFERQHMS	1.75
HAT-	19	KDHLIHNVHKEFHAAHNK	2.31
3 FLAG	22	DYKDDGDYKDDIDYKDDDDK	2.73
Calmodulin-binding peptide	26	KRRWKKNFIAVSAANRFKKISSGAL	2.96
Cellulose-binding domain	27-189	Domains	3.00 - 20.00
SBP	38	MDEKTTGWRGGHVVEGLAGELEQLRARLEH HPQQQREP	4.03
Chitin-binding domain	51	TNPGVSAWQVNTAYTAGQLVTYNGKTYKCL QPHTSLAGWEPSNVPALWQLQ	5.59
Glutathione S-transferase	211	Protein	26.00
Maltose-binding protein	396	Protein	40.00

Table 1.4: Comparison of affinity tag technologies (Lichty *et al.*, 2005)

Tag	Size (aa)	Resin	Eluting agent	Source	Capacity[#]	Cost[#]	Cost/10 mg
MBP	396	Amylose	Maltose	Biolabs	3 mg/mL	\$105/10 mL	\$12
HIS	6	Talon	Imidazole	Clontech	5-14 mg/mL	\$220/25 mL	\$18
		Ni-NTA	Imidazole	Qiagen	5-10 mg/mL	\$257/25 mL	\$21
GST	218	GSH-Sepharose	Glutathione	Amersha	10 mg/mL	\$396/25 mL	\$36
CBP	28	Calmodulin affinity	EGTA	Stratagen	2 mg/mL	\$227/10 mL	\$114
STR	8	Strep-Tactin-Sepharose	Desthiobiotin	IBA	50-100 nmol/mL	\$1100/25	\$293
FLAG	8	Anti-FLAG M2 Mab agarose	FLAG peptide	Sigma	0.6 mg/mL	\$1568/25	\$1,045
HPC	12	Anti-Protein C Mab matrix	EDTA	Roche	2-10 nmol/mL	\$299/1 mL	\$4,983
CYD	5	InaD	DTT	N/A	>0.2 mg/mL [‡]	N/A	N/A

[#] Capacity and cost are for the year 2005 based on manufacturer's catalog and websites.

[‡] The capacity for InaD was experimental calculated by Lichty *et al.*, 2005.

1.3.4: Applications of Encapsulation Processes

There are many applications for encapsulation processes such as in the area of chemical catalysis, biological applications, as well as to demonstrate fundamental aspects of the design and control of artificial host-guest systems. The applications on chemical techniques are mostly based on synthesized organic coats. For example, there has been a report on a water-soluble cavitand (the host component defined as an organic molecule or ion whose binding sites converge in the complex) that acts as a phase transfer catalyst (a type of chemical compound, which facilitates the migration of a particular chemical hydrophobic component from one phase into another phase in a heterogeneous system) (Hooley *et al.*, 2006).

Biological applications of nanotechnology are generally focused in the areas of therapeutics, drug delivery, tissue reconstruction, diagnostics and biolabels (Perkel, 2004). To demonstrate this, some encapsulated metals activated by an exogeneous energy source have been used to heat and destroy surrounding tumors (Hainfeld, 1992). There are many applications for drug encapsulated nanoparticles, which could be made to minimize side effects of drugs, increase bioavailability, and/or enhance solubility of the medicinal agent. For example, a colloidal suspension of nanoscale ferrous oxide has been coupled to antibodies raised against an epithelial cell-adhesion molecule. This facilitates labeling of rare human epithelial cells such as circulating cancer cells in blood. This system could be useful for subsequent automated staining and analysis techniques (Perkel, 2004). For nanoparticles as model systems, there are metal and semiconductor nanoparticles that could make them suitable models for the study of fundamental biological phenomena.

1.4: Possible Aspects for Bacterioferritin Encapsulation

Most of the previous researches on host particles for bFT have been based on metal mineralization, organic, and inorganic encapsulation that had been accomplished by diffusion through the protein's natural pores. A few applications involved encapsulation with partially dissociated subunits. These methods were limited by many factors such as type, size, and amount of guest molecules, while the linkage between host and guest molecules was not the focus of these studies. However, linkage between guest and host may be beneficial for controlling the amount of guest inside the cavity and forming strong interactions, thereby increasing the success of the encapsulation process. Using a chemical linker would eliminate the dependency on guests being randomly entrapped by the reclustered process, rather they would be brought into the cavity directly as the cavity was being formed. This should produce a higher local concentration of host molecules during the encapsulation process.

In this thesis, the interactions between host particles and guest molecules were investigated to broaden the encapsulated applications and overcome limiting factors. Based on the knowledge of host (FT, viral capsid, and etc) encapsulation, there are several possible encapsulating methods for bFT including the use of affinity tags, protein engineering (fusion protein), chemical modification, and heme group interaction. Overall the thesis explores several approaches to carefully control encapsulation processes of complex multisubunit hosts using *E. coli* bFT as the model system. These approaches should be useful in extending controlled encapsulation to larger protein systems.

Affinity Tag

Beyond protein purification applications, the affinity tag approach might be useful in the encapsulation process which could make use of similar interactions to those between immobilized transition metals (stationary phase) and the tagged protein. These affinity-tag systems share the following features: (a) one-step adsorption purification, (b) a minimal effect on tertiary structure and biological activity, (c) easy and specific removal of the tag to produce the native protein, (d) simple and accurate assay of the recombinant protein during purification, and (e) applicability to a number of different proteins (Terpe, 2003). Since the C-terminal bFT is pointing toward the protein cavity, the linkage could be formed between the C-terminal tag and a cognate guest molecule, for example, a nickel nitrilotriacetic acid (Ni^{2+} -NTA)-modified guest (fluorescent probe) (Figure 1.32). Another affinity tag applied to many applications in drug delivery is the antibody-antigen interaction, which normally is utilized for the identification of target proteins. The encapsulation of guest-bFT is possible by generating an antibody linked C-terminal bFT that forms a linkage with a guest molecule that has a recognizable epitope sequence. A commonly used antibody-antigen tag system is the FLAG set of peptides that consist of eight amino acids, DYKDDDDK, which are fused with a protein of interest that has an affinity for a fragment of a monoclonal antibody to this sequence (Terpe, 2003).

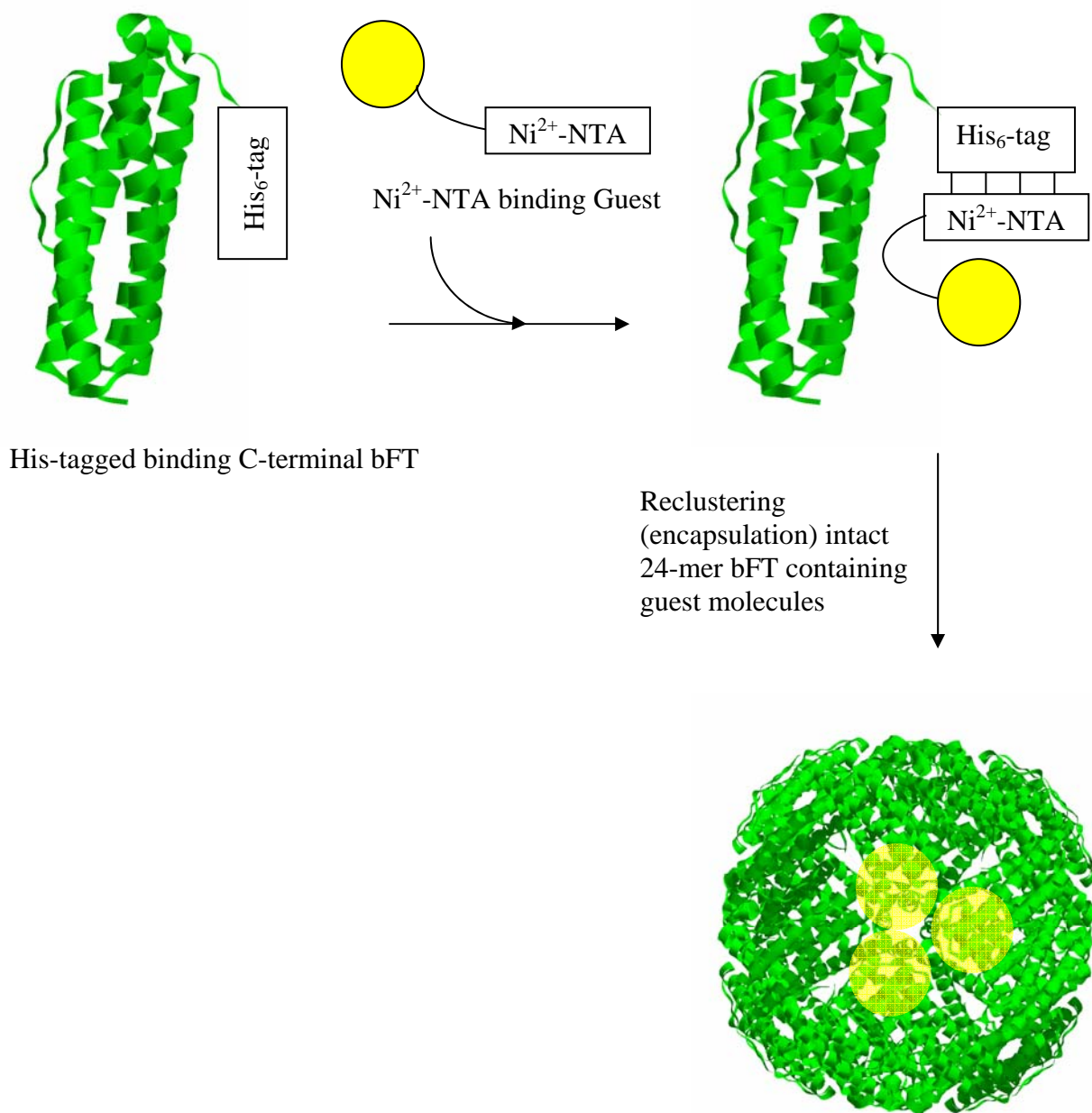


Figure 1.32: The schematic diagram represents the example of a bFT (green ribbon structure) encapsulation using His-tag affinity binding at the C-terminus that interacts with a nickel nitrilotriacetic acid-modified guest (yellow ball).

Protein Engineering

Protein engineering (the alteration of protein sequence by means of recombinant DNA methods) is the most convenient method to introduce new polypeptide sequences into a protein by generating an extended peptide sequence (linker) that can link two proteins. In this case, the fused genetic construct is possible by joining the 3' end of the bFT gene with linker and guest genes. This gene could then be introduced into cells (i.e. *E. coli* cells) and yield an expression system from which the protein fusion can be purified (Figure 1.33). The 24-subunit or higher formation of the fusion protein (guest protein attached to the C-terminal bFT) can be expected after protein purification. Linkers of various lengths may be required for adequate spacing between the guest and host when encapsulation involved the inside of the cavity. A strong affinity interaction between bFT and guest molecules is critical. However, there are several factors that need to be considered for success of this approach such as size of the guest and length of the linker, which may influence reformation of the 24-subunit cluster.

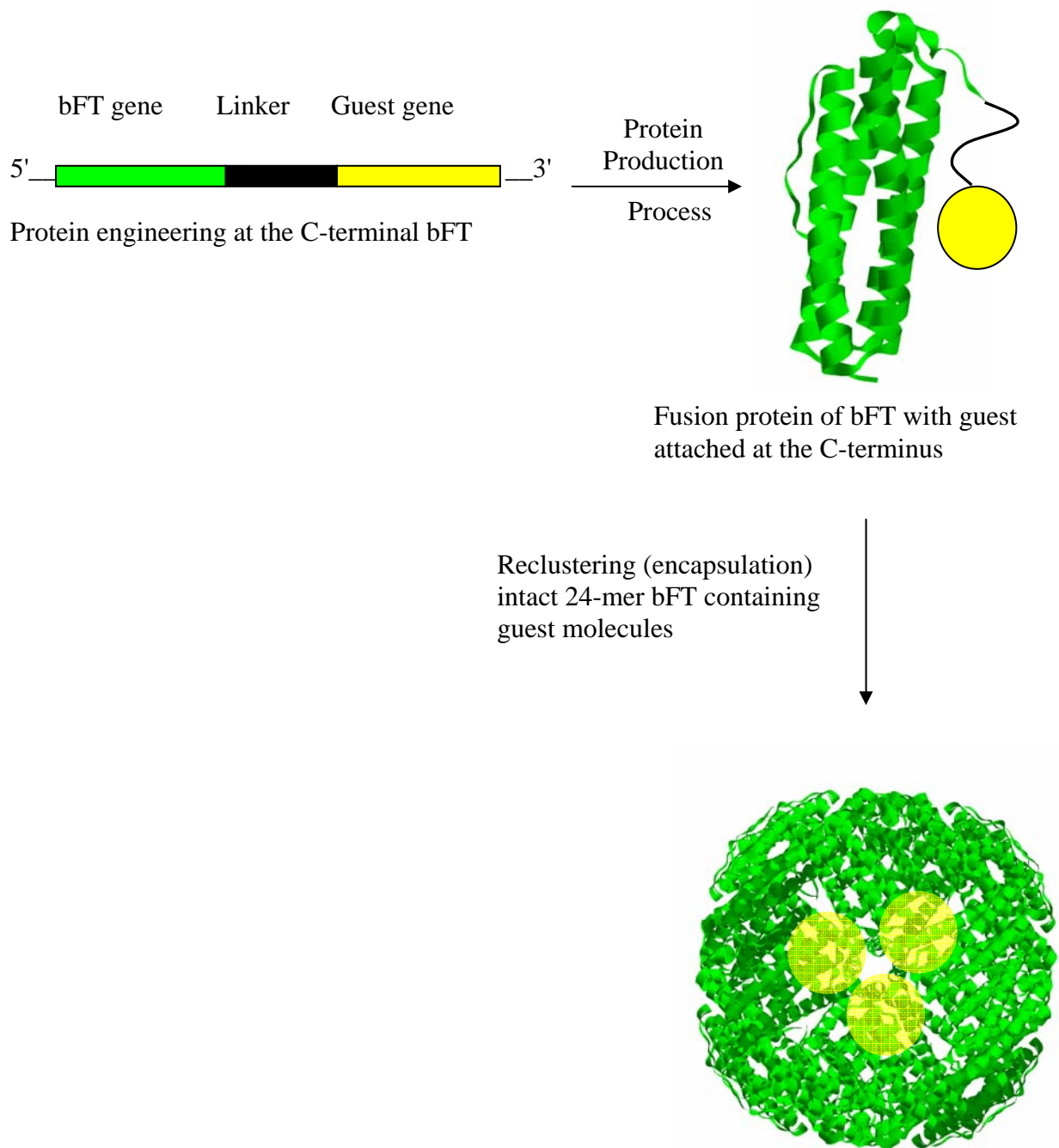


Figure 1.33: The schematic diagram represents a fusion protein approach to encapsulate guest molecules in bFT cavity, which is utilized by a guest gene (yellow) that is attached to the 3' end of the bFT gene (green) with an appropriate linker oligonucleotide (black) in between.

Chemical Modification

Chemical modification of the inner cavity could be also utilized to control encapsulation. Amino acid substitution would be required at the interior of a capsid using site-directed mutagenesis (Hooker *et al.*, 2004). For example, introduction of cysteine is commonly employed to create a reactive site for disulfide bond formation. Wild-type bFT contains no cysteine making this an ideal modification achievable by conventional mutagenesis techniques using the bFT-encoding gene. The guest molecule, containing a thiol group, could then be connected to the protein containing Cys residue through the formation of a mixed disulfide bond. However, there are some limiting factors to this approach such as structure changed, protein stability, and formation of cluster (24-subunit) of the mutated protein that should be considered and controlled.

Another possibility is to use a guest molecule containing a Cys residue or a sulfhydryl (–SH) group, which could react with the heme-iron atom to form a [–S–Fe–] linkage (Figure 1.34). Since heme-iron atom is close to the cavity, the iron attached guest molecule is expected to be encapsulated.

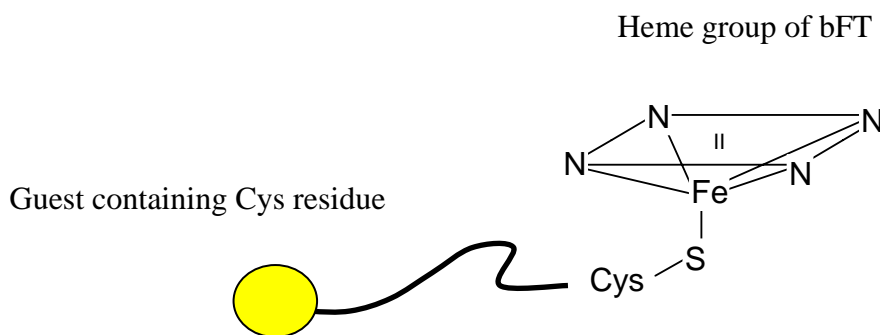


Figure 1.34: The image represents the possible encapsulation of a guest molecule inside bFT cavity by the interaction of a guest containing a Cys residue and heme-iron atom of bFT forming five-coordinate sulfur donor-ligated ferrous heme adducts.

Heme Group Interaction

This proposed encapsulation approach for bFT takes advantage of the heme groups. Since heme propionic acid side chains are pointing into the cavity, the linkage between bFT and a guest molecule can be generated by connecting the guest to these propionate sites. Guest molecules containing a hydroxyl group ($-\text{OH}$) can react with an acid group of exogenous heme ($-\text{CO}_2^-$) to form an ester ($-\text{COOC}-$). This modified heme would then be introduced to declustered bFT and allow for heme incorporation (and guest) into the 24-subunit reclustered protein. Another possibility is a use of amide bond formation ($-\text{CONH}-$), where the propionic acid side chains are reacted with a guest containing amino group ($-\text{NH}_3^+$) (Figure 1.35).

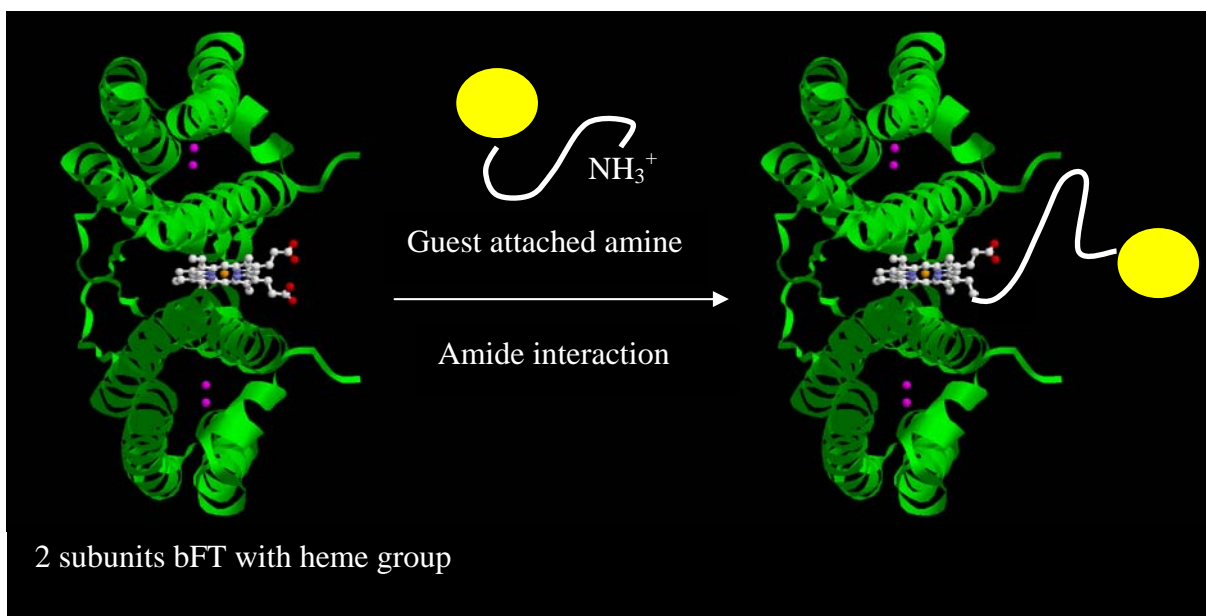


Figure 1.35: The schematic diagram represents possible encapsulated method by using a covalent site chain heme propionate-guest interaction. The formation of the 24-subunit protein is expected to contain the guest inside the protein particle once it is formed.

1.5: Summary of Experimental Objectives Achieved

The encapsulation of guest molecules with bFT using a His-tag affinity approach was an area of interest throughout this thesis. In order to increase the possibility of the encapsulation process for multisubunit host systems of protein bacterioferritin, it may be necessary to allow the subunits of the host molecule to dissociate and form tight interactions with guest molecules, which could then be followed by allowing the subunits to recluster with their tightly held guest molecules being brought inside the cavity during the recluster process (Figure 1.36). Our goal was to find and understand the conditions required to achieve the successful encapsulation of small molecules/biomolecules into the bFT central cavity. Suitable conditions for these encapsulated steps were investigated using apoferritin, a commercially available protein, as a study model and a size standard to visualize the hydrodynamic radius of these proteins under various environments. Since the iron core of bFT as well as the presence of heme groups might influence the encapsulation, ferroxidase- and heme-free bFT mutants were generated by site-directed mutagenesis. The recluster of the 24-subunit of wild-type and mutant bFTs were also examined and studied in terms of protein stability. Using data from optimizing conditions for encapsulation and knowledge of protein stability of these systems, His-tagged bFT was used as a model system for the encapsulation of nickel nitrilotriacetic acid containing guest molecules, which was investigated under studied environments.

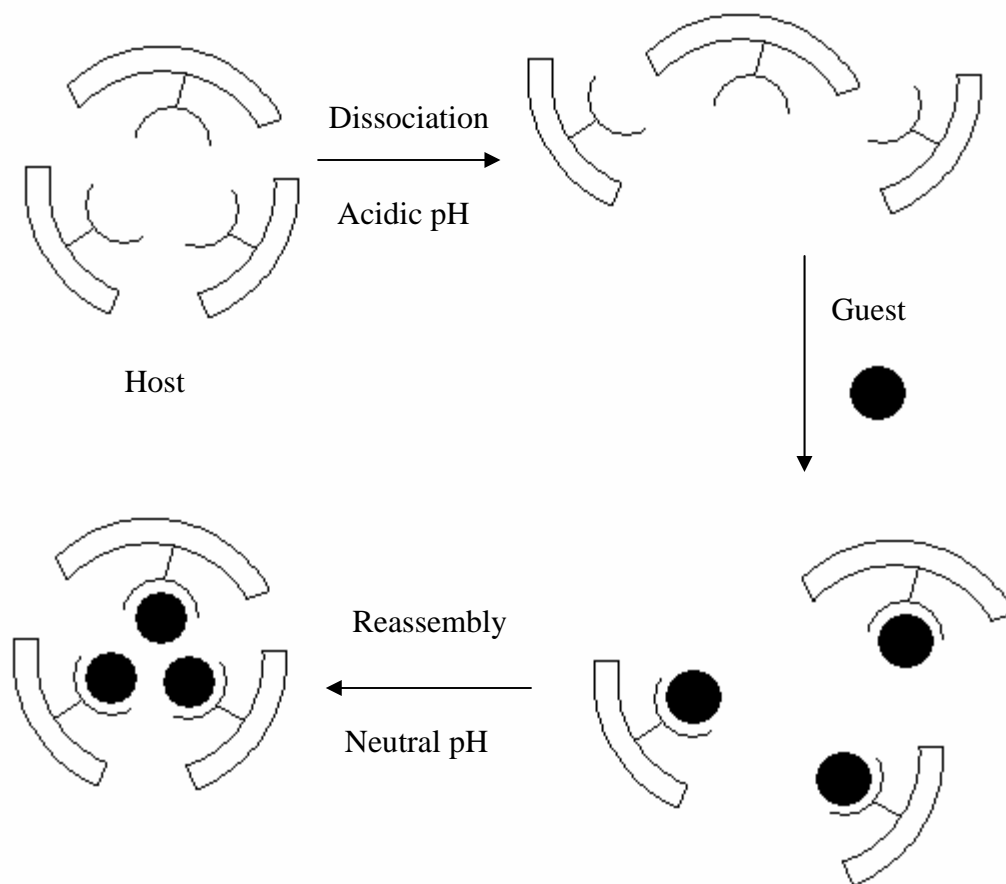


Figure 1.36: The diagram showing the aspect of the guest molecules encapsulated into bFT cavity, which involves declustering of the native 24-subunit cluster in acidic solution, binding with the guest molecules, and reclustering at neutral pH.

CHAPTER 2: CONDITIONAL TESTS FOR DISSOCIATION AND REASSOCIATION OF APOFERRITIN SUBUNITS USING LIGHT SCATTERING TECHNIQUES

2.1: Literature Research on Dissociation and Reassociation of Horse Spleen Apoferritin

Horse spleen apoferritin (apoFT_{HS}) is an iron-free FT that resembles bFT in terms of size and function (Petsev *et al.*, 2000; Lee and Richter, 1976). Horse spleen apoFT was first found to consist of three different multimeric forms that included aggregations of quaternary structure such as two 24-subunit, three 24-subunit, and four 24-subunit forms (Kopp *et al.*, 1963; Suran and Tarver, 1965; Harrison and Gregory, 1965). Several experimental approaches, namely laser light scattering (LLS), starch-gel electrophoresis, and electron microscopy, were used to predict the size of the 24-quaternary structure and higher oligomers (Richter and Walker, 1967; Williams and Harrison, 1968). The interaction causing the formation of higher oligomers was found to be related to water structure around apoFT molecules (Suran and Traver, 1965; Richter and Walker, 1967; Harrison and Gregory, 1968; Williams and Harrison, 1968; Petsev *et al.*, 2000). It was also determined that the interfaces along the 3- and 4-fold axes play the most important roles in the stability of the assembled molecule (Santambrogio *et al.*, 1992; Stefanini *et al.*, 1996; Santambrogio *et al.*, 1970). There are at least five factors that are known to modulate the interaction of inter- and intrasubunits of apoFT. These variables include protein concentration, pH, presence of denaturants, temperature, and ionic strength. Interprotein interactions describe the associative/dissociative factors governing assemblies of intact 24-mers to yield higher order arrangements of the intact

protein. Intraprotein interactions describe factors for association of the polypeptides within a single 24-mer.

Protein concentration was found to affect both inter- and intraprotein interactions. The interchange between 24-subunit and oligomer is dependent upon dilution and concentration (Lee and Richter, 1976). It was found that two 24-subunit quaternary structures were favored when the protein concentration was above 0.1 mg/mL, while higher oligomers were dominant when the protein concentration exceeded 0.4 mg/mL (Jaenicke and Bartmann, 1972). Smaller subunit dissociation of horse spleen apoFT was not detected at concentrations of 4.43×10^3 mg/mL (Crichton *et al.*, 1973).

Size-exclusion chromatography and circular dichroism (CD) experiments were used to investigate (apo)ferritin assembly as a function of pH (Chiaraluce *et al.*, 2000; Stefanini *et al.*, 1987). It was found that the horse spleen apoFT oligomer was stable between pH 2.8–10.6. Aggregation was observed at $\text{pH} \leq 1.0$. Smaller subunit oligomers such as a dimer (2 subunits) and monomer (1 subunit) were detected between pH 1.0–1.6, while higher oligomers, dimer, and monomer were found at pH 1.6–2.8 and pH 10.6–13.0 (Richter and Walker, 1967; Crichton and Bryce, 1973). The relationship between pH and apoFT subunit dissociation can be explained with respect to the protonation states of the protein's amino acid residues. Decreasing the pH results in repulsive interactions, leading to the loss of secondary and tertiary structures. Conversely, for oligomeric proteins, acid denaturation is not limited to the destruction of secondary and tertiary structure of each 24-subunit monomer, but entails the perturbation of intersubunit interactions. In addition, it was found that the presence of the iron core did not influence the acid-induced dissociation of the protein (Chiaraluce *et al.*, 2000).

The denaturants that are widely used in dissociation studies of multisubunit proteins are guanidinium hydrochloride (Gdn-HCl) and urea. It was found that apoFT is stable in 8-10 M urea-containing solutions (Hofmann and Harrison, 1963). FT is dissociated in 9 M urea at pH 2.5 (Otsuka *et al.*, 1981), and *Rhodobacter capsulatus* bFT is completely unfolded in solutions containing more than 10 M urea (Kilic *et al.*, 2003). For Gdn-HCl, apoFT is dissociated in the presence of 7 M Gdn-HCl at pH 4.5, while FT is declustered at the same Gdn-HCl concentration but at a higher pH (Listowsky *et al.*, 1972). The *R. capsulatus* bFT is unfolded when Gdn-HCl concentrations are greater than 5 M (Kilic *et al.*, 2003). The re-association can be achieved by removal of denaturant, in which most of the helical structure has been restored.

FT and bFT are heat stable proteins. FT can tolerate high temperatures up to 80 °C for 10 min at neutral pH (Listowsky *et al.*, 1972; Crichton and Bryce, 1973), while bFT is fully unfolded at 90 °C (Kilic *et al.*, 2003). By using CD measurements in the near and far UV regions, it was found that melting (denaturing) temperature (T_m) of apoFT ($T_m \geq 93$ °C) was higher than FT ($T_m = 77$ °C), in which T_m of apoFT > H-chain FT > L-chain FT (Stefanini *et al.*, 1996). Re-association occurred if the temperature was 5–10 °C lower than T_m , while aggregation occurred if the temperature was higher (Stefanini *et al.*, 1996).

Static light scattering was used to evaluate the effects of electrolytes and the reversible association of apoFT by plotting the second virial coefficient (a representative of the strength of particle-solvent interactions) against concentration (Petsev *et al.*, 2000; Richter and Walker, 1967). It was found that apoFT was stable in solutions containing 0.06–0.34 M NaCl (Richter and Walker, 1967), and while 0.01-0.15 M NaCl decreased repulsion between two 24-
quaternary structures, protein stability was increased outside this range (Petsev *et al.*, 2000).

The salt dependence was also investigated in *L. innocua* Dps, in which the protein was dissociated at $\text{pH} \leq 2.0$; however, with the addition of sodium sulfate (Na_2SO_4) this protein was stable at $\text{pH} \geq 1.5$ (Chiaraluce *et al.*, 2000).

Beyond these factors, only apoFT undergoes partial denaturation, which is the slight re-arrangement of the 24-subunit or the opening of the loop regions in the peptide chain to reveal the hydrophobic regions of the helices. ApoFT can partake in the formation of higher oligomers (Petsev *et al.*, 2000). Denaturations do not significantly change the shape and size of the 24-subunit protein but expose groups that locally decrease the repulsion and increase the attraction between them.

The purpose of this part of the project is to evaluate the behavior of horse spleen apoFT and particularly the stability of oligomers (based on size) in response to pH variation. This protein will be studied initially to obtain some basic information on the declustering and re-clustering phenomenon reported previously in the literature, which will be of use in our studies with *E. coli* bFT encapsulation systems. The effects of protein concentration, pH, ionic strength, presence of glycerol, and incubation time for dissociation and re-association were investigated as to their effects on protein cluster stability. DLS was used to determine the size of the oligomers as a function of the above effects. This technique has been previously utilized to study the interactions of apoFT molecules (Petsev *et al.*, 2000; Richter and Walker, 1967).

Light scattering is mainly elastic scattering, in which the wavelength of incident light is equal to the wavelength of scattering light. If there is an individual molecule in a solution and if it is assumed that the molecule is small relative to the wavelength of incident light, then that molecule may be treated as a point scatterer. The oscillating electric vector of the incident light creates oscillating electrons in the molecules, which in turn cause oscillating dipole

moments and electric fields, whose intensities can be detected by a detector (Van Holde *et al.*, 1998). Laser light scattering allows for two main measurements: (1) the angular distribution of time-averaged scattered intensity or static light scattering (SLS) and (2) time-dependent scattered intensity due to density and concentration fluctuations or dynamic light scattering (DLS). Only DLS provides information on the hydrodynamic radius (R_h), which is used to measure particle size distribution in a given sample.

Dynamic light scattering measures and analyzes the intensity of fluctuations in the scattered light. When laser light interacts with particles, most light will pass through unscattered, while some will be recorded by the detector and causing bright and dark areas of fluctuated particles (Figure 2.1). The bright areas indicate that light is scattered by the particles arriving at the screen with the same phase and interferes constructively to form a bright patch. The dark areas are where the phase additions are mutually destructive and cancel each other out. Since particles move under Brownian motion (a random movement caused by thermal energy), the constructive and destructive phase addition of the scattered light will cause the bright and dark areas to grow and diminish in intensity so that the intensity appears to fluctuate. According to the relationship between diffusion speed and particle size in which smaller particles move more quickly in a liquid than larger particles (Figure 2.2), the particle size can be determined using the Stokes-Einstein relationship, $D = k_B T / 6\pi\eta R_H$, where D is the diffusion coefficient, R_H is the hydrodynamic radius, k_B is Boltzmann's constant, T is temperature in Kelvin, and η is viscosity of the solvent.

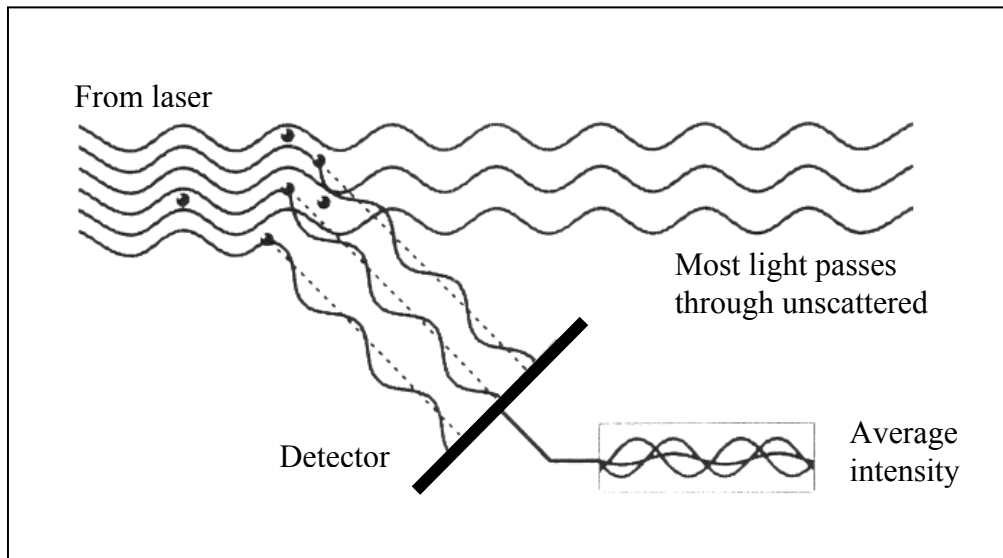


Figure 2.1: The scattered light on the detector shows constructive and destructive phase (Malvern manual, Malvern Instruments Ltd, Worcestershire, England, 2004).

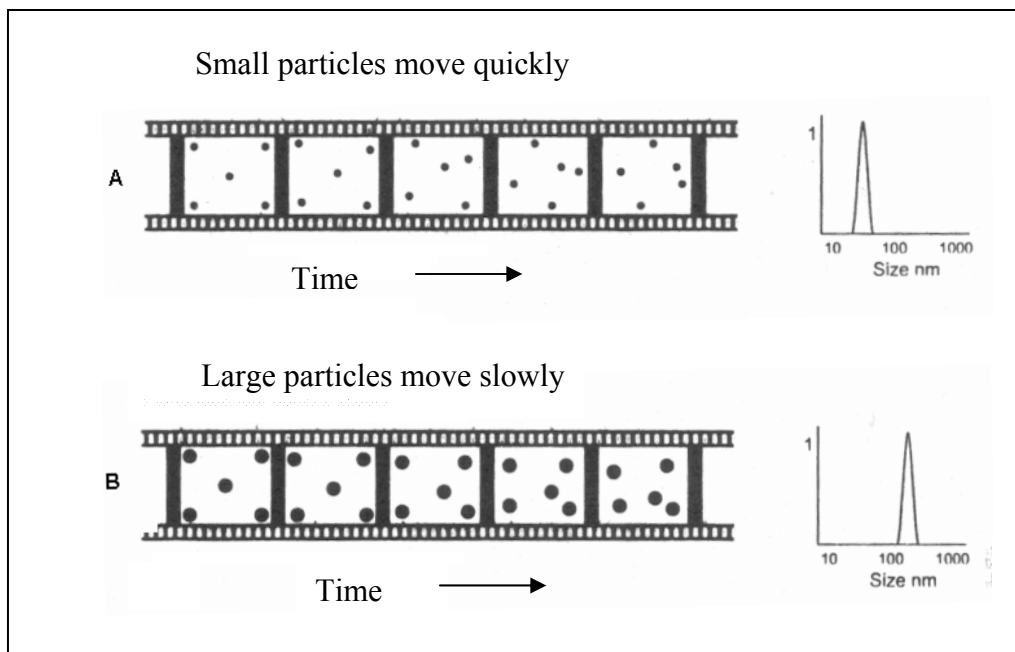


Figure 2.2: The relationship between diffusion speed and size of (A) small particles and (B) large particles (Malvern manual, Malvern Instruments Ltd, Worcestershire, England, 2004).

2.2: Reagents, Materials, and Equipment

Reagents and Materials

Hydrochloric acid (HCl), sodium chloride (NaCl), and glycerol were obtained from EMD Pharmaceuticals (Durham, NC), while sodium hydroxide (NaOH) was obtained from EM Science (Gibbstown, NJ). Horse spleen apoFT (Sigma A3660) was obtained from Sigma Chemical Company, St. Louis, MO). Water used in all experiments was Milli-Q water (18 M Ω -cm conductivity).

Whatman Anotop 10 plus or 0.02 μ m-pore filter membranes were obtained from Whatman Inc. (Florham Park, New Jersey) while 0.2 μ m GHP membrane was obtained from PALL (East Hills, NY).

Equipment

The particle size measurement was performed on a particle sizer (Zetasizer Nano ZS model ZEN3500, Malvern Instruments Ltd, Worcestershire, England) equipped with a He-Ne laser with 4.0 mW power at a 532 nm wavelength using the size measurement (DLS method) as a software protocol. The scattering light is collected at an angle of 90° through fiber optics and converted to an electrical signal by an avalanche photodiode array (APDs). The refraction index was set to 1.450 with 0.001 absorptions. The samples were run in triplicate with the number of runs set to 5 and run duration set to 10 seconds. The particle shape was assumed to be a spherical molecule and can be calculated according to the Stokes-Einstein relationship ($D = k_B T / 6\pi\eta R_H$) as above. For all measurements, dispersant viscosity (η) was set as sample viscosity. The result calculation was in General Purpose mode, which is appropriate for the

majority of dispersions and emulsion (Malvern manual, Malvern Instruments Ltd, Worcestershire, England, 2004).

2.3: Experimental Protocols

The samples were prepared by diluting 25 mg/mL stock horse spleen apoFT (pH 7.0) with Milli-Q water and filtering through 0.2 μm GHP membranes. Samples of 45 μL were gently injected into a low volume quartz cuvette (45 μL) to avoid formation of air bubbles and particulate matter. The z-average diameters (sizes) of the samples were measured at room temperature (25 $^{\circ}\text{C}$).

Effect of protein concentration

The 0.2 mg/mL horse spleen apoFT solution was prepared by diluting stock protein with Milli-Q water. The sample was incubated overnight and the molecular size was re-measured to test for protein stability. The control experiment was performed in order to compare the sizes of the sample with 24-subunit protein. Since the hydrodynamic radius of 24-subunit quaternary structure of apoFT is ~ 12 nm in diameter, only this 24-subunit protein will pass through the 0.02 μm -pore filter membrane, while generally higher oligomers would remain on the filter. The 0.2 mg/mL horse spleen apoFT was filtered through a 0.02 μm pore filter and incubated for 5 min before measurement of the horse spleen apoFT's diameter.

Effect of pH

A 1.0 mg/mL horse spleen apoFT preparation was used in probing pH effects on quaternary structure. The protein was filtered through a 0.02 μm -pore filter membrane and

incubated for 1 min in the solution containing HCl (pH 1.0–3.0 with 0.5 pH interval). Then 45 μ L sample was loaded into small volume quartz cuvettes and the diameter was measured. The graph of apoFT size versus pH was plotted.

Effect of electrolytes

A 0.7 mg/mL horse spleen apoFT solution was prepared and its size was measured. The sample was then filtered through a 0.02 μ m-pore filter membrane and the protein diameter was re-measured. To examine the effect of electrolytes, the protein sample was incubated for 5 min in a solution containing 500 mM NaCl. The whole solution was then filtered through a 0.02 μ m-pore filter membrane and the protein size was measured.

The effect of salt and low pH was then investigated by incubating the solutions of 0.7 mg/mL horse spleen apoFT for 5 min in a solution containing 500 mM NaCl for 5 min, filtered through 0.02 μ m-pore filter membranes, incubated in HCl solution (pH 1.5) for various periods of time (1 min–3 hours), and the protein size was re-measured.

Another set of experiments was to test for suitable salt concentrations that could stabilize the declustered protein. The 0.7 mg/mL horse spleen apoFT solution was incubated for 5 min in solutions containing 50-500 mM NaCl. The whole solution was then filtered through a 0.02 μ m-pore filter membrane and incubated in HCl solution (pH 2.5) for various period of time (1-30 min). The size of the protein was measured by DLS.

Effect of glycerol

The effect of glycerol concentration on native protein was examined by mixing 0.7 mg/mL horse spleen apoFT with 10-60% glycerol (10% glycerol increments). The protein was

then filtered through a 0.02 μm -pore filter membrane, and the protein size was measured by DLS.

The effect of glycerol on protein declustering was tested by mixing 0.7 mg/mL horse spleen apoFT with 10% glycerol, filtering through a 0.02 μm -pore filter membrane, and incubating in HCl solution (pH 2.5) for 1-20 min. The size of the declustered protein was then measured by DLS.

The effect of a combination of glycerol and salt (NaCl) on subunit dissociation was investigated by mixing 0.7 mg/mL horse spleen apoFT with 10% glycerol and 10-300 mM NaCl (10, 50, 100, 200, 300 mM NaCl), filtering through a 0.02 μm -pore filter membrane, and incubating in HCl solution (pH 2.5) for 1 min. The size of declustering protein was measured by DLS.

Further experiments on the effect of glycerol and salt on stability of the protein were performed by mixing 0.7 mg/mL horse spleen apoFT with 10% glycerol and 200 mM NaCl, filtering through a 0.02 μm -pore filter membrane, and incubating in HCl solution (pH 2.5) overnight. The control experiment was done without addition of glycerol.

Effect of incubation time on dissociation

A 0.7 mg/mL horse spleen apoFT solution was mixed with 10% glycerol and 200 mM NaCl, filtered through a 0.02 μm -pore filter membrane, and incubated in HCl solution (pH 1.5) for 1, 5, 8, and 12 min. Then the z-average diameter was measured.

Effect of reassembly time

Horse spleen apoFT (0.7 mg/mL) in solution containing 10% glycerol and 200 mM NaCl was filtered and incubated in HCl solution (pH 1.5) for 8 min. Then a solution of 1 M NaOH was added immediately to neutralize the sample's solution to pH 7.0, and the sample was incubated for 1, 4, and 17 min before measuring protein size.

2.4: Results and Discussion

2.4.1: Effect of Protein Concentration

The Zetasizer Nano ZS instrument requires at least 0.5 mg/mL protein if the size of the particle is less than 10 nm in diameter, while a minimum concentration of 0.1 mg/mL is needed if the particle size is in the range of 10 to 100 nm. The size of 45 μ L of 0.2 mg/mL horse spleen apoFT was measured using DLS, and the average hydrodynamic diameter of peak 1 was \sim 18 nm, while the diameter of peak 2 was \sim 250 nm (red line, Figure 2.3). By comparing with the control experiment (blue line, Figure 2.3), it appeared that peak 1 referred to the size of 24-subunit apoFT and peak 2 was indicative of higher aggregates. The size of 24-mer cluster measured by DLS appears somewhat different from the size measured by electron microscopy and X-ray crystallographic data (\sim 12 nm in diameter) and might be due to the shape of apoFT, which is not perfectly spherical (Smith *et al.*, 1989; Yariv *et al.*, 1981). Similar to reports by Yang and his co-workers, the formation of large aggregates (greater size than the 0.2 μ m pore size of the filter membrane) of apoFT (peak 2) were observed even though all of the protein solution samples were filtered before DLS measurement. These observations might be explained as follows (Yang *et al.*, 1994). Large aggregates might be broken up during filtration but reaggregate quickly after passage through the membrane. This explanation is

consistent with the finding that aggregation was fast under low-salt conditions. The aggregates were not rigid spheres, in which they might be forced to penetrate through the membrane pore during filtration. The size calculation was based on a spherical shape assumption; therefore, nonspherical particles would give larger apparent sizes due to their smaller diffusivity in solution in the DLS measurement.

The protein was found to be quite stable after remaining overnight at room temperature, since the particle size distribution does not change under these conditions (green line, Figure 2.3). However, in order to study the encapsulation reactions of bFT, only the 24-mer cluster is the focus of our studies.

Under acidic conditions, higher protein concentrations were used due to the requirement of the Zetasizer Nano ZS instrument. Some of the protein dissociated into smaller subunits, which could not be detected due to their small size (less than 10 nm in diameter) and lower protein concentration (lower than 0.5 mg/mL). Therefore, higher protein concentrations (1.0 mg/mL) were used in pH dependence experiments. However, high protein concentrations under acidic conditions may contain larger oligomers. This aggregation resulted from the interaction of smaller subunits, which were at high concentrations.

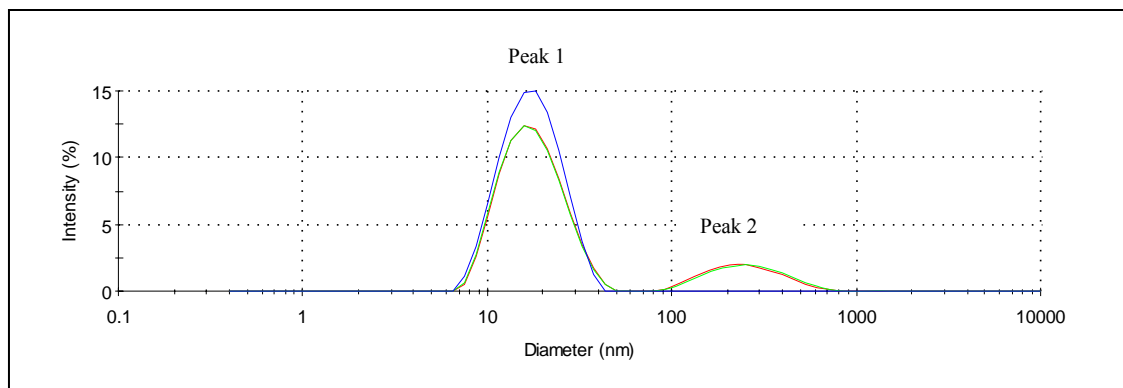


Figure 2.3: The size distribution by intensity plot of 0.2 mg/mL apoFT (pH 7.0) shows the intensity of apoFT that was incubated at room temperature overnight (red line), the intensity of apoFT that was incubated for 5 min (green line), and the intensity of filtered apoFT that was also incubated for 5 min (blue line).

2.4.2: Effect of pH

A rapid decrease in the size of apoFT was found when the pH was decreased from pH 3.0 to 1.5 (Figure 2.4). A size of 9 nm was detected at pH less than 1.5, and 18 nm size was detected at pH greater than 3.0. This decrease in size was almost two times lower (from ~18 nm to ~9 nm) than the normal size of 24-mer apoFT, which indicated the possible subunit dissociation. This dissociation is expected from the changes in charge repulsion that is a result of the protonation of carboxyl residues or charge shielding by Cl⁻ ions that destabilize interhelical interactions (Petsev *et al.*, 2000). Site-directed mutagenesis studies on the residues involved in intersubunit stability of *R. capsulatus* bFT has shown that the carboxylates of Glu128 and Glu135 forming the key salt-bridges with Arg61 and amino-terminal amine, respectively, were disturbed at a pH close to their pKa values (4.3 for Glu and ~7.8 for amino-terminal amine), which lead to dissociation of its 24-mer structure (Kilic *et al.*, 2003). However, after the protein dissociates into smaller clusters, it can quickly form aggregates when incubations are done at high concentrations of acid for long periods of time. This type of

aggregation may be induced by partial denaturation of the 24-mer cluster apoFT, which then exposes hydrophobic portions of the molecule to the water environment and makes aggregation a favored option.

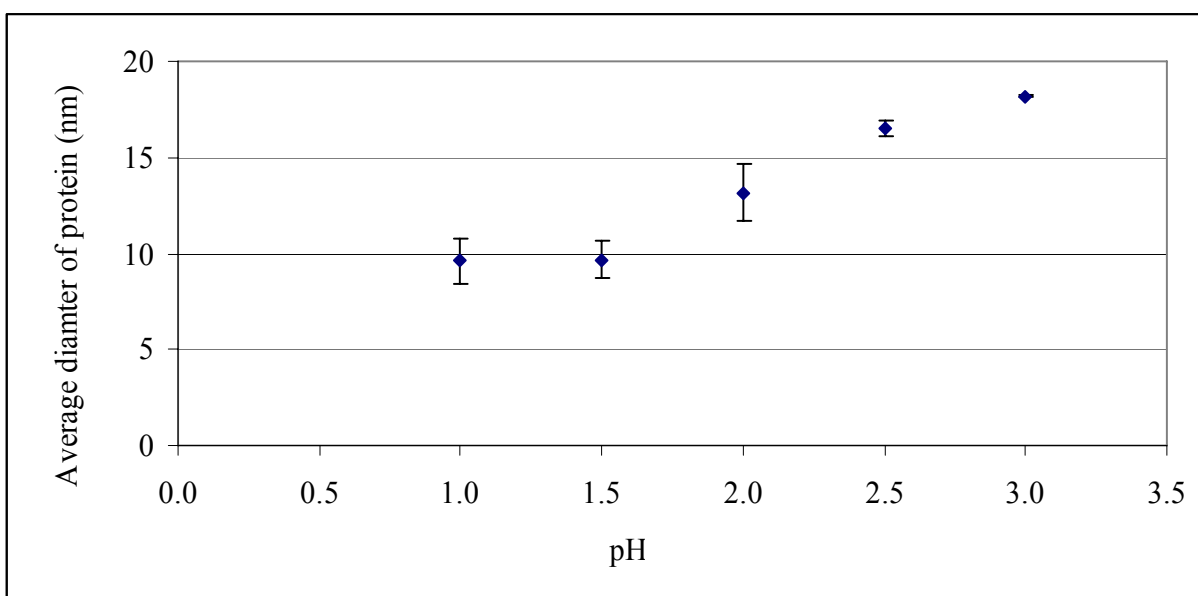


Figure 2.4: The plot of pH of protein solution (HCl addition) versus average size of apoFT (1.0 mg/mL) as determined by DLS shows a rapid decrease in average hydrodynamic diameter of the protein as pH decreases from 3.0 to 1.5.

2.4.3: Effect of Electrolytes

The size measurement of non-filtered apoFT in solution containing no salt gave two forms of protein, the 24-mer cluster with a size of ~18 nm and higher oligomer of ~200 nm (red line, Figure 2.5). It was observed that filtered apoFT through a 0.02 μm -pore membrane aggregated very quickly without addition of salt to form a self-associated cluster with a size of ~150 nm (green line, Figure 2.5), while filtered apoFT in solution containing salt exhibits predominance of stable 24-mer cluster protein (blue line, Figure 2.5).

The protein in a solution containing salt was then declustered at low pH. When the filtered protein in HCl solution (pH 1.5) containing salt was incubated for various times, aggregation was observed. Further experiments on salt concentrations showed that the amount of salt added should be in the range of 300-350 mM in order to stabilize the protein in HCl solutions (pH 2.5). However, it was found that although $[\text{Na}^+]$ did prevent protein aggregation for the first 15 min after incubating with HCl pH 2.5, the protein still aggregated after overnight incubation.

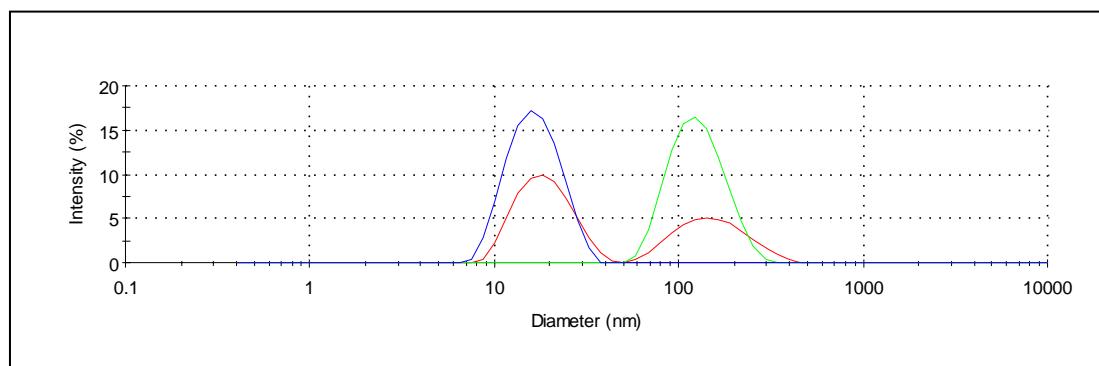


Figure 2.5: The size distribution by intensity plot of apoFT (0.7 mg/mL) with salt control (pH 7.0). The red line represents apoFT before filtering, the green line represents apoFT after filtering, and the blue line represents apoFT after adding NaCl followed by filtration through a 0.02 μm -pore membrane.

2.4.4: Effect of Glycerol

Glycerol is another additive evaluated for influencing protein conformational stability and preventing aggregation. It was found that 10% glycerol stabilized the native protein; however, aggregates were observed when declustering the protein in solution containing HCl (pH 2.5) with the same concentration of glycerol. This indicated that only glycerol was not sufficient to stabilize protein. The combination of salt and glycerol was then prepared to

examine their effect on protein stability. It was found that 10% glycerol with 100–300 mM NaCl stabilized the declustered protein. Further experimentation showed that a combination of 200 mM NaCl and 10% glycerol stabilized declustering protein in acid solution (pH 2.5) over time (green line, Figure 2.6), while the sample in the acidic solution (pH 2.5) containing only 200 mM NaCl (no glycerol) did not (red line, Figure 2.6).

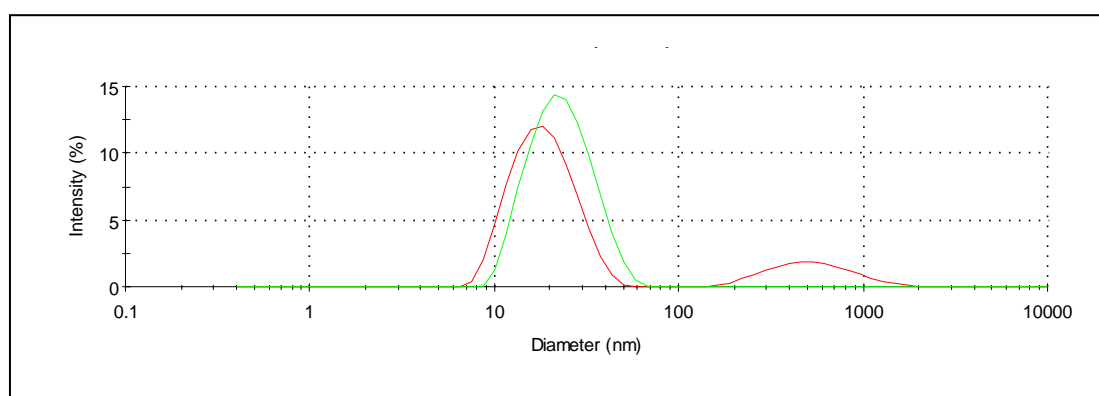


Figure 2.6: The size distribution by intensity plot represents the effects of glycerol on protein stability. The filtered apoFT (0.7 mg/mL) was incubated in solution containing 200 mM NaCl and HCl (pH 2.5) with 10% glycerol (green) and without glycerol (red). The solution was measured after incubating at room temperature overnight.

2.4.5: Effect of Incubation Time on Dissociation

This experiment was done under acidic condition by using HCl solution (pH 1.5) to observe fast dissociation processes. Aggregates were observed after incubation for 5 min under acidic condition (pH 1.5) (green line, Figure 2.7). The 8 min incubation yielded a single peak at ~16 nm, which corresponds to the size of 24-mer cluster (blue line, Figure 2.7). After incubation in acid for 12 min, the peak was shifted to the left of the one incubated in acid for 8 min; however, it also caused a peak shift to the right (~20 nm) and higher aggregation (~1000

nm) (black line, Figure 2.7). This indicated that additional aggregation was occurring. These findings suggest that neutralization to pH 7.0 was necessary after 5 to 8 min to minimize protein aggregation. Another possible cause of aggregates was the direct addition of a high concentration of acid to the protein solution. Therefore, in order to perform encapsulation with bFT, the sample could be dialyzed against a solution containing acid to possibly allow for a more controlled declustering and reclustered process.

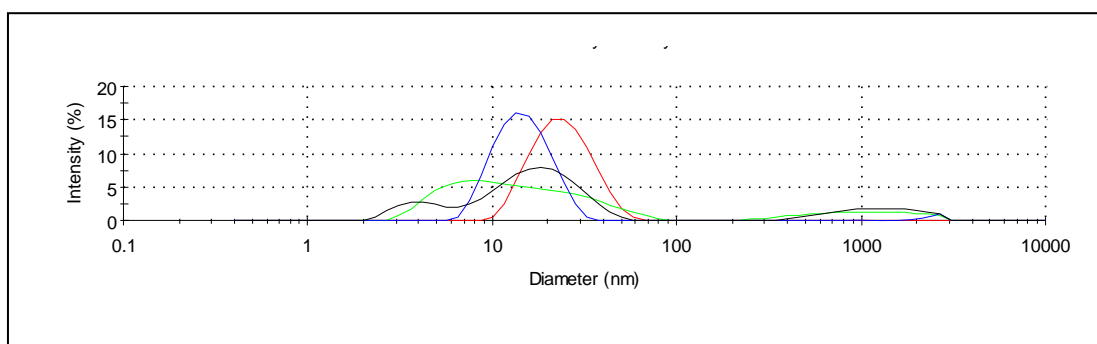


Figure 2.7: The size distribution by intensity plot represents the effects of declustering time. The filtered apoFT (0.7 mg/mL) in solution containing 200 mM NaCl and 10% glycerol was declustering in HCl solution (pH 1.5) for 5 min (green), 8 min (blue), or 12 min (black). The size distribution of the native apoFT is shown in red.

2.4.6: Effect of Reassembly Time

It was shown that declustered protein reformed its 24-subunit quaternary structure (size of 18 nm in diameter) within 1 min of neutralizing with NaOH (green line, Figure 2.8), while aggregation occurred very rapidly after that. Aggregation, which is the formation of amorphous oligomers, might be due to the rapid increase in pH (blue and black lines, Figure 2.8). In order to eliminate aggregation during the reclustered process with bFT, the sample is

dialyzed in solution (pH 7.0) for an extended period of time to allow for a more controlled reassembly process.

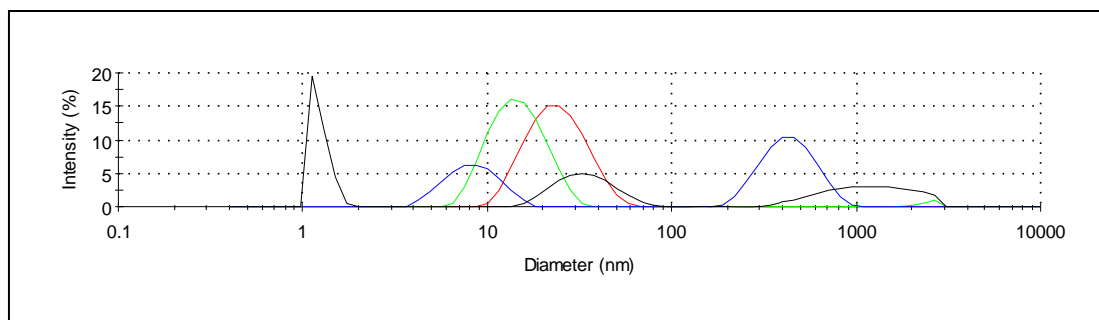


Figure 2.8: The size distribution by intensity plot represents the effects of reassembly time. The filtered 0.7 mg/mL apoFT in solution containing 10% glycerol and 200 mM NaCl was incubated in HCl solution (pH 1.5) for 8 min, then NaOH solution was added to neutralize the protein to pH 7.0. The sample was then measured for the size distribution immediately (green), or it was incubated for 4 min (blue) or for 17 min (black) before measuring the size distribution. The size distribution of the native apoFT is shown in red.

2.5: Conclusions

It was shown that the particle sizer (Zetasizer Nano ZS) can be used to measure the sizes of the spherical particles under specific conditions, in this case, horse spleen apoFT, where the 24-subunit cluster size was ~18 nm comparing to 12 nm in diameter from the literature. This offsize measurement might be explained in terms of apoFT shape, which is not completely spherical (Singh *et al.*, 1991), or the accuracy of the instrument (Zetasizer Nano ZS). Since the duration setting (10 seconds were used in this thesis) was found to affect the accuracy and repeatability of the size results (Malvern manual, Malvern Instruments Ltd, Worcestershire, England, 2004), longer duration might increase the accuracy of the measurements. Another possibility is the error bar of the size measurement for small

molecules using Zetasizer that is larger than that of the large molecules (such that the size measurement of large molecules is more accurate than that of small molecules). This observation is also observed for human FT (Wade *et al.*, 1991). Another peak shown by DLS suggested higher aggregation of apoFT, which was greater than 200 nm in size due to quick reaggregation of apoFT after passage through a filter membrane and its nonspherical shape that caused incorrect diffusivity in solution.

It was demonstrated that horse spleen apoFT declustered under acidic conditions (pH < 3.0), in which the 24-subunit cluster was dissociated into smaller subunits. At least 1 mg/mL samples are required to exceed detection limits of the Zetasizer Nano ZS instrument. The horse spleen apoFT solutions are prepared in a solution containing 200 mM NaCl and 10% glycerol to stabilize subunit dissociation under acidic pH. The slow declustering and reclustered processes are best performed by use of protein dialysis as opposed to direct acid/base titration of the sample. This information will be used and the time for declustering and reclustered steps will be considered for bFT declustering and reclustered experiments.

CHAPTER 3: OVEREXPRESSION AND PURIFICATION OF FERROXIDASE CENTER- AND HEME-FREE BACTERIOFERRITIN

3.1: Literature Research on the Ferroxidase Center- and Heme-free Bacterioferritin

The amino acid residues that are directly involved in the *E. coli* ferroxidase center are Glu18, Glu51, His54, Glu94, Glu127 and His130, while the residue that forms an interaction with the heme moiety is Met52. It was found that mutations of Glu18 to Ala (Glu18→Ala or E18A), Glu51→Ala (E51A), Glu94→Ala (E94A), Glu127→Gln (E127Q), and His130→Glu (H130E) have greatly reduced abilities to store iron and to maintain Fe(II) oxidation activities with no significant affect on the heme environment (Le Brun *et al.*, 1995; Yang *et al.*, 2000; Stillman *et al.*, 2003; Baaghil *et al.*, 2003). It was also found that the E18A mutated protein forms an iron core more slowly than the E94A mutant (Keech *et al.*, 1997). The heme-free bFT can be generated by the replacement of Met52 to Leu (M52L). From site-directed mutagenesis studies, it was found that there were no major differences observed in the overall rate of iron accumulation for M52L compared to wild-type bFT (Andrews *et al.*, 1995). Although the assembly of bFT at physiological pH is not affected by the lack of heme, the iron content of bFT-M52L is at least four times greater than that of wild-type bFT (bFT-WT) (Andrews *et al.*, 1995). The substitution of Met52 might have an affect on the coordinating ability of Glu51, the adjacent residue that provides a carboxylate side chain bridging the two divalent metal ions bound to the ferroxidase center (Figure 1.15). Besides, kinetic studies have shown that heme plays no role in oxygen uptake and iron oxidation (Yang *et al.*, 2000), but bound heme to FT does increase the rate of iron release as observed in a reductive assay system (Kadir *et al.*, 1992).

In order to perform encapsulation experiments with bFT, the iron core must be empty before adding guest molecules into the cavity. There are several methods to empty the iron core including utilization of low concentrations of denaturants such as 1 M urea (Liu *et al.*, 2003), reduction with various thiols such as thioglycolic acid followed by dialysis (Price and Joshi, 1983; Funk *et al.*, 1985; Pead *et al.*, 1995), and mutagenesis of residues involved in pore formation (Jin *et al.*, 2001). Under mild conditions that can be used for subunit declustering (please see Chapter 2) such as low concentration of denaturants or low pH can also apply to iron release. Frequently, literature applications use reducing agents such as ascorbate to reduce Fe(III) stored in the iron core to Fe(II) followed by using an iron chelator such as ferrozine to capture free Fe(II) ions that migrate through the protein channels (Moore *et al.*, 1992b; Lauthère and Briat, 1993; Stookey, 1970). However, these methods were selected for their ability to restore protein quaternary structure after iron release.

In this thesis, the ferroxidase- and heme-ligands in bFT were mutated to examine the effect of the presence of iron atoms and heme molecules on the formation of the 24-subunit cluster. Ferroxidase-free bFT (bFT-E18A/E94A) and heme-free bFT (bFT-M52L) were generated by site-directed mutagenesis. The combination of these two mutants (bFT-E18A/M52L/E94A) yielded ferroxidase- and heme-free bFT. All these bFT variants were then purified using heat denaturation, ammonium sulfate precipitation, and gel filtration chromatography (Superose 6) to investigate how iron core and/or heme groups affect protein stability (Deeb and Hager, 1978; Andrews *et al.*, 1993). As well, other single mutations (bFT-E18A, bFT-E94A, and bFT-M52L) and double mutations (bFT-E18A/E94A, bFT-E18A/M52L, and bFT-M52L/E94A) were also generated to increase our understanding of the ability of the triple mutant to remain a stable 24-subunit protein. Control experiments varying

salt concentration, types of salt, protein concentration, and pH were performed to determine the most suitable conditions for protein purification.

3.2: Reagents, Materials, and Equipment

Reagents and Materials

All reagents and materials used in this section of the thesis are listed below otherwise they are included in Chapter 2.

Salts were obtained from various companies such as sodium bicarbonate (NaHCO_3) from EMD Pharmaceuticals (Durham, NC), ammonium sulfate ($(\text{NH}_4)_2\text{SO}_4$) from BHD (Toronto, ON), calcium chloride (CaCl_2) from Fisher Scientific (Nepean, ON), and sodium azide (NaN_3) from Sigma Chemical Company (St. Louis, MO).

Acid-base reagents acquired from Fisher Scientific (Nepean, ON) were as follows: phosphoric acid, glacial acetic acid ($\text{CH}_3\text{CO}_2\text{H}$), and ethylenediamine tetraacetic acid (EDTA). Trichloroacetic acid (TCA) was obtained from EMD Pharmaceuticals (Durham, NC).

General reagents such as Tris-OH (2-amino-2-(hydroxymethyl)-1, 3-propanediol-hydroxide) was obtained from VWR (Mississauga, ON), acetone was supplied from EMD Pharmaceuticals (Durham, NC), and ethidium bromide and β -mercaptoethanol were from Sigma Chemical Company (St. Louis, MO).

Microbiological reagents acquired from EMD Pharmaceuticals (Durham, NC) were as follows: trypton, yeast extract, and isopropyl- β -D-thiogalactopyranoside (IPTG).

GE Healthcare (Piscataway, NJ) provided sodium dodecyl sulfate polyacrylamide gel electrophoresis (SDS PAGE) gel and buffer stripes. Agarose was obtained from EM Science (Gibbstown, NJ).

Antibiotic ampicillin (Amp) was obtained from Sigma Chemical Company (St. Louis, MO), and carbenicillin (Carb) was obtained from EMD Pharmaceuticals (Durham, NC).

The 100 bp DNA ladder and all restriction enzymes including T4 DNA ligase, *NdeI* and *XhoI* were obtained from New England Biolabs (Beverly, MA), while PWO DNA polymerase was provided by Roche Diagnostics (Laval, QC).

Bovine serum albumin (BSA) was obtained from Sigma Chemical Company (St. Louis, MO). Hen egg white lysozyme was obtained from ICN Biochemicals, Inc. (Costa Mesa, CA). Bio-Rad protein standard for gel filtration chromatography (thyroglobulin, γ -globulin, ovalbumin, myoglobin, and vitamin B₁₂ with molecular weight 670, 158, 44, 17, and 1.35 kDa, respectively) was received from Bio-Rad laboratories (Hercules, CA). Low molecular weight calibration kit for SDS electrophoresis (phosphorylase b, albumin, ovalbumin, carbonic anhydrase, trypsin inhibitor, α -lactalbumin with molecular weight of 97, 66, 45, 30, 20.1, and 14.4 kDa, respectively) was obtained from GE Healthcare (Piscataway, NJ).

Coomassie brilliant blue G-250 was obtained from Eastman Kodak Co. (Rochester, NY), while Coomassie brilliant blue R, and bromophenol blue were supplied from Sigma Chemical Company (St. Louis, MO).

SuperoseTM 6 10/300 GL column was obtained from Amersham Biosciences (now GE Healthcare, Piscataway, NJ). DNA manipulation including DNA purification, DNA digestion, and DNA ligation was performed under construction from QIAprep Spin Miniprep Kit (QIAGEN, Mississauga, ON). Dialysis tubing used in all experiments was Spectra/Por[®] molecular porous membrane with 12-14 kDa molecular weight cutoff (Spectrum laboratories, Inc., Rancho Dominguez, CA). The 0.22 μ m GV filter membrane 0.45 μ m HV filter membrane were obtained from Millipore (Billerica, MA).

Equipment

A Sonicator™ cell disruptor (model W225) with converter model #2 and a standard tapered microtip with the output control set at 5 (Heat Systems-Ultrasonics, Inc., Plainview, NY) was used for cell wall disruption of crude cell extracts in protein purification.

The large volume centrifugation in protein purification steps was performed using a Avanti® J-E Centrifuge from Beckman Coulter, Inc. (Palo Alto, CA), while small volume samples (sample that fits into microcentrifuge tubes) were centrifuged in a tabletop Biofuge A microcentrifuge at 13 000 rpm (Heraeus Sepatech GmbH, Germany).

A fast peptide and protein liquid chromatography (FPLC®) system from Pharmacia (now GE Healthcare, Piscataway, NJ) having a LCC-500 chromatography controller, two P-500 pumps, MV-7 motor valve, UV-M monitor, and REC-482 chart recorder was used to purify protein samples and to test for protein quaternary structure.

A spectrophotometric scanning for confirmation of heme-binding proteins, and optical density reading at the specific wavelength for DNA and protein concentration measurements were performed using a Varian Cary 3 spectrophotometer (Mississauga, ON) with associated software package (designated version 3.04).

Electrospray mass spectrometer used in this thesis was a Micromass Q-TOF Ultima™ Global and supplied by the Waterloo Chemical Analysis Facility, University of Waterloo.

Cell growth for protein expression and induction was performed by using an incubator shaker (series 25) from New Brunswick Scientific Co., Inc. (Edison, NJ) at 220 rpm 37 °C. Antibiotic agar plates for bacterial growth were incubated at 37 °C using a Precision® gravity convection incubator from Precision Scientific, Inc. (Chicago, IL).

All polymerase chain reactions were performed using a Techne (TC-512) Thermal Cycler from Techgene, Inc. (Princeton, NJ).

3.3: Experimental Protocols

3.3.1: Protocols for Control Experiments

The protein was prepared and filtered through a 0.2 μm -pore filter membrane before performing fast peptide and protein liquid chromatography using a SuperoseTM 6 10/300 GL column to separate globular proteins with molecular weight between 5000- 5×10^6 Da. The Superose 6 column was washed with Milli-Q water for 2 hours and sample buffer for another 2 hours before sample loading. The FPLC lamp was warmed up 1 hour prior to sample injection. The samples were filtered through 0.2 μm GHP membrane filters before injecting into a 100 μL loading loop. The pressure was set to 1 MPa (maximum 1.5 MPa) and the flow rate was set to 0.5 mL/min (maximum 1 mL/min). Eluted fractions were collected immediately after the flow was started with sample buffer. After collecting the eluted sample (~ 1 column volume), the column was washed again with sample buffer for 2 hours and continued washing with Milli-Q water for another 2 hours. At this stage, the column could be kept at 4 $^{\circ}\text{C}$ for 1-2 days. To store the column at room temperature, after washing with water the column was washed with 20% ethanol for 2 hours. All buffers and water were filtered either through a 0.22 μm GV filter membrane (for aqueous solution) or a 0.45 μm HV filter membrane (for organic solution) and degassed before use.

Eluted fractions from Superose 6 gel filtration chromatography were visualized by staining of SDS PAGE gels. However, due to low protein concentrations, each eluted fraction was concentrated using TCA precipitation. A mixture of 100 μL of the sample and 100 μL of

20% TCA was vortexed before incubating on ice for 30 min and centrifuging at 13 000 rpm for 15 min at 4 °C using Beckman JA-14 rotor. The collected pellet was washed with 300 μ L acetone and centrifuged for 5 min. The protein pellet was collected by evaporating the acetone under a fume hood.

SDS PAGE was run using a semi-automated electrophoresis apparatus, Pharmacia PhastSystemTM, to separate and visualize proteins in collected fractions. A sample was prepared by dissolving a protein pellet with 10 μ L of loading buffer (150 mM Tris-OH, 2% SDS, 1% β -mercaptoethanol, 10% glycerol, 0.1% Bromophenol blue pH 8.0). The mixture was boiled for 10 min and centrifuged at 13 000 rpm for 30 seconds before loading onto a 8-25% acrylamide gel containing SDS. A staining solution (0.1% Coomassie brilliant blue R, 30% methanol, 10% acetic acid) was used to stain the gel for 2-3 hours before destaining overnight with destaining solution (30% methanol and 10% acetic acid). Then the gel was incubated with a solution containing 5% glycerol and 10% acetic acid to preserve the gel.

The molecular weight (MW) was calculated using Bio-Rad protein standards for Superose 6 gel filtration chromatography, where standard calibration curves of logarithm of molecular weight versus the ratio of elution volume minus void volume to total bed volume minus void volume were plotted (Appendix 7). Superose 6 chromatograms and normalized graphs of proteins in different stability conditions were plotted and analyzed. The control experiments included the effect of salt concentration, type of salt, protein concentration, and pH. All experiments were performed similarly except for the following details.

Effect of Salt Concentration

Three salt concentrations were used to investigate the effect of salt on protein stability and quaternary structure. Horse spleen apoFT (1.35 mg/mL) was diluted into buffer containing 20 mM Tris-OH (pH 8.0) with various concentrations of NaCl (100, 150, and 200 mM). These buffers were also used as running buffer for gel filtration chromatography.

Effect of Salt Type

The 3.35 mg/mL bFT solution was diluted in either buffer containing 20 mM Tris-OH (pH 8.0) and 100 mM NaCl or buffer containing 20 mM Tris-OH (pH 8.0) and 100 mM KCl, which were used as running buffers in gel filtration chromatography.

Effect of Protein Concentration

Lower protein concentrations of 0.34, 0.68, and 1.35 mg/mL horse spleen apoFT in buffer containing 20 mM Tris-OH (pH 8.0) and 100 mM NaCl were prepared before performing gel filtration chromatography to study the effect of protein concentration on the stability of the 24-subunit cluster. Higher protein concentrations were studied using bFT. The 1.35 and 3.35 mg/mL bFT were prepared under the same conditions as horse spleen apoFT as above.

Effect of pH

Two buffers with different pH were investigated by preparing 3.35 mg/mL bFT in (1) buffer containing 20 mM Tris-OH (pH 7.0) and 100 mM NaCl and (2) buffer containing 20

mM Tris-OH (pH 8.0) and 100 mM NaCl. Both buffers were also used as running buffers for gel filtration chromatography.

3.3.2: Protein Engineering

Preparation of Luria-Bertani Media

Luria-Bertani (LB) media was prepared by dissolving 10 g tryptone, 5 g yeast extract, and 5 g NaCl in 1 L distilled deionized water (ddH₂O).

Antibiotic Agar Plate Preparation

Antibiotic agar plates were prepared by dissolving 3 g agar in 250 mL LB in a warm water bath. The mixture was cooled down to ~37 °C before adding 100 µg/mL ampicillin. The solution was then poured onto plastic petri plates, and the gel was allowed to settle for 2-3 hours before being stored at 4 °C.

Preparation of Competent Cells

The stock cell lines (*E. coli* strains DH5 α for cloning processes and BL21 (DE3) for protein expression) were inoculated in LB (3 mL) and shaken at 220 rpm overnight at 37 °C. The culture was transferred to 100 mL LB and shaken until a cell density of OD₆₀₀ was reached 0.4-0.6. The cell pellet was collected by centrifugation (5 min at 4 000 rpm) before resuspension in 50 mL ice-cold 50 mM CaCl₂. The mixture was kept on ice for 30 min and centrifuged for another 5 min at 4 000 rpm to collect the cell pellet, which then was resuspended in 10 mL of 50 mM CaCl₂ containing 15% glycerol. The competent cells were then kept on ice for 4 hours before being stored at -80 °C.

Site-directed Mutagenesis, DNA Manipulation, and Cloning

Site-directed mutagenesis was performed on pT7bFT, the stock plasmid generated from the insertion of the bFT encoding gene into the pET-22b(+) plasmid (Novagen, Mississauga, ON) (generated by Dr. Elisabeth Daub and Liz Gargatsougias, the Honek Lab, 2004) by utilization of the polymerase chain reaction (PCR). The complement primers were obtained from Sigma-Genosys Canada (Oakville, ON) and were designed as in Table 3.1. The mutation was generated by the QuikChange[®] Site-Directed Mutagenesis method, where complementary primers were used to extend each strand of the vector in its entirety while incorporating the codon for the desired amino acid substitution. PCR reagents and plasmids were set up as in Table 3.2 and programmed as in Table 3.3. Standard DNA manipulation and bacterial cloning were performed as stated using standard molecular biology protocols (Sambrook *et al.*, 1989). PCR plasmids were digested with *DpnI* restriction enzyme that was specific to methylated DNA before heat shock transforming into competent *E. coli* cells (strain DH5 α) followed by growth on Amp containing agar plates overnight at 37 °C. A single colony was picked and inoculated overnight with 5 mL LB containing Amp (50 μ g/mL LB) at 37 °C in a 220 rpm shaker. Plasmid purification was performed using a QIAprep Spin Miniprep Kit.

The concentration of purified DNA was calculated by measuring the OD₂₆₀, in which one unit optical density at OD₂₆₀ was approximately 50 μ g/mL of DNA. DNA samples were sent for sequencing when appropriate (Mobix Central facility, DNA Synthesis Laboratory, The Institute for Molecular Biology and Biotechnology, McMaster University, Hamilton, ON). The determined DNA sequences were compared with that of wild-type bFT using BLAST2 program (Tatusova and Madden, 1999) to check and confirm successful mutagenesis.

The purified plasmid was used for generating double and triple mutations by repeating the site-directed mutagenesis steps. The double mutation, bFT-E18A/M52L, was generated using bFT-E18A as the host plasmid with bFT-M52L.For and bFT-M52L.Rev oligonucleotides as primers. The DNA for bFT-E18A/E94A was generated similarly. The plasmid generated for bFT-M52L/E94A used bFT-M52L as host plasmid and bFT-E94A.For and bFT-E94A.Rev as primers. The triple mutation, bFT-E18A/M52L/E94A, was generated using double mutation, bFT-E18A/E94A, as host plasmid and bFT-M52L.For and bFT-M52L.Rev as primers. The protocols are summarized in the flow chart in Appendix 1.

All single, double, and triple mutations were generated using the QuikChange[®] Site-Directed Mutagenesis method except for the bFT-E94A mutation. This single mutation was generated by digesting bFT-E18A/E94A and bFT-WT plasmids with *BsmI* and *HindIII* restriction enzymes at 37 °C for 3 hours. Digested DNA was mixed with sample buffer provided by New England Biolabs (Beverly, MA) before loading to 1% agarose gel, which was prepared by dissolving agarose (1 g) with 100 mL TAE (Tris-acetate-EDTA buffer containing 40 mM Tris-OH (pH 8.0), 20 mM glacial acetic acid, and 1 mM EDTA) with the addition of 10 µL of ethidium bromide, poured into a plastic chamber and allowing the gel to settle. The agarose gel was run at 100 V for approximately 2 hours before visualization under UV light. The bands containing the desired DNA were cut and plasmid purification was performed using a QIAprep Spin Miniprep Kit. Ligations were performed using T4 ligase enzyme (3 hours at 14-16 °C) to insert the E94A fragment into the bFT-WT plasmid. Plasmid DNA was transformed into heat shocked *E. coli* cells (strain DH5α) followed by visualizing similar cloning protocols as other variants generated by PCR (Appendix 2).

Table 3.1: The forward and reverse primers used to generate each mutation by site-directed mutagenesis.

Mutation	Primer name	Sequence of primer (5' to 3')
bFT-E18A [†]	bFT-E18A.For bFT-E18A.Rev	CTG TTG GGA AAT GCG [‡] CTT GTC GCA ATC GAT TGC GAC AAG CGC ATT TCC CAA CAG
bFT-M52L [†]	bFT-M52L.For bFT-M52L.Rev	CC ATT GAT GAG CTG AAA CAC GCC G C GGC GTG TTT CAG CTC ATC AAT GG
bFT-E94A [†]	bFT-E94A.For bFT-E94A.Rev	GAT CTG GCA CTT GCG CTG GAT GGC GCG CGC GCC ATC CAG CGC AAG TGC CAG ATC

[‡] The bold-italics indicate the codons modified to obtain the desired amino acid substitutions.

[†] The melting temperature (T_m) for bFT-E18A primers is 61 °C, for bFT-M52L primers is 59 °C, and for bFT-E94A primers is 67 °C.

Table 3.2: PCR recipe for bFT variants except bFT-E94A derived from QuikChange[®] Site-Directed Mutagenesis Instruction Manual from Stratagene (La Jolla, CA).

Plasmids/Reagents	Stock Concentration	Amount Used (μL)	Final Concentration
DNA	a	x	20 ng
Primer.For	1 μ M	5.0	1 pmol
Primer.Rev	1 μ M	5.0	1 pmol
dNTP	10 mM	1.0	0.2 mM
PWO Buffer	10 \times	5.0	
Mg ²⁺	25 mM	y	b
ddH ₂ O		z	
PWO polymerase		0.5	
Total		50.0	

a depends on efficiency of plasmid purification and b depends on amount of Mg²⁺ used.

x depends on DNA stock concentration and will yield same final concentration of 20 ng DNA.

y is variable, which normally was 1, 2, or 3 μ L (0.5 mM, 1.0 mM, and 1.5 mM, respectively) used to maximize PCR products.

z is amount of distill water (ddH₂O) used to fulfill the final PCR volume (50 μ L).

Table 3.3: PCR Programming protocols for QuikChange[®] Site-Directed Mutagenesis method.

Steps	Temperature (°C)	Time	
Initial Denaturation [†]	95	5 min	
Hot Start [‡]	85		
Denaturation	95	30 sec	} Repeat 16 cycles
Annealing*	55	1 min	
Elongation	72	10 min	
Final Extension	72	10 min	
Hold	4		

[†] Initial denaturing temperature was used to ensure DNA template denaturation.

[‡] Hot start was used to maintain the temperature at 85 °C during adding PWO DNA polymerase to minimize self annealing of primers.

* Annealing temperature was altered depending on the T_m of the primers (~6 °C lower than T_m) i.e. annealing temperature for generating bFT-E18A, bFT-E18A/M52L, bFT-E18A/E94A, and bFT-E18A/M52L/E94A is 55 °C, for bFT-M52L is 53 °C, and for bFT-M52L/E94A is 60 °C.

3.3.3: Protein Expression, Induction, and Purification

The purified plasmid was heat shock transformed into competent *E. coli* cells (strain BL21 (DE3)), and the transformed cells were grown on agar plates containing Amp (overnight at 37 °C). Single colonies of *E. coli* cells containing desired plasmids were picked and inoculated overnight with LB (5 mL) containing Amp (50 µg/mL LB) at 37 °C incubator shaker (shaken at 220 rpm). The culture was then transferred into 1 L LB containing 40 µg/mL carbenicillin and allowed to grow for 3 hours at 37 °C with shaking (220 rpm or until OD_{600} reached 0.6). The proteins were induced by addition of 1 mM IPTG, and shaking was continued at the same speed for 3 hours. The culture was then centrifuged (10 000 g for 10 min) using Beckman JA-14 rotor. The supernatant was discarded, and the remaining pellet was resuspended in a minimal volume of buffer containing 20 mM Tris-OH (pH 8.0) and 0.5 M NaCl before centrifugation at 15 000 g for an additional 10 min. The cell pellet was then collected and flash frozen in liquid nitrogen before storing at -80 °C.

The frozen pellet was resuspended in buffer containing 20 mM Tris-OH (pH 8.0) with the addition of 1 mg/mL hen egg white lysozyme. The temperature shock by placing the suspension in liquid nitrogen and then warm water immediately (repeated 5 times) was used to rupture the cells. Heat denaturation was used for deactivation of lysozyme and was performed by warming the suspension in a water bath (60-70 °C) for 15 min before cooling to 4 °C. Sonication was performed at the same temperature (4 °C) for 15-20 rounds (10 sec each) using Sonicator™ cell disruptor. The suspension was then centrifuged at 20 000 rpm for 15 min using a JA-25.50 rotor. The pellet was discarded, while the supernatant was heated in a hot water bath (60-70 °C) for 15 min followed by cooling to 4 °C to eliminate *E. coli* proteins before continuing centrifugation at the same speed and time to collect the supernatant. *E. coli* proteins in this supernatant were eliminated by slow addition of a 25% (w/v) ammonium sulfate solution on ice followed by centrifugation at 15 000 g for 30 min. The supernatant after this centrifugation contained bFT, which was collected by addition of a 40% (w/v) ammonium sulfate solution on ice and centrifuged at 15 000 g for 30 min. The protein pellet was solubilized by dialysis for 2 days against 20 mM Tris buffer (pH 8.0) which contained 100 mM NaCl (dialysis buffer was changed twice) using a 12-14 kDa cutoff dialysis membrane, which was prepared as follows. In order to eliminate other chemicals that might contaminate the protein during the preparation, the dialysis tubing was boiled in a wash solution (300 mL ddH₂O, 6 g NaHCO₃, and 150 mg EDTA) for 10 min, then rinsed with ddH₂O several times. The clean dialysis tubing was then stored at 4 °C in Milli-Q water containing 0.02% sodium azide to prevent bacterial growth. The overall protein purification is shown as a flow chart in Appendix 3.

The existence of the proteins was confirmed by mass spectrometry (MS). In order to determine their molecular weight by positive ion mode-electrospray mass spectrometry, the samples were prepared by exchanging sample buffer with Milli-Q water using Nanosep[®] Centrifugal devices with 10K molecular weight cutoff (PALL, East Hills, NY). The samples were then diluted into a solution containing 50/50 acetonitrile/water with 0.2% formic acid in the ratio of 1:1 before injecting into the mass spectrometer.

The Bradford assay was used to determine protein concentration (Bradford, 1976). Bradford dye was prepared by dissolving 100 mg Coomassie Brilliant Blue G-250 with 50 mL 95% ethanol. Then 100 mL of 85% (w/v) phosphoric acid was added to the solution, which was then diluted to 0.5 L with ddH₂O. The solution was mixed and added up to 1 L with ddH₂O before filtering through Whatman#1 filter paper. The reference sample was prepared by diluting 10 mg/mL BSA to 1 mg/mL with the same buffer as the unknown samples. The Bradford assay standard curves were plotted (OD₅₉₅ vs. BSA concentrations) by preparing triplicate sets of different concentrations of BSA (0, 5, 15, 25, 35, 45 μL). Each standard sample was made up to 50 μL with sample buffer before addition of 2.5 mL of dye solution. The solution was vortexed, and absorption at 595 nm was measured using spectrophotometry. Bradford assays for samples were performed similarly to standard samples. The protein concentration was calculated by comparing OD₅₉₅ values with those of Bradford assay standard curve values.

Heme-binding was investigated using spectroscopic methods. The protein samples were prepared by filtering through 0.2 μm-pore filter membranes before loading onto 1 mL quartz cuvettes. Absorption was scanned from 300-600 nm at room temperature. The values of absorption versus wavelength were plotted. The comparison between wild-type bFT and

each bFT variant's chromatograms demonstrated the absorption of heme groups present in the mutant bacterioferritin.

Gel filtration chromatography (Superose 6) was used for further purification and investigation of protein stability (ability to maintain 24-subunit clusters for bFT wild-type and variants). The protein samples were diluted with running buffer containing 20 mM Tris-OH (pH 8.0) and 100 mM NaCl to 1.35 mg/mL before filtering through a 0.2 μ m-pore filter membrane. The running buffer was filtered through a 0.22 μ m GV filter membrane and degassed before use. To detect proteins presented in each eluted peak, Superose 6 fractions were concentrated by TCA precipitation before visualization by dye staining of SDS PAGE gels. The molecular weight was calculated using a Bio-Rad protein standard plot for gel filtration chromatography. This MW was related to protein size and its conformation (i.e. MW with two times greater than that of literature subunit MW represented dimeric subunits). The normalized Superose 6 gel filtration chromatograms of bFT-WT and bFT variants were also plotted to demonstrate the overlap of eluted peaks that contained similar protein quaternary structure. For the triple mutant, bFT-E18A/M52L/E94A, the eluted 2-subunit and 24-subunit fractions from Superose 6 gel filtration chromatography were concentrated by centrifuging at 10 000 rpm using Nanosep[®] Centrifugal devices with 10K molecular weight cutoff until reaching minimal volume (~300 μ L). The concentrations of these concentrated proteins were measured using the Bradford assay. The protein samples were then reloaded onto Superose 6 to test for 2-subunit and 24-subunit stability.

3.4: Results and Discussion

3.4.1: Control Experiments

Effect of Salt Concentration

Superose 6 gel filtration chromatograms of commercial apoFT in various salt concentrations contained two peaks, which eluted at the time ~25 and 29 min (Figure 3.1). The MW calculation from the Bio-Rad protein standard plots for gel filtration chromatography was used to determine that peak 1 consisted of self-associated cluster of apoFT with MW ~1000 kDa and peak 2 was the native 24-subunit containing native protein (MW ~330 kDa). The comparison of these chromatograms showed that salt concentrations between 100-200 mM possessed similar effects on protein quaternary structure (Figure 3.2). Since the MW of the 24-subunit apoFT in buffer containing 100 mM NaCl was similar to that of the literature (~440 kDa), then buffer conditions might be appropriate to stabilize the 24-subunit cluster protein (Table 3.4).

A small difference in MW between experimental and literature protein suggested possible interference of salt with the interaction between the protein and resin in Superose 6 column. It was found that nitric reductase behaved similarly (smaller MW determined by gel filtration chromatography than MW estimated by other methods), in which the authors suggested that gel filtration was not suitable for the MW determination and the MW could not be used to determine the behavior of the macromolecules upon gel filtration (Husain and Sadana, 1974). In addition, the plot of MW versus relative mobility measured by SDS PAGE was used to evaluate MW (Husain and Sadana, 1974). It was also suggested that the gel filtration chromatography could be used to determine Stokes radius (Husain and Sadana, 1974; Siegel and Monty, 1966). By plotting the graph of Stokes radius versus elution volumes of

protein standards, the Stokes radius of protein sample could be predicted. It is showed that by plotting experimental elution volume of protein standards with their known Stokes radius (Appendix 7) (Qasim and Salahuddin, 1979; Andrews, 1970; Cui *et al.*, 2002; Husain and Sadana, 1974; Siegel and Monty, 1966), the experimental Stokes radius of apoFT (14.5 mL elution volume) is 62.8 Å, which corresponds to that of the literature (67.1 Å Stokes radius) (De Haën, 1987). By using the combination of the Stokes-Einstein and Svedberg equations and literature sedimentation coefficient (17S) (Notides and Williams-Ashman, 1967; Rothen, 1944) (calculation is shown in Appendix 7), it is found that the calculated molecular weight of 24-subunit apoFT is 446 kDa. It was also found that the literature elution volume of FT is 14.82 mL determined by Superose 6 gel filtration chromatography (14.5 mL elution volume for apoFT) (Chilkova *et al.*, 2003). Therefore, from this data it is suggested that the experimental elution volume at ~29 min (14.5 mL) corresponds to the 24-subunit protein. It is also suggested that the low MW of protein samples determined by Superose 6 gel filtration chromatography might be shape dependence, in which the protein samples loading into the Superose 6 column might possess packed quaternary structures (smaller size than the native proteins), causing smaller MW than that of the literature MW. In addition, if the sedimentation coefficient is known (with the uses of the plot of Stokes radius versus elution volume and the combination of the Stokes-Einstein and Svedberg equations), then the correct MW of bFT can be calculated. However, Superose 6 gel filtration chromatography can be used to demonstrate a degree of protein quaternary structures, even though their MW is not correct.

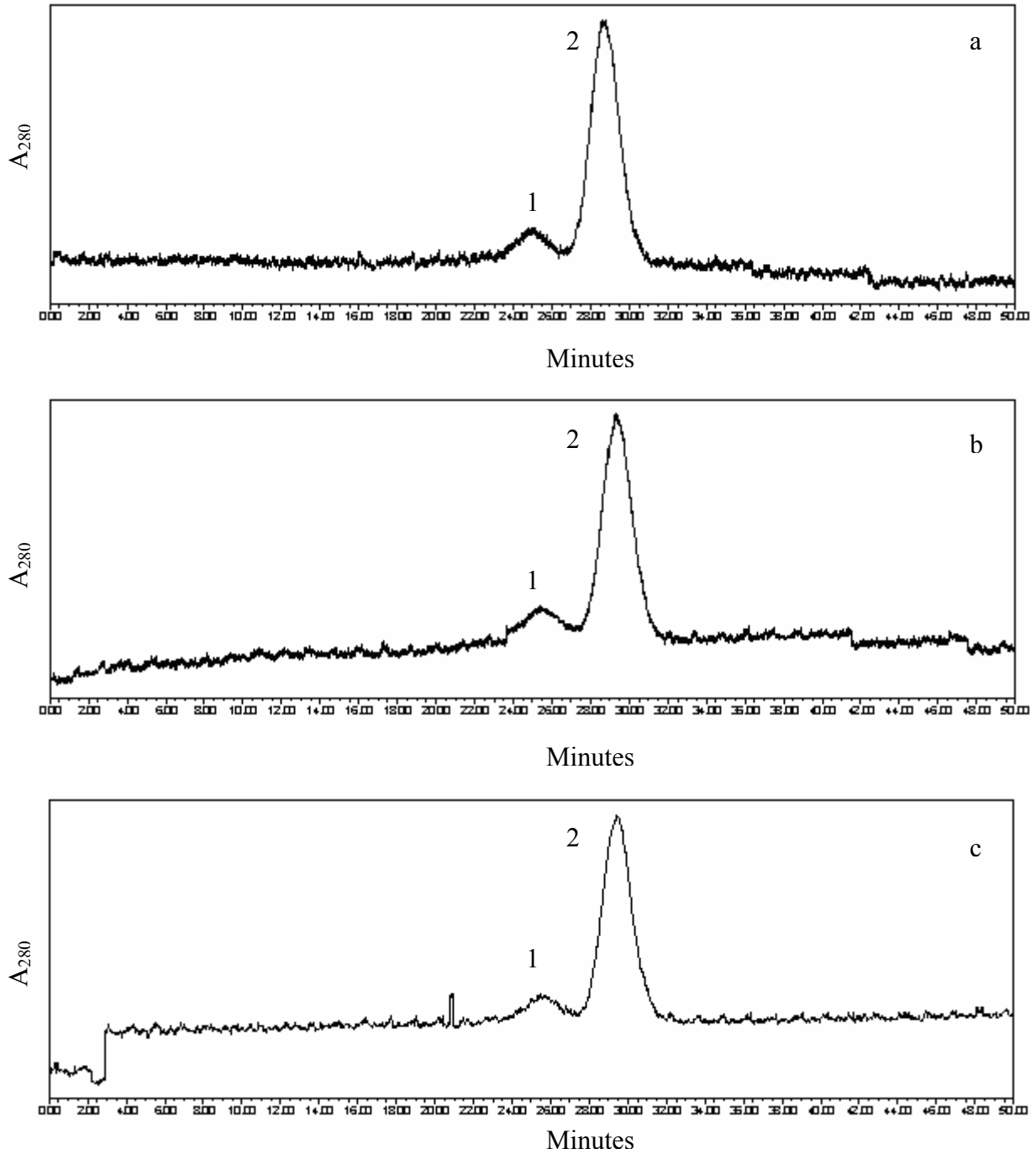


Figure 3.1: Superose 6 gel filtration chromatograms of 1.35 mg/mL apoFT in buffer containing 20 mM Tris-OH (pH 8.0) and either 100 mM (a), or 150 mM (b), or 200 mM (c) NaCl show two peaks of eluted protein, which are marked as peak 1 and peak 2.

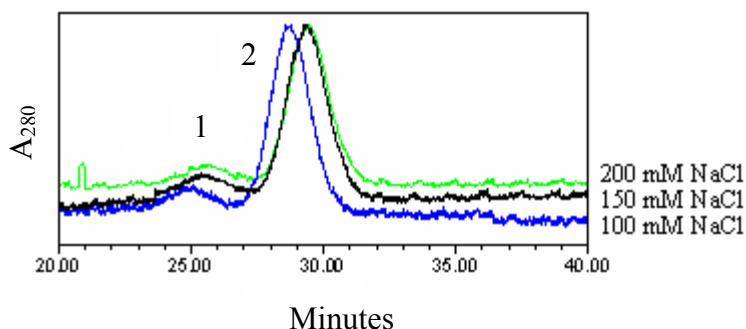


Figure 3.2: Normalized Superose 6 gel filtration chromatograms of apoFT in 20 mM Tris-OH (pH 8.0) containing 100 mM (blue), 150 mM (black), or 200 mM (green) NaCl. The molecular weight of peak 1 and 2 are shown in Table 3.4.

Table 3.4: The molecular weight of each eluted peak of Superose 6 gel filtration chromatography varies under different salt concentrations.

[NaCl] (mM)	Molecular weight (kDa)	
	Peak 1	Peak 2
100	1034	359
150	1034	334
200	898	312

Effect of Salt Type

Different types of salts might generate particular effects on protein quaternary structure and/or interaction between protein and Superose 6 resin due to ion characteristics such as charge, size, and electrostatic properties. Superose 6 gel filtration chromatograms of bFT-WT in Tris buffer (pH 8.0) containing two types of salts, NaCl and KCl, showed the overlap of 24-subunit peaks (Figure 3.3). Since this protein was experimentally purified, it might contain smaller subunit combinations of bFT that are observed as eluted peaks after 35 min. The MW of the 24-subunit bFT-WT in buffer containing NaCl was 250 kDa, while that of protein in buffer containing KCl was 231 kDa. Since the MW of the protein in buffer containing NaCl is

closer to that of the literature, NaCl might be a better choice of salt to stabilize the 24-mer quaternary structure than KCl.

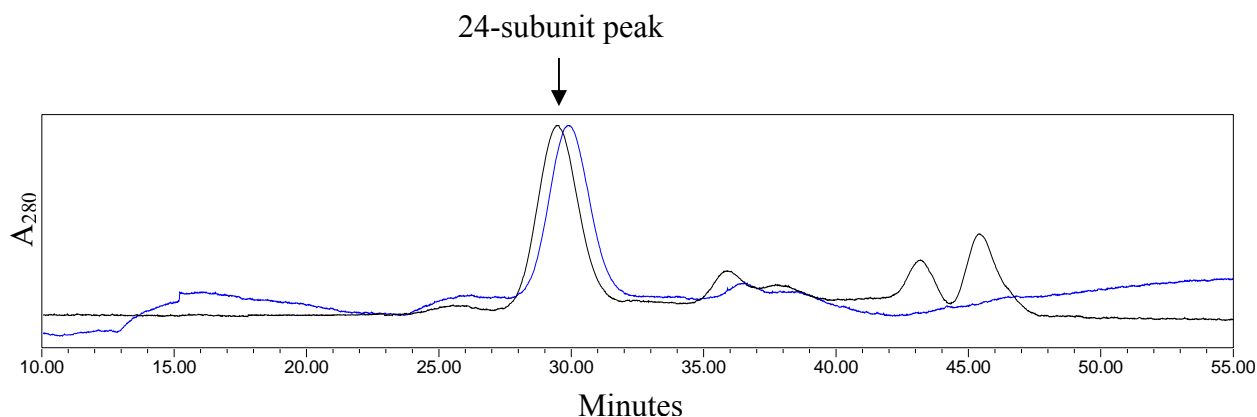


Figure 3.3: The normalized Superose 6 gel filtration chromatograms of 3.35 mg/mL bFT-WT in buffer containing 20 mM Tris-OH (pH 8.0) and either 100 mM KCl (blue) or 100 mM NaCl (black).

Effect of Protein Concentration

It was suggested in the Introduction section of Chapter 2 that protein concentration has an effect on the formation of 24-subunit apoFT (Lee and Richter, 1976). It was shown that the protein concentration is related to stability of the 24-subunit cluster, in which high apoFT concentration yielded a greater amount of 24-subunit formation (Figure 3.4). However, Superose 6 chromatograms and MW calculations for different concentrations of apoFT demonstrated the overlap of 24-subunit peaks with similar MWs (334.6, 335.0, and 359.0 kDa for 0.34, 0.67, and 1.35 mg/mL protein, respectively) (Figure 3.4). A greater amount of self-associated clusters (eluted peak at ~25 min) at higher protein concentration (1.35 mg/mL) suggested strong interaction between clusters with higher possibility to form aggregates. The smaller subunits (eluted peak after 35 min) were not observed even in low protein concentration, indicating stable formation of the 24-subunit cluster of commercial apoFT.

The effects of protein concentration were similar for bFT, where the normalized Superose 6 gel filtration chromatograms of 1.35 mg/mL and 3.35 mg/mL bFT in Tris buffer (pH 8.0) containing 100 mM NaCl represented the overlap of 24-subunit peaks (Figure 3.5). It was confirmed that protein concentration for both apoFT and bFT had similar effects on protein stability, in which a higher protein concentration yielded higher 24-subunit cluster quantities.

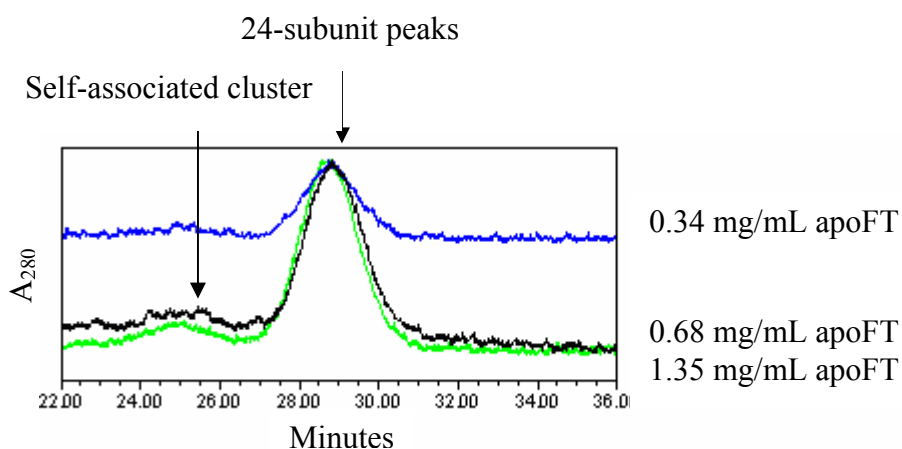


Figure 3.4: The normalized Superose 6 gel filtration chromatograms of 0.34 (blue), 0.68 (black), and 1.35 (green) mg/mL apoFT in buffer containing 20 mM Tris-OH (pH 8.0) and 100 mM NaCl represents the overlap of different intensity of 24-subunit peaks and the formation of self-associated clusters at higher protein concentrations.

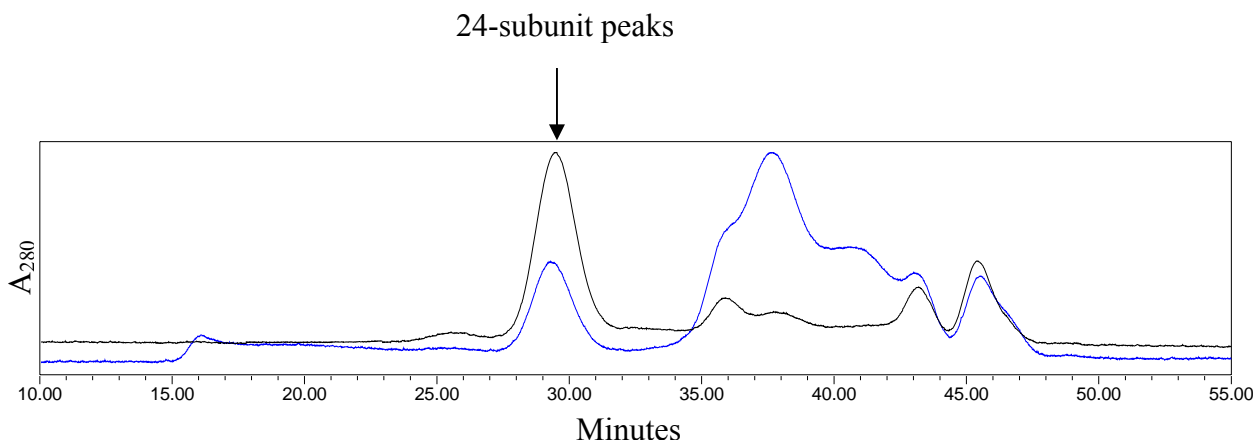


Figure 3.5: The normalized Superose 6 gel filtration chromatograms of 1.35 mg/mL bFT-WT (blue) and 3.35 mg/mL bFT-WT (black) in 20 mM Tris-OH (pH 8.0) and 100 mM NaCl show the overlap peaks of the 24-subunit cluster.

Effect of pH

Buffer at different pHs might influence the protonation of acidic residues in the proteins, which would in turn affect protein-protein interactions and/or protein-resin interactions. Two buffers with pH 7.0 and 8.0 were examined as to how and as to which one would yield higher native protein structure stability. It was shown that protein in both buffers yielded similar 24-subunit peak intensities (MW = 187 and 250 kDa, respectively) (Figure 3.6). Since the MW of the protein in solution at pH 8.0 was closer to that of the literature, this buffer was more suitable for stabilizing the 24-mer quaternary structure than buffer with pH 7.0.

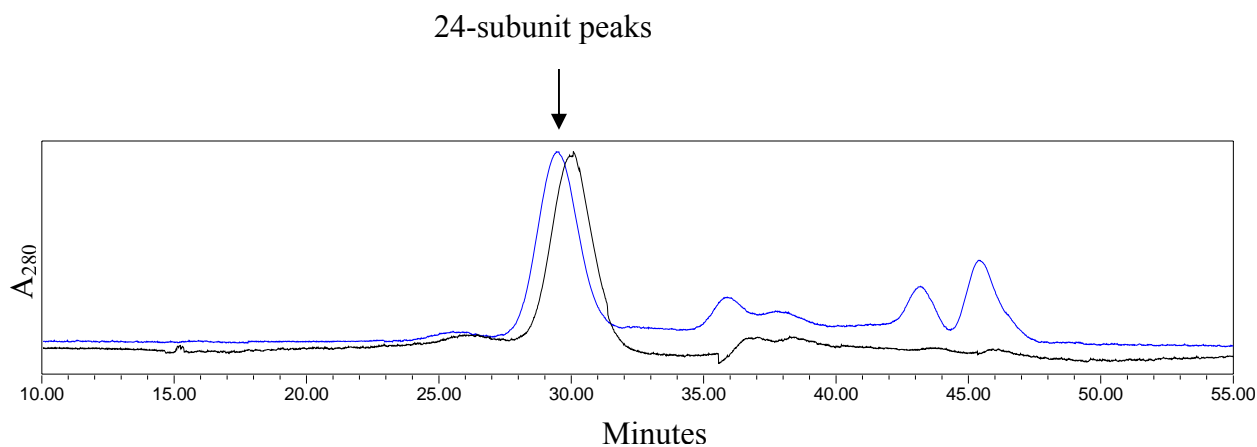


Figure 3.6: The normalized Superose 6 gel filtration chromatograms of 3.35 mg/mL bFT-WT in buffer containing 100 mM NaCl and either 20 mM Tris-OH (pH 8.0) (blue) or 20 mM Tris-OH (pH 7.0) (black).

3.4.2: Cloning of Wild-type and Bacterioferritin Mutants

The results for cloning, all the sequences of wild-type bFT and bFT variants, are presented in Appendix 4. All sequences were compared with the sequence of bFT-WT using the online BLAST2 program (<http://www.ncbi.nlm.nih.gov/blast/bl2seq/wblast2.cgi>), which confirmed successful mutagenesis. The 1% agarose gel of bFT-E94A that was generated by

inserting the E94A fragment into bFT-WT plasmid is shown in Figure 3.7. The digested DNA fragment of bFT-WT was ~5400-base pair (bp) and that of bFT-E18A/E94A was ~300 bp. The inserted fragment was not clearly shown due to its small size. The difficulty of generating this single mutation by QuikChange[®] Site-Directed Mutagenesis method suggested a strong self-secondary structure of the primers even with high annealing temperature (61 °C). Another possibility due to the successful insertion of E94A into bFT-E18A and bFT-M52L by PCR was that bFT-WT DNA might form a strong hairpin or complicated loop at this area (E94), so that it would require higher temperatures for primers to anneal.

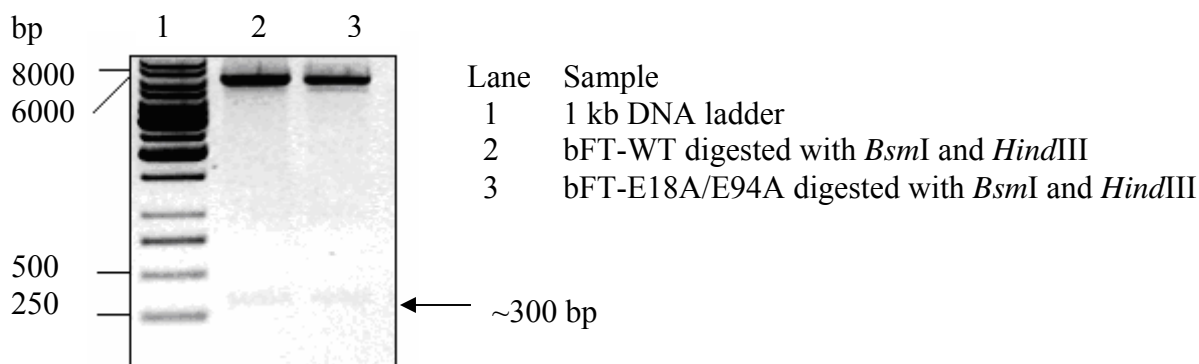


Figure 3.7: The 1% agarose gel illustrates the digestion of bFT-WT and bFT-E18A/E94A with *BsmI* and *HindIII*. The 100 bp DNA ladder is shown (in bp).

3.4.3: Overexpression and Purification of Wild-type and Bacterioferritin Mutants

The purification of wild-type bFT and all variants yielded similar results. The purification protocols were sufficient, yielding pure proteins after a final dialysis step. The most effective method in the purification was found to be the heat treatment at 65-70 °C. Indeed, it would appear that heat stability is a universal property of bFT and FT, possibly reflecting the need for an iron-storage molecule that does not easily denature and release its insoluble iron core in an uncontrolled manner. The example of SDS PAGE of bFT-E18A

showed two bands at 40 and 18.5 kDa (Figure 3.8), which corresponded to the size of a dimer (2 subunits) and a monomer (1 subunit). The 40 kDa MW suggests a strong interaction between two subunits, which could not be completely denatured. It is believed that a dimer subunit is the main multimeric form of the protein compared to other possible oligomers other than the intact 24-mer cluster.

Mass spectrometry of all wild-type and bFT variants support the proper molecular weight of each protein sample, in which MW calculated from the amino acid residues was similar within experimental error to the MW determined by MS (Appendix 5).

UV spectroscopy provided evidence for the presence of heme in the protein samples, in which the absorption peaks at 418, 525, and 560 nm associated with the Soret, β , and α bands of the oxidized heme moiety, respectively, are present (Appendix 6). An example of the UV spectrum from the chromatogram of bFT-WT represents a clearly observed peak at 418 nm and two small peaks at 525 and 560 nm (Figure A6.1). The peak at 418 nm was absent in the chromatogram of bFT without the heme group (i.e. bFT-M52L) (Figure A6.3). The low iron content of overproduced bFT was expected and was presumably due to the increased iron storage capacity of the overproducing strain relative to the cellular iron content.

Superose 6 gel filtration chromatograms of wild-type bFT and all bFT variants were plotted, MW of eluted peaks containing proteins were calculated (using Bio-Rad standard protein plot), and eluted peaks containing proteins were visualized by staining the SDS PAGE gels (Appendix 7). For example, the Superose 6 gel filtration chromatogram of 3.35 mg/mL bFT-WT consisted of six main peaks, which were found to be a self-associated cluster at ~26 min (919 kDa), 24-subunit at 29 min (247 kDa), a dimer at 36 min (27 kDa), and a monomer at 38 min (19 kDa) of the running time (Figure 3.9, Figure 3.10, and Table 3.5). By comparing

this chromatogram with that of apoFT, similar eluted peak at ~29 min from both chromatograms supports the existence of the 24-mer cluster. The molecular weight of the 24-subunit cluster calculated by protein standards was off by approximately 250 kDa (literature MW is 440 kDa), which might be due to similar reasons as those of apoFT as above. It was also shown that 24-subunit was a dominated quaternary structure. The eluted peak at 44 and 46 min (peak 5 and 6 in Figure 3.9) might contain small proteins, nucleic acids, or heme-containing proteins. Spectroscopic analysis of the chromatograms of peak 5 and peak 6 were similar. There were no absorptions at 418 nm, which indicated no heme-binding protein or a low amount of heme-containing protein, which could not be detected by UV (Figure 3.11). A less intense peak at 280 nm suggested low protein concentration in this fraction, while absorption at ~250-260 nm suggested a trace of nucleic acid (Figure 3.12). Therefore, these two eluted peaks might contain low concentration of protein or no protein, in which they might be nucleic acid, small proteins, or peptides.

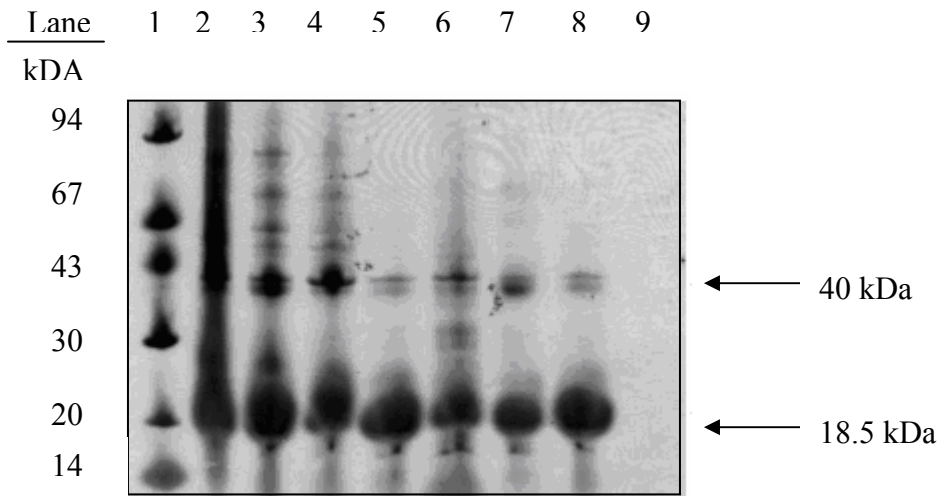


Figure 3.8: SDS PAGE gel of the protein purification of bFT-E18A by heat denaturation and ammonium sulfate precipitation. The molecular weight at 18.5 kDa represents a monomer and 40 kDa represents a dimer bFT mutant. The list below indicates each step of the purification protocol.

Lane	Sample	Lane	Sample
1	MWM	6	Pellet from 25% ammonium sulfate
2	Pellet from sonication	7	Supernatant from 25% ammonium sulfate
3	Supernatant from sonication	8	Pellet from 40% ammonium sulfate
4	Pellet from heat denaturation	9	Supernatant from 40% ammonium sulfate
5	Supernatant from heat denaturation		

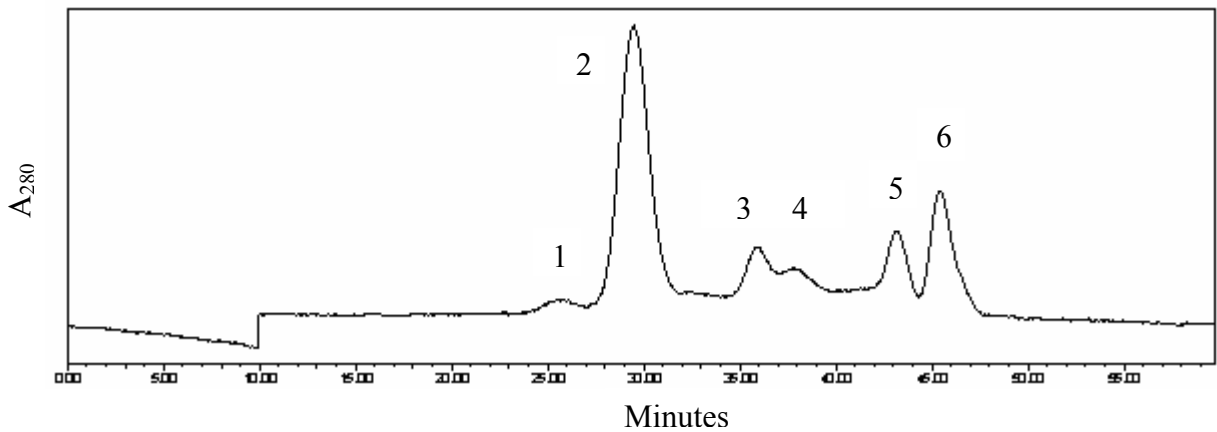


Figure 3.9: The Superose 6 chromatogram of 3.35 mg/mL bFT-WT in 20 mM Tris-OH (pH 8.0) and 100 mM NaCl. The table below shows the MW of each eluted peak.

Table 3.5: The calculated molecular weight of each eluted peak from gel filtration chromatography (Superose 6) of 3.35 mg/mL bFT-WT in 20 mM Tris-OH (pH 8.0) and 100 mM NaCl calculated using the Bio-Rad protein standard.

bFT-WT	MW (kDa)	log (MW)	Ve (mL)	Ka
Peak 1 (self-associated cluster)	919.39	2.9635	12.80	0.3000
Peak 2 (24-mer)	247.05	2.3928	14.70	0.4188
Peak 3 (dimer)	27.01	1.4316	17.90	0.6188
Peak 4 (monomer)	19.12	1.2814	18.40	0.6500
Peak 5	2.09	0.3202	21.60	0.8500
Peak 6	0.98	-0.0102	22.70	0.9188

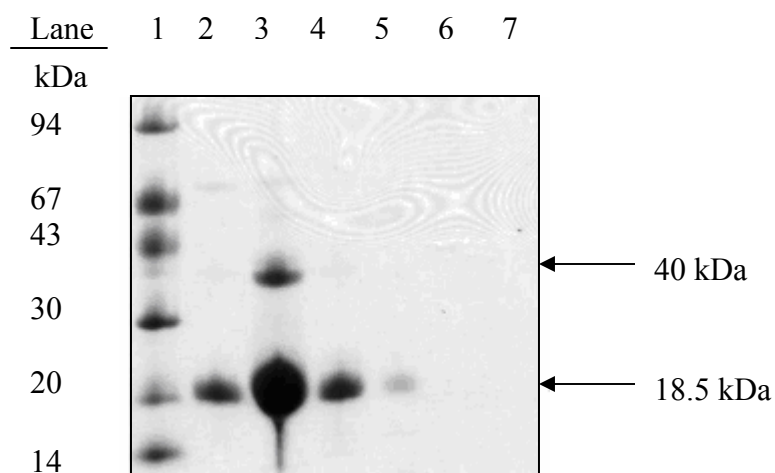


Figure 3.10: SDS PAGE results of Superose 6 eluted peaks of 3.35 mg/mL bFT-WT in 20 mM Tris-OH (pH 8.0) and 100 mM NaCl. The list below indicates loading samples (Superose 6 eluted peak) in each lane.

Lane	Sample
1	MWM
2	Eluted peak 1 of bFT-WT
3	Eluted peak 2 of bFT-WT
4	Eluted peak 3 of bFT-WT
5	Eluted peak 4 of bFT-WT
6	Eluted peak 5 of bFT-WT
7	Eluted peak 6 of bFT-WT

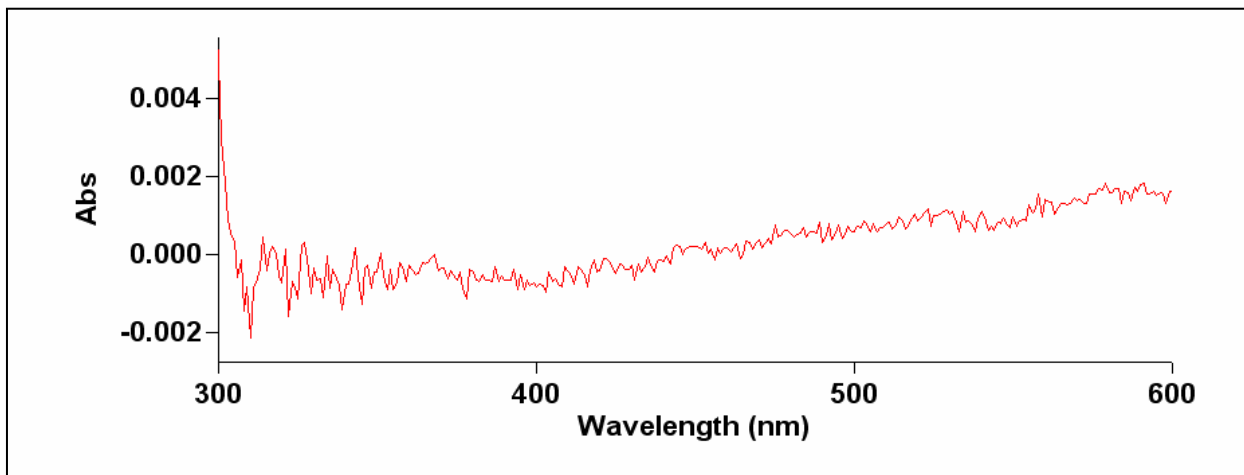


Figure 3.11: The UV-visible spectrum of peak 6 bFT-WT from Superose 6 (peak 6 in Figure 3.9) scanned from 300-600 nm shows that there is no absorption at 418 nm wavelength (corresponding to Soret band of the oxidized heme moiety), which indicated the presence of heme in this fraction.

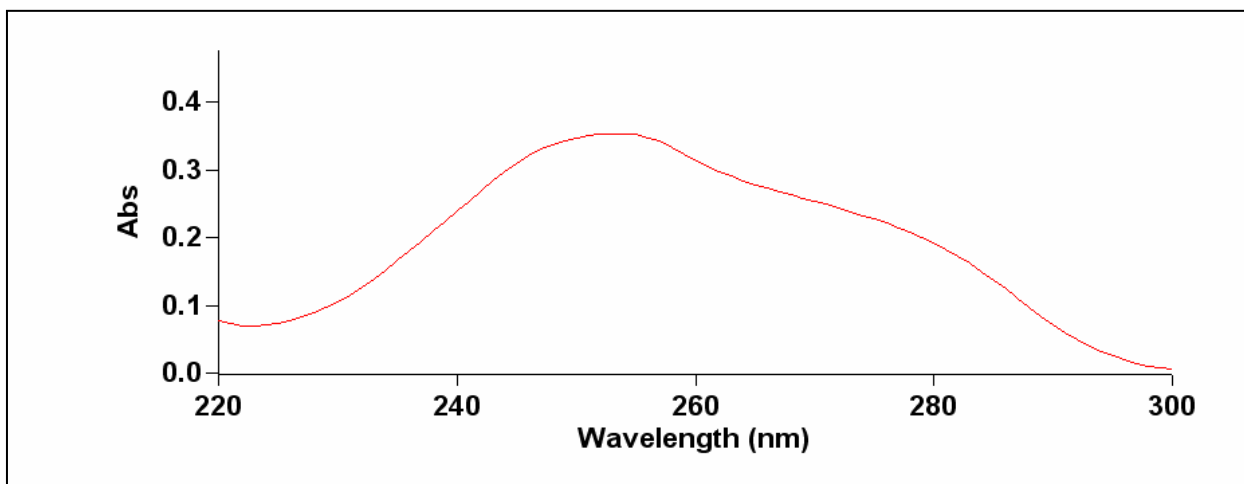


Figure 3.12: The UV spectrum of peak 6 bFT-WT from Superose 6 (peak 6 in Figure 3.9) scanned from 220-300 nm shows an intense peak at ~260 nm and small peak at 280 nm.

3.4.4: Protein Stability of Wild-type and Bacterioferritin Mutants

Protein stability was examined by Superose 6 gel filtration chromatography by comparing chromatograms of bFT-WT with bFT variants. All single mutations (bFT-E18A, bFT-M52L, and bFT-E94A) possessed similar Superose 6 chromatograms. It was shown that

bFT-E18A formed 24-mer, 12-mer, dimeric, and monomeric oligomers (Figure 3.13). However, the 12-mer peak was not clearly shown, and the dimer was a stable conformation for this mutation. For bFT-M52L, it was shown that only the 24-subunit cluster and the dimer were the stable forms, and the dimer was more stable than the 24-mer (Figure 3.14). The Superose 6 chromatogram of Bfr-E94A represented the presence of a higher amount of the 24-mer cluster than the dimer (Figure 3.15). From these single mutations, it was observed that the bFT-E94A mutation stabilized the highest proportion of 24-subunit cluster, which was the lowest fraction in bFT-E18A even though both amino acids (E18 and E94) are components of the ferroxidase center (Table 3.6). The positions of Glu18 and Glu94 that are located at the outer helices of bFT face the inner core and have less possibility to affect protein-protein interactions, which may relate to the formation of the 24-subunit cluster (Figure 3.22).

For double mutations, it was shown that bFT-E18A/M52L and bFT-E18A/E94A exist predominantly as the 24-mer cluster and the monomer (Figure 3.16 and 3.17). However, bFT-E18A/M52L possessed a higher proportion of single subunits, which was probably a result from the combination of single mutations (bFT-E18A and bFT-M52L) that also yielded greater proportion of smaller subunits than 24-mer cluster (Table 3.6). For bFT-E18A/E94A, the 24-subunit formation is higher than that of bFT-E18A/M52L. A possible explanation is that the single mutation bFT-E94A yielded more 24-mer proportionally to that of bFT-M52L. The 12-mer might exist in bFT-E18A/E94A; however, this peak in the chromatogram was not clearly observed. The Superose 6 chromatogram of bFT-M52L/E94A showed a favored dimeric structure (Figure 3.18), suggesting the effect of M52L and E94A to the structure of 24-subunit. However, the positions of these two amino acid residues had less possibility to interfere with protein-protein interactions. The 24-subunit and the smaller subunits of bFT-M52L were in

reverse proportion to those of bFT-E94A; therefore, the combination of both mutants was expected to yield 50/50:24-subunit/smaller subunits (Table 3.4). However, this prediction was not correct.

The triple mutant, bFT-E18A/M52L/E94A, had a similar Superose 6 chromatogram to that of bFT-WT (Figure 3.19), and it consisted of three forms of protein, 24-subunit cluster, a dimer, and a monomer. However, the dimer was found to be the predominant form. The proportion of the 24-subunit and smaller subunits were also considered from its components of single mutations and double mutations. Since all mutants except bFT-E94A yielded higher proportions of smaller subunits than the 24-mer, it was expected that the triple mutant would possess similar proportions (Table 3.6). In order to test for stability of the dimer, the eluted dimeric peak was concentrated and reloaded onto the Superose 6 column. It was shown that the concentrated dimer does not reform the 24-mer. However, this might be due to its lower protein concentration (0.40 mg/mL) (Figure 3.20). The eluted 24-subunit fraction was also concentrated and similarly tested for stability. It was observed that this protein fraction retained its quaternary structure (Figure 3.21).

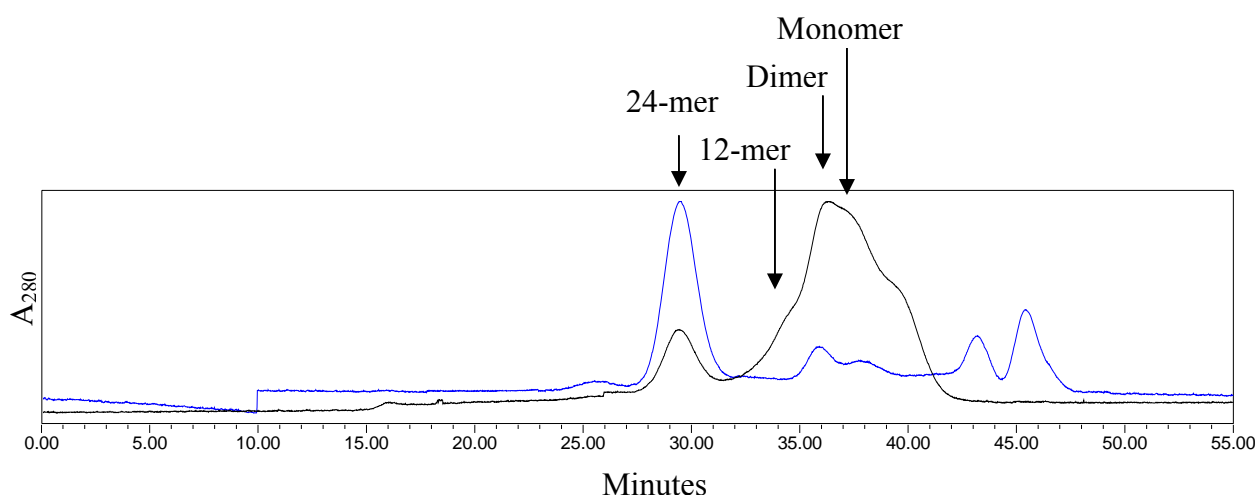


Figure 3.13: The normalized Superose 6 chromatograms of 3.35 mg/mL bFT-WT (blue) and 1.35 mg/mL bFT-E18A (black) in 20 mM Tris-OH (pH 8.0) and 100 mM NaCl showing the overlap of 24-subunit, dimer, and monomer peaks.

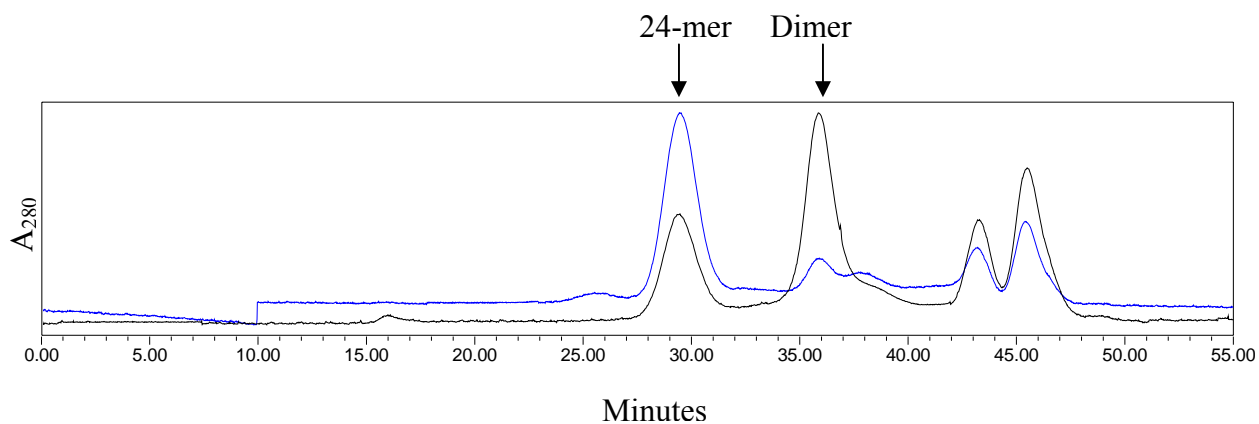


Figure 3.14: The normalized Superose 6 chromatograms of 3.35 mg/mL bFT-WT (blue) and 1.35 mg/mL bFT-M52L (black) in 20 mM Tris-OH (pH 8.0) and 100 mM NaCl showing the overlap of 24-subunit and dimer peaks.

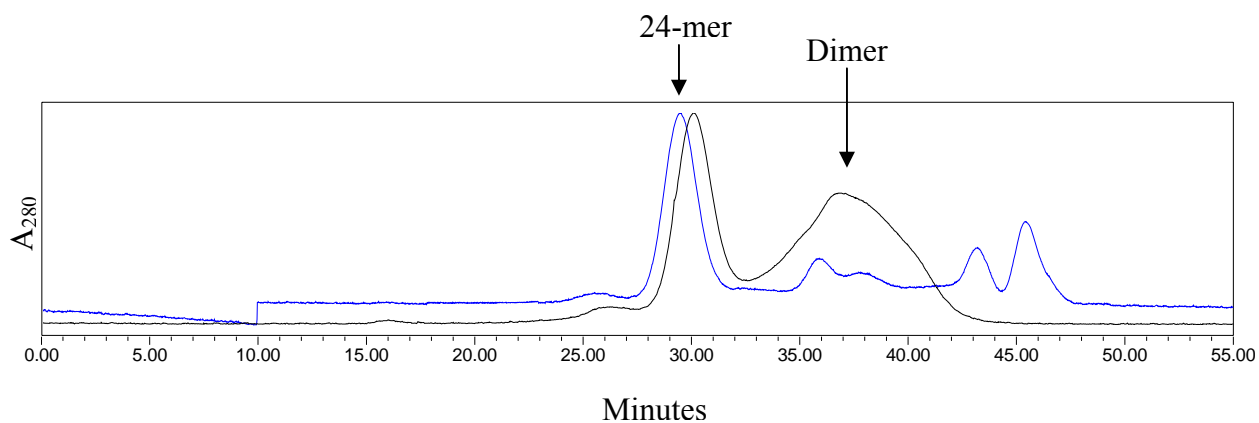


Figure 3.15: The normalized Superose 6 chromatograms of 3.35 mg/mL bFT-WT (black) and 1.35 mg/mL bFT-E94A (blue) in 20 mM Tris-OH (pH 8.0) and 100 mM NaCl showing the overlap of 24-subunit and dimer peaks.

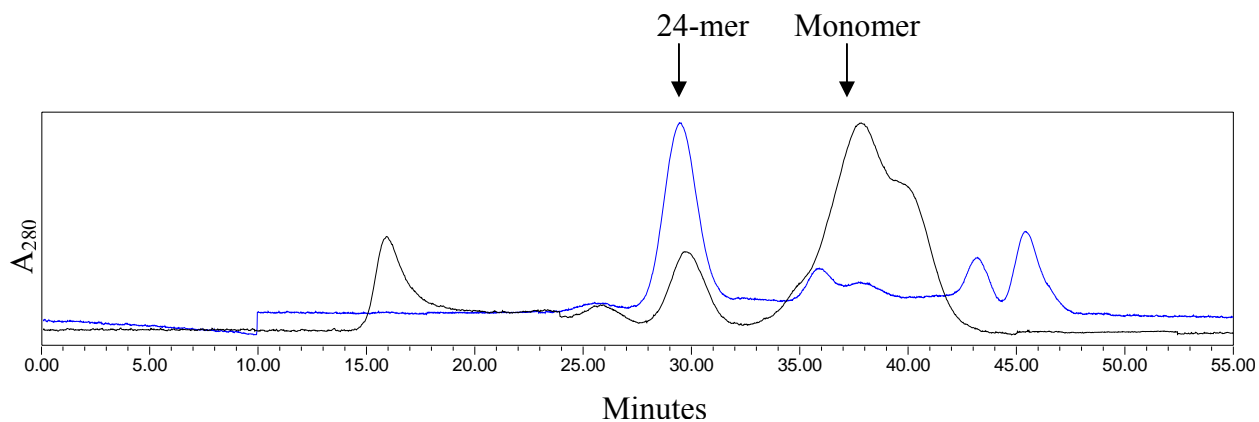


Figure 3.16: The normalized Superose 6 chromatograms of 3.35 mg/mL bFT-WT (blue) and 1.35 mg/mL bFT-E18A/M52L (black) in 20 mM Tris-OH (pH 8.0) and 100 mM NaCl showing the overlap of 24- and monomer peaks.

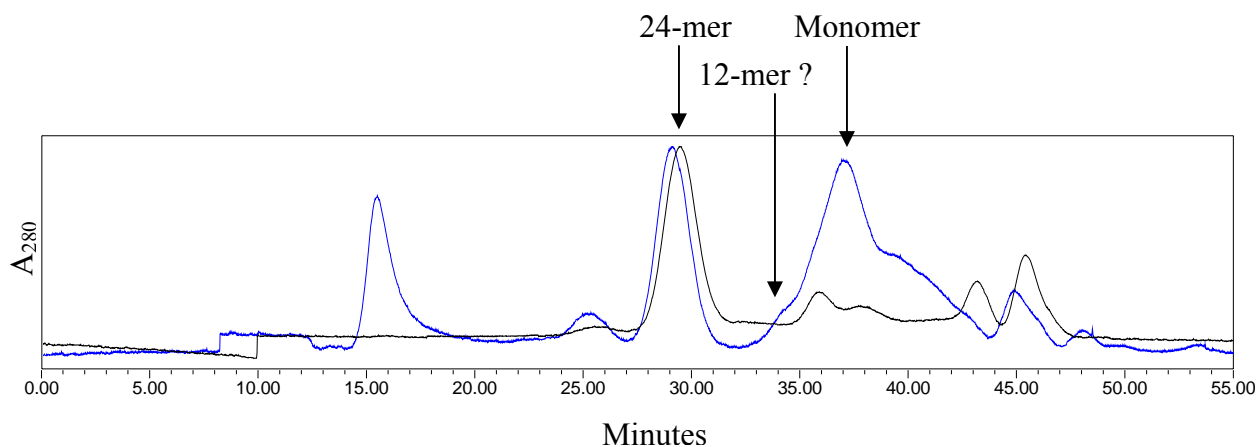


Figure 3.17: The normalized Superose 6 chromatograms of 3.35 mg/mL bFT-WT (black) and 1.35 mg/mL bFT-E18A/E94A (blue) in 20 mM Tris-OH (pH 8.0) and 100 mM NaCl showing the overlap of 24-mer and monomer peaks. The variant might contain a 12-mer peak.

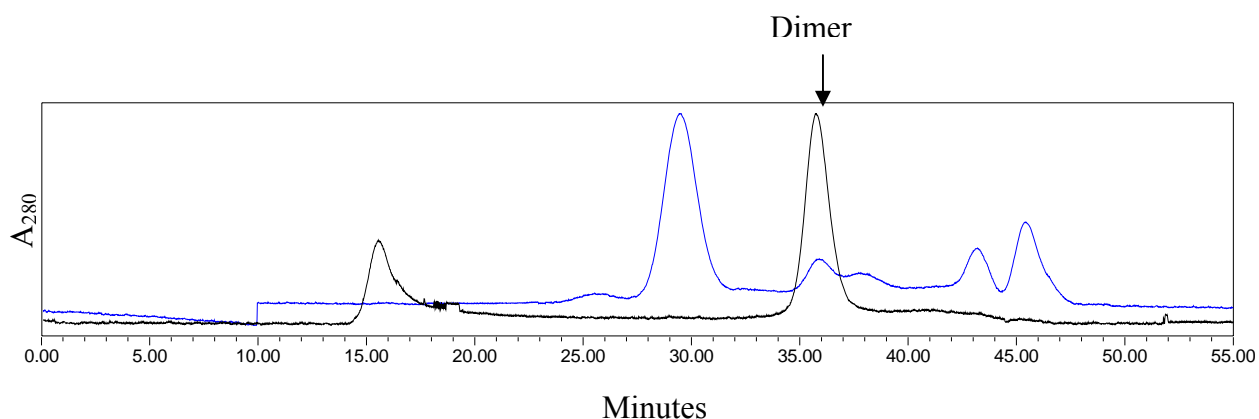


Figure 3.18: The normalized Superose 6 chromatograms of 3.35 mg/mL bFT-WT (blue) and 1.35 mg/mL bFT-M52L/E94A (black) in 20 mM Tris-OH (pH 8.0) and 100 mM NaCl showing the overlap of a dimer peak.

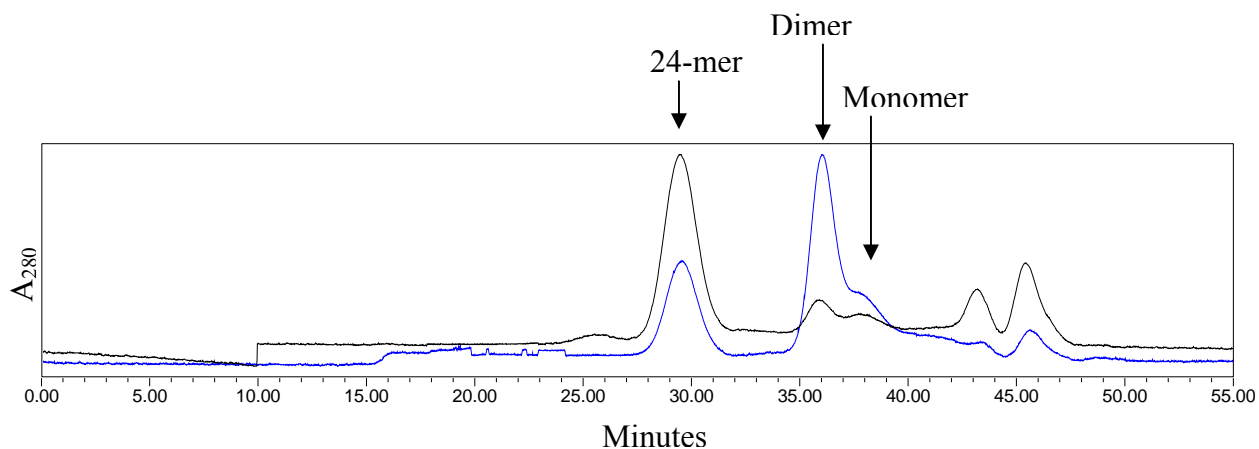


Figure 3.19: The normalized Superose 6 chromatograms of 3.35 mg/mL bFT-WT (black) and 3.35 mg/mL bFT-E18A/M52L/E94A (blue) in 20 mM Tris-OH (pH 8.0) and 100 mM NaCl showing the overlap of 24-subunit, dimer, and monomer peaks.

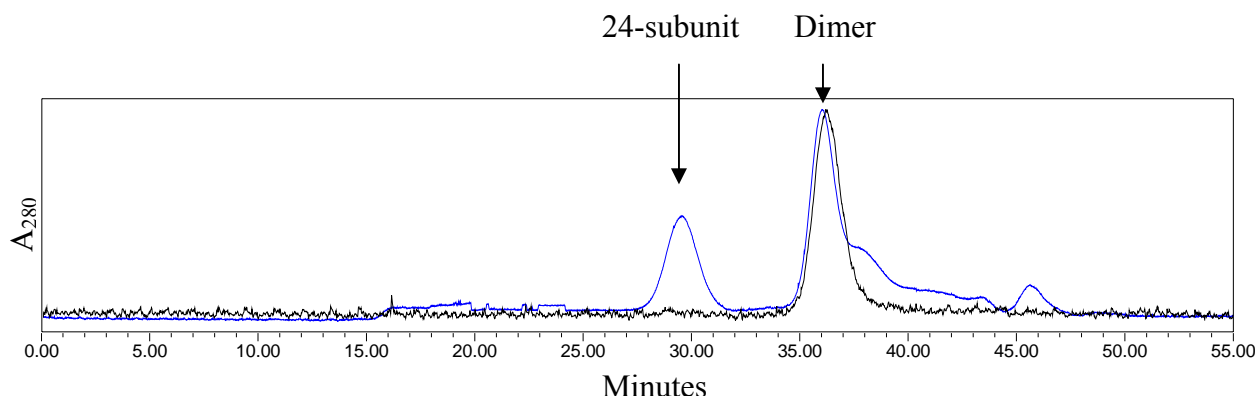


Figure 3.20: The normalized Superose 6 chromatograms of 3.35 mg/mL bFT-E18A/M52L/E94A (blue) and 0.40 mg/mL 2-subunit peak of bFT-E18A/M52L/E94A (black) in 20 mM Tris-OH (pH 8.0) and 100 mM NaCl showing the overlap of the dimer peak.

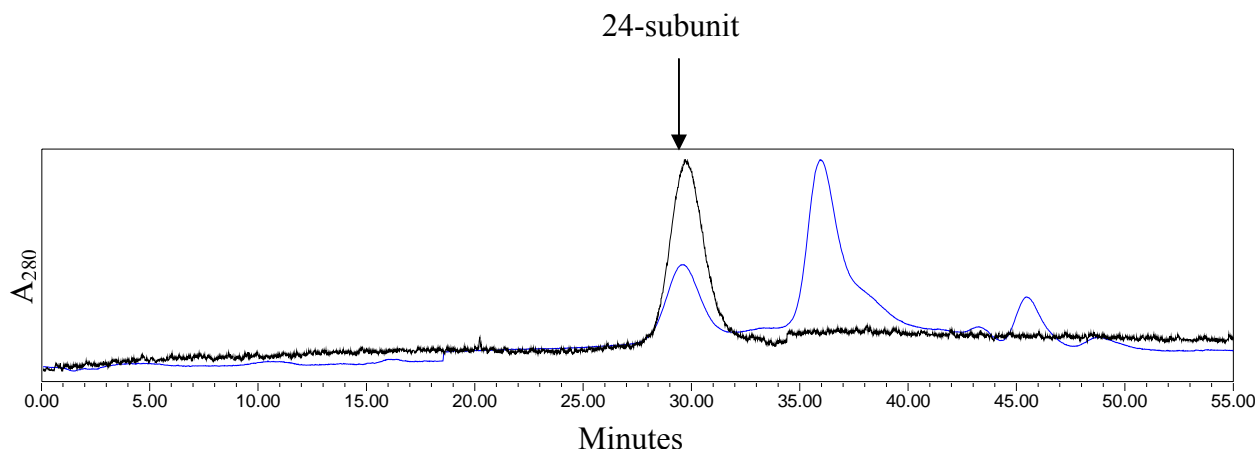


Figure 3.21: The normalized Superose 6 chromatograms of 1.01 mg/mL 24-mer peak (black) and 5.89 mg/mL bFT-E18A/M52L/E94A (blue) in 20 mM Tris-OH (pH 8.0) and 100 mM NaCl show the overlap of 24-mer peak.

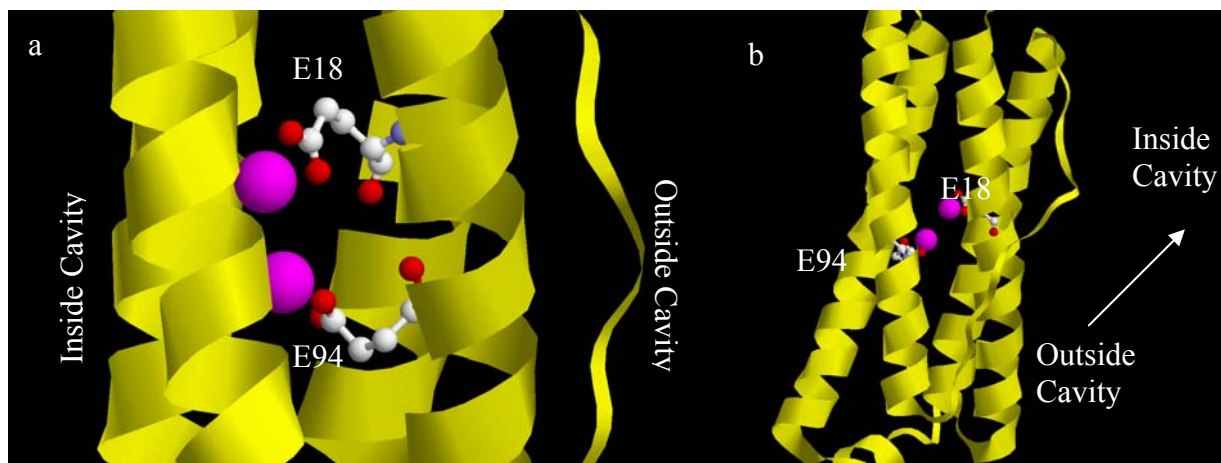


Figure 3.22: The ribbon structure of *E. coli* bFT showing Glu18 and Glu94, which are facing the inner core (a) and locating at the outer helices (b) (PDB entry 1BCF) (Frolow *et al.*, 1994). The di-iron atoms are shown in pink.

Table 3.6: A summary of the protein structure, 24-subunit and smaller subunits (dimer and monomer), of wild-type bFT compared with bFT variants.

Samples	Protein concentration (mg/mL)	Protein conformation [‡] (%)	
		24-subunit	Dimer and monomer
bFT-WT	3.35	80	20
bFT-E18A	1.35	20	80
bFT-M52L	1.35	40	60
bFT-E94A	1.35	60	40
bFT-E18A/M52L	1.35	25	70
bFT-E18A/E94A	1.35	40	60
bFT-M52L/E94A	1.35	0	100
bFT-E18A/M52L/E94A	3.35	30	70

[‡] The approximated values from area under curves

3.5: Conclusions

The control experiments suggest that a suitable condition for stabilizing the 24-subunit structure includes use of high protein concentration in buffer containing 20 mM Tris-OH (pH 8.0) and 100 mM NaCl. The heat denaturation and ammonium sulfate precipitation steps were sufficient methods for protein purification. The Superose 6 gel filtration chromatographic results indicate the approximate amount of 24-subunit clusters of bFT-WT and bFT variants. All except bFT-M52L/E94A formed mixtures of the self-associated cluster, 24-subunit, and smaller subunit conformations. The only mutant that showed significant presence of dimer was the bFT-M52L/E94A mutant. All variants were unable to remain high proportion of completely in the intact 24-subunit form after purification as bFT-WT, although the specific amino acid positions seemed to have no easily explainable reason for their effect on the 24-mer formation.

In order to study the use of bFT in encapsulation, it is necessary to use bFT or a variant that produces high levels of stable 24-mer cluster. Since the dimer structure is favored in the ferroxidase- and heme-free variant (bFT-E18A/M52L/E94A), wild-type bFT was used for further study of the potential for this protein to be useful in encapsulation studies as shown in the next chapter.

CHAPTER 4: OVEREXPRESSION, PURIFICATION, AND ENCAPSULATION PROPERTIES OF C-TERMINAL HIS₆-TAGGED BACTERIOFERRITIN

4.1: Literature Research on C-terminal Extension and Encapsulation of Bacterioferritin

The work by Andrews and co-workers had previously shown that the bFT subunits with an extra 14 amino acid residues at the C-terminus could form a normal protein shell, in which they called this C-terminal extension bFT a BFR- λ hybrid protein (Andrews *et al.*, 1990). This hybrid replaced four C-terminal residues (REEG) in bFT-WT by 18 residues (RLPFTSCAVCLQDSMRSR). Based on native PAGE, heat denaturation, Q-Sepharose anion-exchange chromatography, and Superose 6 gel permeation chromatography, it was found that both wild type and hybrid proteins had similar functions and properties. These results suggested that the additional residues at the C-terminus project into the central molecular cavity and do not disrupt the protein shell or influence the properties of the external surface. Further information based on crystallization experiments had shown that these extra 14 amino acid residues filled roughly 60% of the hollow cavity and possibly blocked the access of iron ions such that the BFR- λ hybrid protein failed to take up iron *in vitro*. They also suggested that many of the heme-binding pockets of the protein might be disrupted.

Andrews and co-workers later developed protocols to purify the wild-type bFT and BFR- λ hybrid proteins (Andrews *et al.*, 1993). Their results showed that the overproduction of wild-type bFT protein was 120-fold, while it was only 50-fold for the hybrid protein. The X-ray diffraction patterns showed that the additional C-terminus residues were present within the cavity of the 24-subunit protein, and the visible spectrum showed that the heme content of the

λ hybrid was approximately 1-2 hemes/tetracosamer, while bFT-WT had 3.5-10.5 hemes/tetracosamer. Non-denaturing PAGE experiments indicated that the BFR- λ hybrid was stabilized by the presence of the additional C-terminal residues.

While most published applications of protein cages for host-guest studies are based on FT with various types of guest molecules i.e. metals, peptides, small protein, or drugs (Chapter 1.3), previous encapsulation studies using bFT have focused on the replacement of the Fe(III) core with other metals. Further study on kinetics of metals binding to bFT (in term of dissociation constant) had shown that the order of divalent metal ion binding was Cu(II) < Co(II) < Zn(II) (Baaghil *et al.*, 2002; Le Brun *et al.*, 1996).

Based on the study of dissociation and reassociation of horse spleen apoFT (Chapter 2) and knowledge of suitable conditions for maintaining its quaternary structure (Chapter 3), the encapsulation of bFT was examined in this thesis under three steps of encapsulation, which included (1) subunit-declustering in acidic solution, (2) encapsulation of guest molecules, and (3) reclustered at neutral pH (Figure 4.1). The conditions used to maximize the amount of encapsulated guest molecules and allow for the 24-subunit reclustered after declustering in acidic solution were investigated. The encapsulations were studied using the bFT subunit derivative with a His₆-tag at the C-terminal end of the protein as host. It was anticipated that this system would provide a protein cage for binding of a nickel nitrilotriacetic acid (Ni²⁺-NTA) derivative (dye molecules in Pro-Q[®] sapphire 365 oligohistidine gel stain) that acts as a guest molecule. The linkage was the interaction between His-tag protein and Ni²⁺-NTA derivative. Since the C-terminal bFT points toward the protein cavity, the host-guest interaction could provide for the encapsulation of guest molecules inside the protein cage. The host protein containing the affinity tag was generated by PCR amplification and insertion into

the pET-22b(+) vector. The properties of the dye molecules in Pro-Q[®] sapphire 365 oligohistidine gel stain (Invitrogen Molecular Probes) including extinction coefficient, MW, dye concentration, and possible dye structure were also investigated. The amount of Ni²⁺ contained in the dye solution was quantitated by metal analysis. The encapsulation of the dye molecules into the protein cavity was demonstrated using fluorescence spectroscopy. The stability of the host-guest complex after encapsulation was tested using Superose 6 gel filtration chromatography and laser light scattering techniques. The number of encapsulated dye molecules under optimized conditions was calculated along with its efficiency. In addition, the effect of the presence of heme groups and iron ions incorporated into bFT on encapsulation was investigated.

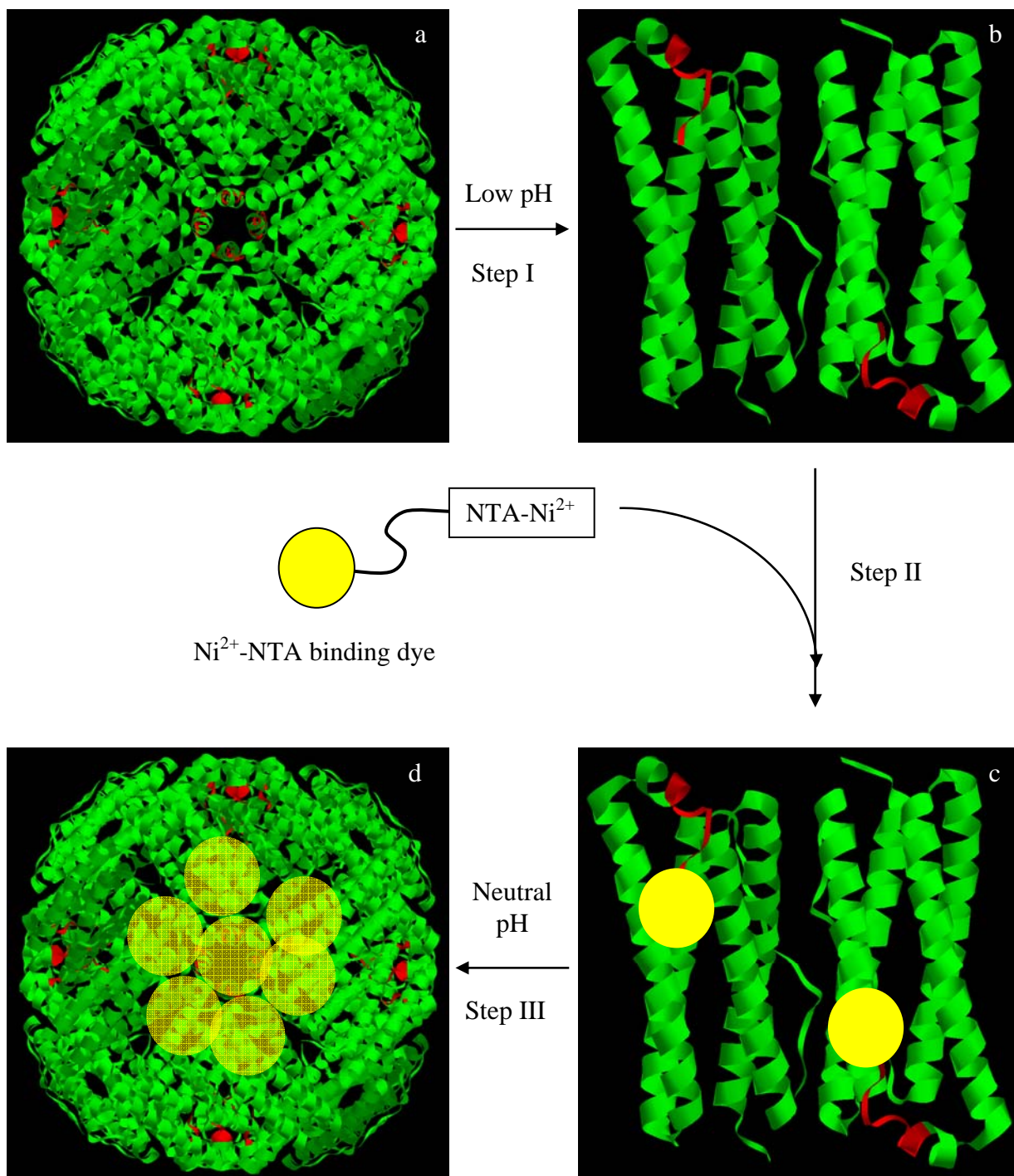


Figure 4.1: A schematic representation of the encapsulation process using bFT as host particle. The 24-subunit bFT (green) with His₆-tag at the C-terminus (red) (a) is declustered in acidic solution yielding subunits (b). By adding Ni²⁺-NTA binding dye (yellow), the interaction between His₆-tag and Ni²⁺-NTA is formed (c). The encapsulation of dye inside protein cavity (reclustering) is expected when altering the pH back to neutral, which would allow for protein reclustering to the 24-mer (d).

4.2: Reagents, Materials, and Equipment

Reagents and materials

All reagents and materials used in this chapter are stated below otherwise they are included in Chapter 2 and 3.

Dye reagents including Pro-Q[®] sapphire 365 oligohistidine gel stain was obtained from Invitrogen Molecular Probes (Burlington, ON) and 1,4-piperazinebis(ethanesulfonic acid) (PIPES) was obtained from J.T Baker (Toronto, ON). Denaturant, guanidinium hydrochloride (Gdn-HCl), was obtained from Sigma Chemical Company (St. Louis, MO).

Equipment

All equipment used in this chapter is listed below otherwise they are included in Chapter 2 and 3.

Fluorescence measurements used in the study of dye in corporation and extinction coefficient determination of Pro-Q[®] sapphire 365 oligohistidine gel stain were achieved using a PTI Fluorometer with light source supplied from a LPS-220B Lamp (Model 101M monochromator), Photon-Counting Photomultiplier Detector (Model 814 Analog), and FeliX32 software (version 1.0) from PTI Photo Technology International, PicoQuant GmbH (Berlin, Germany).

4.3: Experimental Protocols

4.3.1: PCR Amplification and Insertion into pET-22b(+)

The protocols to generate bFT with His₆-tag at the C-terminal were similar to that of bFT-E94A in Chapter 3. First, bFT-WT plasmids with a *Nde*I digestion site at the N-terminus

and a *XhoI* digestion site at the C-terminus were generated by PCR using pT7bFT as host plasmid, the forward primers had a *NdeI* digestion site, and the reverse primers had a *XhoI* digestion site (Table 4.1). PCR reagents and materials were prepared under optimized conditions as shown in Table 4.2 and PCR protocols were programmed as in Table 4.3. The DNA product from the PCR reaction was digested with *NdeI* and *XhoI* restriction enzymes for 3 hours at 37 °C. The DNA fragments were purified by using DNA electrophoresis (1% agarose gel) before visualizing under UV light. The gel containing the desired DNA fragment was cut and purified using a QIAprep Spin Miniprep Kit before it was inserted into pET-22b(+) vectors that were digested with the same restriction enzymes. The ligation using T4 ligase enzyme was performed at 14-16 °C for 3 hours. Since pET-22b(+) vector possesses six histidine residues next to the *XhoI* digestion site, this ligation yielded bFT-WT DNA with a His₆-tag at the C-terminus. The ligated DNA was heat shock transformed into *E. coli* cells (strain DH5 α), which were then subsequently grown on agar plates containing Amp overnight at 37 °C. A single colony was selected and inoculated into 5 mL LB containing Amp (50 μ g/mL LB) and left to shake overnight at 37 °C (220 rpm). Plasmid purification was performed using a QIAprep Spin Miniprep Kit. The DNA concentration was measured spectrophotometrically (OD₂₆₀) before samples were sent for DNA sequencing (Mobix Central facility). The successful insertion was confirmed by analysis of the obtained DNA sequence with the expected sequence using the BLAST2 program.

Table 4.1: The forward and reverse primers used to generate bFT-WT with a *NdeI* cutting site at the 5' end and a *XhoI* cutting site at the 3' end.

Primers	Sequences of primers (5' to 3')	Melting temperature (T _m)
BfrNdeI.For	CCAGGATCCATATGAAAGGTGATACTAAAG [‡]	59
BfrXhoI.Rev	CCGCTCGAGACCTTCTTCGCG [‡]	60

[‡]The bold letters represent digesting sites.

Table 4.2: PCR conditions for generating a bFT-WT construct with a *NdeI* cutting site at the 5' end and a *XhoI* cutting site at the 3' end.

Plasmids/Reagents	Stock Concentration	Amount Used (μL)	Final Concentration
bFT-WT template	115 ng	10	23 ng
Primer.For	10 μM	3	600 nM
Primer.Rev	10 μM	3	600 nM
dNTP	10 mM	1.0	200 μM
PWO Buffer	10×	5.0	
Mg ²⁺	25 mM	x	y
ddH ₂ O		z	
PWO polymerase		0.5	
Total		50.0	

x were 1, 2, or 3 μL Mg²⁺, where y was the final concentration of Mg²⁺ used (0.5 mM, 1.0 mM, and 1.5 mM, respectively) to maximize PCR products.

z is amount of distill water (ddH₂O) used to fill the final PCR volume to 50 μL.

Table 4.3: PCR Programming sets for generating the bFT-WT construct with a *NdeI* cutting site at the 5' end and a *XhoI* cutting site at the 3' end.

Steps	Temperature (°C)	Time	
Initial Denaturation	95	2 min	
Hot Start	85		
Denaturation	95	30 sec	} Repeat 30 cycles
Annealing	55	1 min	
Elongation	72	45 sec	
Final Extension	72	2 min	
Hold	4		

4.3.2: Protein Expression, Induction, and Purification

Protein expression, induction, and purification of bFT with His₆-tag at the C-terminus was similar to those of bFT-WT and bFT variants described in Chapter 3 except the last step where dialysis buffer and running buffer for the Superose 6 gel filtration chromatograph was replaced by buffer containing 10 mM PIPES buffer (pH 8.0) and 100 mM NaCl.

4.3.3: Identification of Dye Molecule

Little information on the exact chemical structure of the dye used in the Pro-Q[®] sapphire 365 oligohistidine gel stain was available from Invitrogen Molecular Probes due to the proprietary nature of the dye. Hence some effort was made to determine additional information on the dye. The dye molecules have fluorescent absorption with a maximum excitation wavelength at 345 nm and maximum emission wavelength at 440 nm (Figure 4.2). However, the UV-visible spectrum of the dye solution represents the highest absorption at 345 nm, while there is low intensity at 440 nm (Figure 4.3). The dye molecules were dissolved in PIPES solution (soluble at pH > 6.1). This dye solution is commercially sold for the detection of oligohistidine fusion proteins in SDS PAGE gels. Other properties of the dye in Pro-Q[®] sapphire 365 oligohistidine gel stain such as its molecular weight, predicted structure, and extinction coefficient were investigated.

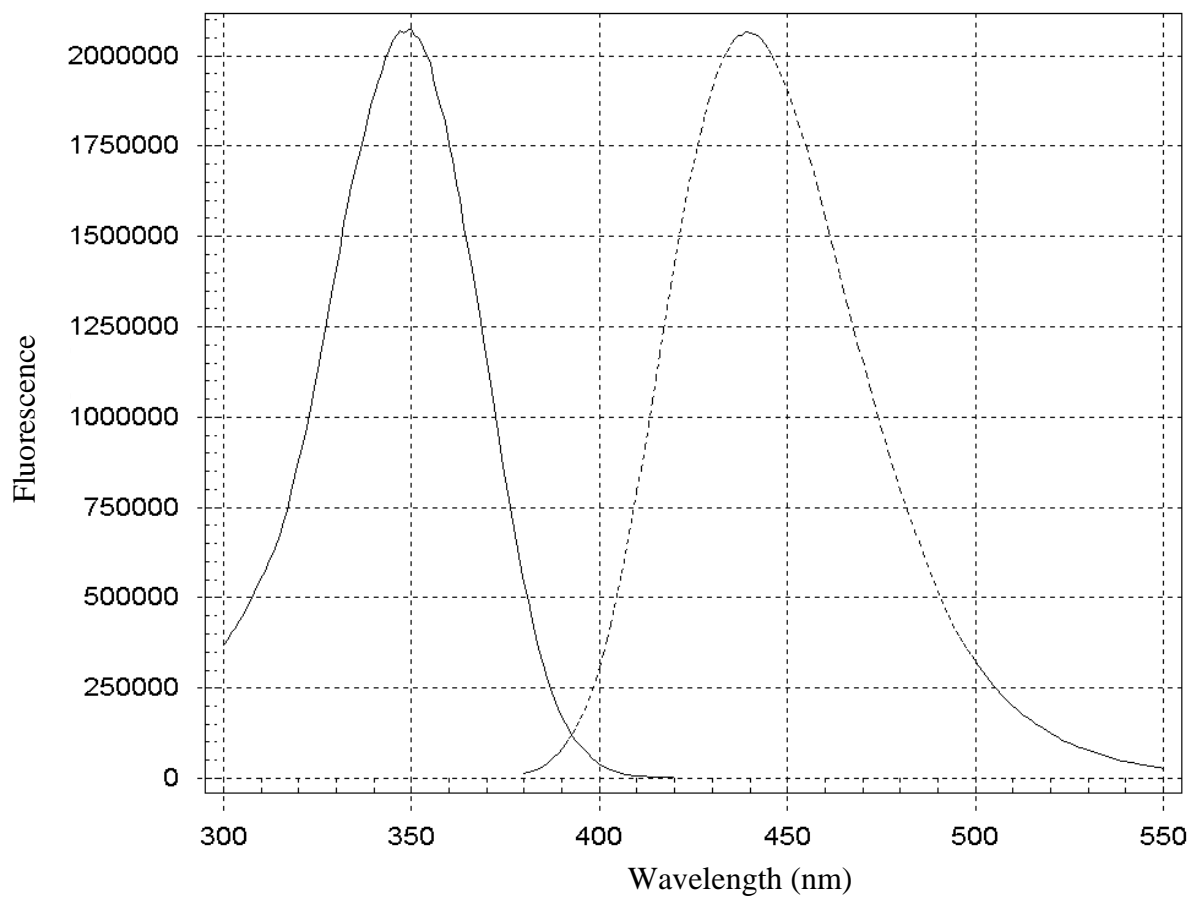


Figure 4.2: The excitation spectrum scanning from 300-420 nm with the fixed emission wavelength at 440 nm (—) and the emission spectrum scanning from 380-550 nm with the fixed excitation wavelength at 345 nm (---) of Pro-Q[®] sapphire 365 oligohistidine gel stain using a fluorometer.

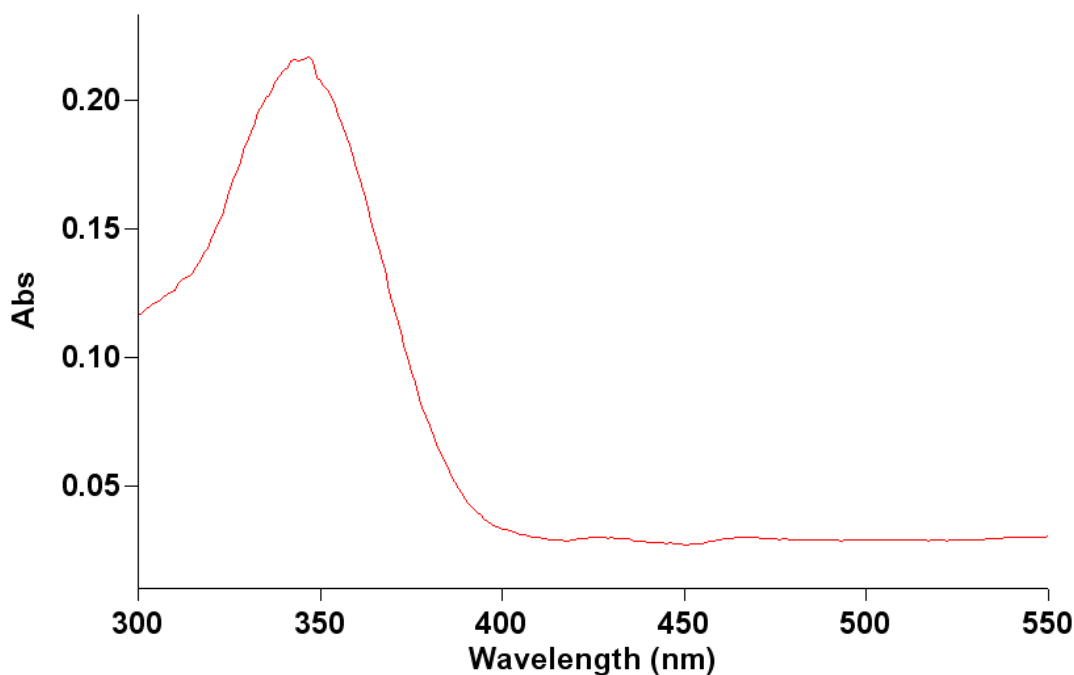


Figure 4.3: The UV-visible spectrum of Pro-Q[®] sapphire 365 oligohistidine gel stain scanned from 300-550 nm showing the highest absorption at 345 nm.

The molecular weight of the dye molecule was examined by electrospray MS. Since the stock solution of Pro-Q[®] sapphire 365 oligohistidine gel stain contained a high concentration of PIPES (57.3 mM) that can interfere with MS, PIPES was precipitated out under acidic solution. A 200 μ L stock solution of stain was mixed with 2% formic acid and then PIPES was allowed to precipitate for two days at 4 °C. The solution was centrifuged at 13 000 rpm for 30 seconds before withdrawing a 100 μ L supernatant aliquot. The sample was then diluted 10 times with 50/50 acetonitrile to water containing 0.2% formic acid before measuring the mass spectrum.

The predicted structure of the dye molecules in this stain was searched using an internet patent database, International Application Published under the Patent Cooperation Treaty

(PCT) of World Intellectual Property Organization, using the key word “site-specific labeling of affinity tags in fusion proteins”. The predicted structure with known molecular weight was used for the calculation of the dye concentration in Pro-Q[®] sapphire 365 oligohistidine gel stain and to estimate the extinction coefficient of the dye molecules.

The estimated extinction coefficient was predicted from a comparison between a fluorophore of the dye and the known compound that possesses the same fluorophore (or its derivative). If the solvent of the known compound with similar maximum excitation wavelength and emission wavelength as the dye molecules (excitation wavelength at 345 nm and emission wavelength at 440 nm) was the same as the solvent of the dye solution, then their extinction coefficients were similar.

In order to compare the actual extinction coefficient of the dye with the estimated extinction coefficient that was determined from the dye related structure, the experimental extinction coefficient was calculated using the Beer-Lambert law. The dye samples were prepared by diluting a stock solution of Pro-Q[®] sapphire 365 oligohistidine gel stain with Milli-Q water in the following series dilution: 100%, 50%, 25%, 12.5%, 7.25%, and 3.125% of dye (v/v) concentration. The samples were loaded into a low volume quartz cuvette (45 μ L) before scanning for the emission wavelength between 400-550 nm with a fixed excitation at 345 nm. Another set of experiments was to scan the excitation wavelength between 300-400 nm with a fixed emission wavelength at 440 nm. The size of the incoming slit and the outgoing slit were set to 1 nm with a 1 nm step size and a 1 second integration. All measurements were done in duplicate at room temperature. The reading at 440 nm was collected for the emission scan, and the reading at 345 nm was obtained for the excitation scan. A graph of emission intensities versus dye concentration and the graph of excitation intensity

versus dye concentration were plotted. The extinction coefficient of dye molecule could be calculated from the expected linear trend of each experiment, which corresponded to the Beer-Lambert law, $A = \epsilon'_{345}BC$, where A is absorbance, ϵ'_{345} is the fluorescence determined extinction coefficient ($\text{cm}^{-1}\text{M}^{-1}$) at 345 nm, B is the path length of cuvette (1 cm), and C is concentration (M). The measurement was performed at room temperature using a 57.3 mM PIPES solution (same concentration as stock solution) as blank.

Since dye molecules that might be in close proximity may possess their fluorescence quenching (decrease in fluorescent intensity), which might affect the fluorescence intensities in the measurement of the encapsulated dye molecules in bFT, this extinction coefficient might not be correct. Therefore, the extinction coefficient measured by UV-visible spectroscopy was calculated to compare with the extinction coefficient that was determined by the fluorescence experiment. The extinction coefficient of the dye solution determined by a UV-visible spectrophotometer was performed similarly to that of the fluorescence determinations. The samples were prepared with the same dilution factor (100%, 50%, 25%, 12.5%, and 6.25% v/v dye). The protein samples were loaded into 1 mL quartz cuvettes before measuring their optical density at 345 nm. The extinction coefficient was determined from the linear trend of the plot between OD_{345} and dye concentration, which corresponds to the Beer-Lambert law, $A = \epsilon_{345}BC$, where A is absorbance, ϵ_{345} is the UV-visible extinction coefficient ($\text{cm}^{-1}\text{M}^{-1}$) at 345 nm, B is the path length of cuvette (1 cm), and C is concentration (M).

The concentration of the dye in Pro-Q[®] sapphire 365 oligohistidine gel stain was calculated using the Beer-Lambert law, $A = \epsilon_{345}BC$. The measurement for the absorption of the dye was performed in duplicate at room temperature by loading 45 μL of Pro-Q[®] sapphire

365 oligohistidine gel stain to a low volume quartz cuvette (45 μ L). The absorption of the sample was measured at 345 nm using spectrophotometer.

The quenching of dye molecules in Pro-Q[®] sapphire 365 oligohistidine gel stain can be evaluated using fluorescence experiments. The dye solution was diluted with 6 M Gdn-HCl (final concentration of 5 M Gdn-HCl with total volume of 400 μ L) and was incubated at room temperature for 2 hours. The sample was loaded into a low volume quartz cuvette (45 μ L) before scanning for the emission wavelength between 400-550 nm with a fixed excitation at 345 nm. The size of the incoming slit and the outgoing slit were set to 1 nm with a 1 nm step size and a 1 second integration. The control experiments were (1) the dye solution that was diluted in PIPES buffer (pH 8.0) containing 100 mM NaCl (same dye dilution factor as the one that diluted in Gdn-HCl solution), (2) PIPES buffer (pH 8.0) containing 100 mM NaCl, and (3) 6 M Gdn-HCl solution.

In addition to the attempts to determine the extinction coefficient and the structure of the dye molecules, the amount of Ni²⁺ contained in Pro-Q[®] sapphire 365 oligohistidine gel stain was examined by metal analysis (ETL Chemspec Analytical Ltd., Waterloo, ON). The dye sample was 5 times diluted from stock solution with Chelex treated water with the total volume of solution being 20 mL. Two identical samples were analyzed by Inductively Coupled Plasma Mass Spectrometry (ICP-MS) and a Chelex treated water solution was also used as a control. The concentration of Ni²⁺ and the ratio of Ni²⁺ to NTA-binding dye molecule were calculated. Chelex treated water was prepared by filtering Milli-Q water through a 0.22 μ m GV filter membrane before pumping it through a 5-10 mL plastic column packed with Chelex[®] 100 chelating ion exchange resin (Bio-Rad, Hercules, CA) (flow rate ~1-2 mL/min). Containers used for the samples were soaked in 10% nitric acid for 30 min before

rinsing with ddH₂O followed by rinsing several times with Chelex treated water. The containers were then allowed to dry overnight.

4.3.4: Preparation for Encapsulation Experiments

The 24-subunit protein samples, wild-type bFT with and without His₆-tag at the C-terminus (Histag and WT protein, respectively) were prepared by performing Superose 6 gel filtration chromatography. The concentrations of isolated 24-subunit proteins were calculated by the Bradford assay method. The size and stability of the proteins were investigated by laser light scattering and Superose 6 gel filtration chromatography. The proteins were then used for further experiments on optimizing declustering and reclustered, and hence the effect of declustering time, encapsulating time, protein subunit homogeneity, protein concentration, and dialysis time were evaluated. Control experiments that included attempts to encapsulate the dye into wild-type bFT, elimination of non-specific dye binding, and the use of proteins with non-encapsulated dye, which were performed to evaluate the encapsulation of dye molecules by bFT with His₆-tag at the C-terminus. The encapsulation processes studied included declustering of the protein in acidic solution (pH 2.0), binding dissociated His₆-tag protein subunits with Ni²⁺-NTA binding dye (Pro-Q[®] Sapphire 365 oligohistidine gel stain), and reclustered at neutral pH. The general concept of the encapsulating protocols is shown as a flow chart in Figure 4.4. The lists below represent the specific terms that were used for the encapsulation experiments:

- Histag protein: wild-type bFT with an extend His₆-tagged C-terminus
- WT: wild-type bFT

- 24-mer protein: the 24-subunit protein that was isolated by Superose 6 gel filtration chromatography
- protein with encapsulated dye: the protein after encapsulation experiments, which included incubating in acidic pH solution, binding with dye molecules, reclustered at neutral pH, and removing non-specific binding of the dye
- non-specific dye binding protein: the protein that was not declustered (was not exposed to acidic pH) but was directly incubated with dye at pH 8.0
- non-encapsulated protein: the protein that was declustered in acidic pH solution and then directly reclustered in neutral pH solution by skipping the encapsulation with dye molecules

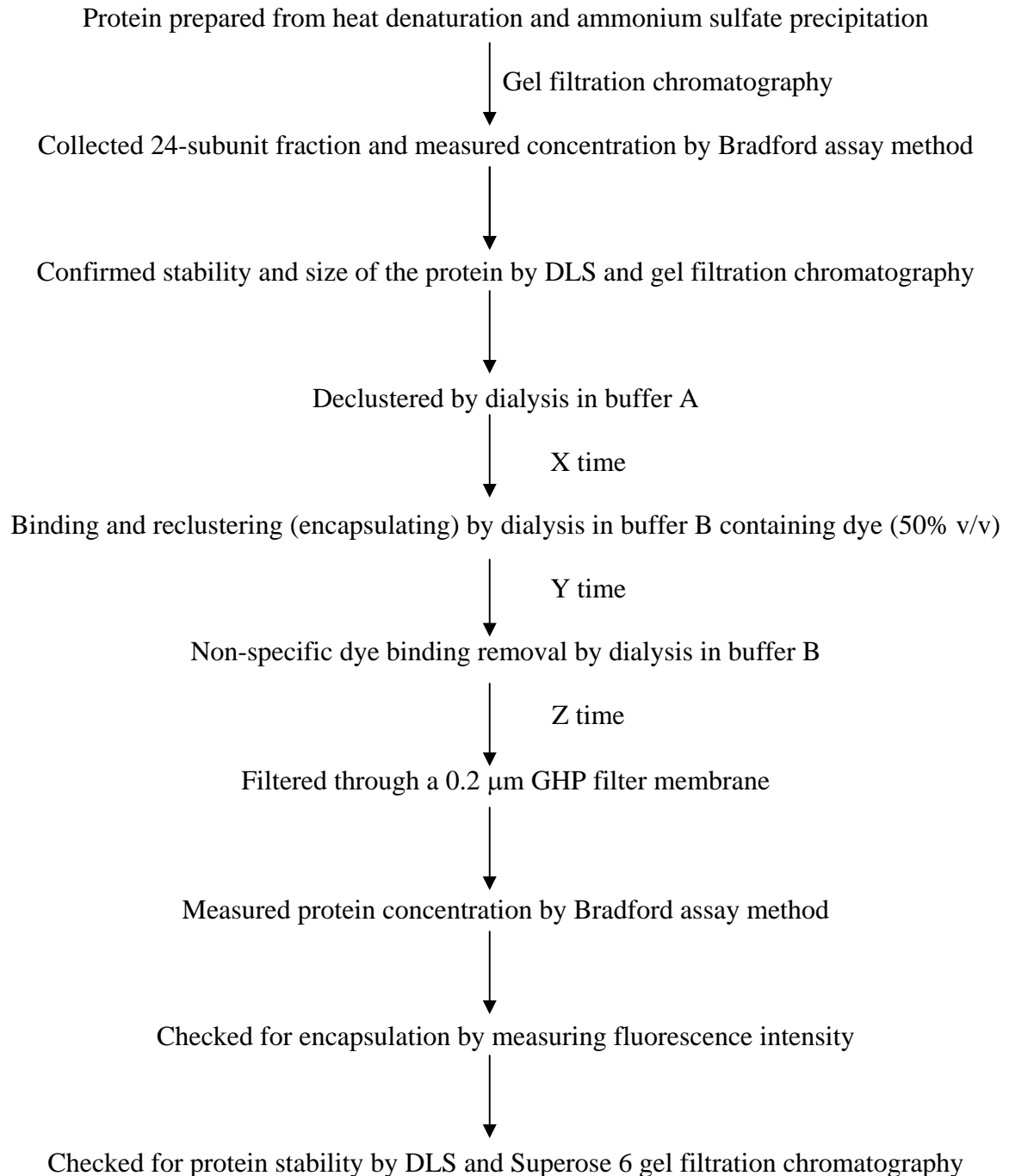


Figure 4.4: A summary showing the encapsulating protocols, where buffer A is 10 mM PIPES (pH 2.0) solution containing 150 mM NaCl and 10% glycerol and buffer B is 10 mM PIPES (pH 8.0) solution containing 100 mM NaCl. The X, Y, and Z are the variables that were altered to optimize conditional tests.

After encapsulation, the proteins were filtered through a 0.2 μm GHP membrane and their concentration was re-measured using the Bradford assay method. Since the fluorescence intensities of the Pro-Q[®] sapphire 365 oligohistidine gel stain are more sensitive than the optical densities presenting in the UV-visible spectrum, the existence of successful encapsulation of the dye was examined by measuring the fluorescence intensity using a fluorescence spectrophotometer. The excitation wavelength was fixed at 345 nm, while the emission intensity was scanned at wavelengths between 400-550 nm. The size of the incoming slit was set to 1 nm and the outgoing slit was set to 14 nm to maximize the detected intensity. The step size was 1 nm with an integration of 1 second. A low volume quartz cuvette (45 μL) was used. Superose 6 gel filtration chromatography and light scattering analysis of these protein samples were then re-performed to investigate protein stability and confirm the existence of the 24-subunit cluster after encapsulation had been completed.

Effect of Declustering Time

Gel filtration chromatography of His-tagged bFT was performed, and the 24-subunit protein was declustered by dialysis against buffer containing 10 mM PIPES (pH 2.0), 150 mM NaCl, and 10% glycerol for 30, 60, and 90 min. Then the declustered protein was incubated in a solution containing dye solution (50% v/v) for 3 hours, and the reclustered step was performed by dialysis in buffer containing 10 mM PIPES (pH 8.0) and 100 mM NaCl overnight. The Histag protein after the encapsulation procedure had been performed are called Histag protein with encapsulated dye. In order to evaluate non-specific surface binding of the dye to the protein, some experiments used proteins that were not declustered but were directly incubated with dye at pH 8.0 and 100 mM NaCl as above.

Effect of Encapsulation Time

Superose 6 gel filtration chromatography was performed on the Histag protein, which was dialyzed (90 min) against buffer containing 10 mM PIPES (pH 2.0), 150 mM NaCl, and 10% glycerol (declustering step). The binding and reclustered step were varied by 1, 2, and 3 hours incubation time with dye solution (50% v/v). Then the elimination of non-specific dye binding was accomplished by dialysis of the encapsulated protein in buffer containing 10 mM PIPES (pH 8.0) and 100 mM NaCl overnight. The Superose 6 gel filtration chromatography and DLS of the 24-subunit Histag protein were performed as control experiments. In addition, protein concentrations after the various binding and reclustered steps were calculated.

Effect of Protein Subunit Homogeneity

Superose 6 gel filtration chromatography of Histag and WT bFT yielded 24-subunit proteins, which were then mixed at various combinations of 100% Histag (100/0:Histag/WT), 60% Histag with 40% WT (60/40:Histag/WT), 50% Histag with 50% WT (50/50:Histag/WT), 40% Histag with 60% WT (40/60:Histag/WT), and 100% WT (0/100:Histag/WT). The declustering step was then done on these mixtures under dialysis condition in the buffer containing 10 mM PIPES (pH 2.0), 150 mM NaCl, and 10% glycerol for 90 min. The binding and reclustered step was undertaken for two hours in duration with dye (50% v/v) and then followed by overnight dialysis against buffer containing 10 mM PIPES (pH 8.0) and 100 mM NaCl. The protein concentrations were measured to determine suitable protein combinations that yielded maximum dye encapsulation.

Effect of Protein Concentration

The 24-subunit cluster of Histag protein (0.5 mg/mL) from Superose 6 gel filtration chromatography was adjusted to 0.15 mg/mL and 0.45 mg/mL and then declustered in buffer containing 10 mM PIPES (pH 2.0), 150 mM NaCl, and 10% glycerol for 90 min. The proteins were encapsulated with dye (50% v/v) for 3 hours. The elimination of non-specific dye binding step was performed by dialysis against buffer containing 10 mM PIPES (pH 8.0) and 100 mM NaCl overnight. The control sample, 24-subunit Histag, was performed utilizing DLS and Superose 6 gel filtration chromatography.

Effect of Dialysis Time

The 24-subunit proteins of Histag and WT bFT from gel filtration chromatography were mixed in a combination of 100% Histag (100/0:Histag/WT) and 60% Histag with 40% WT (60/40:Histag/WT), in which both protein combinations were declustered in buffer containing 10 mM PIPES (pH 2.0), 150 mM NaCl, and 10% glycerol for 90 min. The proteins were then permitted to interact with dye (50% v/v) for two hours, then the elimination of non-specific dye binding in buffer containing 10 mM PIPES (pH 8.0) and 100 mM NaCl overnight was accomplished. The dialysis buffer was changed and dialysis was continued for an additional 5 hours. After measuring protein concentration, half of the samples were adjusted to a concentration of 0.23 mg/mL before measuring fluorescence, DLS, and Superose 6 gel filtration chromatography in parallel with the samples, whose protein concentrations were not adjusted.

Encapsulation by Wild-type Bacterioferritin

The bFT-WT protein was purified using Superose 6 gel filtration chromatography to obtain pure 24-subunit cluster. This was then declustered in buffer containing 10 mM PIPES (pH 2.0), 150 mM NaCl, and 10% glycerol for 90 min. The encapsulation was then undertaken by incubating the subunits with dye (50% v/v) for 3 hours. This was followed by the elimination of non-specific dye binding by dialysis against buffer containing 10 mM PIPES (pH 8.0) and 100 mM NaCl overnight. The dialysis buffer was changed and dialysis continued for an additional 5 hours.

Elimination of Non-specific Dye Binding

Superose 6 gel filtration chromatography in this set of experiments was performed on WT and Histag protein. The declustering step was skipped and the intact protein was simply incubated with dye (50% v/v) for 3 hours. The proteins were then dialyzed against buffer containing 10 mM PIPES (pH 8.0) and 100 mM NaCl overnight followed by an additional 5 hours with fresh dialysis buffer.

Non-encapsulated Proteins

The 24-subunit WT and Histag proteins were isolated from Superose 6 gel filtration chromatography. The combination of 100% Histag (100/0:Histag/WT), 60% Histag with 40% WT (60/40:Histag/WT), and 100% WT (0/100:Histag/WT) were declustered in buffer containing 10 mM PIPES (pH 2.0), 150 mM NaCl, and 10% glycerol for 90 min. The encapsulation processes skipped the binding of the dye but were reclustered, in which the protein samples were dialyzed against buffer containing 10 mM PIPES (pH 8.0) and 100 mM

NaCl overnight followed by an additional 5 hours of dialysis time with fresh dialysis buffer.

The proteins, 100% Histag (100/0:Histag/WT), 60% Histag with 40% WT (60/40:Histag/WT), and 100% WT (0/100:Histag/WT), after encapsulation process were called non-encapsulated Histag, non-encapsulated 60/40:Histag/WT, and non-encapsulated WT, respectively.

4.3.5: Determination of the Fluorescence Quenching

In the encapsulation experiments, the fluorescence of the encapsulated dye might be quenched by other dye molecules in close proximity or by proteins, causing lower fluorescence intensity than the one of non-encapsulated dye. The fluorescence quenching of the dye molecules encapsulated in the proteins was determined by denaturing proteins in a high concentration of Gdn-HCl, allowing dye molecules to become exposed to the solvent. The dye molecules were then expected to exhibit their actual fluorescence properties. In order to investigate the fluorescence quenching, the 24-subunit of Histag and WT proteins isolated by Superose 6 gel filtration chromatography were mixed at a combinations of 60% Histag with 40% WT (60/40:Histag/WT). The mixture was declustering in the buffer containing 10 mM PIPES (pH 2.0), 150 mM NaCl, and 10% glycerol for 90 min. The encapsulating step was undertaken for two hours (with 50% v/v dye) and then followed by overnight dialysis against buffer containing 10 mM PIPES (pH 8.0) and 100 mM NaCl. The mixture with encapsulated dye was incubated with 6 M Gdn-HCl for 2 hours at room temperature (final concentration of 4 M Gdn-HCl with total volume of 50 μ L). The sample was then loaded into a low volume quartz cuvette (45 μ L) before scanning for the emission wavelength between 400-550 nm with a fixed excitation at 345 nm. The size of the incoming slit and the outgoing slit were set to 1 nm with a 1 nm step size and a 1 second integration. The control experiments were (1) the

60/40:Histag/WT mixture with encapsulated dye in PIPES buffer (pH 8.0) containing 100 mM NaCl (same dye dilution factor as the one that diluted in Gdn-HCl solution), (2) 24-mer Histag protein in 6 M Gdn-HCl solution, and (3) 6 M Gdn-HCl solution.

4.3.6: Measurement of Heme Groups Incorporated in Bacterioferritin

The absorption at 417 nm (hem group absorbance) for the protein samples, native bFT-WT, native bFT with His₆-tag at the C-terminus, and bFT with His₆-tag at the C-terminus with encapsulated dye were measured using a UV-visible spectrophotometer at room temperature. These were performed by filtering 0.42 mg/mL samples through 0.2 μm GHP membranes before loading them into low volume quartz cuvettes (45 μL). The 24-subunit fractions of native proteins isolated by Superose 6 gel filtration chromatography were scanned directly for absorption at 417 nm. The proteins with encapsulated dye were performed as before: (1) dialysis of samples for 90 min against buffer containing 10 mM PIPES (pH 2.0), 150 mM NaCl, and 10% glycerol, (2) incubation of these declustered proteins with dye (50% v/v) in buffer containing 10 mM PIPES (pH 8.0) and 100 mM NaCl for 3 hours, and (3) dialysis against buffer containing 10 mM PIPES (pH 8.0) and 100 mM NaCl overnight with/without an additional 5 hours of dialysis time with fresh dialysis buffer. The extent of encapsulation of the dye molecules was examined by fluorescence spectroscopy, and protein stability was evaluated by Superose 6 gel filtration chromatography as well as dynamic light scattering stated in section 4.3.2.

The number of heme groups incorporated into protein samples was calculated from the Beer-Lambert law, $A = \epsilon BC$, where A is absorption measured at 417 nm, B is the cuvette path length (1 cm), C is the concentration of heme incorporated in samples, and ϵ_{417} is the extinction

coefficient at 417 nm ($\epsilon_{417} = 137\,000\text{ cm}^{-1}\text{M}^{-1}$ per heme per *E. coli* ferricytochrome protein) (Yariv *et al.*, 1981).

4.3.7: Determination of the Presence of Iron Atoms in Bacterioferritin

The 24-subunit fraction obtained from Superose 6 gel filtration chromatography was dialyzed in Chelex treated water overnight at 4 °C. The protein concentration was measured by the Bradford assay method. All containers and dialysis tubing were soaked in Chelex treated water before use. The sample was diluted six times with Chelex treated water to a final volume of 15 mL. This sample was sent for metal analysis in duplicate (ETL Chemspec Analytical Ltd.). The dialysis buffer that was also prepared similarly for metal analysis was sent as a control.

4.3.8: Determination of the Number of Dye Molecules Encapsulated into Bacterioferritin

The protein samples with encapsulated dye used for the calculation of the number of encapsulated dye molecules inside the protein cavity were bFT-WT with a His₆-tag at the C-terminus (100% Histag protein) and the combination of 60% bFT with His₆-tag at the C-terminus with 40% bFT-WT without His₆-tag at the C-terminus (60/40:Histag/WT mixture). The dye molecules were encapsulated under the following conditions: (1) dialysis of the protein samples for 90 min against buffer containing 10 mM PIPES (pH 2.0), 150 mM NaCl, and 10% glycerol, (2) declustering of the proteins in the presence of 50% dye (v/v) in buffer containing 10 mM PIPES (pH 8.0) and 100 mM NaCl for 2 hours, and (3) dialysis against buffer containing 10 mM PIPES (pH 8.0) and 100 mM NaCl overnight followed by an additional 5 hours of dialysis time with fresh dialysis buffer. The proteins with encapsulated

dye were filtered through 0.2 μm GHP membranes before calculating their protein concentration using the Bradford assay method. The samples were then examined by fluorescence spectroscopy, Superose 6 gel filtration chromatography, and DLS to investigate the stability of the 24-subunit clusters and the extent of successful encapsulation (similar protocols as in section 4.3.4). The UV-visible spectrophotometer was operated to measure absorption at 345 nm at room temperature using a 1 mL quartz cuvette. Each sample was performed in duplicate. The buffer containing 20 mM PIPES (pH 8.0) and 100 mM NaCl was used as a blank. The concentrations of encapsulated dye were calculated from the Beer-Lambert law with the experimental extinction coefficient (the results from section 4.3.3). The number of encapsulated dye molecules was determined from the ratio of these calculated dye concentrations and the protein concentrations measured after the encapsulation processes.

4.4: Results and Discussion

4.4.1: DNA Cloning and Protein Purification

The PCR products of bFT-WT with *NdeI* and *XhoI* cutting sites (~470 bp) are shown in Figure 4.5. This fragment was then inserted into the pET-22b(+) vector to generate a plasmid containing the gene coding for bFT with a His₆-tag at the C-terminus (sequence is shown in Appendix 4). The results of overexpression and protein purification utilizing heat denaturation and ammonium sulfate precipitation are shown in the SDS PAGE gel figure (Figure 4.6). A monomeric subunit of bFT with a His₆-tag at the C-terminus is shown as a band with MW ~18.5 kDa. It should be noted that based on experiment, the bFT proteins have tight interaction in the dimeric form such that some dimer is observed in gels (MW ~40 kDa) even under SDS PAGE conditions. The existence of monomeric subunit mass was confirmed by

electrospray MS (Appendix 5). Further purification was accomplished by Superose 6 gel filtration chromatography (Appendix 7). This technique was also used to test for protein stability.

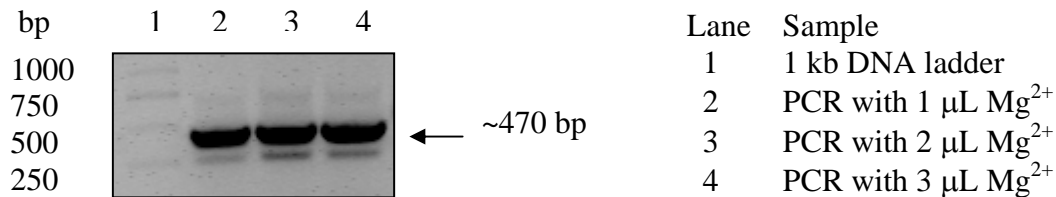


Figure 4.5: The 1% agarose gel representing PCR products of bFT-WT with *NdeI* cutting site at the N-terminus and *XhoI* cutting site at the C-terminus.

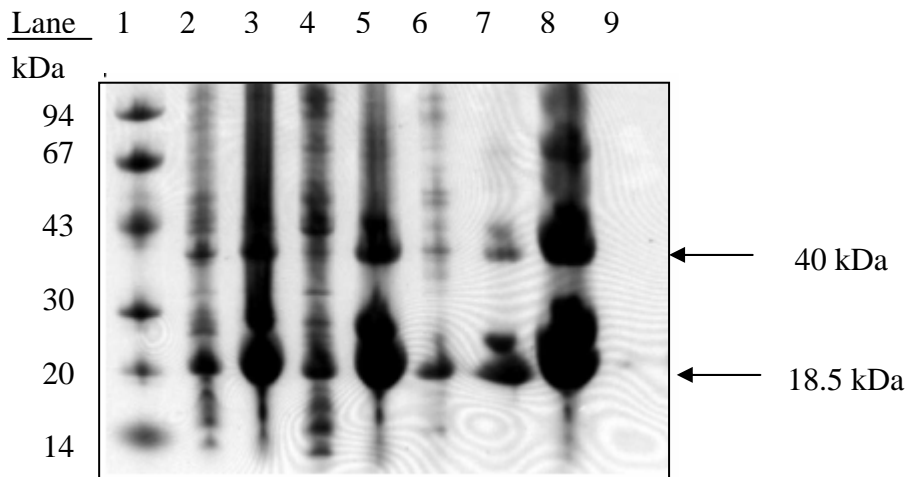


Figure 4.6: SDS PAGE of protein purification of bFT with His₆-tag at the C-terminus by heat denaturation and ammonium sulfate precipitation. The molecular weight at 18.5 kDa represents monomer and 40 kDa represents dimeric bFT mutant. The samples that were loaded in each lane are shown as followed.

Lane	Sample	Lane	Sample
1	MWM	6	Pellet from 25% ammonium sulfate
2	Pellet from sonication	7	Supernatant from 25% ammonium sulfate
3	Supernatant from sonication	8	Pellet from 40% ammonium sulfate
4	Pellet from heat denaturation	9	Supernatant from 40% ammonium sulfate
5	Supernatant from heat denaturation		

4.4.2: Dye Identification

Pro-Q[®] sapphire 365 oligohistidine gel stain is a commercially available fluorescent dye containing a nickel-NTA group that shows high affinity to His-tag containing proteins. As such it is used for fluorescent identification of His-tag proteins, especially useful for gel staining (Hart *et al.*, 2003). Rather than synthesizing our own fluorescent labeled nickel-NTA dye, we utilized this well known dye in our attempts to develop methods to encapsulate host molecules into the cavity of bFT (or rather bFT with a C-terminal Histag). Although described in a patent application (PCT-WO 2004/025259 A2, site-specific labeling of affinity tags in fusion proteins) by Molecular Probes, we wished to confirm some of the properties of this dye. Hence an analysis of the commercial dye stain was undertaken. The commercial solution (P21876) is said to contain 57.3 mM PIPES buffer, but no mention is made of Ni²⁺ or dye concentrations. Molecular Probes declined supplying additional information on this dye. The first investigation we undertook was to determine the mass spectrum of the dye solution.

The literature search retrieved from a patent application for a site-specific labeling of affinity tags in fusion proteins suggested that the dye molecules in Pro-Q[®] sapphire 365 oligohistidine gel stain might have a structure related to coumarin (Figure 4.7a). The patent search suggested that the potential dye might be 7-amino-3-(1-carboxy-1-(bis(carboxymethyl)amino)-5-(acetyl amino))pentyl-4-methylcoumarin-6-sulfonic acid (MW = 553 Da) (Figure 4.7b).

By incubating the dye solution with 2% formic acid to precipitate PIPES that might interfere with the electrospray MS, the MW of dye molecules was calculated. The electrospray mass spectrum of commercial PIPES shows the intensities at 347 m/z, which might correspond to the mass of one molecule of PIPES (MW = 302 Da) with two adducts of Na⁺, at 671 m/z,

which might be the mass of two molecules of PIPES with three adducts of Na^+ , and at 995 m/z, which is similar to the MW of three molecules PIPES with four adducts Na^+ (Figure 4.8). Comparing the MS of pure PIPES, it is observed that the intensity at 631 m/z might be the potential MW of 7-amino-3-(1-carboxy-1-(bis(carboxymethyl)amino)-5-(acetylamino))pentyl-4-methylcoumarin-6-sulfonic acid (MW = 553 Da) with one adduct of Ni^{2+} and one adduct of Na^+ (Figure 4.9). The intensity at 641 m/z might correspond to the MW of one dye molecule with four adducts of Na^+ . The high intensity at 437 m/z might correspond to the MW of one molecule PIPES with six adducts of Na^+ (MW = 440 Da).

From the predicted structure of the dye, it is found that Alexa Fluoro 350 (aminocoumarin conjugate) has a similar structure (Figure 4.7c). Alexa Fluoro[®] 350 carboxylic acid is a product of Invitrogen Molecular Probes (Burlington, ON) that can be used in many multicolor fluorescence applications. Alexa Fluoro 350 is an amine-reactive 7-aminocoumarin derivative with the maximum absorption at 346 nm and maximum emission intensity at 445 nm. Its extinction coefficient measured at 346 nm in a solvent pH 7.0 is 19 000 $\text{M}^{-1}\text{cm}^{-1}$ (data retrieved from the Handbook of Fluorescent Probes and Research Products, Invitrogen Molecular Probes, Burlington, ON). Since both compounds share the same fluorophore (coumarin) as a part of their structures, they should have very similar if not identical extinction coefficients. By using the Beer-Lambert law ($A = \epsilon BC$), the extinction coefficient of the dye molecule determined by a fluorescence measurement and UV-visible spectrum was calculated to be 23 000 $\text{cm}^{-1}\text{M}^{-1}$ (Appendix 8), which is similar to the estimated extinction coefficients (19 000 $\text{cm}^{-1}\text{M}^{-1}$) determined by the related structure of the dye molecule.

The dye concentration was calculated by this experimental extinction coefficient using the Beer-Lambert law, $A = \epsilon_{345}BC$, where A is absorption of Pro-Q[®] sapphire 365 oligohistidine gel stain measured at 345 nm (average OD_{345} of the dye is 0.2117), B is the cuvette path length (1 cm), C is the concentration of the dye in a solution, and ϵ_{345} is the experimental extinction coefficient at 345 nm ($23\,000\text{ M}^{-1}\text{cm}^{-1}$), the concentration of the dye in Pro-Q[®] sapphire 365 oligohistidine gel stain was approximately $9.2\ \mu\text{M}$.

The amount of metals present in the Pro-Q[®] sapphire 365 oligohistidine gel stain were evaluated in Appendix 11. It was determined by ICP-MS that only Ni^{2+} and Na^{+} ions are present in the stain. The concentration of Ni^{2+} was determined to 7.125 mg/L ($60.7\ \mu\text{M}$), and the ratio of Ni^{2+} /dye molecule was approximated 6.6 in the Pro-Q[®] sapphire 365 oligohistidine gel stain. The sodium concentration was found to be 120 mM .

The fluorescence quenching of the dye molecules might occur in the Pro-Q[®] sapphire 365 oligohistidine gel stain, causing low fluorescence intensity. This quenching might have resulted from the dye molecules that are blocked by their neighbors such that when the samples were excited at 345 nm, only some part of the fluorescence was emitted. Other possibilities are these dye molecules might form a complex once they are in a close proximity or it might be due to the ionic strength of these dye molecules. To investigate the dye quenching, the dye molecules in Pro-Q[®] sapphire 365 oligohistidine gel stain were treated with 6 M Gdn-HCl , isolating the dye complex to be free from each other. The emission spectra with the fixed excitation at 345 nm show that the denaturant-treated dye molecules possess higher emission intensity than the native dye (Figure 4.10). Once the encapsulations of the dye molecules into bFT proteins are performed, the measured fluorescence intensity is expected to be lower than that of the actual dye molecules.

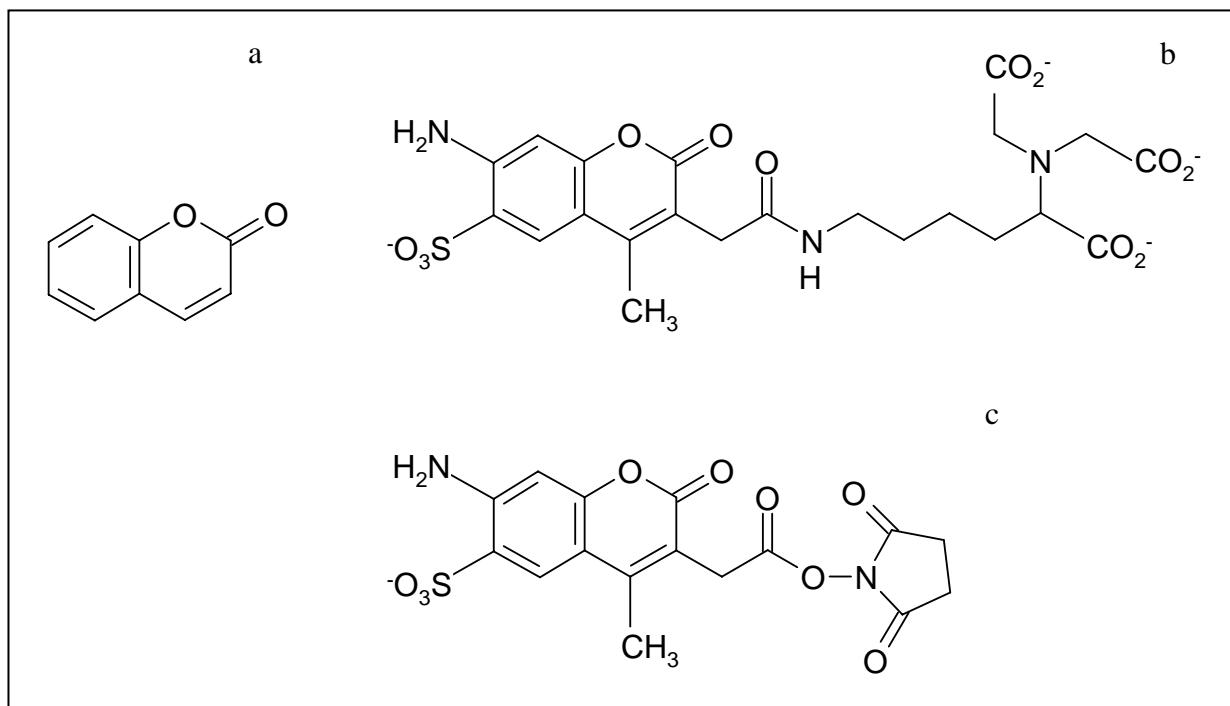


Figure 4.7: The structure of coumarin (a), 7-amino-3-(1-carboxy-1-(bis(carboxymethyl)amino)-5-(acetamino))pentyl-4-methylcoumarin-6-sulfonic acid (b), and Alexa Fluoro 350 carboxylic acid (c).

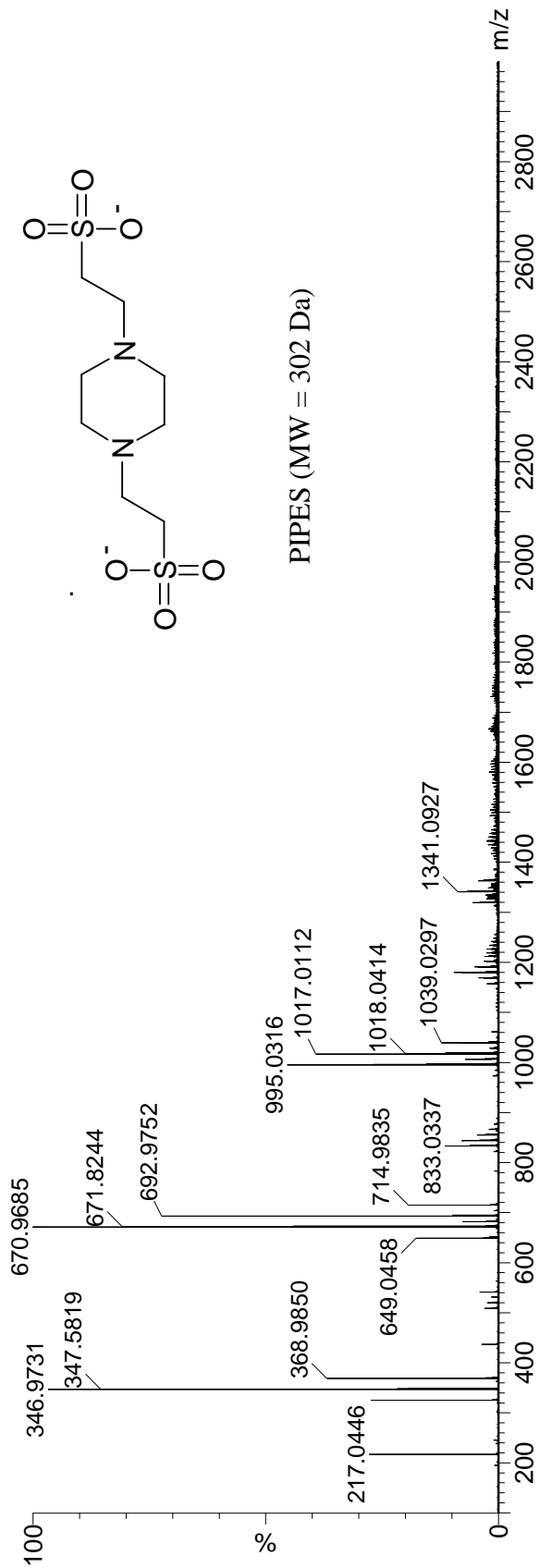


Figure 4.8: The electrospray mass spectrum of commercial PIPES (literature MW = 302 Da) representing the series of intensity at 347 m/z, which might correspond to the MW of one molecule PIPES and two molecules Na⁺, at 671 m/z, which is similar to the MW of two molecules PIPES and three molecules Na⁺, and at 995 m/z, which might be the MW of three molecules PIPES and four molecules Na⁺.

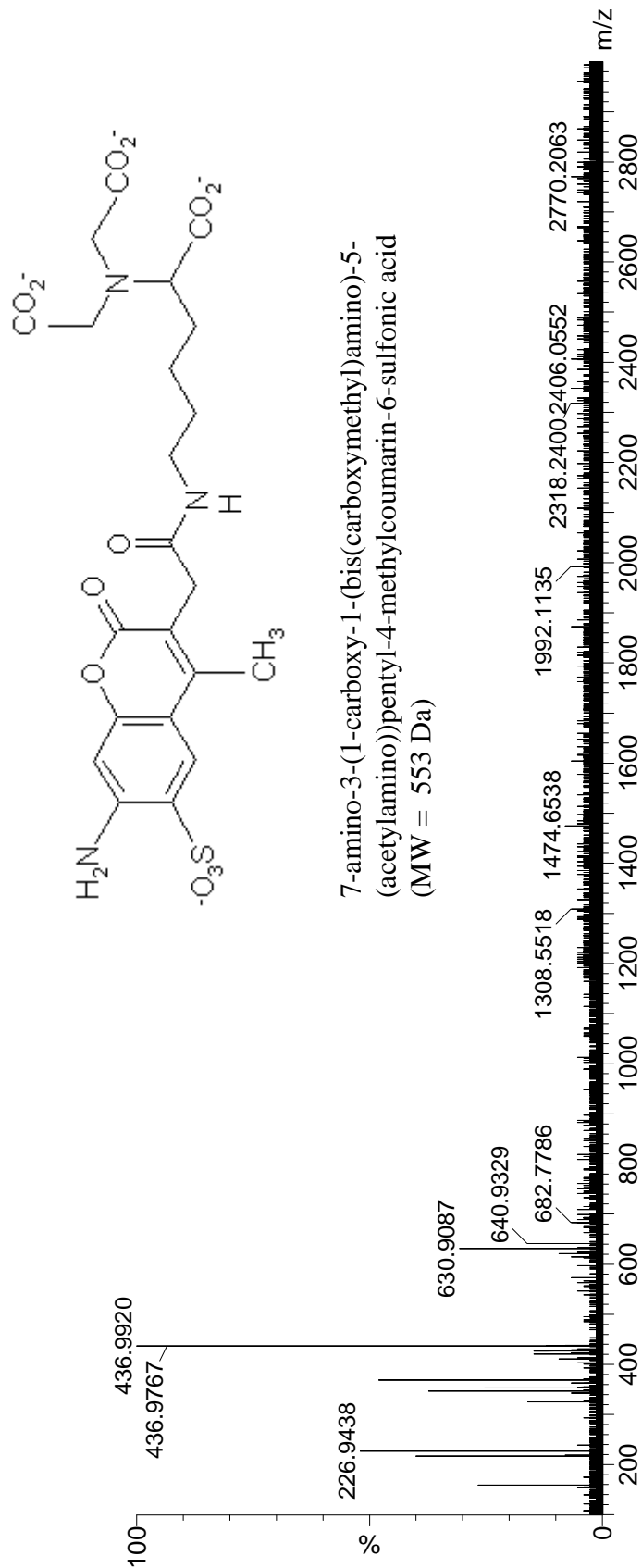


Figure 4.9: The electrospray mass spectrum of dye molecules in Pro-Q[®] sapphire 365 oligohistidine gel stain, which was determined after incubating the dye solution with 2% formic acid to precipitate PIPES, representing the intensity at 631 m/z that might be the MW of one dye molecule (MW = 553 Da) with one adduct of Ni²⁺ and one adduct of Na⁺. The intensity at 641 m/z might correspond to the MW of one dye molecule with four adducts of Na⁺.

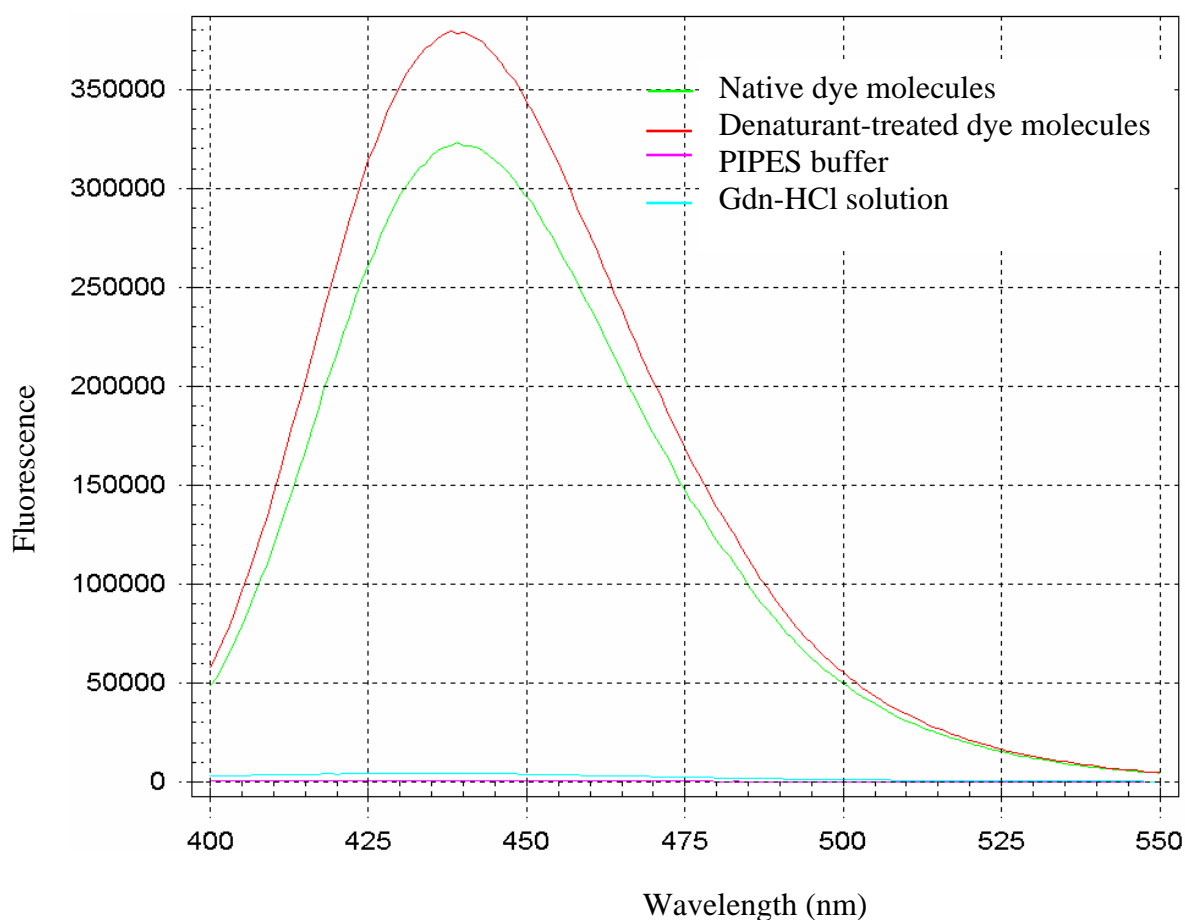


Figure 4.10: The emission spectra scanned between wavelengths 400-550 nm with the fixed excitation at 345 nm of the native dye molecules in Pro-Q[®] sapphire 365 oligohistidine gel stain (PIPES buffer pH 7.0), the denaturant-treated dye molecules in 6 M Gdn-HCl solution, PIPES buffer, and 6 M Gdn-HCl solution showing maximum fluorescence intensity at 440 nm.

4.4.3: Optimum Conditions for Encapsulation of Bacterioferritin

Effect of Declustering Time

The collected 24-mer fraction of Histag protein from the Superose 6 gel filtration chromatography yielded ~0.50 mg/mL, which were reduced to ~0.45 mg/mL after the encapsulation process. The decreased protein concentration could be due to poor solubility over the pH range 3.5-5.4 resulting in aggregation close to the protein's pI of 4.6. From fluorescence measurements, it was shown that the highest fluorescence intensity of

encapsulated dye was obtained for the protein using a 90 min declustering time (Figure 4.11). The Superose 6 gel filtration chromatograms showed that the proteins were stable under the encapsulated conditions, in which the intensity of 24-subunit peak (~30 min eluted time) was higher than that of the dimer peak (~35 min eluted time) (Figure 4.12c, d, e), and they behaved similarly to those of the 24-mer Histag protein (Figure 4.12a) and non-specific dye binding protein (Figure 4.12b). The DLS results, on the other hand, showed that the proteins with encapsulated dye were not as stable as the 24-subunit cluster such that there was small peak at ~50 nm (aggregates) presented in the sample with 90 min declustering time, while the other two samples formed broad peaks (Figure 4.13).

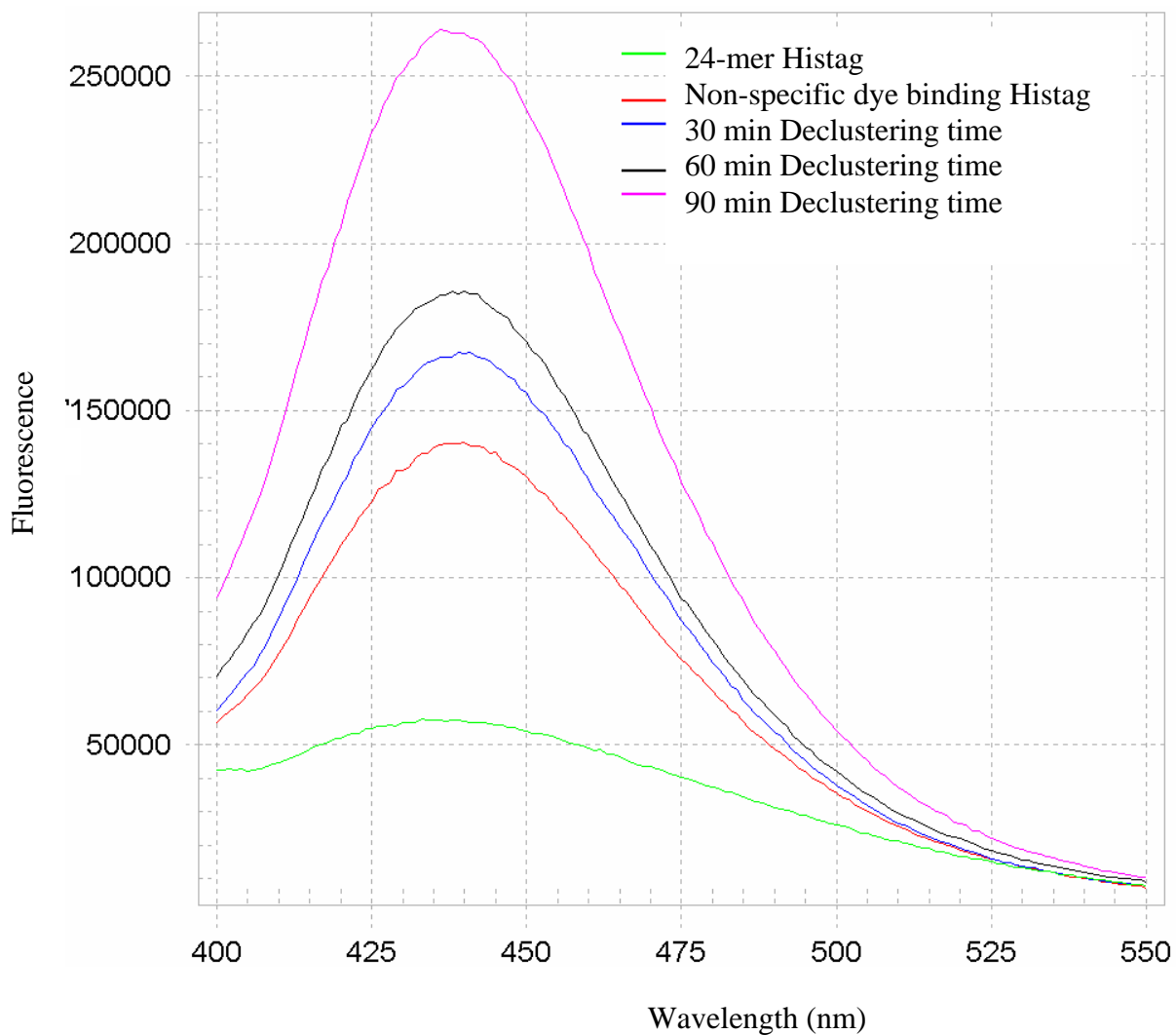


Figure 4.11: The emission spectra scanned between wavelengths 400-550 nm with the fixed excitation at 345 nm of the 24-mer Histag protein, non-specific dye binding Histag protein, Histag protein after 30, 60, and 90 min declustering time showing maximum fluorescence intensity at 440 nm.

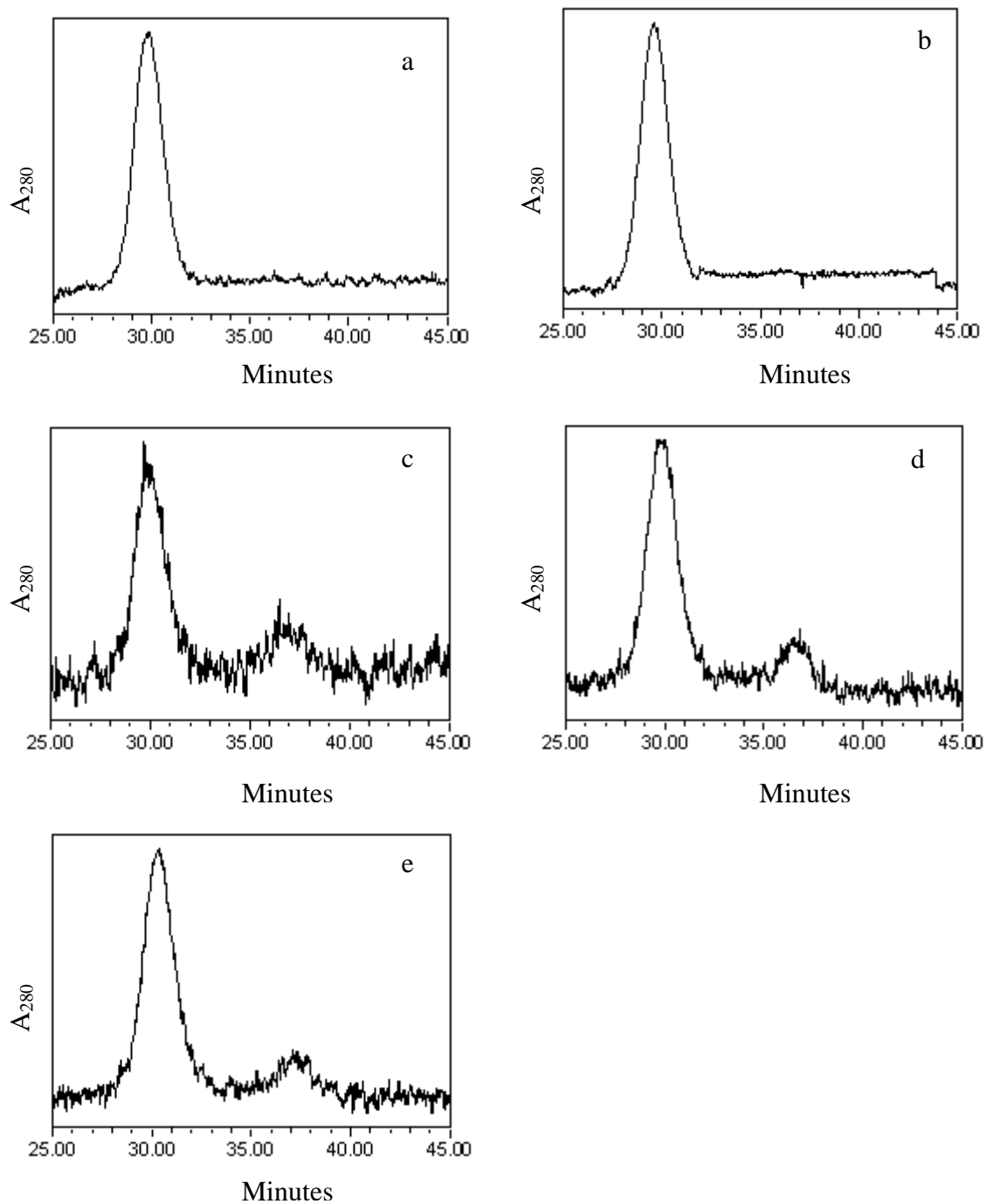


Figure 4.12: The Superose 6 gel filtration chromatograms of 24-mer Histag protein (a), non-specific dye binding Histag protein (b), Histag protein with encapsulated dye after 30 min declustering time (c), Histag protein with encapsulated dye after 60 min declustering time (d), Histag protein with encapsulated dye after 90 min declustering time (e). The first peak at ~30 min represents 24-mer and the second peak at ~37 min represents dimer protein.

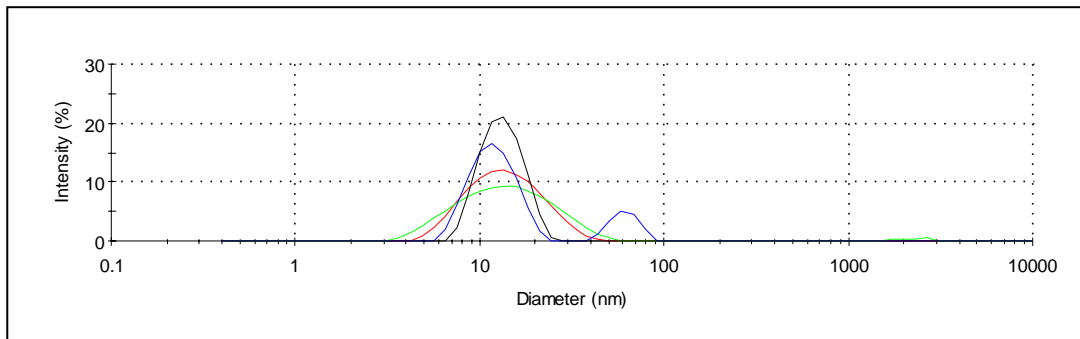


Figure 4.13: The size distribution by intensity plot of 24-subunit Histag protein (black), Histag protein with encapsulated dye after 30 min (red), 60 min (green), and 90 min (blue) declustering time. The peak at ~16 nm represents 24-subunit protein and the peak at higher diameter represents higher self-aggregation (multi 24-subunit clusters).

Effect of Encapsulation Time

The 24-subunit fraction used for encapsulation was ~0.50 mg/mL and yielded ~0.23 mg/mL after the encapsulating process. It was shown that the two-hour encapsulation time yielded the highest fluorescence intensity of dye associated protein (Figure 4.14). However, the calculation of protein concentration suggested that the longer encapsulation time resulted in greater amounts of protein aggregation (i.e. less protein concentration after encapsulation process) (Table 4.4). Therefore, two hours might be the most suitable encapsulation time for these specific conditions. The results from Superose 6 gel filtration chromatography showed that proteins were less stable after the encapsulation process compared to that of an intact 24-subunit Histag starting protein (Figure 4.15), while DLS results showed that protein stability for the two-hour encapsulation time was better than the others, in which higher self-aggregation (~100 nm in diameter cluster) was not observed in this sample (Figure 4.16).

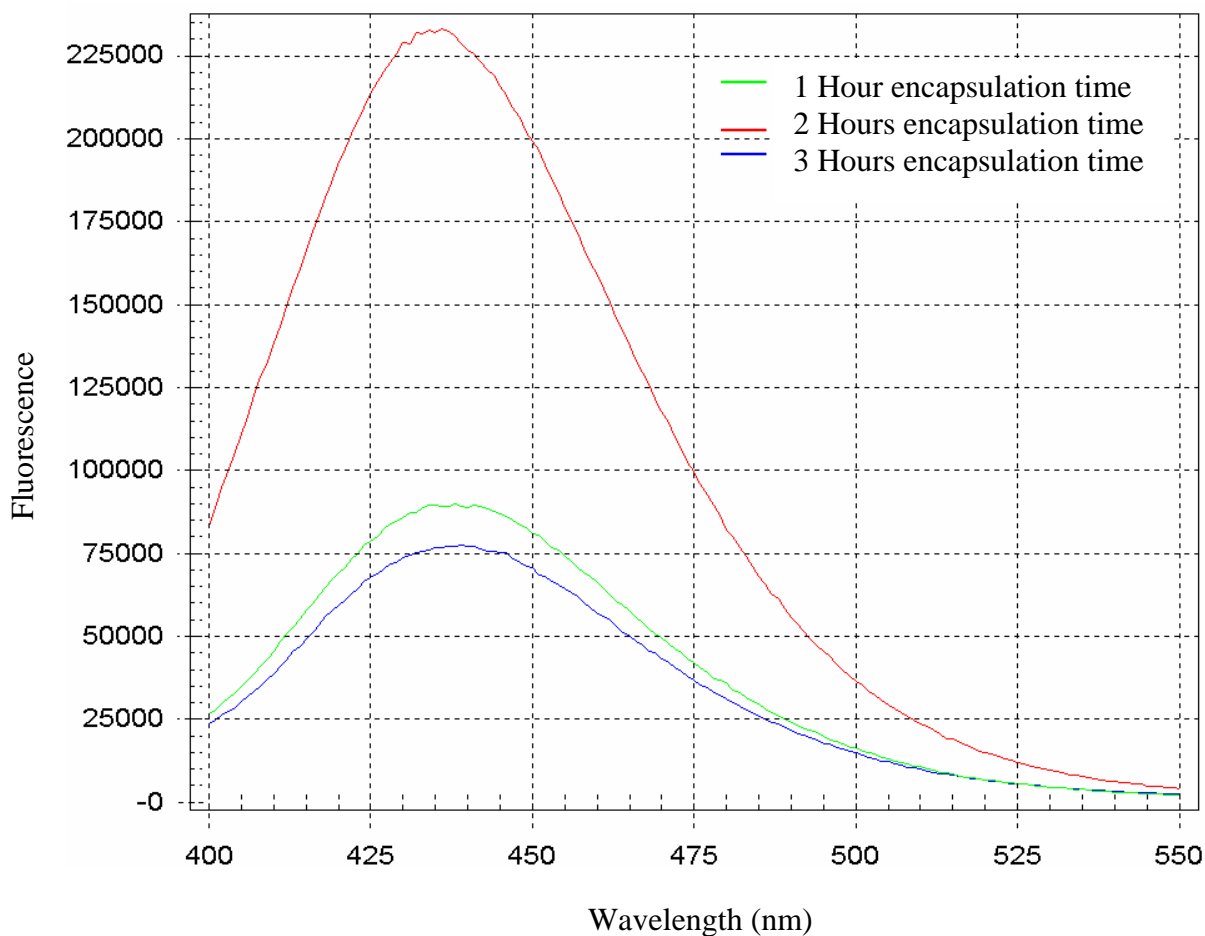


Figure 4.14: The emission spectra scanned between wavelengths 400-550 nm with the fixed excitation wavelength at 345 nm of Histag protein after encapsulated with dye molecules for 1, 2, and 3 hours showing maximum fluorescence intensity at 440 nm.

Table 4.4: The protein concentrations of the Histag protein that encapsulated dye molecules at various periods encapsulating time were calculated after dialysis overnight.

Sample	Concentration after dialysis (mg/mL)
Histag protein after encapsulated with dye for 1 hour	0.30
Histag protein after encapsulated with dye for 2 hours	0.29
Histag protein after encapsulated with dye for 3 hours	0.15

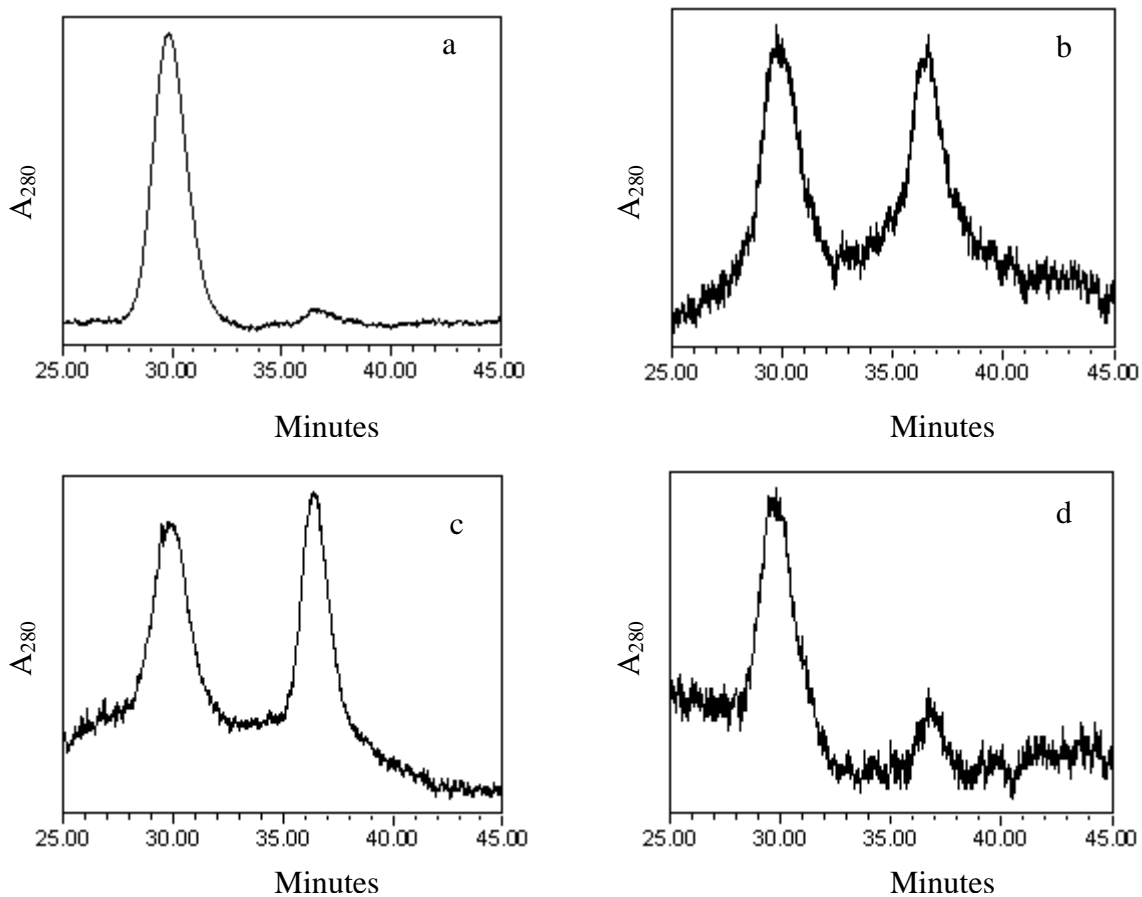


Figure 4.15: The Superose 6 gel filtration chromatograms of 24-mer Histag protein (a), Histag protein after encapsulated with dye molecules for 1 hour (b), 2 hours (c), and 3 hours (d). The first peak at ~30 min represents 24-subunit and the second peak at ~37 min represents dimer protein.

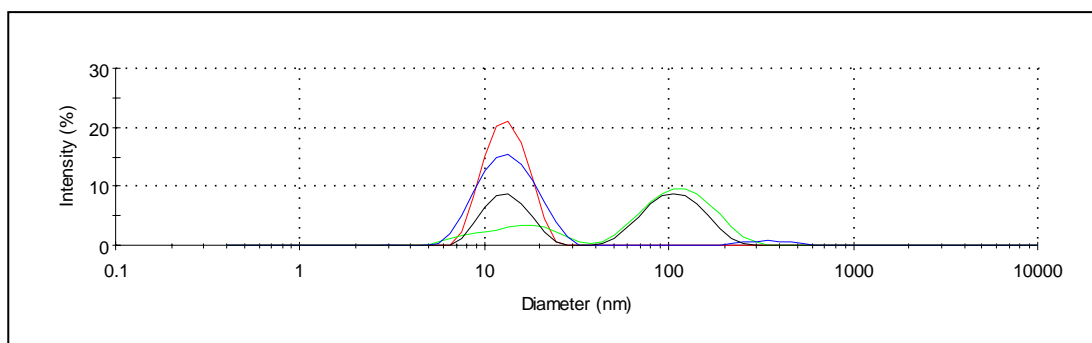


Figure 4.16: The size distribution by intensity plot of 24-mer Histag protein (red), Histag protein after encapsulated with dye molecules for 1 hour (green), 2 hours (blue), and 3 hours (black). The peak at ~16 nm represents 24-subunit protein and the peak at ~100 nm represents higher self-aggregation.

Effect of Protein Subunit Homogeneity

The concentration of ~0.50 mg/mL for the 24-subunit proteins prepared by Superose 6 gel filtration chromatography was decreased after the encapsulation experiments due to aggregation proportional to the increasing amount of the Histag protein present in the mixture (Histag:WT proteins) (Table 4.5). This suggested that the encapsulation of the dye could cause some steric effects that interfered with successful reclustering. While 100% Histag protein seemed to produce the highest aggregation, it was also found to have the highest fluorescence intensity or consequently the highest amount of dye encapsulated inside the protein cavity (Figure 4.17). The combination of 60/40:Histag/WT mixture yielded the second highest fluorescence intensity, while the rest gave much lower intensities. Therefore, in order to compare and consider advantages between using 100% Histag or a 60/40:Histag/WT ratio for encapsulation studies, Superose 6 gel filtration chromatograms and DLS results were evaluated. The Superose 6 chromatograms for the 100% Histag experiments yielded a higher intensity of 24-subunit than dimer quaternary structure, while that of the 60/40:Histag/WT mixture yielded similar intensity for these two forms (Figure 4.18c, d). It was suggested that 100% Histag protein might be more stable than 60/40:Histag/WT mixture after the encapsulation experiments. The DLS results indicated that stability of 100% Histag protein was lower than the 60/40:Histag/WT mixture, because the 100% Histag protein system formed self-associated clusters with diameters of ~1000 nm (Figure 4.19).

Table 4.5: The protein concentrations of Histag/WT mixtures calculated after dialysis overnight.

Sample	Concentration after dialysis (mg/mL)
100/0:Histag/WT	0.23
60/40:Histag/WT	0.34
50/50:Histag/WT	0.48
40/60:Histag/WT	0.44
0/100:Histag/WT	0.54

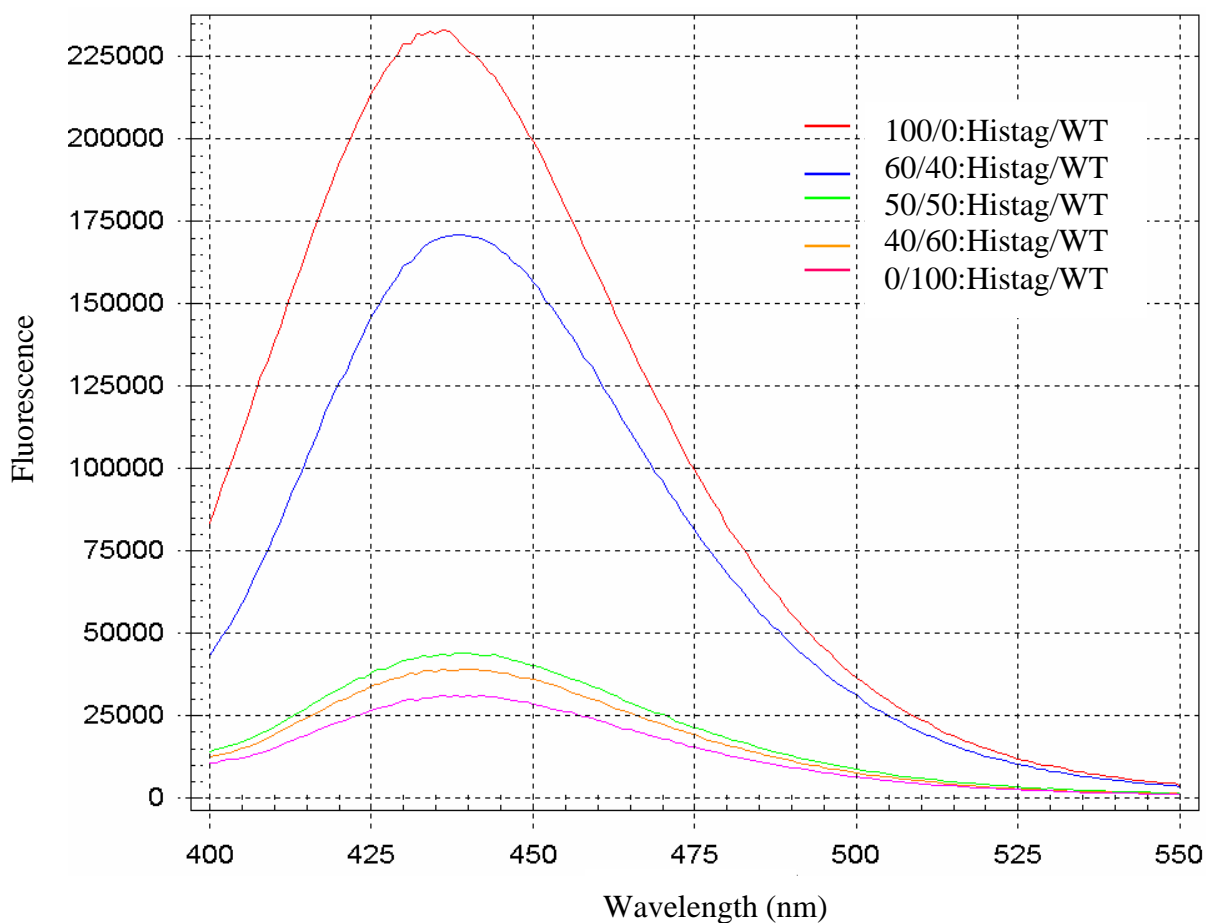


Figure 4.17: The emission spectra scanned between wavelengths 400-550 nm with the fixed excitation at 345 nm of the various combinations of Histag/WT mixture with encapsulated dye showing maximum fluorescence intensity at 440 nm.

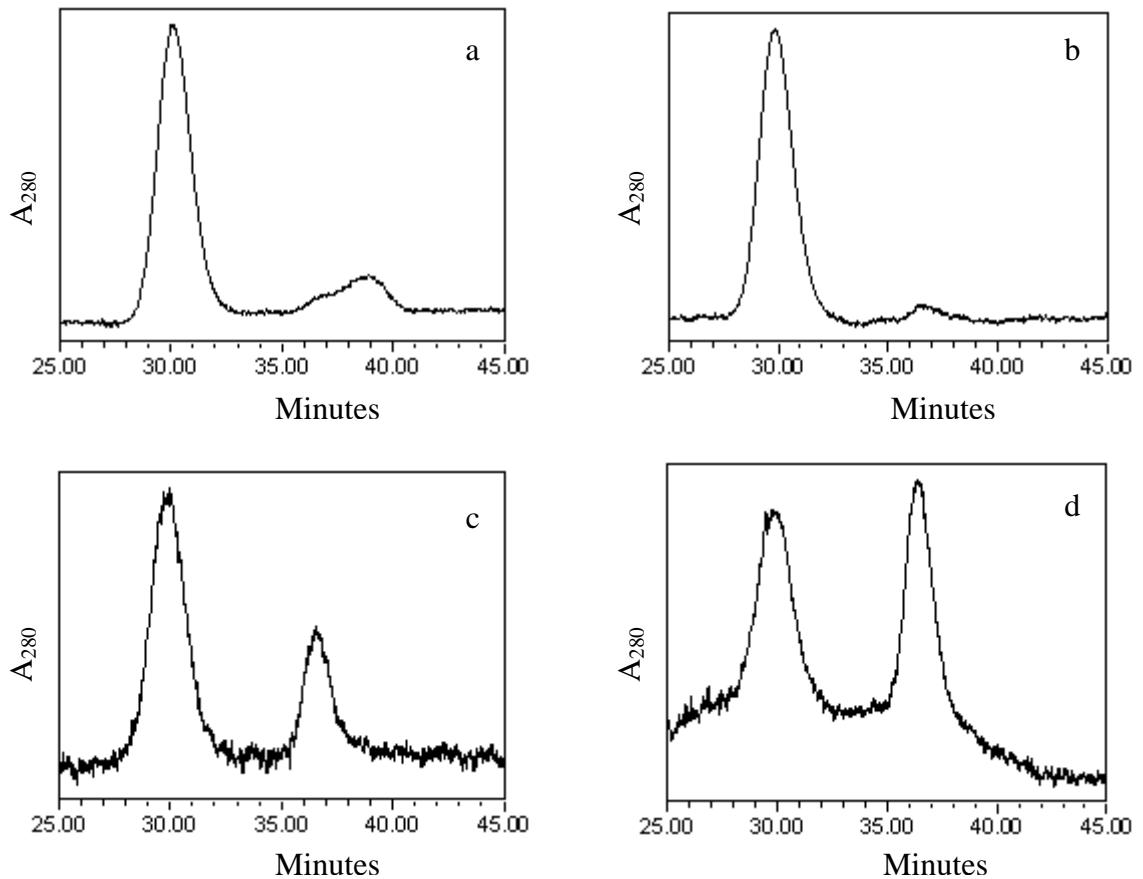


Figure 4.18: The Superose 6 gel filtration chromatograms of 24-mer WT protein (a), 24-mer Histag protein (b), 100/0:Histag/WT mixture with encapsulated dye (c), and 60/40:Histag/WT mixture with encapsulated dye (d). The first peak at ~30 min represents 24-subunit and the second peak at ~37 min represents dimer protein.

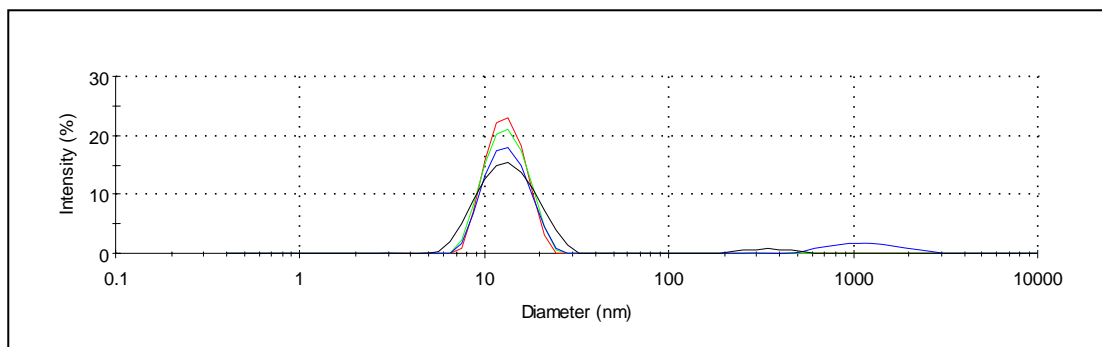


Figure 4.19: The size distribution by intensity plot of 24-mer Histag protein (green), 24-mer WT protein (red), 100/0:Histag/WT mixture with encapsulated dye (blue), and 60/40:Histag/WT mixture with encapsulated dye (black). The peak at ~16 nm represents 24-mer protein and the peak at higher diameter represents higher self-aggregation.

Effect of Protein Concentration

The concentration of the ~0.50 mg/mL 24-subunit of Histag protein was adjusted to 0.15 mg/mL and 0.45 mg/mL used for the encapsulation experiments. It was found that higher protein concentrations yielded higher fluorescence intensity after encapsulation experiments, where a larger amount of protein could accept more dye molecules for encapsulation (Figure 4.20). The results from Superose 6 chromatograms (Figure 4.21) and DLS (Figure 4.22) showed that protein stability was dependent on protein concentration, in which a greater protein concentration yielded higher stability. In addition, lower protein concentration tended to form higher self-associated clusters than single 24-subunit protein (Figure 4.22).

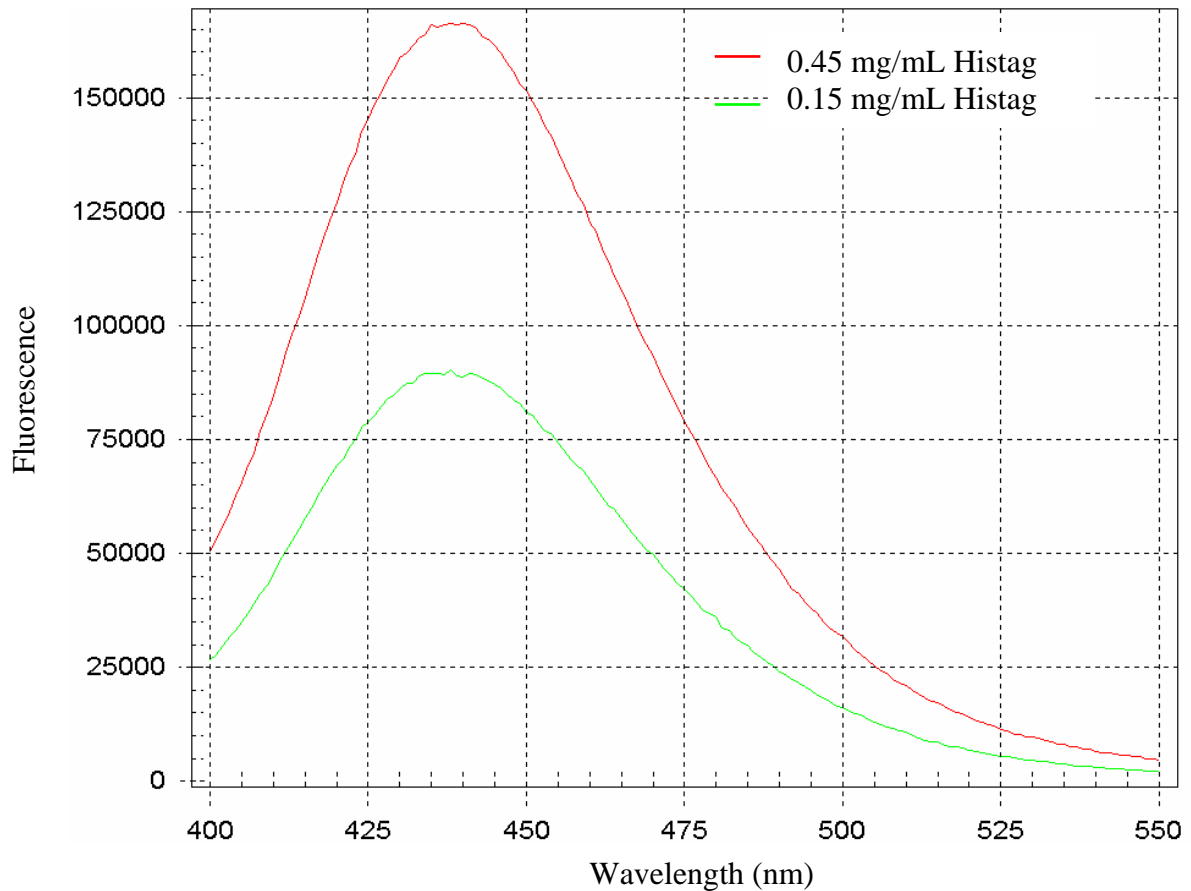


Figure 4.20: The emission spectra scanned between wavelengths 400-550 nm with the fixed excitation wavelength at 345 nm of 0.15 and 0.45 mg/mL Histag protein with encapsulated dye showing maximum fluorescence intensity at 440 nm.

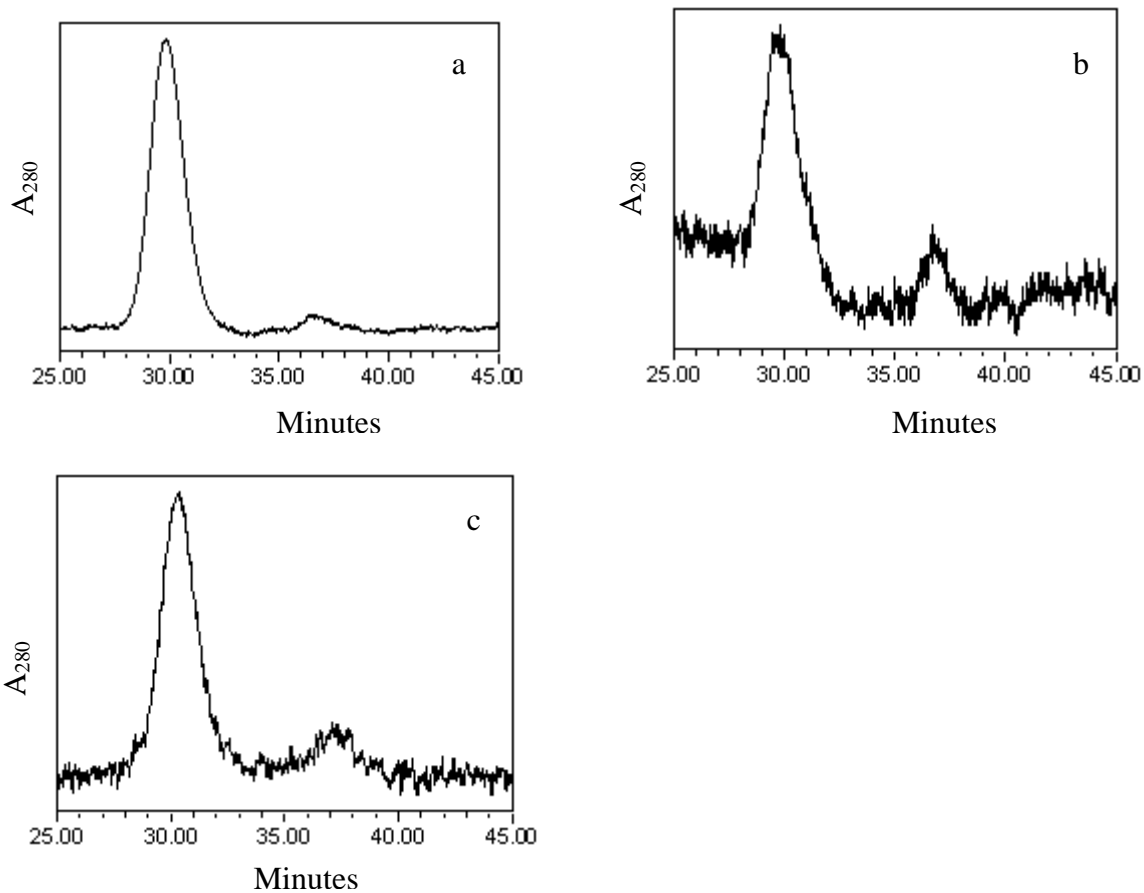


Figure 4.21: The Superose 6 gel filtration chromatograms of 24-mer Histag protein (a), 0.15 mg/mL (b) and 0.45 mg/mL (c) Histag protein with encapsulated dye. The first peak at ~30 min represents 24-subunit and the second peak at ~37 min represents dimer protein.

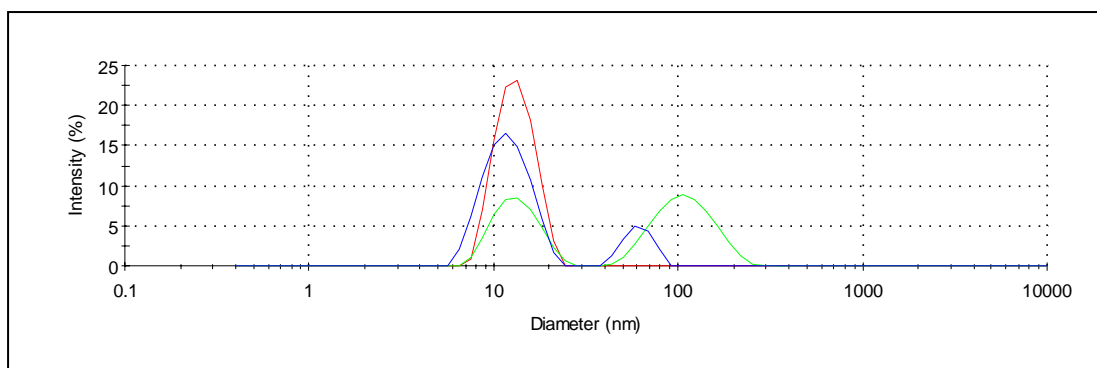


Figure 4.22: The size distribution by intensity plot of 24-mer Histag (red), 0.15 mg/mL (green) and 0.45 mg/mL (blue) Histag protein with encapsulated dye. The peak at ~16 nm represents 24-mer protein and the peak at higher diameter represents self-aggregation.

Effect of Dialysis Time

A ~0.5 mg/mL protein solution of purified 24-subunit Histag was prepared for encapsulation experiments. It was found that by performing an additional 5 hours of dialysis time with fresh dialysis buffer (other than overnight dialysis) could eliminate non-specific surface binding of the dye as well as perhaps remove dye produced from unstable 24-subunit proteins that allow encapsulated dye molecules to escape from their cavity (Figure 4.23). Low amount of protein aggregation was observed in the encapsulation experiments with an additional 5 hours of dialysis time. This can be determined by protein concentration (Table 4.6). Compared with the protein concentration in the encapsulation experiments without an additional dialysis step, the higher protein concentrations for both 100% Histag protein (0.37 mg/mL) and 60/40:Histag/WT mixture (0.67 mg/mL) with an additional 5 hours of dialysis time were observed. However, after adjusting all protein concentrations to 0.23 mg/mL, it was observed that 100% Histag protein yielded a higher fluorescence intensity for both before and after elimination of the non-specific surface binding of the dye (Figure 4.23). Since a higher intensity of dimeric protein was found after an additional 5 hours of dialysis time on Superose 6 gel filtration chromatograms, this additional dialysis time might relate to protein stability such that this procedure increases amounts of dimeric protein. In contrast to 60/40:Histag/WT mixture, it was also found that the 24-subunit peak using 100% Histag protein was higher than the dimer peak, which suggested a greater ability of the 100% Histag system to maintain 24-subunit quaternary structures than that of the 60/40:Histag/WT mixture (Figure 4.24 and 4.25). The stability tests by DLS were similar for both the 100% Histag protein and 60/40:Histag/WT mixture, although the 100% Histag protein was found to be more stable (similar intensity as 24-mer Histag) (Figure 4.26 and 4.27).

Table 4.6: The protein concentrations of Histag protein and the combination of Histag/WT mixture calculated after dialysis overnight with and without an additional 5 hours of dialysis time.

Sample	Protein Concentration (mg/mL)
100/0:Histag/WT	0.23
60/40:Histag/WT	0.34
100/0:Histag/WT after an additional 5 hrs of dialysis time	0.37
60/40:Histag/WT after an additional 5 hrs of dialysis time	0.67

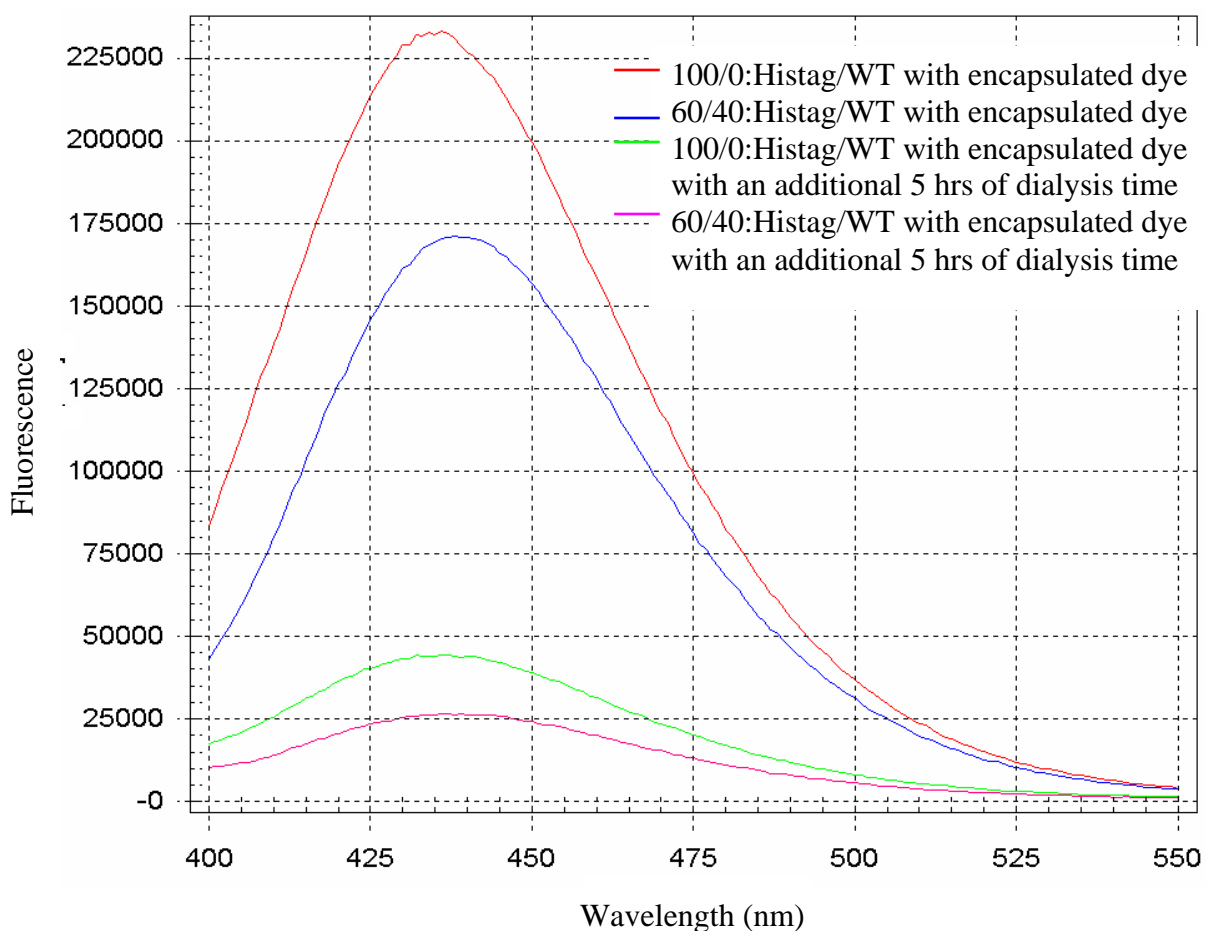


Figure 4.23: The emission spectra scanned between wavelengths 400-550 nm with the fixed excitation wavelength at 345 nm of 0.23 mg/mL of 100% Histag protein with encapsulated dye with and without an additional 5 hours of dialysis time and 0.23 mg/mL of 60/40:Histag/WT mixture with encapsulated dye with and without an additional 5 hours of dialysis time showing maximum fluorescence intensity at 440 nm.

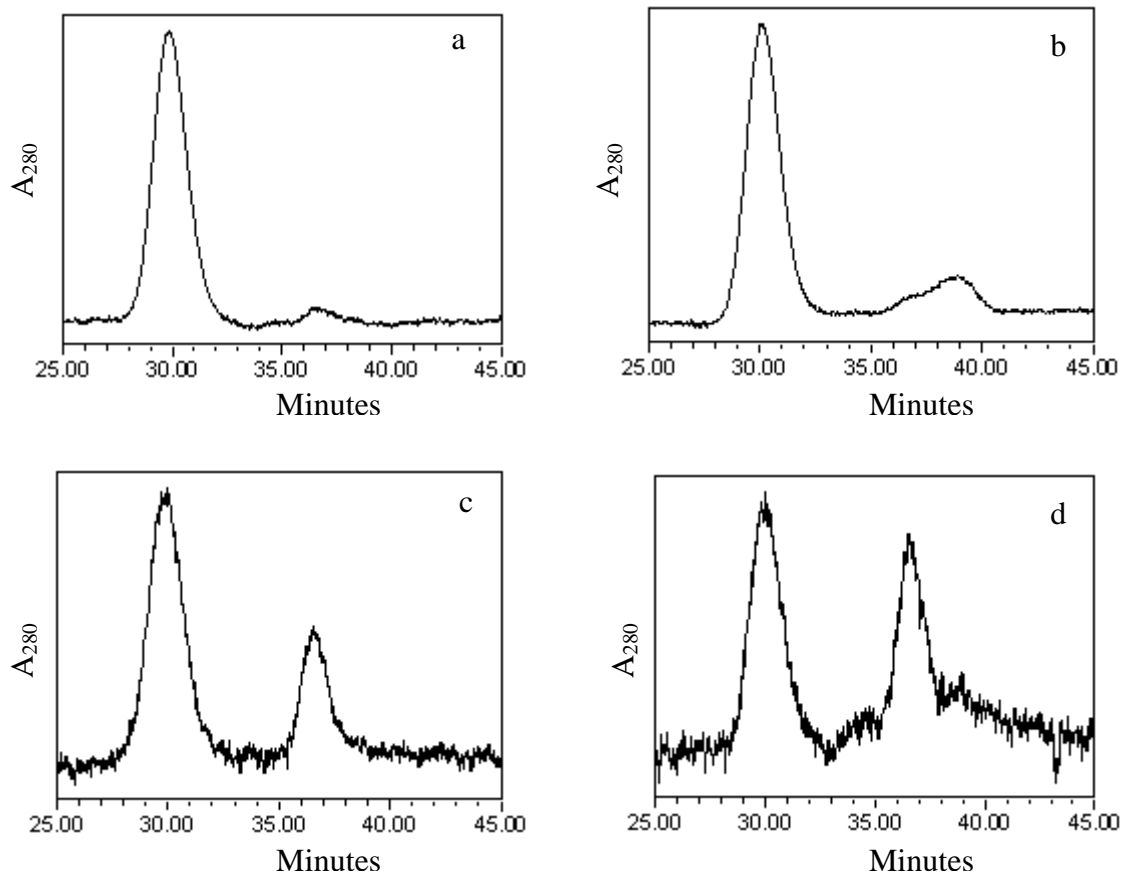


Figure 4.24: The Superose 6 gel filtration chromatograms of 24-mer Histag protein (a), 24-mer WT protein (b), 100/0:Histag/WT mixture with encapsulated dye before an additional 5 hours of dialysis time (c), and 100/0:Histag/WT mixture with encapsulated dye after an additional 5 hours of dialysis time (d) without adjusting protein concentration. The first peak at ~30 min represents 24-subunit and the second peak at ~37 min represents dimeric protein.

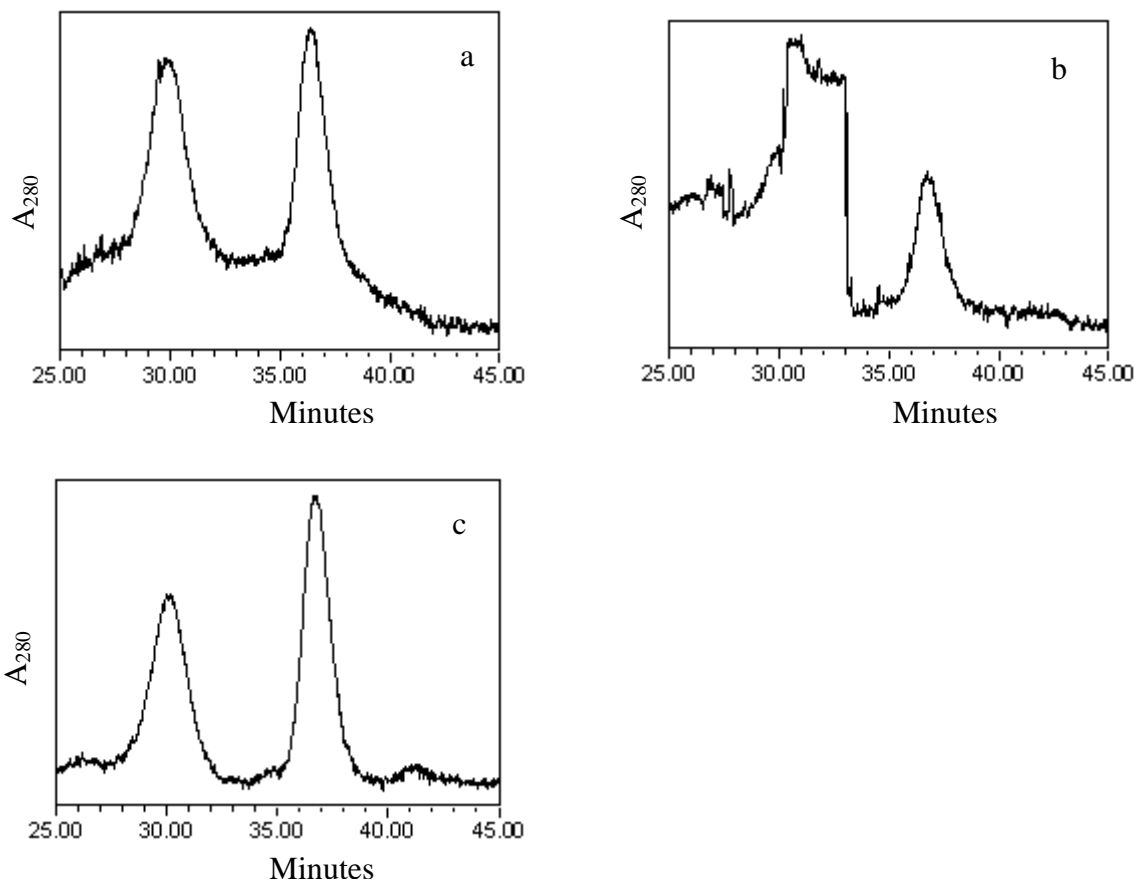


Figure 4.25: The Superose 6 gel filtration chromatograms of 60/40:Histag/WT mixture with encapsulated dye before an additional 5 hours of dialysis time (a), 60/40:Histag/WT mixture with encapsulated dye after an additional 5 hours of dialysis time (b), 60/40:Histag/WT mixture with encapsulated dye after an additional 5 hours of dialysis time (without adjusting protein concentration) (c). The first peak at ~30 min represents 24-subunit and the second peak at ~37 min represents dimeric protein.

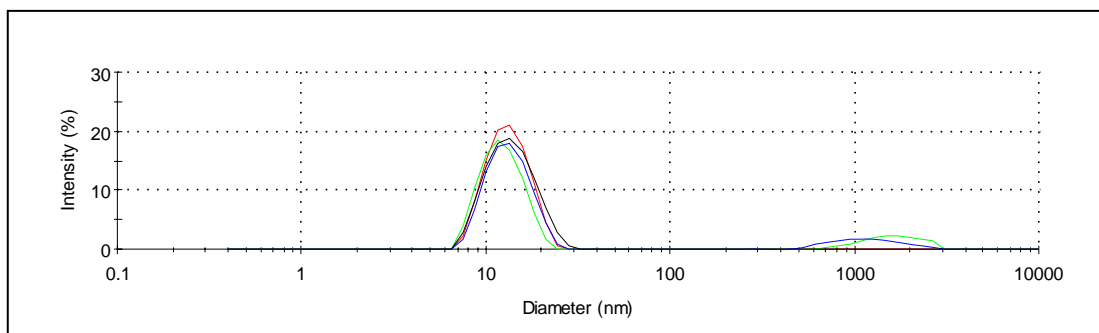


Figure 4.26: The size distribution by intensity plot of 24-mer Histag protein (red), 100/0:Histag/WT mixture with encapsulated dye (blue), 100/0:Histag/WT mixture with an additional 5 hours of dialysis time (green), and 100/0:Histag/WT mixture with an additional 5 hours of dialysis time without adjusting protein concentration (black).

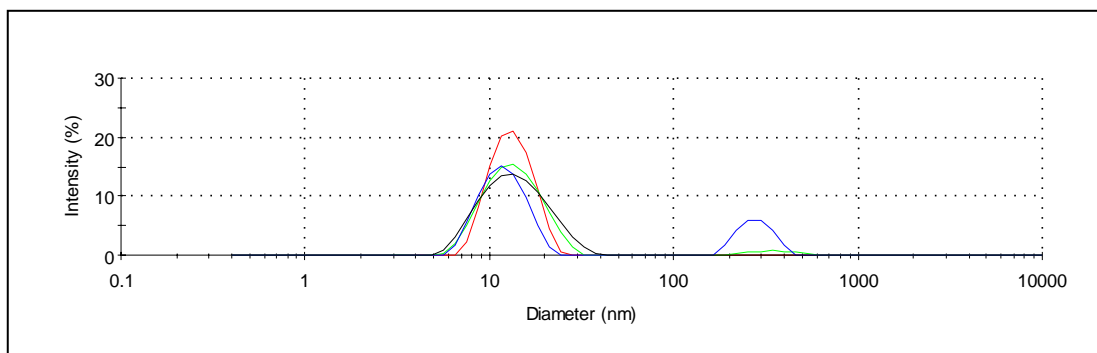


Figure 4.27: The size distribution by intensity plot of 24-mer Histag protein (red), 60/40:Histag/WT mixture with encapsulated dye (green), 60/40:Histag/WT mixture with an additional 5 hours of dialysis time (blue), 60/40:Histag/WT mixture with an additional 5 hours of dialysis time without adjusting protein concentration (black).

4.4.4: Control Experiments for Encapsulation by Bacterioferritin

Encapsulation by Wild-type Bacterioferritin

A 0.7 mg/mL solution of the 24-subunit WT protein was investigated for its ability to act as an encapsulation protein. The protein concentrations before and after the encapsulation processes were similar, and it was found that no dye was encapsulated within the WT cavity (Figure 4.28). By comparing these results with the 100% Histag system, it was found that the encapsulation of the dye seemed to lead to some protein aggregation. The decrease in fluorescence intensity for dye encapsulated into WT protein with an additional 5 hours of dialysis time confirmed that non-specific binding of the dye could be eliminated by this method. The dimer peak in Superose 6 gel filtration chromatograms was higher than that of the 24-subunit for WT protein in encapsulation experiments with and without an additional 5 hours of dialysis time (Figure 4.29b and 4.29c). DLS results showed that both WT proteins (with/without an additional 5 hours of dialysis time) had a smaller size than a starting 24-mer

WT protein (Figure 4.30). These results suggest that the encapsulation of dye might support the re-formation of the 24-subunit structure.

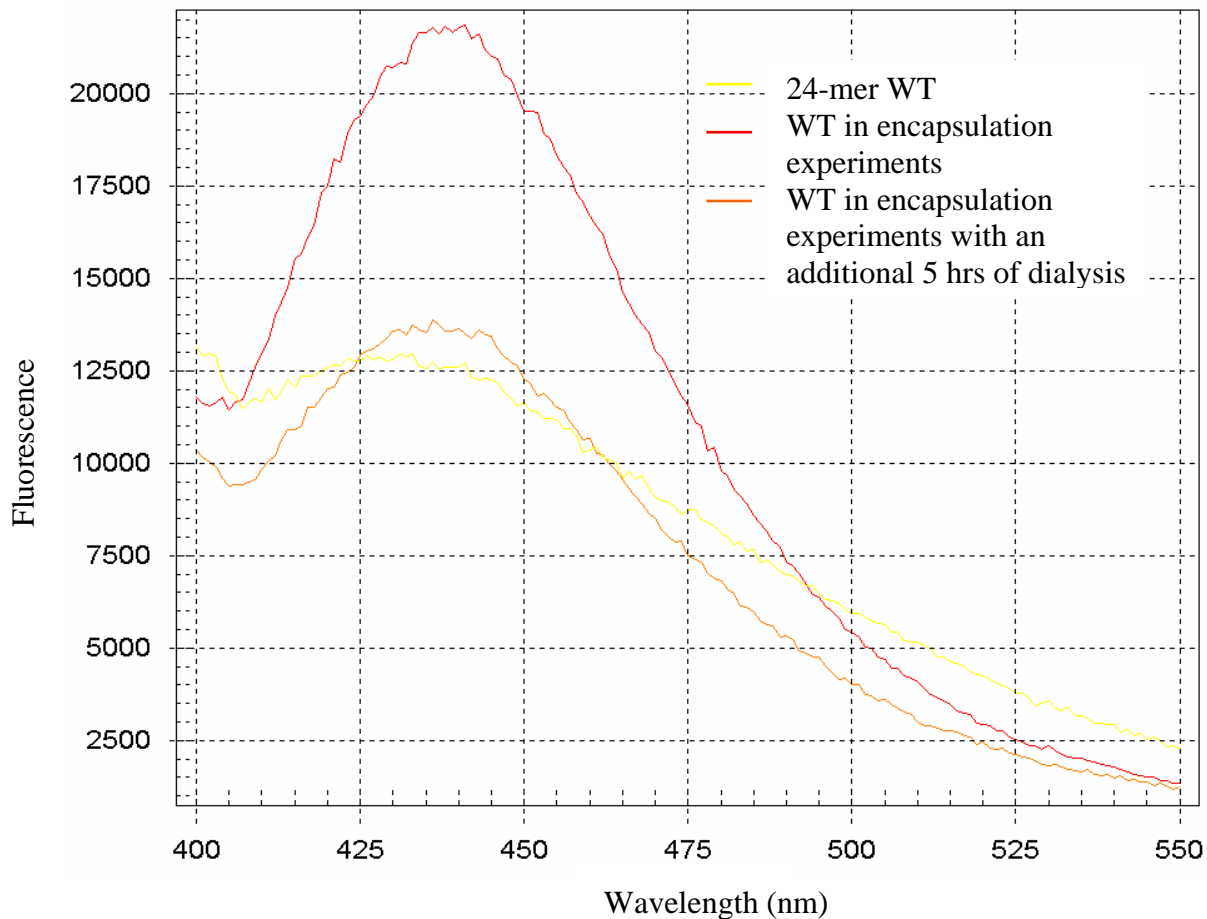


Figure 4.28: The emission spectra scanned between wavelengths 400-550 nm with the fixed excitation wavelength at 345 nm of 24-mer WT protein, WT protein in encapsulation experiments, and WT protein in encapsulation experiments with an additional 5 hours of dialysis time showing maximum fluorescence intensity at 440 nm.

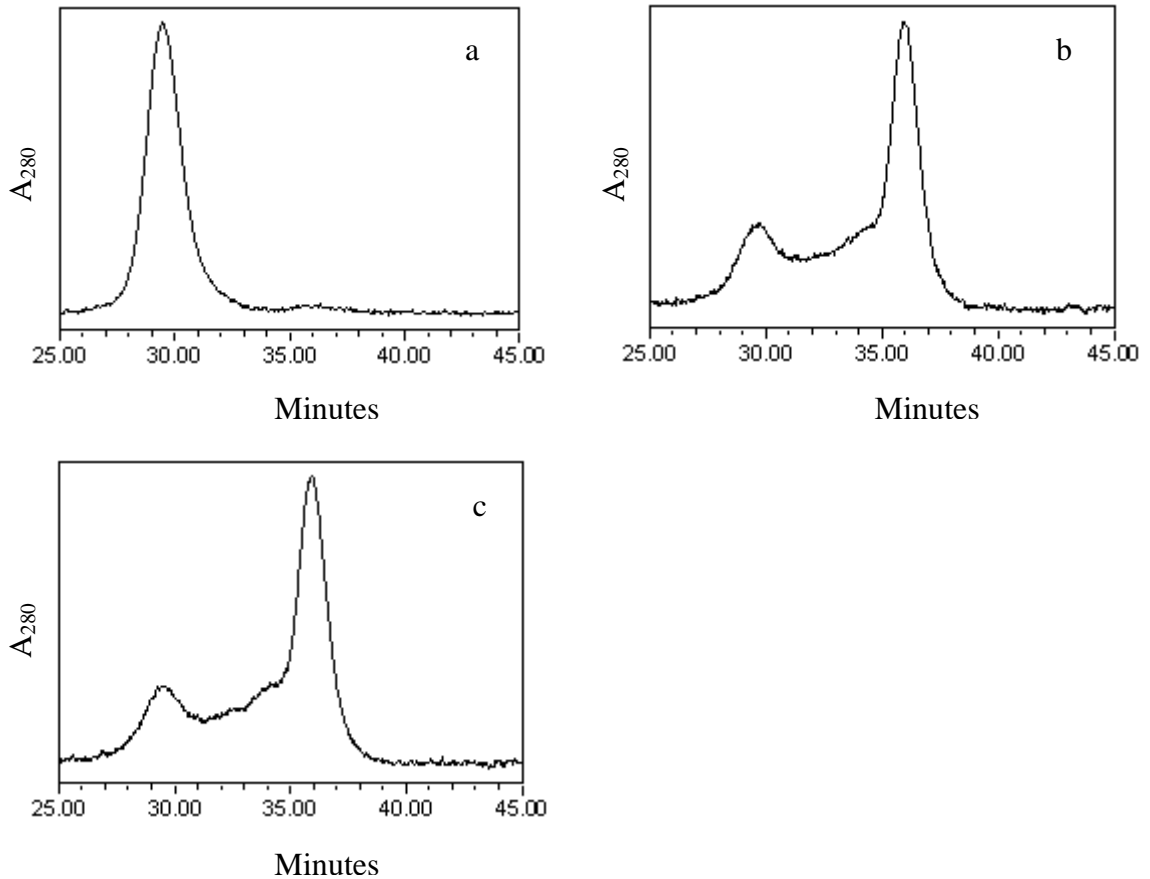


Figure 4.29: The Superose 6 gel filtration chromatograms of 24-mer WT protein (a), WT protein in encapsulation experiments after dialysis overnight (b), and WT protein in encapsulation experiments with an additional 5 hours of dialysis time (c). The first peak at ~30 min represents 24-subunit and the second peak at ~36 min represents dimer protein.

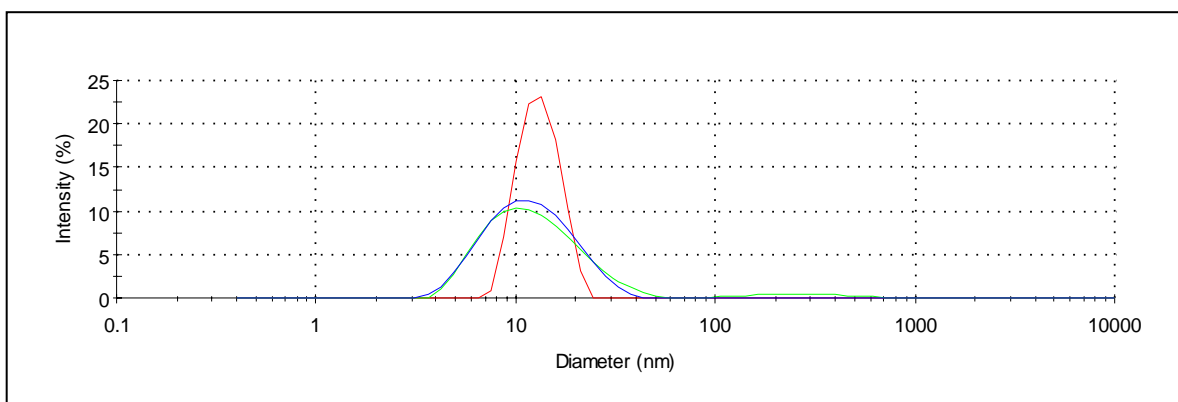


Figure 4.30: The size distribution by intensity plot of 24-mer WT protein (red), WT protein in encapsulation experiments (blue), and WT protein in encapsulation experiments with an additional 5 hours of dialysis time (green).

Elimination of Non-specific Dye Binding

A 0.65 mg/mL solution of the 24-subunit Histag and WT proteins were used in encapsulation studies without a declustering step (so called non-specific dye binding Histag and non-specific dye binding WT, respectively) to investigate non-specific binding of the dye. Compared to the non-specific dye binding proteins without an extend dialysis time (both Histag and WT), a large decrease in fluorescence intensity after an additional 5 hours of dialysis time suggested the elimination of non-specific binding of the dye (Figure 4.31). The Superose 6 chromatograms and DLS results indicated that stable proteins for both with and without an additional 5 hours of dialysis time were produced (Figure 4.32, 4.33, and 4.34). Therefore, the decrease of fluorescence intensity of the protein with encapsulated dye after extensive dialysis is due to the elimination of non-specific (possibly surface binding) dye binding and little contribution from effects on protein stability.

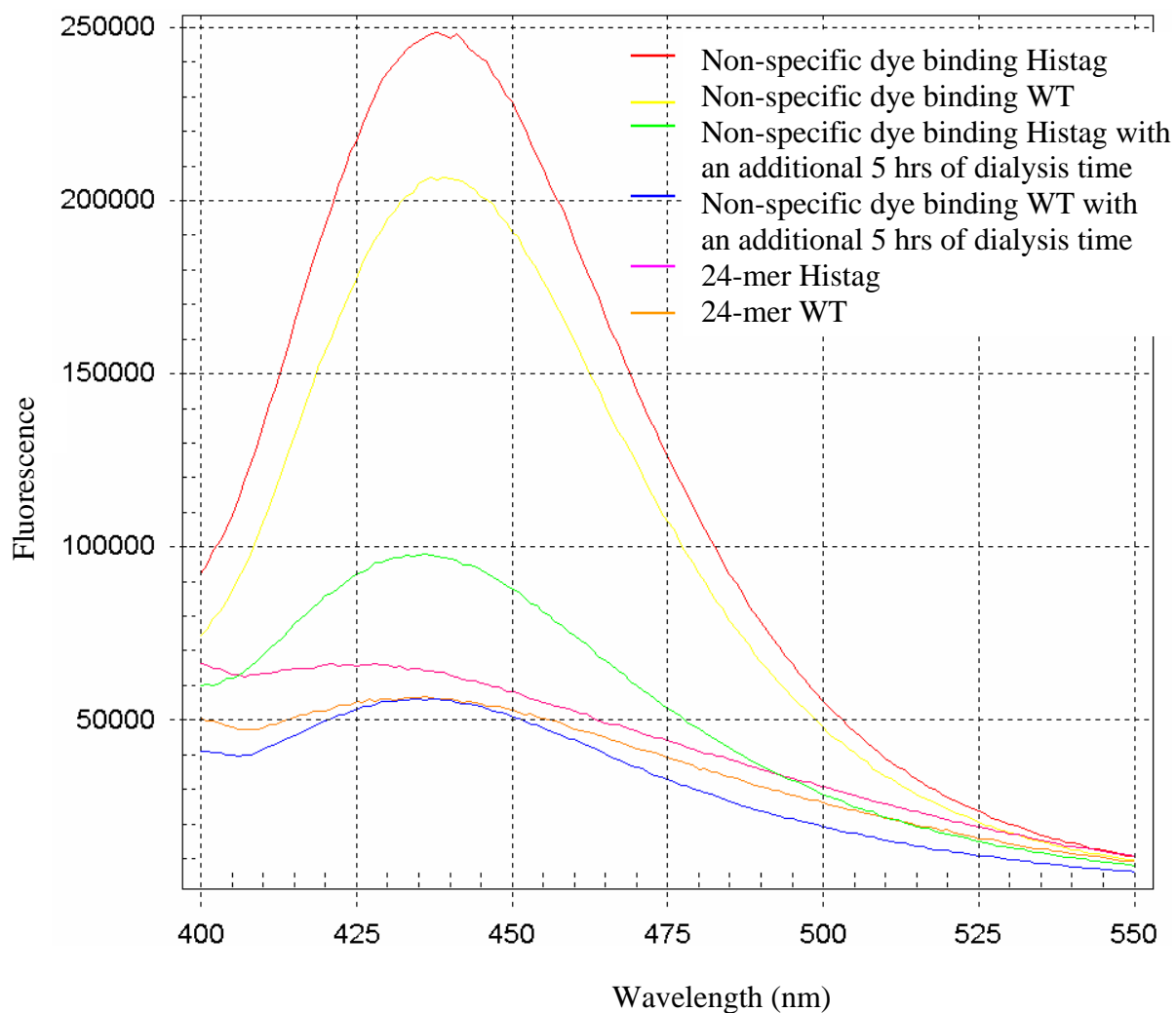


Figure 4.31: The emission spectra scanned between wavelengths 400-550 nm with the fixed excitation wavelength at 345 nm of 24-mer Histag protein, 24-mer WT protein, non-specific dye binding Histag protein with and without an additional 5 hours of dialysis time, and non-specific dye binding WT protein with and without an additional 5 hours of dialysis time showing maximum fluorescence intensity at 440 nm.

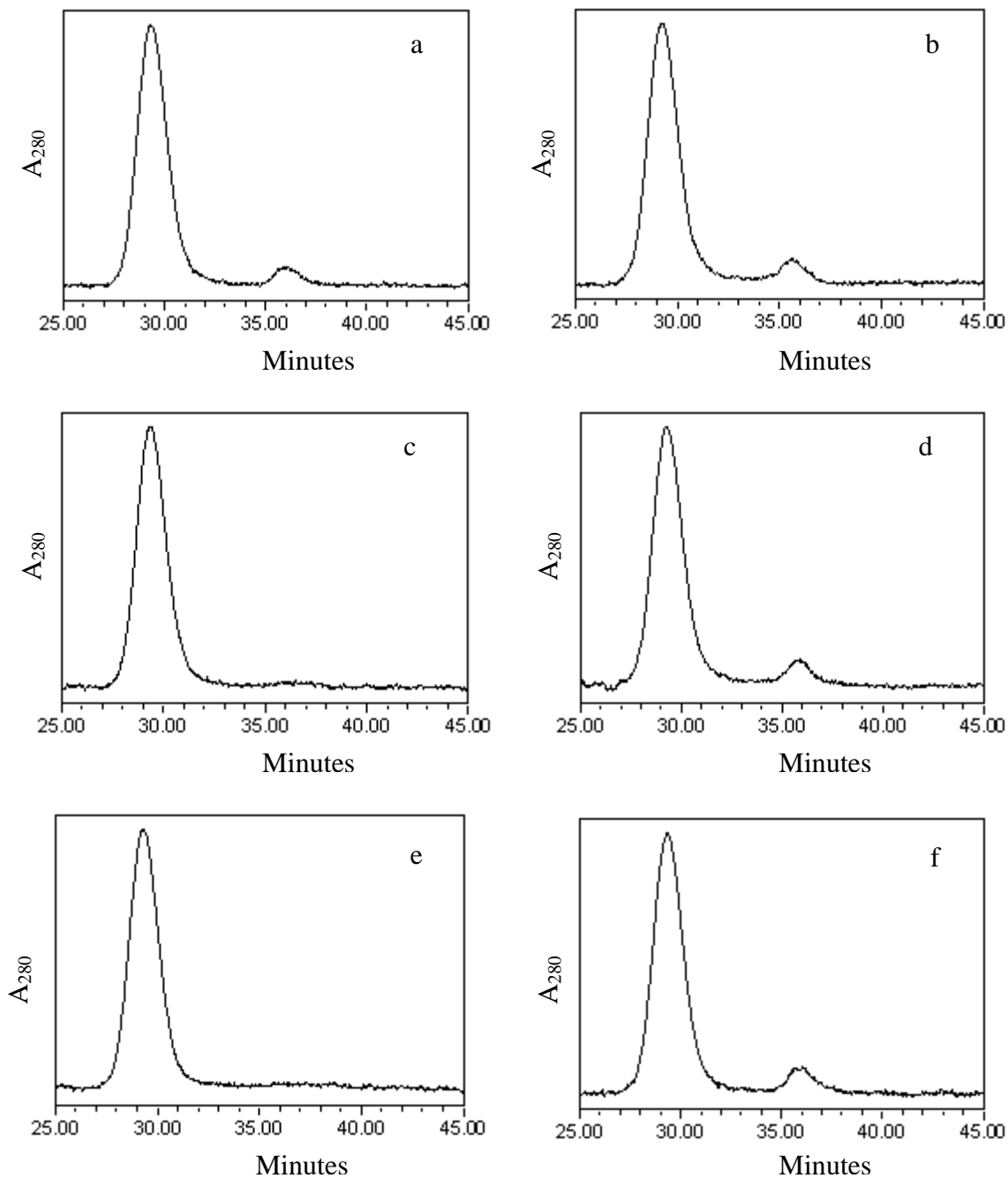


Figure 4.32: The Superose 6 gel filtration chromatograms of 24-mer Histag protein (a), 24-mer WT protein (b), non-specific dye binding Histag protein without (c) and with (e) an additional 5 hours of dialysis time, and non-specific dye binding WT protein without (d) and with (f) an additional 5 hours of dialysis time. The first peak at ~30 min represents 24-subunit and the second peak at ~37 min represents dimer protein.

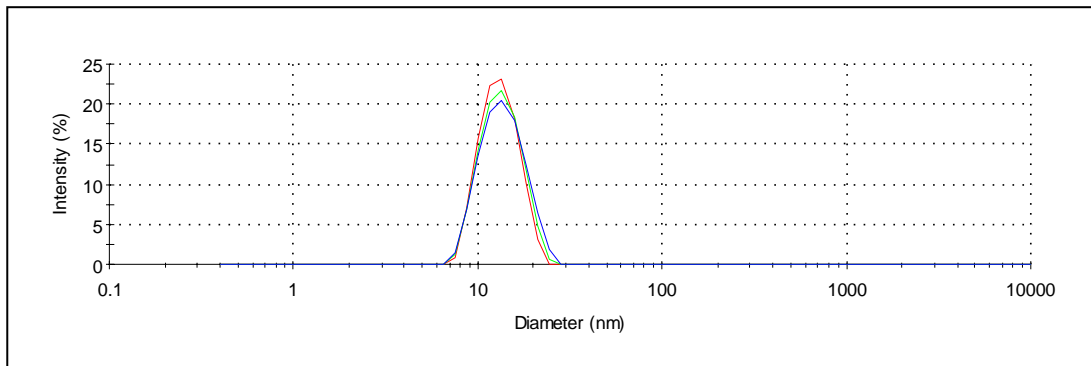


Figure 4.33: The size distribution by intensity plot of 24-mer WT protein (red), non-specific dye binding WT protein with an additional 5 hours of dialysis time (blue), and non-specific dye binding WT protein without an additional 5 hours of dialysis time (green). The peak at ~16 nm represents 24-subunit protein.

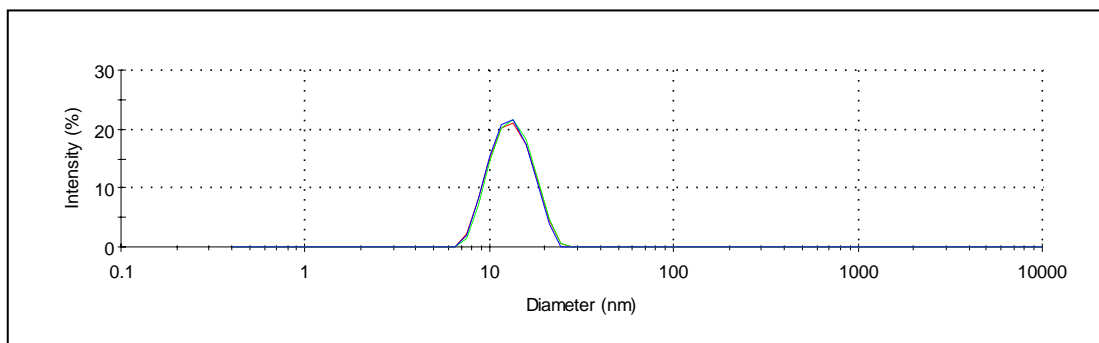


Figure 4.34: The size distribution by intensity plot of 24-mer Histag protein (red), non-specific dye binding Histag protein with an additional 5 hours of dialysis time (blue), and non-specific dye binding Histag protein without an additional 5 hours of dialysis time (green). The peak at ~16 nm represents 24-subunit protein.

Non-encapsulated Proteins

Solutions of 0.7 mg/mL of the 24-subunit proteins (Histag and WT) were reduced to 0.65 mg/mL after the encapsulation procedures. In order to investigate protein stability, these experiments skipped the encapsulating step. By comparing these results with those involving the encapsulating step (section 4.4.3), the Superose 6 chromatograms exhibited higher amounts of dimeric protein for both with and without an additional 5 hours of dialysis time (Figure 4.35

and 4.36), and the sizes of non-encapsulated proteins were smaller than 24-mer size as shown in DLS results (Figure 4.37 and 4.38). These results suggest that encapsulation of dye might support protein reclustering.

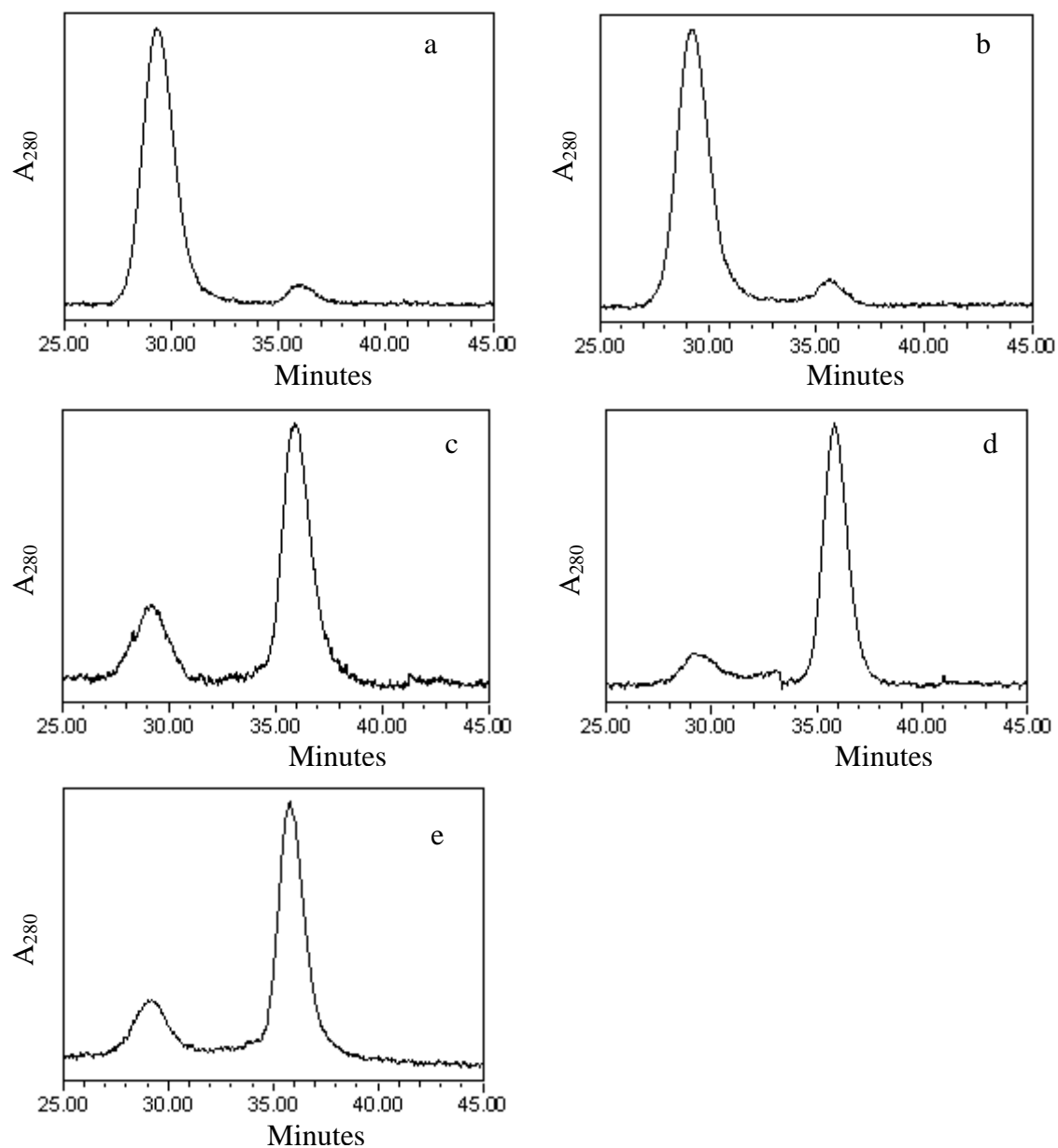


Figure 4.35: The Superose 6 gel filtration chromatograms of 24-mer Histag protein (a), 24-mer WT protein (b), non-encapsulated Histag protein (c), non-encapsulated WT protein (d), and non-encapsulated 60/40:Histag/WT mixture (e). All non-encapsulated proteins were dialyzed overnight. The first peak at 29 min represents 24-subunit and the second peak at ~36 min represents dimer protein.

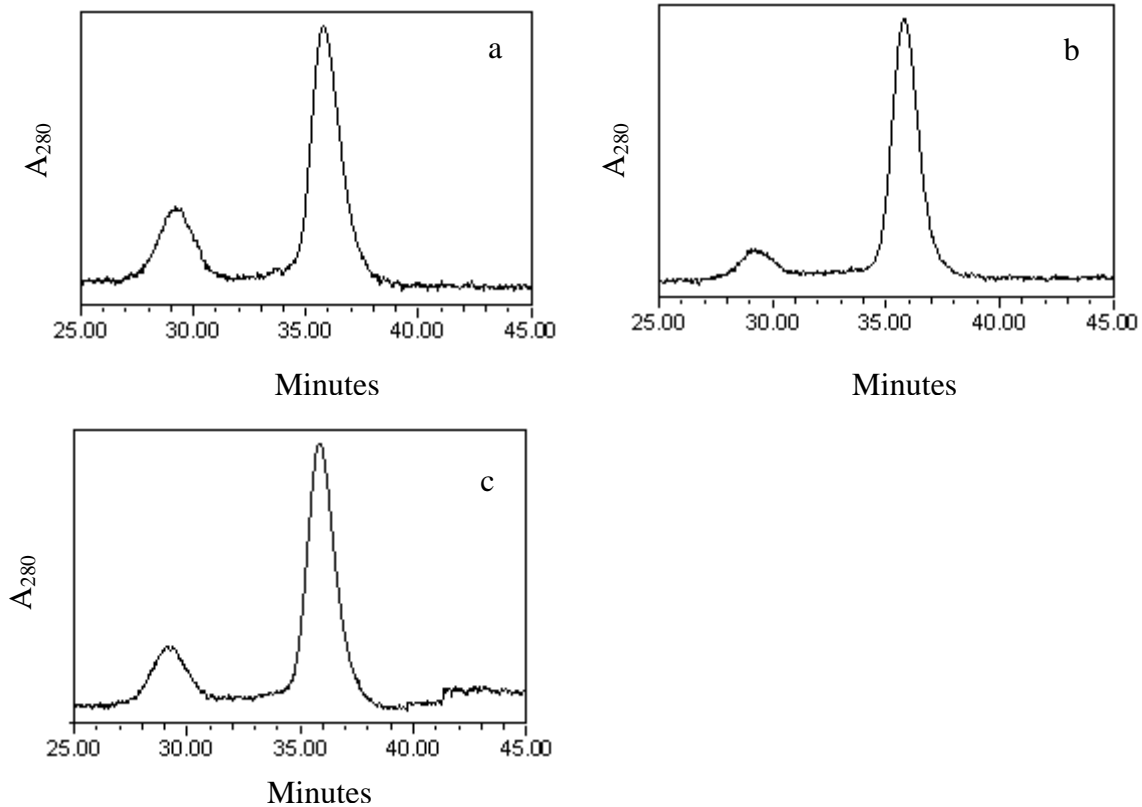


Figure 4.36: The Superose 6 gel filtration chromatograms of non-encapsulated Histag protein (a), non-encapsulated WT protein (b), and non-encapsulated 60/40:Histag/WT mixture (c). All non-encapsulated proteins were dialyzed overnight followed by change of dialysis buffer and then dialyzed for an additional 5 hours. The first peak at ~29 min represents 24-subunit and the second peak at ~36 min represents dimer protein.

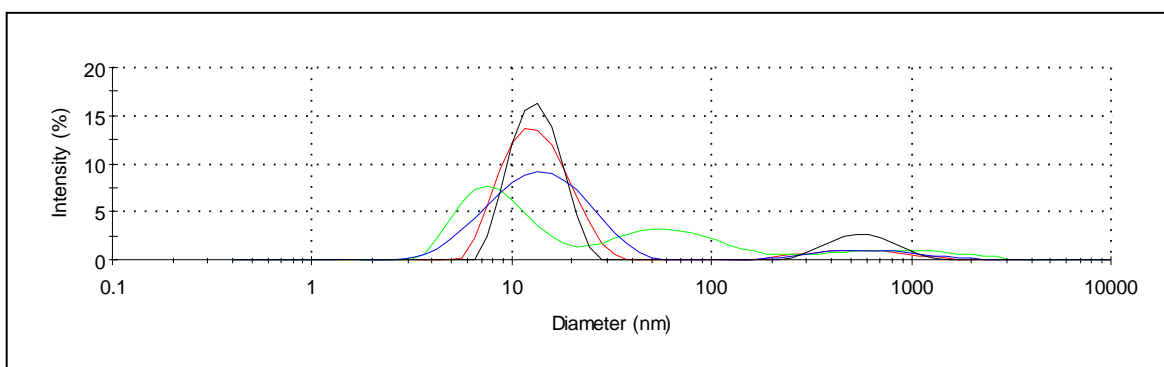


Figure 4.37: The size distribution by intensity plot of 24-mer Histag protein (black), non-encapsulated Histag protein (red), non-encapsulated WT protein (green), and non-encapsulated 60/40:Histag/WT mixture (blue). All non-encapsulated proteins were dialyzed overnight. The peak at ~16 nm represents 24-mer protein, the peak at higher diameter represents self-aggregation, and the peak with lower diameter represents smaller subunit formation.

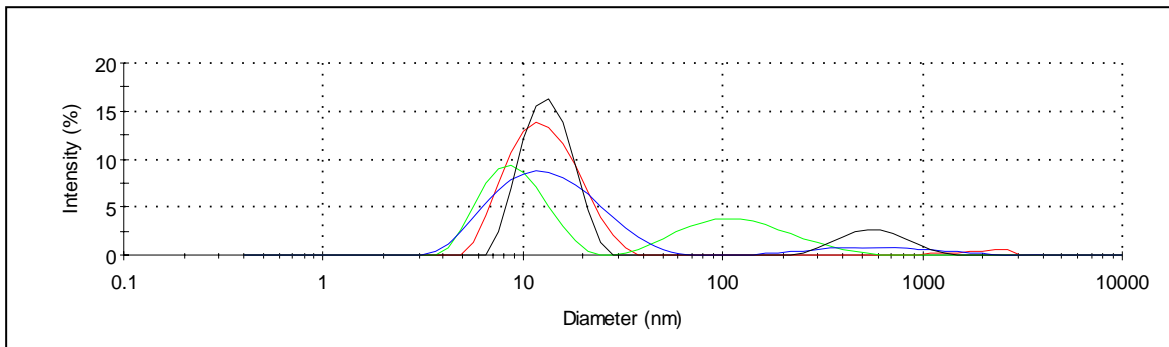


Figure 4.38: The size distribution by intensity plot of 24-mer Histag protein (black), non-encapsulated Histag protein (red), non-encapsulated WT protein (green), and non-encapsulated 60/40:Histag/WT mixture (blue). All non-encapsulated proteins were dialyzed overnight followed by change of dialysis buffer and then dialyzed for an additional 5 hours.

4.4.5: Fluorescence Quenching of the Dye Encapsulated Bacterioferritin

The results from section 4.4.2 suggest that the dye molecules might quench each other if they are in a close distance (high concentration of the dye). However, only 50% (v/v) dye was used in the encapsulation experiments, so the fluorescence quenching of the encapsulated dye molecules might come from their interaction with the protein. The fluorescence measurements of the denatured 60/40:Histag/WT mixture with encapsulated dye compared with the native 60/40:Histag/WT mixture with encapsulated dye suggest that the protein shells might prevent some emission of the encapsulated dye molecules (Figure 4.39).

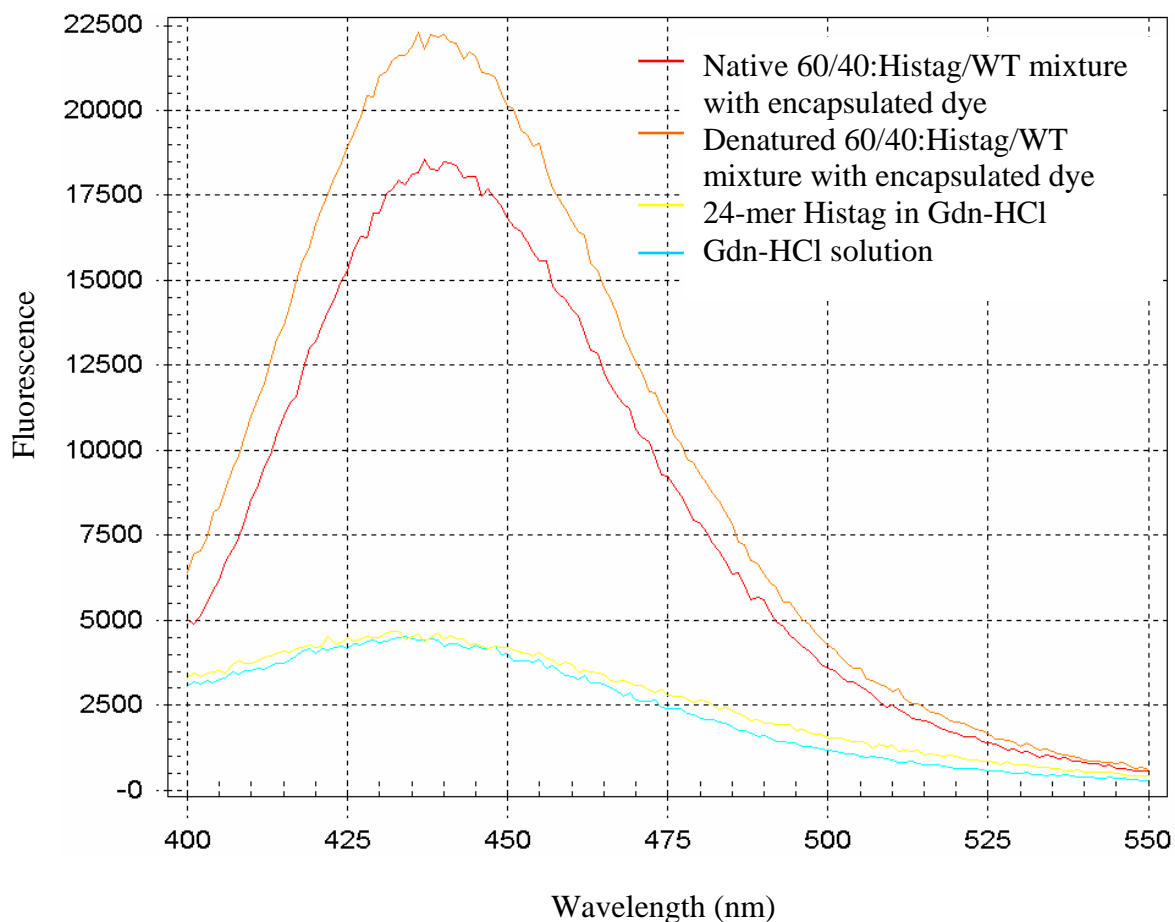


Figure 4.39: The emission spectra scanned between wavelengths 400-550 nm with the fixed excitation at 345 nm of the 60/40:Histag/WT mixture with encapsulated dye, the denatured 60/40:Histag/WT mixture with encapsulated dye (with 6 M Gdn-HCl solution), denatured 24-mer Histag protein (with 6 M Gdn-HCl), and 6 M Gdn-HCl solution showing maximum fluorescence intensity at 440 nm.

4.4.6: Heme-incorporated Encapsulated Bacterioferritin

The results for fluorescence measurement, Superose 6 gel filtration chromatography, and DLS of encapsulation with bFT with His₆-tag at the C-terminus with/without an additional 5 hours of dialysis time were similar to those of the encapsulation with 100/0:Histag/WT protein (section 4.4.3). The determination of the heme groups present in bFT is presented in Appendix 9. It was demonstrated that the amount of heme groups in bFT-WT with and

without His₆-tag at the C-terminus were similar (~12 heme groups per 24-subunit protein). Therefore, the presence of the His-tag as well as the encapsulation process itself does not seem to affect the heme binding pocket.

4.4.7: Iron Storage in Bacterioferritin

The results from metal analysis of the 24-subunit bFT containing His₆-tag at the C-terminus isolated by Superose 6 gel filtration chromatography showed that this protein possessed low amounts of iron atoms (Appendix 12). High amount of sodium and zinc, which are common ions found in water, might be the contaminants from environments such as container, air, or even from Chelex treated water. A trace of sulfur might also come from environments and might be related to amino acid residue such as methionine in the protein.

4.4.8: Dye Molecules Encapsulated in Bacterioferritin

Protein concentration of 100% Histag and the combination of 60/40:Histag/WT as determined in section 4.4.3 (Table 4.6) were used to determine the average number of dye molecules encapsulated by the declustering and recluster procedure. The fluorescence measurements that suggested successful encapsulation were presented in Figure 4.23. The stabilities for encapsulated dye molecules in the protein were represented by the Superose 6 gel filtration chromatograms (Figure 4.24 and 4.25) and the size distribution by intensity plots (Figure 4.26 and 4.27). The calculation of encapsulated dye molecules is shown in Appendix 10. It was calculated that for both the 100% Histag protein and the 60/40:Histag/WT mixture, dye encapsulation was similar (~6-7 molecules). However, since 100% Histag had higher

possibility to capture dye molecules, its efficiency (~25%) was lower than that of the combination (~43%).

4.5: Conclusions

Dye molecules in Pro-Q[®] sapphire 365 oligohistidine gel stain possess the following properties: (1) maximum excitation wavelength at 345 nm and maximum emission wavelength at 440 nm, (2) a MW of 553 Da, (3) an extinction coefficient (ϵ_{345}) of $\sim 19\,000\text{--}23\,000\text{ cm}^{-1}\text{M}^{-1}$, (4) a concentration of $\sim 9.2\ \mu\text{M}$ in the stock solution, and (5) approximately a 6.6 ratio of Ni^{2+} /dye molecule. The predicted structure of the dye molecules was expected to be a coumarin based dye system.

It was determined that the encapsulation of Ni^{2+} -NTA linked dye by bFT with His₆-tag at the C-terminus required three steps to be successful: (1) declustering of the native protein for 90 min by dialysis against an acidic solution (pH 2.0) containing 10 mM PIPES, 150 mM NaCl and 10% glycerol, (2) binding and reclustering (encapsulating) of the Ni^{2+} -NTA dye with His₆-tag protein and reclustering in buffer pH 8.0 for 2 hours, and (3) eliminating non-specific binding of the dye by dialysis against wash buffer (pH 8.0) containing 10 mM PIPES and 100 mM NaCl overnight and then for an additional 5 hours with fresh dialysis buffer. A high protein concentration was required to maintain the 24-subunit clusters after the encapsulation experiments. The experimental data suggests that at least 0.5 mg/mL of the 24-subunit protein prepared by Superose 6 gel filtration chromatography is needed for step 1 of the encapsulation experiments. The protein combination of 60/40:Histag/WT mixture had higher recoveries after the encapsulation process, while the 100% Histag protein system had greater protein stability to maintain 24-subunit cluster after encapsulation. Although both proteins yielded similar

amounts of encapsulated dye (~6-7 molecules), the combination of 60/40:His₆/WT mixture had higher dye encapsulation efficiency (~43%) for the number of His-tag sites available. Small amount of encapsulated dye molecules in the 100% His₆ protein suggested that all His₆-tags at the C-terminal bFT subunits were not available for dye binding (Figure 4.40). Steric or electrostatic interactions among adjacent His-tag regions or secondary interactions between other parts of the protein and variants His-tags may reduce the number of final His-tag binding sites available for dye interaction. In addition, it was found that encapsulation does not influence the heme binding pocket and low amount of iron atoms were found to have no effect on the encapsulation process.

Control experiments to study the encapsulation by bFT-WT taking into account non-specific binding confirmed the results of the encapsulation process. There was no encapsulation of dye molecules for bFT-WT, which is consistent with the interaction between His₆-tag protein and Ni²⁺-NTA binding dye, while non-encapsulated protein provided information on protein stability and non-specific binding of the dye. It is suggested that the encapsulated dye molecules might be involved in 24-subunit reformation. There are two possibilities to explain the observation that fluorescence decreased with utilization of an additional 5 hours of dialysis time in the reclustering step. One possibility is the elimination of non-specific dye binding and the second could be protein dissociation. The loss of fluorescence for non-specific binding of the dye on native proteins confirmed that the decrease in fluorescence intensity for the protein with encapsulated dye after extensive dialysis was most likely caused by elimination of non-specific surface binding of the dye.

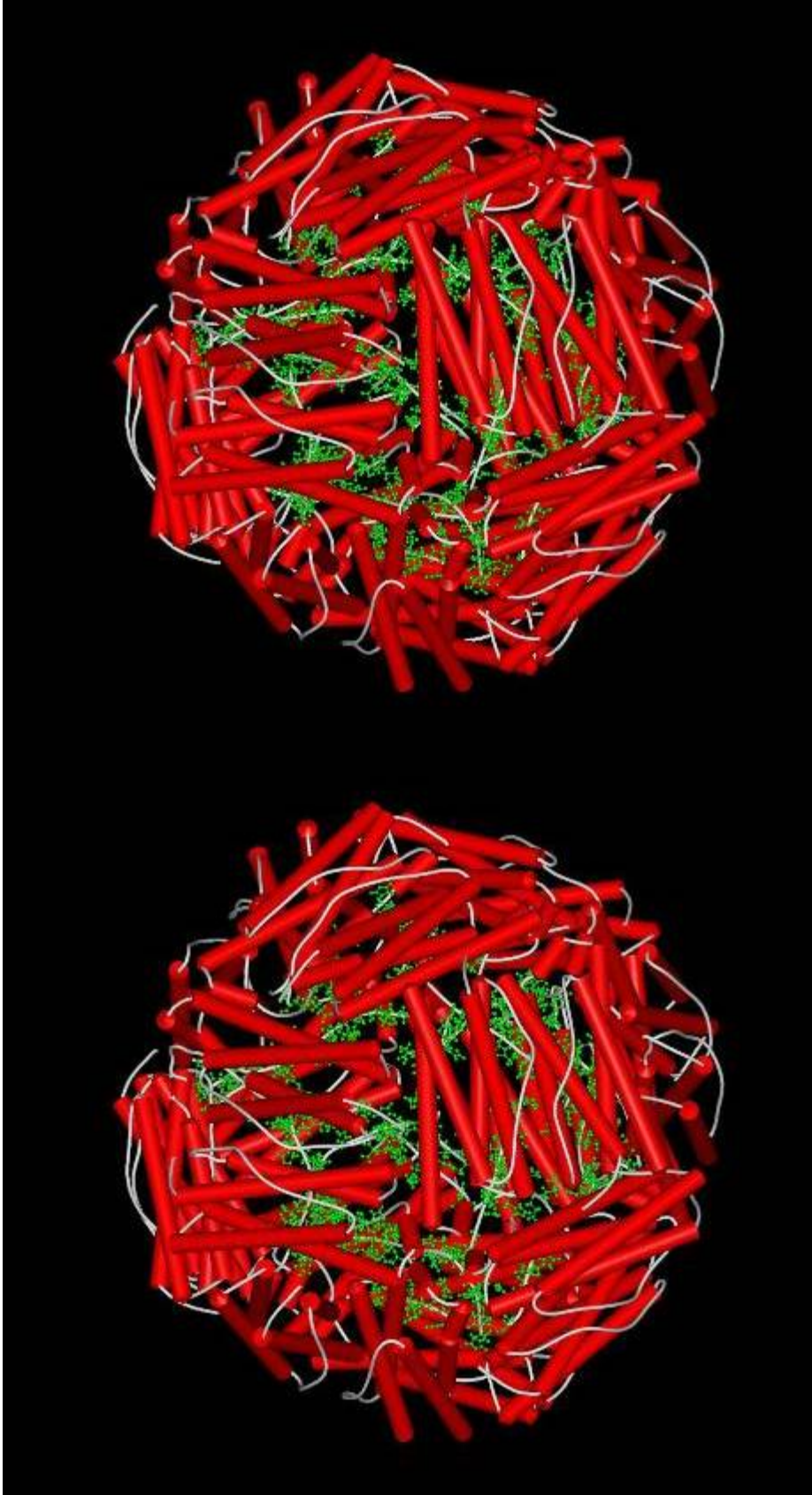


Figure 4.40: Structural modeling of the 24-mer His-tag bFT. The pdb file (1BCF) for *E. coli* bacterioferritin was imported into Sybyl (Tripos) and the sequence, Leu-Glu-His-His-His-His-His, was added in a random conformation on to the C-terminal 158 residue for each of the 24 protein chains followed by simulated annealing for each new side chain using Amber4.1 force field (1000 iterations using the Amber4.1 force field with loaded charges and a dielectric constant of 78 and NBCutoff = 8.0).

CHAPTER 5: SUMMARY AND FUTURE WORK

5.1: Summary

The bacterial protein, bFT, consisting of 24 identical subunits with a maximum of 12 heme groups was used as a host particle in encapsulation experiments. Each subunit possesses two iron atoms forming a ferroxidase center. Encapsulation of a dye using bFT requires three main steps to complete an encapsulation process and include (1) subunit dissociation in acidic pH (declustering), (2) binding of each subunit with a guest molecule, and (3) reassociation at neutral pH (reclustering).

The development of dissociation and reassociation conditions was preliminarily performed on commercially available apoFT, an iron-free FT that resembles bFT in terms of its size and function. The optimized conditions for declustering and reclustering of multisubunit apoFT were investigated by measuring the size of the protein using dynamic light scattering methods. It was found that the apoFT subunit dissociation can be accomplished at pH between 1.0-2.5 in the presence of 200 mM NaCl and 10% glycerol. Multisubunit reassociation can be achieved by raising the pH to neutral. A high protein concentration is required due to the sensitivity of the particle sizer.

In order to encapsulate guest molecules, the internal protein cavity needs to be free of its iron core. The ferroxidase- and heme-free bFT mutant (bFT-E18A/M52L/E94A), as well as other variants that are composed of various combinations of these three mutations, were generated by site directed mutagenesis. Protein purifications were performed using a sequence of steps, which included heat denaturation, ammonium sulfate precipitation, and gel filtration chromatography. Protein stability was investigated by Superose 6 gel filtration

chromatography and the protein sizes were determined by DLS. Optimized conditions to isolate these proteins by Superose 6 gel filtration chromatography required (1) at least 0.5 mg/mL of protein concentration, and (2) buffer (pH 8.0) containing 20 mM Tris-OH and 100 mM NaCl. All bFT variants except for bFT-E94A resulted in high amounts of smaller subunit structures (dimer and monomer). It was also found that the bFT-M52L/E94A variant (not previously reported) only possessed dimeric quaternary structure. Since only bFT-WT exhibited a stable 24-subunit quaternary structure isolated by Superose 6 gel filtration chromatography, it was used for the encapsulation experiments and not the variants of the wild-type bFT.

By obtaining knowledge of the optimized conditions needed for the declustering and reclustered of apoFT, the optimized conditions for the isolation of bFT by gel filtration chromatography, and the investigation of the stability of the 24-subunit quaternary structure of these proteins, the encapsulation experiments using bFT with His₆-tag at the C-terminus as a host particle and dye molecules in Pro-Q[®] sapphire 365 oligohistidine gel stain as encapsulated guests were studied. The electrospray MS and the patent searching suggest that this commercial dye is 7-amino-3-(1-carboxy-1-(bis(carboxymethyl)amino)-5-(acetylamino))pentyl-4-methylcoumarin-6-sulfonic acid (MW = 553 Da), which is a Ni²⁺-NTA derivative. This dye possesses the following properties: (1) maximum excitation wavelength at 345 nm and maximum emission wavelength at 440 nm, (2) dye concentration of ~9.2 μM in Pro-Q[®] sapphire 365 oligohistidine gel stain, (3) an estimated extinction coefficient (ϵ_{345}) of 23 000 M⁻¹cm⁻¹, (4) a 6.6 ratio of Ni²⁺/dye molecule. This Ni²⁺-NTA derivative dye (structure resembling coumarin) is able to form strong interactions with His₆-tag at the C-terminal bFT in the encapsulation experiments, yielding evidence for encapsulated dye in the bFT cavity. The

optimized conditions for dye encapsulation were (1) subunit dissociations occur during ~90 minutes in the acidic solution (pH 2.0) containing 10 mM PIPES, 150 mM NaCl, and 10% glycerol, (2) encapsulation and reclustering of dye molecules for 2 hours in buffer (pH 8.0) containing 10 mM PIPES and 100 mM NaCl, and (3) elimination of non-specific dye binding by overnight dialysis in buffer (pH 8.0) containing 10 mM PIPES and 100 mM NaCl followed by an additional 5 hours of dialysis with fresh buffer. In addition, it was found that the heme groups and iron atoms do not affect the encapsulation experiments. The amount of encapsulated dye molecules was found to be similar for both 100% bFT with His₆-tag at the C-terminus and the combination of 60% bFT with His₆-tag at the C-terminus and 40% bFT without His₆-tag at the C-terminus (~6-7 molecules). However, the encapsulation efficiency of 100% bFT with His₆-tag at the C-terminus (~25%) was lower than the one of the combination of 60% bFT with His₆-tag at the C-terminus and 40% bFT without His₆-tag at the C-terminus (~43%). These results suggest that not all His₆-tag at the C-terminal bFT are available for dye binding.

5.2: Future Work

Since there are only small amounts of dye molecules that could be encapsulated within the His-tagged bFT, methods to increase the number of encapsulated dye molecules in the encapsulation experiments should be developed. One possibility is to separate the binding step and the reclustering step and allow a longer time for the binding step. In our encapsulation experiments, these two steps were performed together (the declustered proteins in acidic buffer (pH 2.0) were bound with dye molecules in the dye solution (pH 8.0)). If the binding time for

dye molecules and the protein is allowed to be longer before the reclustering step, perhaps a greater number of encapsulated dye molecules will be obtained.

Other host-guest affinity methods such as use of a S-tag could also be useful for future encapsulation studies. S-tag is a 15 amino-acid peptide, which can form a stable interaction with S-protein (S-fragment of RNaseA) (Terpe, 2003). However, the cost of this affinity tag is higher than that of the His-tag affinity. Other linkage that can form strong interaction between host particle and a guest molecule is to perform protein engineering (fusion protein), in which a guest gene is directly linked to the host gene. In this case, a linker with various sizes between host and guest might be required. In addition, the reclustering to reform 24-subunit of this fusion protein should be investigated.

REFERENCES

- Abbing, A., Blaschke, U., Grein, S., Kretschmar, M., Stark, C., Thies, M., Walter, J., Weigand, M., Woith, D., Hess, J. and Reiser, C. 2004. Efficient intracellular delivery of a protein and a low molecular weight substance via recombinant polyomavirus-like particles. *J Biol Chem.* 279(26): 27410-27421
- Abdul-Tehrani, H., Hudson, A., Chang, Y., Timms, A., Hawkins, C., Williams, J., Harrison, P., Guest, J. and Andrews, S. 1999. Ferritin Mutants of *Escherichia coli* Are Iron Deficient and Growth Impaired, and *fur* Mutants are Iron Deficient. *Journal of Bacteriology.* 181(5): 1415-1428
- Abraham, S., Edwards, K., Karlsson, G., MacIntosh, S., Mayer, L., McKenzie, C. and Bally, M. 2002. Formation of transition metal-doxorubicin complexes inside liposomes. *Biochim Biophys Acta.* 1565(1): 41-54
- Allen, M., Willits, D., Young, M. and Douglas, T. 2003. Constrained Synthesis of Cobalt oxide nanomaterials in the 12-subunit Protein cage from *Listeria innocua*. *Inorg Chem.* 42: 6300-6305
- al-Massad, F., Kadir, F. and Moore, G. 1992. Animal ferritin and bacterioferritin contain quinines. *Biochem J.* 283(Pt 1): 177-180
- Andrews, P. 1970. Estimation of molecular size and molecular weights of biological compounds by gel filtration. *Methods Biochem Anal.* 18: 1-53
- Andrews, S. 1998. Iron storage in bacteria. *Adv Microb Physiol.* 40: 281-351
- Andrews, S., Findlay, J., Guest, J., Harrison, P., Keen, J. and Smith, J. 1991. Physical, chemical and immunological properties of the bacterioferritins of *Escherichia coli*, *Pseudomonas aeruginosa* and *Azotobacter vinelandii*. *Biochim Biophys Acta.* 1078(1): 111-116 (Andrews *et al.*, 1991a)
- Andrews, S., Le Brun, N., Barynin, V., Thomson, A., Moore, G., Guest, J. and Harrison, P. 1995. Site-directed Replacement of the Coaxial Heme Ligands of Bacterioferritin Generates Heme-free Variants. *J Biol Chem.* 270(40): 23268-23274
- Andrews, S., Harrison, P. and Guest, J. 1989. Cloning, Sequencing, and Mapping of the Bacterioferritin Gene (*bfr*) of *Escherichia coli* K-12. *Journal of Bacteriology.* 171(7): 3940-3947 (Andrews *et al.*, 1989a)
- Andrews, S., Robinson, A. and Rodríguez-Quinones, F. 2003. Bacterial iron homeostasis. *FEMS Microbiology Reviews.* 27: 215-237

- Andrews, S., Smith, J., Guest, J. and Harrison, P. 1989. Amino acid sequence of the bacterioferritin (cytochrome *b_f*) of *Escherichia coli*-K12. *Biochem Biophys Res Commun.* 158(2): 489-496 (Andrews *et al.*, 1989b)
- Andrews, S., Smith, J., Guest, J. and Harrison, P. 1990. Genetic and structural characterization of the bacterioferritin of *Escherichia coli*. *Biochem Soc Trans.* 18(4): 658-659
- Andrews, S., Smith, J., Hawkins, C., Williams, J., Harrison, P. and Guest, J. 1993. Overproduction, purification and characterization of the bacterioferritin of *Escherichia coli* and a C-terminally extended variant. *Eur J Biochem.* 213(1): 329-338
- Andrews, S., Smith, J., Yewdall, S., Guest, J. and Harrison, P. 1991. Bacterioferritins and ferritins are distantly related in evolution. Conservation of ferroxidase-centre residues. *FEBS Lett.* 293(1-2): 164-168 (Andrews *et al.*, 1991b)
- Anobom, C., Albuquerque, S., Albernaz, F., Oliveira, A., Silva, J., Peabody, D., Valente, A. and Almeida, F. 2003. Structural studies of MS2 bacteriophage virus particle disassembly by nuclear magnetic resonance relaxation measurements. *Biophys J.* 84(6): 3894-3903
- Baaghil, S., Lewin, A., Moore, G. and Le Brun, N. 2003. Core Formation in *Escherichia coli* Bacterioferritin Requires a Functional Ferroxidase Center. *Biochemistry.* 42(47): 14047-14056
- Baaghil, S., Thomson, A., Moore, G. and Le Brun, N. 2002. Studies of copper(ii)-binding to bacterioferritin and its effect on iron(II) oxidation. *Journal of the Chemical Society, Dalton Transactions.* (5): 811-818
- Baichoo, N. and Helmann, J. 2002. Recognition of DNA by Fur: a Reinterpretation of the Fur Box Consensus Sequence. *Journal of bacteriology.* 184(21): 5826-5832
- Bartsch, R., Kakuno, T., Horio, T. and Kamen, M. 1971. Preparation and Properties of *Rhodospirillum rubrum* Cytochromes *c₂*, *c_c*, and *b_{557.5}*, and Flavin Mononucleotide Protein. *The Journal of Biological Chemistry.* 246(14): 4489-4496
- Basu, G., Allen, M., Willits, D., Young, M. and Douglas, T. 2003. Metal binding to cowpea chlorotic mottle virus using terbium(III) fluorescence. *J Biol Inorg Chem.* 8(7): 721-725
- Bou-Abdallah, F., Lewin, A., Le Brun, N., Moore, G. and Chasten, N. 2002. Iron Detoxification Properties of *Escherichia coli* Bacterioferritin. *The Journal of Biological Chemistry.* 277(4): 37064-37069
- Bradford, M. 1976. A rapid and sensitive method for the quantitation of microgram quantities of protein utilizing the principle of protein-dye binding. *Anal Biochem.* 72: 248-254

- Braig, K., Otwinowski, Z., Hegde, R., Boisvert, D., Joachimiak, A., Horwich, A. and Sigler, P. 1994. The crystal structure of the bacterial chaperonin GroEL at 2.8 Å. *Nature*. 371(6498): 578-586
- Bulen, W., LeComte, J. and Lough, S. 1973. A hemoprotein from *Azotobacter* containing non-heme iron: Isolation and crystallization. *Biochemical and Biophysical Research Communications*. 54(4): 1274-1281
- Bullen, J., Rogers, H. and Griffiths, E. 1978. Role of iron in bacterial infection. *Curr Top Microbiol Immunol*. 80: 1-35
- Carrondo, M. 2003. Ferritins, iron uptake and storage from the bacterioferritin viewpoint. *The EMBO Journal*. 22(9): 1959-1968
- Cartron, M., Maddocks, S., Gillingham, P., Craven, C. and Andrews, S. 2006. Feo-transport of ferrous iron into bacteria. *Biometals*. 19 (2): 143-157
- Cavalli, R., Bargoni, A., Podio, V., Muntoni, E., Zara, G. and Gasco, M. 2003. Duodenal administration of solid lipid nanoparticles loaded with different percentages of tobramycin. *J Pharm Sci*. 92(5): 1085-1094
- Chasteen, N. 1998. Ferritin. Uptake, storage, and release of iron. *Met Ions Biol Syst*. 35: 479-514
- Cheesman, M., Kadir, F., Al-Basseet, J., Al-Massad, F., Farrar, J., Greenwood, C., Thomson, A. and Moore, G. 1992. E.p.r. and magnetic circular dichroism spectroscopic characterization of bacterioferritin from *Pseudomonas aeruginosa* and *Azotobacter vinelandii*. *Biochem J*. 286: 361-367
- Cheesman, M., Le Brun, N., Kadir, F., Thomson, A., Moore, G., Andrews, S., Guest, J., Harrison, P., Smith, J. and Yewdall, S. 1993. Haem and non-haem iron sites in *Escherichia coli* bacterioferritin: spectroscopic and model building studies. *Biochem J*. 292: 47-56
- Cheesman, M., Thomson, A., Greenwood, C., Moore, G. and Kadir, F. 1990. Bis-methionine axial ligation of haem in bacterioferritin from *Pseudomonas aeruginosa*. *Nature*. 346: 771-773
- Chen, M. and Crichton, R. 1982. Purification and Characterization of a Bacterioferritin from *Azotobacter Chroococcum*. *Biochimica et Biophysica Acta*. 707: 1-6
- Cheung, C., Camarero, J., Woods, B., Lin, T., Johnson, J. and De Yoreo, J. 2003. Fabrication of assembled virus nanostructures on templates of chemoselective linkers formed by scanning probe nanolithography. *J Am Chem Soc*. 125(23): 6848-6849

- Chiaraluce, R., Consalvi, V., Cavallo, S., Ilari, A., Stefanini, S. and Chiancone, E. 2000. The unusual dodecameric ferritin from *Listeria innocua* dissociates below pH 2.0. *Eur. J. Biochem.* 267: 5733-5741
- Chilkova, O., Jonsson, B. and Johansson, E. 2003. The quaternary structure of DNA polymerase ϵ from *Saccharomyces cerevisiae*. *The Journal of Biological Chemistry.* 278(16): 14082-14086
- Cobessi, D., Huang, L., Ban, M., Pon, N., Daldal, F. and Berry, E. 2002. The 2.6 Å resolution structure of *Rhodobacter capsulatus* bacterioferritin with meter-free dinuclear site and heme iron in a crystallographic 'special position'. *Acta Crystallographica Section D: Biological Crystallography.* D58: 29-38
- Coelho, A., Macedo, S., Matias, P., Thompson, A., LeGall, J. and Carrondo, M. 2001. Structure determination of bacterioferritin from *Desulfovibrio desulfuricans* by the MAD method at the Fe K-edge. *Acta Cryst.* D57: 326-329
- Conn, M. and Rebek, J. 1997. Self-Assembling Capsules. *Chem Rev.* 97(5): 1647-1668
- Crichton, R. and Bryce, C. 1973. Subunit interactions in horse spleen apoferritin. Dissociation by extremes of pH. *Biochem J.* 133(2): 289-299
- Crichton, R., Eason, R., Barclay, A. and Bryce, C. 1973. The Subunit Structure of Horse Spleen Apoferritin: the Molecular Weight of the Oligomer and its Stability to Dissociation by Dilution. *Biochem J.* 131: 855-857
- Cui, S., Klima, R., Ochem, A., Arosio, D., Falaschi, A. and Vindigni, A. 2002. Characterization of the DNA-unwinding Activity of Human RECQ1, a Helicase Specifically Stimulated by Human Replication Protein A. *J Biol Chem.* 278(3): 1424-1432
- Dautant, A., Meyer, J., Yariv, J., Precigoux, G., Sweet, R., Kalb, A. and Frolow, F. 1998. Structure of a Monoclinic Crystal Form of Cytochrome b_1 (Bacterioferritin) from *E. coli*. *Acta Crystallogr D Biol Crystallogr.* 54: 16-24
- De Haën, C. 1987. Molecular weight standards for calibration of gel filtration and sodium dodecyl sulfate-polyacrylamide gel electrophoresis: ferritin and apoferritin. *Analytical Biochemistry.* 166: 235-245
- Deeb, S. and Hager, L. 1964. Crystalline Cytochrome b_1 from *Escherichia coli*. *The Journal of Biological Chemistry.* 239(4): 1024-1031
- Domínguez-Vera, J. 2004. Iron(III) complexation of Desferrioxamine B encapsulated in apoferritin. *Journal of Inorganic Biochemistry.* 98: 469-472
- Domínguez-Vera, J. and Colacio, E. 2003. Nanoparticles of Prussian Blue Ferritin: A New Route for Obtaining Nanomaterials. *Inorganic Chemistry.* 42: 6983-6985

- Douglas, T. and Stark, V. 2000. Nanophase cobalt oxyhydroxide mineral synthesized within the protein cage of ferritin. *Inorg Chem.* 39: 1828-1830
- Douglas, T. and Young, M. 1998. Host-guest encapsulation of materials by assembled virus protein cages. *Nature.* 393: 152-155
- Douglas, T. and Young, M. 1999. Virus Particles as Templates for Materials Synthesis. *Advanced Materials.* 11(8): 679-681
- Ensign, D., Young, M. and Douglas, T. 2004. Photocatalytic synthesis of copper colloids from CuII by the ferrihydrite core of ferritin. *Inorg Chem.* 43(11): 3441-3446
- Escolar, L., Pérez-Martin, J. and de Lorenzo, V. 1998. Binding of the Fur (Ferric Uptake Regulator) Repressor of *Escherichia coli* to Arrays of the GATAAT sequence. *J Mol Biol.* 283: 537-547
- Evans Jr., D., Evans, D., Lampert, H. and Nakano, H. 1995. Identification of four new prokaryotic bacterioferritins, from *Helicobacter pylori*, *Anabaena variabilis*, *Bacillus subtilis* and *Treponema pallidum*, by analysis of gene sequences. *Gene.* 153(1): 123-127
- Flenniken, M., Liepold, L., Crowley, B., Willits, D., Young, M. and Douglas, T. 2005. Selective attachment and release of a chemotherapeutic agent from the interior of a protein cage architecture. *Chem Commun (Camb).* (4): 447-449
- Flenniken, M., Willits, D., Harmsen, A., Liepold, L., Harmsen, A., Young, M. and Douglas, T. 2006. Melanoma and lymphocyte cell-specific targeting incorporated into a heat shock protein cage architecture. *Chem Biol.* 13(2): 161-170
- Frolow, F., Kalb(Gilboa), A. and Yariv, J. 1993. Location of Haem in Bacterioferritin of *E.coli*. *Acta Cryst.* D49: 597-600
- Frolow, F., Kalb(Gilboa), A. and Yariv, J. 1994. Structure of a unique two-fold symmetric haem-binding site. *Nat Struct Biol.* 1: 453-460
- Funk, F., Lenders, J., Crichton, R. and Schneider, W. 1985. Reductive mobilisation of ferritin iron. *Eur J Biochem.* 152: 167-172
- Futaki, S., Niwa, M., Nakase, I., Tadokoro, A., Zhang, Y., Nagaoka, M., Wakako, N. and Sugiura, Y. 2004. Arginine carrier peptide bearing Ni(II) chelator to promote cellular uptake of histidine-tagged proteins. *Bioconjug Chem.* 15(3): 475-481
- George, G., Richards, T., Bare, R., Gea, Y., Prince, R., Stiefel, E. and Watt, G. 1993. Direct Observation of Bis-Sulfur Ligation to the Heme of Bacterioferritin. *J Am Chem Soc.* 115: 7716-7718

- Gerl, M., Jaenicke, R., and Smith, J. and Harrison, P. 1988. Self-assembly of apoferritin from horse spleen after reversible chemical modification with 2,3-dimethylmaleic anhydride. *Biochemistry*. 27(11): 4089-4096
- Gillitzer, E., Willits, D., Young, M. and Douglas, T. 2002. Chemical modification of a viral cage for multivalent presentation. *Chem Commun (Camb)*. (20): 2390-2391
- Grady, J., Shao, J., Arosio, P., Santambrogio, P. and Chasteen, N. 2000. Vanadyl(IV) binding to mammalian ferritins. An EPR study aided by site-directed mutagenesis. *J Inorg Biochem*. 80(1-2): 107-113
- Grossman, M., Hinton, S., Minak-Bernero, V., Slaughter, C. and Stiefel, E. 1992. Unification of the ferritin family of proteins. *Proc Natl Acad Sci USA*. 89(6): 2419-2423
- Guerinot, M. 1994. Microbial iron transport. *Annu Rev Microbiol*. 48: 743-772
- Hainfeld, J. 1992. Uranium-loaded apoferritin with antibodies attached: Molecular design for uranium neutron-capture therapy. *Proc Natl Acad Sci USA*. 89: 11064-11068
- Hamburger, A., West Jr., A., Hamburger, Z., Hamburger, P. and Bjorkman, P. 2005. Crystal structure of a secreted insect ferritin reveals a symmetrical arrangement of heavy and light chains. *J Mol Biol*. 349: 558-569
- Harker, A. and Wullstein, L. 1985. Evidence for Two Nonidentical Subunits of Bacterioferritin from *Azotobacter vinelandii*. *Journal of Bacteriology*. 162(2): 651-655
- Harrison, P. and Arosio, P. 1996. The ferritins: molecular properties, iron storage function and cellular regulation. *Biochim Biophys Acta*. 1275(3): 161-203
- Harrison, P. and Gregory, D. 1965. Evidence for the existence of stable "aggregates" in horse ferritin and apoferritin. *J Mol Biol*. 14(2): 626-629
- Harrison, P. and Gregory, D. 1968. Reassembly of apoferritin molecules from subunits. *Nature*. 120(167): 578-580
- Harrison, P., Hempstead, P., Artymiuk, P. and Andrews, S. 1998. Structure-function relationships in the ferritins. *Met Ions Biol Syst*. 35: 435-477
- Hart, C., Schulenberg, B., Diwu, Z., Leung, W. and Patton, W. 2003. Fluorescence detection and quantitation of recombinant proteins containing oligohistidine tag sequences directly in sodium dodecyl sulfate polyacrylamide gels. *Electrophoresis*. 24: 599-610
- Heymann, J., Cheng, N., Newcomb, W., Trus, B., Brown, J. and Steven, A. 2003. Dynamics of herpes simplex virus capsid maturation visualized by time-lapse cryo-electron microscopy. *Nat Struct Biol*. 10(5): 334-341

- Hofmann, T. and Harrison, P. 1963. The structure of apoferritin: degradation into and molecular weight of subunits. *J Mol Biol.* 6: 256-267
- Hooker, J., Kovacs, E. and Francis, M. 2004. Interior Surface Modification of Bacteriophage MS2. *J Am Chem Soc.* 126: 3718-3719
- Hooley, R., Biro, S. and Rebek, J. 2006. A deep, water-soluble cavitand acts as a phase-transfer catalyst for hydrophobic species. *Angew Chem Int Ed Engl.* 45(21): 3517-3519
- Hudson, A., Andrews, S., Hawkins, C., Williams, J., Izuhara, M., Meldrum, F., Mann, S., Harrison, P. and Guest, J. 1993. Overexpression, purification and characterization of the *Escherichia coli* ferritin. *Eur J Biochem.* 218: 985-995
- Husain, M. and Sadana, J. 1974. Nitrite Reductase from *Achromobacter fischeri*: Molecular Weight and Subunit Structure. *Eur J Biochem.* 42: 283-289
- Ilari, A., Latella, M., Ceci, P., Ribacchi, F., Su, M., Giangiacomo, L., Stefanini, S., Chasteen, D. and Chiancone, E. 2005. The unusual intersubunit ferroxidase center of *Listeria innocua* Dps is required for hydrogen peroxide detoxification but not for iron uptake. A Study with site-specific mutants. *Biochemistry.* 44: 5579-5587
- Ilari, A., Stefanini, S., Chiancone, E. and Tsernoglou, D. 2000. The dodecameric ferritin from *Listeria innocua* contains a novel intersubunit iron-binding site. *Nat Struct Biol.* 7(1): 38-43
- Ishii, D., Kinbara, K., Ishida, Y., Ishii, N., Okochi, M., Yohda, M. and Aida, T. 2003. Chaperonin-mediated stabilization and ATP-triggered release of semiconductor nanoparticles. *Nature.* 423: 628-632
- Izuhara, M., Takamune, K. and Takata, R. 1991. Cloning and sequencing of an *Escherichia coli* K12 gene which encodes a polypeptide having similarity to the human ferritin H subunit. *Mol Gen Genet.* 225: 510-513
- Jaenicke, R. and Bartmann, P. 1972. Dissociation-association properties of apoferritin in the milligram and microgram range. *Biochem Biophys Res Commun.* 49(4): 884-890
- Jin, W., Takagi, H., Pancorbo, B. and Theil, E. 2001. "Opening" the Ferritin Pore for Iron Release by Mutation of Conserved Amino Acids at Interhelix and Loop Sites. *Biochemistry.* 40: 7525-7532
- Kadir, F., al-Massad, F. and Moore, G. 1992. Haem binding to horse spleen ferritin and its effect on the rate of iron release. *Biochem J.* 282(Pt 3): 867-870
- Kadir, F. and Moore, G. 1990. Bacterial ferritin contains 24 haem groups. *FEBS Lett.* 271(1-2): 141-143

- Kammler, M., Schon, C. and Hantke, K. 1993. Characterization of the ferrous iron uptake system of *Escherichia coli*. *J Bacteriol.* 175: 6212-6219
- Keech, A., Le Brun, N., Wilson, M., Andrews, S., Moore, G. and Thomson, A. 1997. Spectroscopy Studies of Cobalt(II) Binding to *Escherichia coli* Bacterioferritin. *The Journal of Biological Chemistry.* 272(1): 422-429
- Keilin, D. 1934. Cytochrome and the supposed direct spectroscopic observation of oxidase. *Nature.* 133: 290-291
- Keilin, D. and Harpley, C. 1941. Cytochrome System in *Bacterium coli* Commune. *Biochem J.* 35: 688-692
- Kickhoefer, V., Garcia, Y., Mikiyas, Y., Johansson, E., Zhou, J., Raval-Fernandes, S., Minoofar, P., Zink, J., Dunn, B., Stewart, P. and Rome, L. 2005. Engineering of vault nanocapsules with enzymatic and fluorescent properties. *PANS.* 102(12): 4348-4352
- Kilic, M., Spiro, S. and Moore, G. 2003. Stability of a 24-meric homopolymer: Comparative studies of assembly-defective mutants of *Rhodobacter capsulatus* bacterioferritin and the native protein. *Protein Science.* 12: 1663-1674
- Kim, K., Kim, R. and Kim, S. 1998. Crystal structure of a small heat-shock protein. *Nature.* 394(6693): 595-599
- Kong, L., Siva, A., Kickhoefer, V., Rome, L. and Stewart, P. 2000. RNA location and modeling of a WD40 repeat domain within the vault. *RNA.* 6(6): 890-900
- Kopp, R., Vogt, A. and Maass, G. 1963. Separation of Iron-containing Ferritin from Horse-spleen into Three Distinct Fractions by Starch-gel Electrophoresis. *Nature.* 198: 892-893
- Köster, W. 2001. ABC transporter-mediated uptake of iron, siderophores, heme and vitamin B₁₂. *Res Microbiol.* 152: 291-301
- Kramer, R., Li, C., Carter, D., Stone, M. and Naik, R. 2004. Engineered protein cages for nanomaterial synthesis. *J Am Chem Soc.* 126(41): 13282-13286
- Langlois d'Estaintot, B., Santambrogio, P., Granier, T., Gallois, B., Chevallier, J., Precigoux, G., Levi, S. and Arosio, P. 2004. Crystal Structure and Biochemical Properties of the Human Mitochondrial Ferritin and its Mutant Ser144Ala. *J Mol Biol.* 340: 277-293
- Laulhère, J. and Briat, J. 1993. Iron release and uptake by plant ferritin: effects of pH, reduction and chelation. *Biochem J.* 290(Pt 3): 693-699

- Lawson, D., Artymiuk, P., Yewdall, S., Smith, J., Livingstone, J., Treffry, A., Luzzago, A., Levi, S., Arosio, P., Cesareni, G., Thomas, C., Shaw, W. and Harrison, P. 1991. Solving the structure of human H ferritin by genetically engineering intermolecular crystal contacts. *Nature*. 349: 541-544
- Le Brun, N., Andrews, S., Guest, J., Harrison, P., Moore, G. and Thomson, A. 1995. Identification of the ferroxidase centre of *Escherichia coli* bacterioferritin. *Biochem J*. 312: 385-392
- Le Brun, N., Keech, A., Mauk, M., Mauk, A., Andrews, S., Thomson, A. and Moore, G. 1996. Charge compensated binding of divalent metals to bacterioferritin: H⁺ release associated with cobalt(II) and zinc(II) binding at dinuclear metal sites. *FEBS Lett*. 397(2-3): 159-163
- Le Brun, N., Wilson, M., Andrews, S., Guest, J., Harrison, P., Thomson, A. and Moore, G. 1993. Kinetic and structural characterization of an intermediate in the biomineralization of bacterioferritin. *FEBS Letters*. 333(1-2): 197-202
- Lee, S. and Richter, G. 1976. The monomers and oligomers of ferritin and apoferritin: Association and dissociation. *Biochemistry*. 15(1): 65-70
- Levi, S., Santambrogio, P., Corsi, B., Cozzi, A. and Arosio, P. 1996. Evidence that residues exposed on the three-fold channels have active roles in the mechanism of ferritin iron incorporation. *Biochem J*. 317(Pt 2): 467-473
- Li, M. and Mann, S. 2004. DNA-directed assembly of multifunctional nanoparticle networks using metallic and bioinorganic building blocks. *J Mater Chem*. 14: 2260-2263
- Li, M., Wong, K. and Mann, S. 1999. Organization of Inorganic Nanoparticles Using Biotin-Streptavidin Connectors. *Chem Mater*. 11: 23-26
- Lichty, J., Malecki, J., Agnew, H., Michelson-Horowitz, D. and Tan, S. 2005. Comparison of affinity tags for protein purification. *Protein Expr Purif*. 41(1): 98-105
- Liepold, L., Revis, J., Allen, M., Oltrogge, L., Young, M. and Douglas, T. 2005. Structural transitions in Cowpea chlorotic mottle virus (CCMV). *Phys Biol*. 2(4): S166-172
- Listowsky, I., Blauer, G., Englard, S. and Bethel, J. 1972. Denaturation of Horse Spleen Ferritin in Aqueous Guanidinium Chloride Solutions. *Biochemistry*. 11: 2176-2182
- Litwin, C. and Calderwood, S. 1993. Role of iron in regulation of virulence genes. *Clin Microbiol Rev*. 6: 137-149
- Liu, H., Zhou, H., Xing, W., Zhao, J., Li, S., Huang, J. and Bi, R. 2004. 2.6 Å Resolution Crystal Structure of the Bacterioferritin from *Azotobacter vinelandii*. *FEBS Lett*. 573(1-3): 93-98

- Liu, X., Jin, W. and Theil, E. 2003. Opening protein pores with chaotropes enhances Fe reduction and chelation of Fe from the ferritin biomineral. *Proc Natl Acad Sci USA*. 100(7): 3653-3658
- Liu, X. and Theil, E. 2005. Ferritins: Dynamic Management of Biological Iron and Oxygen Chemistry. *Acc Chem Res*. 38(3): 167-175
- Macedo, S., Romao, C., Mitchell, E., Matias, P., Liu, M., Xavier, A., LeGall, J., Teixeira, M., Lindley, P. and Carrondo, M. 2003. The nature of the di-iron site in the bacterioferritin from *Desulfovibrio desulfuricans*. *Nature Structural Biology*. 10(4): 285-290
- Malvern manual, Malvern Instruments Ltd, Worcestershire, England, 2004
- Mann, S., Williams, J., Treffry, A. and Harrison, P. 1987. Reconstituted and Native Iron-cores of Bacterioferritin and Ferritin. *J Mol Biol*. 198(3): 405-416
- Mann, S., Shenton, W., Li, M., Connolly, S. and Fitzmaurice, D. 2000. Biologically Programmed Nanoparticle Assembly. *Advanced Materials*. 12(2): 147-150
- Marlovits, T., Haase, W., Herrmann, C., Aller, S. and Unger, V. 2002. The membrane protein FeoB contains an intramolecular G protein essential for Fe(II) uptake in bacteria. *Proc Natl Acad Sci USA*. 99: 16243-16248
- Massé, E. and Arguin, M. 2005. Ironing out the problem: new mechanisms of iron homeostasis. *TRENDS in Biochemical Sciences*. 30(8): 462-468
- Massé, E. and Gottesman, S. 2002. A small RNA regulates the expression of genes involved in iron metabolism in *Escherichia coli*. *Proc Natl Acad Sci USA*. 99(7): 4620-4625
- Meldrum, F., Douglas, T., Levi, S., Arosio, P. and Mann, S. 1995. Reconstitution of manganese oxide cores in horse spleen and recombinant ferritins. *J Inorg Biochem*. 58(1): 59-68
- Miller, C., Kim, Y., Walsh, M. and Anderson, A. 2000. Characterization and expression of the *pseudomonas putida* bacterioferritin alpha subunit gene. *Gene*. 247: 199-207
- Modis, Y., Trus, B. and Harrison, S. 2002. Atomic model of the papillomavirus capsid. *The EMBO Journal*. 21(18): 4754-4762
- Moore, G. 1991. Bacterial 4-alpha-helical Bundle Cytochromes. *Biochim Biophys Acta*. 1058(1): 38-41
- Moore, G., Mann, S. and Bannister, J. 1986. Isolation and Properties of the Complex Nonheme-iron-containing Cytochrome *b*₅₅₇ (bacterioferritin) from *Pseudomonas aeruginosa*. *J Inorg Biochem*. 28(2-3): 329-336

- Moore, G., Cheesman, M., Kadir, F., Thomson, A., Yewdall, S. and Harrison, P. 1992. Spectroscopic identification of the haem axial ligands of haemoferritin and location of possible haem-binding sites in ferritin by molecular modeling. *Biochem J.* 287: 457-460 (Moore *et al.*, 1992a)
- Moore, G., Kadir, F. and Al-Massad, F. 1992. Haem Binding to Ferritin and Possible Mechanisms of Physiological Iron Uptake and Release by Ferritin. *J Inorg Biochem.* 47(3-4): 175-181 (Moore *et al.*, 1992b)
- Naumann, C., Roman, E., Peinador, C., Ren, T., Patrick, B., Kaifer, A. and Sherman, J. 2001. Expanding cavitand chemistry: the preparation and characterization of [n]cavitands with $n \geq 4$. *Chemistry.* 7(8): 1637-1645
- Niemeyer, C. 2001. Nanoparticles, proteins, and Nucleic Acids: Biotechnology Meets Materials Science. *Angew Chem Int Ed.* 40: 4128-4158
- Notides, A. and Williams-Ashman, H. 1967. The basic protein responsible for the clotting of guinea pig semen. *Biochemistry.* 58: 1991-1995
- Notredame, C., Higgins, D. and Heringa, J. 2000. T-Coffee: A novel method for multiple sequence alignments. *Journal of Molecular Biology.* 302: 205-217
- Orino, K., Miura, T., Muto, S. and Watanabe, K. 2005. Sequence analysis of canine and equine ferritin H and L subunit cDNAs. *DNA Seq.* 16(1): 58-64
- Otsuka, S., Maruyama, H. and Listowsky, I. 1981. Structure, Assembly, Conformation, and Immunological Properties of the Two Subunit Classes of Ferritin. *Biochemistry.* 20: 5226-5232
- Palmer, L. and Rebek, J. 2004. The ins and outs of molecular encapsulation. *Org Biomol Chem.* 2(21): 3051-3059
- Palmer, L. and Rebek, J. 2005. Hydrocarbon binding inside a hexameric pyrogallol[4]arene capsule. *Org Lett.* 7(5): 787-789
- Palmer, L., Zhao, Y., Houk, K. and Rebek, J. 2005. Diastereoselection of chiral acids in a cylindrical capsule. *Chem Commun (Camb).* (29): 3667-3669
- Pandey, R., Sharma, S. and Khuller, G. 2005. Oral solid lipid nanoparticle-based antitubercular chemotherapy. *Tuberculosis (Edinb).* 85(5-6): 415-420
- Pandey, R., Sharma, A., Zahoor, A., Sharma, S., Khuller, G. and Prasad, B. 2003. Poly (DL-lactide-co-glycolide) nanoparticle-based inhalable sustained drug delivery system for experimental tuberculosis. *J Antimicrob Chemother.* 52(6): 981-986

- Pead, S., Durrant, E., Webb, B., Larsen, C., Heaton, D., Johnson, J. and Watt, G. 1995. Metal Ion Binding to Apo, Holo, and Reconstituted Horse Spleen Ferritin. *Journal of Inorganic Biochemistry*. 59: 15-27
- Pecora, R. 1985. Dynamic light scattering: Applications of photon correlation spectroscopy; Plenum Press: New York
- Perkel, J. 2004. The Ups and Downs of Nanobiotech. *The Scientist*. 18(16): 14-18
- Petsev, D., Thomas, B., Yau, S. and Vekilov, P. 2000. Interactions and aggregation of apoferritin molecules in solution: Effects of added electrolytes. *Biophysical Journal*. 78: 2060-2069
- Polanams, J., Ray, A. and Watt, R. 2005. Nanophase Iron Phosphate, Iron Arsenate, Iron Vanadate, and Iron Molybdate Minerals Synthesized within the Protein Cage of Ferritin. *Inorganic Chemistry*. 44(9): 3203-3209
- Post, P., Tyska, M., O'Connell, C., Johung, K., Hayward, A. and Mooseker, M. 2002. Myosin-IXb Is a Single-headed and Processive Motor. *The Journal of Biological Chemistry*. 277(14): 11679-11683
- Price, D. and Joshi, J. 1983. Ferritin: Binding of beryllium and other divalent metal ions. *The Journal of Biological Chemistry*. 258(18): 10873-10880
- Puig, S., Askeland, E. and Thiele, D. 2005. Coordinated remodeling of cellular metabolism during iron deficiency through targeted mRNA degradation. *Cell*. 120(1): 99-110
- Qasim, M. and Salahuddin, A. 1979. The Conformational Consequences of Maleylation of Amino Groups in Ovalbumin. *J Biochem*. 85(4): 1029-1035
- Ratledge, C. and Dover, L. 2000. Iron metabolism in pathogenic bacteria. *Annu Rev Microbiol*. 54: 881-941
- Rebek, J. 2005. Simultaneous encapsulation: molecules held at close range. *Angew Chem Int Ed Engl*. 44(14): 2068-2078
- Richter, G. and Walker, G. 1967. Reversible association of apoferritin molecules. Comparison of light-scattering and other data. *Biochemistry*. 6(9): 2871-2880
- Romão, C., Louro, R., Timkovich, R., Lubben, M., Liu, M., LeGall, J., Xavier, A. and Teixeira, M. 2000. Iron-coproporphyrin III is a Natural Cofactor in Bacterioferritin from the Anaerobic Bacterium *Desulfovibrio desulfuricans*. *FEBS Lett*. 480(2-3): 213-216 (Romão *et al.*, 2000a)

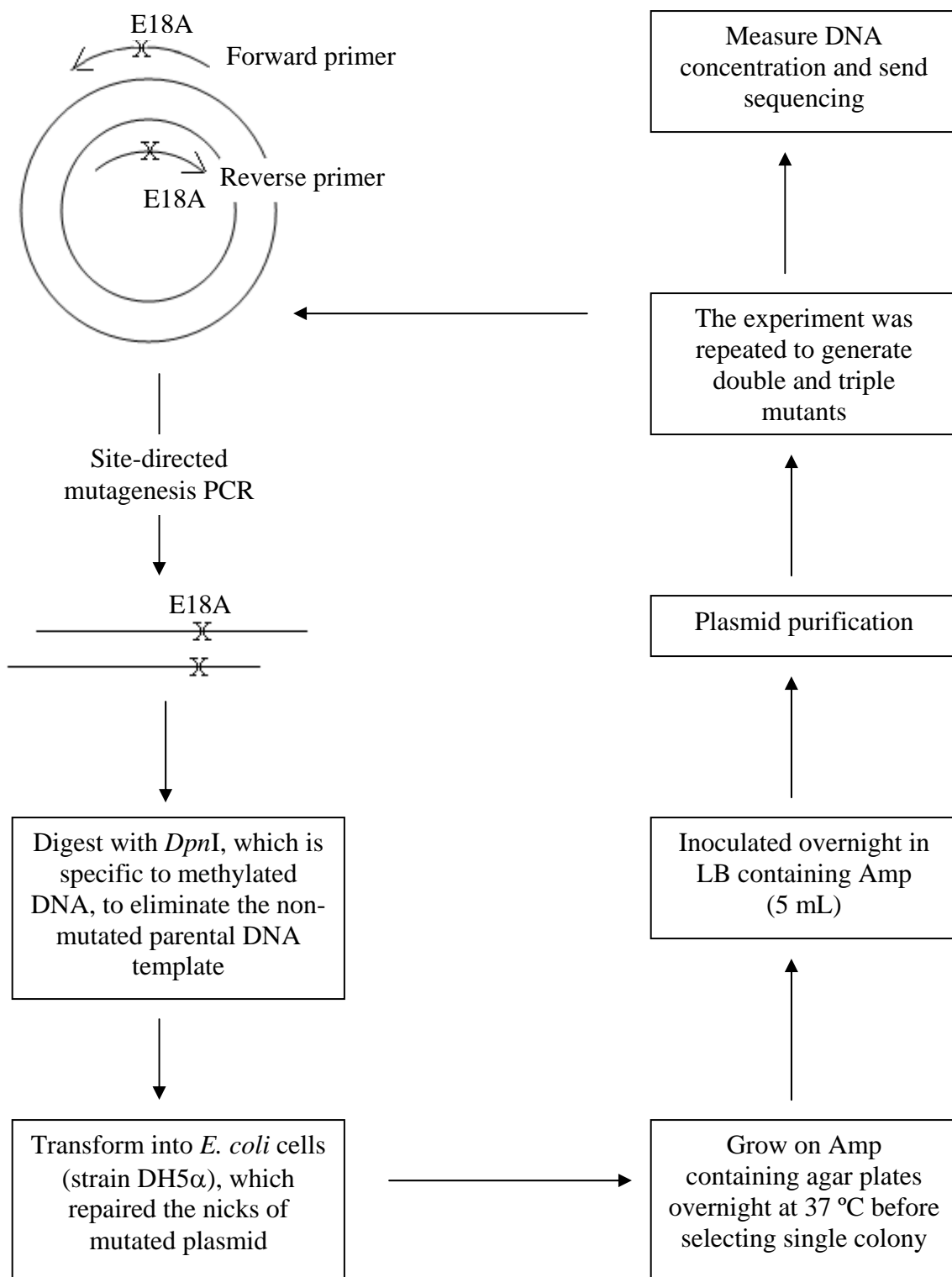
- Romão, C., Regalla, M., Xavier, A., Teixeira, M., Liu, M. and Le Gall, J. 2000. A Bacterioferritin from the Strict Anaerobe *Desulfovibrio desulfuricans* ATCC 27774. *Biochemistry*. 39(23): 6841-6849 (Romão *et al.*, 2000b)
- Rothen, A. 1944. Ferritin and Apoferritin in the Ultracentrifuge. Studies on the Relationship of Ferritin and Apoferritin; Precision Measurements of the Rates of Sedimentation of Apoferritin. *Journal of Biological Chemistry*. 152: 679-693
- Sambrook, J., Fritsch, E. and Maniatis, T. 1989. *Molecular Cloning: A laboratory Manual*. Cold Spring Harbour Laboratory Press, Plainsview, NY.
- Santambrogio, P., Levi, S., Arosio, P., Palagi, L., Vecchio, G., Lawson, D., Yewdall, S., Artymiuk, P., Harrison, P., Jappelli, R. and Cesareni, G. 1992. Evidence That a Salt Bridge in the Light Chain Contributes to the Physical Stability Difference between Heavy and Light Human Ferritins. *The Journal of Biological Chemistry*. 267(20): 14077-14083
- Santambrogio, P., Pinto, P., Levi, S., Cozzi, A., Rovida, E., Albertini, A., artymiuk, P., Harrison, P. and Arosio, P. 1997. Effects of modifications near the 2-, 3- and 4-fold symmetry axes on human ferritin renaturation. *Biochem. J.* 322: 461-468
- Sharma, A., Pandey, R., Sharma, S. and Khuller, G. 2004. Chemotherapeutic efficacy of poly (DL-lactide-co-glycolide) nanoparticle encapsulated antitubercular drugs at sub-therapeutic dose against experimental tuberculosis. *Int J Antimicrob Agents*. 24(6): 599-604
- Shenton, W., Douglas, T., Young, M., Stubbs, G. and Mann, S. 1999. Inorganic-Organic Nanotube Composites from Template Mineralization of Tobacco Mosaic Virus. *Advanced Materials*. 11(3): 253-256
- Siegel, L. and Monty, K. 1966. Determination of molecular weights and frictional ratios of proteins in impure systems by use of gel filtration and density gradient centrifugation. Application to crude preparations of sulfite and hydroxylamine reductases. *Biochim Biophys Acta*. 112(2): 346-362
- Simsek, E. and Kilic, M. 2005. Magic ferritin: a novel chemotherapeutic encapsulation bullet. *Journal of Magnetism and Magnetic Materials*. 293(1): 509-513
- Singh, B., Bohidar, H. and Chopra, S. 1991. Heat aggregation studies of phycobilisomes, ferritin, insulin, and immunoglobulin by dynamic light scattering. *Biopolymers*. 31: 1387-1396
- Smith, J. 1991. Bacterioferritin: Structural Modelling and Molecular Symmetry of *Escherichia coli* BFR. *Biochem Soc Trans*. 19(3): 337S
- Smith, J. 2004. The physiological role of ferritin-like compounds in bacteria. *Crit Rev Microbiol*. 30(3):173-185

- Smith, J., Ford, G., Harrison, P., Yariv, J. and Kalb, A. 1989. Molecular Size and Symmetry of the Bacterioferritin of *Escherichia coli*. X-ray Crystallographic Characterization of Four Crystal Forms. *J Mol Biol.* 205(2): 465-467
- Smith, J., Quirk, A., Plank, R., Diffin, F., Ford, G. and Harrison, P. 1988. The identity of *Escherichia coli* bacterioferritin and cytochrome *b_l*. *Biochem J.* 255: 737-740
- Starnes, S., Rudkevich, D. and Rebek, J. 2001. Cavitand-porphyrins. *J Am Chem Soc.* 123(20): 4659-4669
- Stefanini, S., Cavallo, S., Wang, C., Tataseo, P., Vecchini, P., Giartosio, A. and Chiancone E. 1996. Thermal Stability of Horse Spleen Apoferritin and Human Recombinant H Apoferritin. *Archives of Biochemistry and Biophysics.* 325(1): 58-64
- Stefanini, S., Vecchini, P. and Chiancone, E. 1987. On the Mechanism of Horse Spleen Apoferritin Assembly: A Sedimentation Velocity and Circular Dichroism Study. *Biochemistry.* 26: 1831-1837
- Stiefel, E. and Watt, G. 1979. *Azotobacter* cytochrome *b_{557.5}* is a bacterioferritin. *Nature.* 279: 81-83
- Stillman, T., Connolly, P., Latimer, C., Morland, A., Quail, M., Andrews, S., Treffry, A., Guest, J., Artymiuk, P. and Harrison, P. 2003. Insights into the Effects on Metal Binding of the Systematic Substitution of Five Key Glutamate Ligands in the Ferritin of *Escherichia coli*. *The Journal of Biological Chemistry.* 278(28): 26275-26286
- Stillman, T., Hempstead, P., Artymiuk, P., Andrews, S., Hudson, A., Treffry, A., Guest, J. and Harrison, P. 2001. The High-resolution X-ray Crystallographic Structure of the Ferritin (EcFtnA) of *Escherichia coli*; Comparison with Human H Ferritin (HuHF) and the Structures of the Fe³⁺ and Zn²⁺ Derivatives. *J Mol Biol.* 307: 587-603
- Stoddart, F. 1988. Unnatural product synthesis. *Nature.* 334: 10-11
- Stookey, L. 1970. Ferrozine-A New Spectrophotometric Reagent for Iron. *Analytical Chemistry.* 42(7): 779-781
- Stothard, P. 2000. The sequence manipulation suite: JavaScript programs for analyzing and formatting protein and DNA sequences. *BioTechniques.* 28: 1102-1104
- Su., M., Cavallo, S., Stefanini, S., Chiancone, E. and Chasteen, N. 2005. The So-Called *Listeria innocua* Ferritin Is a Dps Protein. Iron Incorporation, Detoxification, and DNA Protection Properties. *Biochemistry.* 44: 5572-5578
- Suran, A. and Tarver, H. 1965. Heterogeneity of Horse Spleen Ferritin and Apoferritin: Comparison of Electrophoretic and Chromatographic Fractions. *Archives of Biochemistry and Biophysics.* 111: 399-406

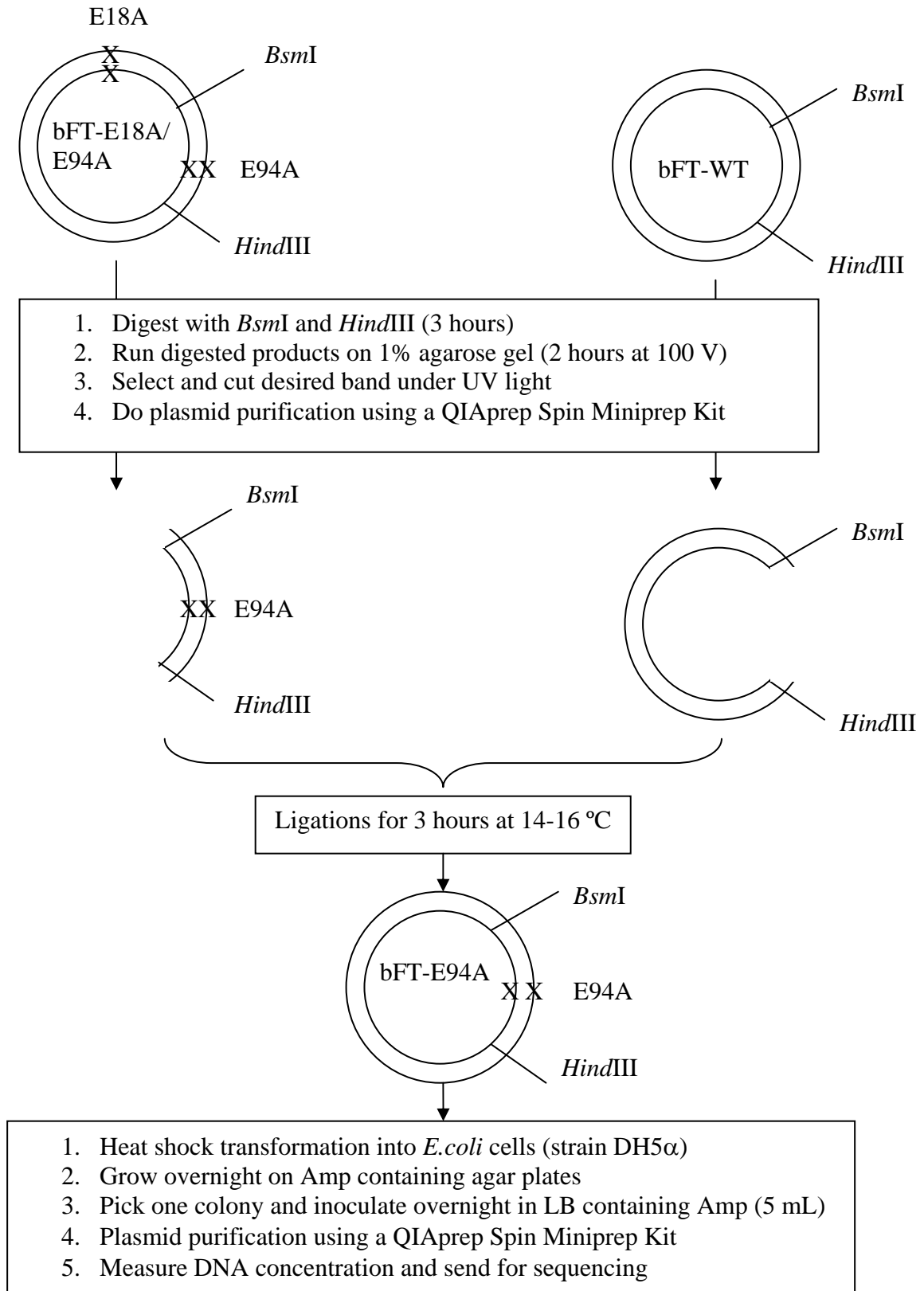
- Takeda, S., Ohta, M., Ebina, S. and Nagayama, K. 1993. Cloning, expression and characterization of horse L-ferritin in *Escherichia coli*. *Biochim Biophys Acta*. 1174(2): 218-220
- Tatusova, T. and Madden, T. 1999. BLAST 2 Sequences, a new tool for comparing protein and nucleotide sequences. *FEMS Microbiol Lett*. 174(22): 247-250
- Terpe, K. 2003. Overview of tag protein fusions: from molecular and biochemical fundamentals to commercial systems. *Appl Microbiol Biotechnol*. 60: 523-533
- Theil, E. 1987. Ferritin: structure, gene regulation, and cellular function in animals, plants, and microorganisms. *Annu Rev Biochem*. 56: 289-315
- Treffry, A., Bauminger, E., Hechel, D., Hodson, N., Nowik, I., Yewdall, S. and Harrison, P. 1993. Defining the roles of the threefold channels in iron uptake, iron oxidation and iron-core formation in ferritin: a study aided by site-directed mutagenesis. *Biochem J*. 296(Pt 3): 721-728
- Treffry, A., Zhao, Z., Quail, M., Guest, J. and Harrison, P. 1997. Dinuclear Center of Ferritin: Studies of Iron Binding and Oxidation Show Differences in the Two Iron Sites. *Biochemistry*. 36: 432-441
- Trus, B., Heymann, J., Nealon, K., Cheng, N., Newcomb, W., Brown, J., Kedes, D. and Steven, A. 2001. Capsid structure of Kaposi's sarcoma-associated herpesvirus, a gammaherpesvirus, compared to those of an alphaherpesvirus, herpes simplex virus type 1, and a betaherpesvirus, cytomegalovirus. *J Virol*. 75(6): 2879-2890
- Tsugita, A. and Yariv, J. 1985. Preliminary results for the primary structure of bacterioferritin of *Escherichia coli*. *Biochem J*. 231: 209-212
- Van Holde, K., Johnson, W. and Ho, P. 1998. Principles of Physical Biochemistry. Prentice Hall: New Jersey
- Varpness, Z., Peters, J., Young, M. and Douglas, T. 2005. Biomimetic synthesis of a H₂ catalyst using a protein cage architecture. *Nano Lett*. 5(11): 2306-2309
- Velayudhan, J., Hughes, N., McColm, A., Bagshaw, J., Clayton, C., Andrews, S. and Kelly, D. 2000. Iron acquisition and virulence in *Helicobacter pylori*: a major role for FeoB, a high-affinity ferrous iron transporter. *Mol Microbiol*. 37: 274-286
- Venkatesh, S. and Deshpande, V. 1999. A comparative review of the structure and biosynthesis of thyroglobulin. *Comp Biochem Physiol C Pharmacol Toxicol Endocrinol*. 122(1): 13-20
- Wade, V., Levi, S., Arosio, P., Treffry, A., Harrison, P. and Mann, S. 1991. Influence of Site-directed Modifications on the Formation of Iron Cores in Ferritin. *J Mol Biol*. 221: 1443-1452

- Wandersman, C. and Delepelaire, P. 2004. Bacterial Iron Sources: From Siderophores to Hemophores. *Annu Rev Microbiol.* 58: 611-647
- Wang, Q., Lin, T., Tang, L., Johnson, J. and Finn, M. 2002. Icosahedral virus particles as addressable nanoscale building blocks. *Angew Chem Int Ed Engl.* 41(3): 459-462
- Wiedenheft, B., Mosolf, J., Willits, D., Yeager, M., Dryden, K., Young, M. and Douglas, T. 2005. An archaeal antioxidant: Characterization of a Dps-like protein from *Sulfolobus solfataricus*. *PNAS.* 102(30): 10551-10556
- Wilderman, P., Sowa, N., FitzGerald, D., FitzGerald, P., Gottesman, S., Ochsner, U. and Vasil, M. 2004. Identification of tandem duplicate regulatory small RNAs in *Pseudomonas aeruginosa* involved in iron homeostasis. *PNAS.* 101(26): 9792-9797
- Williams, M. and Harrison, P. 1968. Electron-Microscopic and Chemical Studies of Oligomers in Horse Ferritin. *Biochem J.* 110: 265-280
- Xu, C., Xu, K., Gu, H., Zhong, X., Gua, Z., Zheng, R., Zhang, X. and Xu, B. 2004. Nitrilotriacetic Acid-Modified Magnetic Nanoparticles as a General Agent to Bind Histidine-Tagged Proteins. *J Am Chem Soc.* 126: 3392-3393
- Yang, S., Marchio, J. and Yen, J. 1994. A dynamic light scattering study of β -galactosidase: Environmental effects on protein conformation and enzyme activity. *Biotechnol Prog.* 10: 525-531
- Yang, X., Le Brun, N., Thomson, A., Moore, G. and Chasteen, N. 2000. The Iron Oxidation and Hydrolysis Chemistry of *Escherichia coli* Bacterioferritin. *Biochemistry.* 39(16): 4915-4923
- Yariv, J. 1983. The identity of bacterioferritin and cytochrome b_1 . *BJ Letters.* 211: 527
- Yariv, J., Kalb, A., Sperling, R., Bauminger, E., Cohen, S. and Ofer, S. 1981. The composition and the structure of bacterioferritin of *Escherichia coli*. *Biochem J.* 197: 171-175
- Zhao, G., Ceci, P., Ilari, A., Giangiacomo, L., Laue, T., Chiancone, E. and Chasteen, N. 2002. Iron and hydrogen peroxide detoxification properties of DNA-binding protein from starved cells. A ferritin-like DNA-binding protein of *Escherichia coli*. *J Biol Chem.* 277(31): 27689-27696

Appendix 1: Flow Chart for QuikChange[®] Site-directed Mutagenesis PCR



Appendix 2: Flow Chart for Site-directed Mutagenesis of bFT-E94A



Appendix 4: Sequencing Results for Wild Type and Variants of Bacterioferritin

All DNA samples, wild-type bFT and bFT variants, were sent for sequencing (Mobix, McMaster). The sequencing process required at least 100 ng/ μ L (for double strand DNA < 10 kb). The forward primer for the promoter T7 was used for sequencing of bFT-WT and mutated bFT, so the results were in the forward direction (5' to 3'). For the sequence of bFT with His₆-tag at the C-terminus, the result from Mobix is in the reverse form due to the position of tag. The reverse primer of promoter T7 was used for this sequencing. The forward sequence was received using Reverse Complement software (http://bioinformatics.org/sms/rev_comp.html) (Stothard, 2000). The results are in two forms, FASTA format and sequencing chromatogram. The mutated sequence in FASTA format was checked using the BLAST2 program (<http://www.ncbi.nlm.nih.gov/blast/bl2seq/wblast2.cgi>) (Tatusova and Madden, 1999). Blast2 results represent Query as literature sequence of wild-type bFT and Sbjct as experimental cloning sequence. The bold letters and number above the specific three amino acids (emphasized by highlight) show correctly mutated residues. The sequencing chromatograms were used to confirm the FASTA format and check for the possibility of “n” (uncertain or unknown amino acid) in experimental cloning sequence.

Sequence for pT7.Bfr-WT

FASTA Format Results:

```
GAGGGGGGGCGGNTAAACAATTNCCCCTGCTAGNAAATAATTTTGTTTAACTTTAAGNAAGGNAGNATATACATAT
GAAAGGTGATACTAAAGTTATAAAATTATCTCAACAAACTGTTGGGAAATGAGCTTGTTCGCAATCAATCAGTACTTT
CTCCATGCCCGAATGTTTAAAAACTGGGGTCTCAAACGTCTCAATGATGTGGAGTATCATGAATCCATTGATGAGA
TGAAACACGCCGATCGTTATATTGAGCGCATTCTTTTTCTGGAAGGTCTTCCAAACTTACAGGACCTGGGCAAAC
GAACATTGGTGAAGATGTTGAGGAAATGCTGCGTTCTGATCTGGCACTTGAGCTGGATGGCGCGAAGAATTTGCGT
GAGGCAATTGGTTATGCCGATAGCGTTCATGATTACGTCAGCCGCGATATGATGATAGAAATTTTGCCTGATGAAG
AAGGCCATATCGACTGGCTGGAAACGGAACCTTGATCTGATTGAGAAGATGGGCCCTGCAAAAATTATCTGCAAGCACA
GATCCGCGAAGAAGGTTGAGGATCCGAATTCGAGCTCCGTCGACAAGCTTGCGGCCGCACTCGAGCACCACCACCA
CCACCACTGAGATCCGGCTGCTAACAAAGCCCGAAAGGAAGCTGAGTTGGCTGCTGCCACCGCTGAGCAATAACTA
GCATAACCCCTTGGGGCTCTAAACGGGCTTGGAGGGTTTTTTTGTGAAAGGAGGAACTATATCCNGATTGGCG
AATGGGACGCGCCCTGTAGCGGCGATTAAAGCGCGCNGNTGTGGTGGTTACCCCCCGCCGTGACCCGCTACACT
TGCCAGCGCCCTAGCGCCGCTNCTTTTCGCTTTCTNCCCTTNTTNTCGCCACGTTCCGCCGGCTTTTCCCGTCAAG
CTCTAATCGGGGGCTCCCTTNANGGTTCCATTTANTGCTTNCGGCACCTGACCCCAAAAACCTGTTAGGGTGTGG
TCACNTATGGGCATCCCTGNNGACGGTTTNGCCTTGNCGTTGAGCCNCGTCTTAATANNGNCTCTGTCAACTGGA
CACNCCACCTTTCGNCTTNTTTGATTATAGNCTTGC
```

Blast2 Result :

```
Query: 1 atgaaaggtgataactaaagttataaattatctcaacaaactgttgggaaatgagcttgtc 60
|||||
Sbjct: 75 atgaaaggtgataactaaagttataaattatctcaacaaactgttgggaaatgagcttgtc 134

Query: 61 gcaatcaatcagtacttttctccatgcccgaatgtttaaaaactggggtctcaaactgtctc 120
|||||
Sbjct: 135 gcaatcaatcagtacttttctccatgcccgaatgtttaaaaactggggtctcaaactgtctc 194

Query: 121 aatgatgtggagtatcatgaatccattgatgagatgaaacacgccgatcgttatattgag 180
|||||
Sbjct: 195 aatgatgtggagtatcatgaatccattgatgagatgaaacacgccgatcgttatattgag 254

Query: 181 cgcattcttttctggaaggtcttccaaacttacaggacctgggcaaactgaacattggt 240
|||||
Sbjct: 255 cgcattcttttctggaaggtcttccaaacttacaggacctgggcaaactgaacattggt 314

Query: 241 gaagatgttgaggaaatgctgcttctgatctggcacttgagctggatggcgcaagaat 300
|||||
Sbjct: 315 gaagatgttgaggaaatgctgcttctgatctggcacttgagctggatggcgcaagaat 374

Query: 301 ttgctgaggcaattggttatgccgatagcgttcatgattacgtcagccgcgatatgatg 360
|||||
Sbjct: 375 ttgctgaggcaattggttatgccgatagcgttcatgattacgtcagccgcgatatgatg 434

Query: 361 atagaaatTTTgctgatgaagaaggccatatcgactggctggaaacggaacttgatctg 420
|||||
Sbjct: 435 atagaaatTTTgctgatgaagaaggccatatcgactggctggaaacggaacttgatctg 494

Query: 421 attcagaagatgggctgcaaaaattatctgcaagcacagatccgcgaagaaggttga 477
|||||
Sbjct: 495 attcagaagatgggctgcaaaaattatctgcaagcacagatccgcgaagaaggttga 551
```

Sequence for pT7.Bfr-E18A

FASTA Format Results:

```
GANGNGNCCGTAACAATTNCCCCTNCTAAAAATAATTTTGTTTAACTTTAAGNAAGGAGNATATACATATGAAAG
GTGATACTAAAGTTATAAAATTATCTCAACAAACTGTTGGGAAATGCGCTTGTGCGCAATCAATCAGTACTTTCTCCA
TGCCCGAATGTTTAAAAACTGGGGTCTCAAACGTCTCAATGATGTGGAGTATCATGAATCCATTGATGAGATGAAA
CACGCCGATCGTTATATTGAGCGCATTCTTTTTCTGGAAGGCTTCCAAACTTACAGGACCTGGGCAAACCTGAACA
TTGGTGAAGATGTTGAGGAAATGCTGCGTTCGATCTGGCACTTGGAGCTGGATGGCGCGAAGAATTTGCGTGAGGC
AATTGGTTATGCCGATAGCGTTCATGATTACGTCAGCCGCGATATGATGATAGAAATTTTGGCTGATGAAGAAGGC
CATATCGACTGGCTGGAAACGGAACTTGATCTGATTTCAGAAAGATGGGCCCTGCAAAATTTATCTGCAAGCACAGATCC
GCGAAGAAGGTTGAGGATCCGAATTCGAGCTCCGTCGACAAGCTTGGCGCCGCACTCGAGCACCACCACCACCACC
ACTGAGATCCGGCTGCTAACAAAGCCCGAAAGGAAGCTGAGTTGGCTGCTGCCACCCTGAGCAATAACTAGCATA
ACCCCTTGGGGCTCTAAACGGGCTTTGAGGGGTTTTTTGCTGAAAGGAGGAACTATATCCGGATTGGCGAATGGG
GACGCGCCCTGTAGCGGCGCATTAACGCCGGCGGGTGTGGTGGTTACGCCAGCGTGACCGCTNCACCTTGCCAGCG
CCCTAGCGCCNGCTCCTTTTCGCTTTTTCCCTTCTTTTTTCGNCACGTTNGCCGGCTTTCCCGTCAGCTNTAATCGG
GGCCCCCTTNAGGGTCCGATTAAGTGCCTTAGGNCNCCGNCCAAACTGNTTAGGGGATGGTCCCGNNTGGGCNN
CCCTGANAACGGTTTCNCCCTTGNGTGGAGTCNCNNNNTANANGGNCNTGTCAAACCTGGACANCTACCTTTTGG
GCNTTTTTTGTTTAAGGAATTG
```

Blast2 Result:

```
Query: 1 atgaaaggtgataactaaagttataaattatctcaacaaactgttgggaaatgagcttgtc 60
          |||
Sbjct: 70 atgaaaggtgataactaaagttataaattatctcaacaaactgttgggaaatgagcttgtc 129
          |||

Query: 61 gcaatcaatcagtaactttctccatgcccgaatgtttaaactggggctctcaaactgtctc 120
          |||
Sbjct: 130 gcaatcaatcagtaactttctccatgcccgaatgtttaaactggggctctcaaactgtctc 189
          |||

Query: 121 aatgatgtggagtatcatgaatccattgatgagatgaaacacgccgatcgttatattgag 180
          |||
Sbjct: 190 aatgatgtggagtatcatgaatccattgatgagatgaaacacgccgatcgttatattgag 249
          |||

Query: 181 cgcattcttttctggaaggctcttccaaacttacaggacctgggcaactgaacattggt 240
          |||
Sbjct: 250 cgcattcttttctggaaggctcttccaaacttacaggacctgggcaactgaacattggt 309
          |||

Query: 241 gaagatggtgaggaaatgctgcttctgatctggcacttgagctggatggcgcaagaat 300
          |||
Sbjct: 310 gaagatggtgaggaaatgctgcttctgatctggcacttgagctggatggcgcaagaat 369
          |||

Query: 301 ttgctgaggcaattgggttatgccgatagcgttcatgattacgtcagccgcatatgatg 360
          |||
Sbjct: 370 ttgctgaggcaattgggttatgccgatagcgttcatgattacgtcagccgcatatgatg 429
          |||

Query: 361 atagaaatTTTgctgatgaagaaggccatatacactggctggaaacggaacttgatctg 420
          |||
Sbjct: 430 atagaaatTTTgctgatgaagaaggccatatacactggctggaaacggaacttgatctg 489
          |||

Query: 421 attcagaagatgggctgcaaaattatctgcaagcacagatccgcgaagaaggttga 477
          |||
Sbjct: 490 attcagaagatgggctgcaaaattatctgcaagcacagatccgcgaagaaggttga 546
          |||
```


Sequence for pT7.Bfr-E94A

FASTA Format Results:

```
GANGNGNCGGTAACAATTTCCCTNCTAGNAAATAATTTTGTTTAACTTTAAGNAAGGAGNATATACATATGAAA
GGTGATACTAAAGTTATAAAATTATCTCAACAAACTGTTGGGAAATGAGCTTGTTCGCAATCAATCAGTACTTTCTCC
ATGCCCGAATGTTTAAAAACTGGGGTCTCAAACGTCTCAATGATGTGGAGTATCATGAATCCATTGATGAGATGAA
ACACGCCGATCGTTATATTGAGCGCATCTTTTTCTGGAAGGCTTCCAAACTTACAGGACCTGGGCAAACCTGAAC
ATTGGTGAAGATGTTGAGGAAATGCTGCGTTCTGATCTGGCACTTGCCTGGATGGCGCGAAGAATTTGCGTGAGG
CAATTGGTTATGCCGATAGCGTTTCATGATTACGTACGCCGCGATATGATGATAGAAATTTTGCCTGATGAAGAAGG
CCATATCGACTGGCTGGAAACGGAACCTTGATCTGATTTCAGAAGATGGGCCCTGCAAAAATTATCTGCAAGCACAGATC
CGCGAAGAAGGTTGAGGATCCGAATTCGAGCTCCGTCGACAAGCTTGGCGCCGCACTCGAGCACCACCACCACCAC
CACTGAGATCCGGCTGCTAACAAAGCCCGAAAGGAAGCTGAGTTGGCTGCTGCCACCGCTGAGCAATAACTAGCAT
AACCCCTTGGGGCTCTAAACGGGTCTTGAGGGGTTTTTTTGTGAAAGGAGGAACATATCCGGATTGGCGAATGG
GACGCGCCCTGTAGCGCGCATTAAAGCGCGGGGTGTGGTGGTTACGCGCAGCGTGACCGCTACACTTGCAGCG
CCCTAGCGCCCGCTCTTTTCGCTTTCTTCCCTTCTTCTCGCCACGTTTCGCCGCTTTCCCGTCAGCTCTAATC
GGGGGCTCCCTTTAGGGTTCCGATTAAGTGCTTACGGCCCTCGCCCCAAAACTTGATAGGGTGATGGTCCGTAGT
GGGCATCGCTGATAGACGTTTTTCGCCCTTGCCTGAGTCACGCTTTATAGTGACTCTGTCAACTGGACACCTCAN
CCTTCTCGTTTCTTTGTTATANGAATTCGATTTCGCTTGGTAAATGACTGATTACAAATTACNGATTTACAAATAC
CTNATTAGNGCCTTCGGAATGNCGACCTT
```

Blast2 Result :

```
Query: 1 atgaaaggtgataactaaagttataaattatctcaacaaactggtgggaaatgagcttgtc 60
      |||
Sbjct: 71 atgaaaggtgataactaaagttataaattatctcaacaaactggtgggaaatgagcttgtc 130

Query: 61 gcaatcaatcagtactttctccatgcccgaatgtttaaaaactggggctctcaaacgtctc 120
      |||
Sbjct: 131 gcaatcaatcagtactttctccatgcccgaatgtttaaaaactggggctctcaaacgtctc 190

Query: 121 aatgatgtggagtatcatgaatccattgatgagatgaaacacgccgatcggtatattgag 180
      |||
Sbjct: 191 aatgatgtggagtatcatgaatccattgatgagatgaaacacgccgatcggtatattgag 250

Query: 181 cgcattcttttctggaaggtcttccaaacttacaggacctgggcaaactgaacattggt 240
      |||
Sbjct: 251 cgcattcttttctggaaggtcttccaaacttacaggacctgggcaaactgaacattggt 310

Query: 241 gaagatgtgaggaaatgctgcttctgatctggcacttgagctggatggcgcaagaat 300
      |||
Sbjct: 311 gaagatgtgaggaaatgctgcttctgatctggcacttgagctggatggcgcaagaat 370

Query: 301 ttgctgaggcaattggttatgccgatagcgttcatgattacgtcagccgcgatatgatg 360
      |||
Sbjct: 371 ttgctgaggcaattggttatgccgatagcgttcatgattacgtcagccgcgatatgatg 430

Query: 361 atagaaatTTGCGTGATGAAGAAGGCCATATCGACTGGCTGGAACGGAACCTGATCTG 420
      |||
Sbjct: 431 atagaaatTTGCGTGATGAAGAAGGCCATATCGACTGGCTGGAACGGAACCTGATCTG 490

Query: 421 attcagaagatgggctgcaaaattatctgcaagcacagatccgcaagaaggttga 477
      |||
Sbjct: 491 attcagaagatgggctgcaaaattatctgcaagcacagatccgcaagaaggttga 547
```

Sequence for pT7.Bfr-E18A/E94A

FASTA Format Results:

```
GATNGkGagCGGwwAACAAATCCCCTCTAGAAATAATTTTGTTTAACTTTAAGAAGGAGATATACATATGAAAGGT
GATACTAAAGTTATAAAATTATCTCAACAAACTGTTGGGAAATGCGCTTGTTCGCAATCAATCAGTACTTTCTCCATG
CCCGAATGTTTAAAAACTGGGGTCTCAAACGTCTCAATGATGTGGAGTATCATGAATCCATTGATGAGATGAAACA
CGCCGATCGTTATATTGAGCGCATTCTTTTTCTGGAAGGTCTTCCAAACTTACAGGACCTGGGCAAACCTGAACATT
GGTGAAGATGTTGAGGAAATGCTGCGTTCGATCTGGCACTTGCCTGGATGGCGCGAAGAATTTGCGTGAGGCAA
TTGGTTATGCCGATAGCGTTCATGATTACGTCAGCCGCGATATGATGATAGAAATTTTGCCTGATGAAGAAGGCCA
TATCGACTGGCTGGAAACGGAACTTGATCTGATTTCAGAAAGATGGGCCCTGCAAAAATTATCTGCAAGCACAGATCCGC
GAAGAAGGTTGAGGATCCGAATTCGAGCTCCGTCGACAAGCTTGC GGCCGCACTCGAGCGCCACCACCACCACCAC
TGAGATCCGGCTGCTAACAAAAGCCCGAAAGGAAAGCTGAGTTGGCTGCTGCCACCCTGAGCAATAACTAGCATAAC
CCCTTGGGGCTCTAAACGGGTCTTGAGGGTTTTTTGTCTGAAAGGAGGAACTATATCCGGATTGGCgATGGGACG
CGCCCTGTAGCGCGCATTAAGCGCGCGGGTGTGGTGGTTACCgCGCANCNGACCCTAACTTGCCAGCGCCCC
TAGCGCCCGNTCCCTTTCCCTTTNTCCCTTCCCTTCTCGCNCCTTNCNCCGGCTTTCCCGTCAAGGCTNTAAATCGGGG
CGTCCCTTTAGGTTCCANTTAGNGGNTTTACGNCCCCCTCCCCAAAAACTTGATAGGGGNTGGTNCGTANGGGCCCN
CCCCNTGNAACGNTTTTNCNCTTGNCTTGGGGCCNNTNTTAAANNGGNNTGTTNCNANTGGNNNCNCCCCCN
CCGGCTNTTTTTTGNNTNAG
```

Blast2 Result:

```
Query: 1 atgaaaggtgataactaaagttataaattatctcaacaaactggtgggaaatgagcttgtc 60
          |||
Sbjct: 68 atgaaaggtgataactaaagttataaattatctcaacaaactggtgggaaatgagcttgtc 127
          |||

Query: 61 gcaatcaatcagtaactttctccatgcccgaatggttaaaaactggggctctcaaacgtctc 120
          |||
Sbjct: 128 gcaatcaatcagtaactttctccatgcccgaatggttaaaaactggggctctcaaacgtctc 187
          |||

Query: 121 aatgatgtggagtatcatgaatccattgatgagatgaaacacgccgatcggtatattgag 180
          |||
Sbjct: 188 aatgatgtggagtatcatgaatccattgatgagatgaaacacgccgatcggtatattgag 247
          |||

Query: 181 cgcattcttttctggaaggtcttccaaacttacaggacctgggcaaacgaacattggt 240
          |||
Sbjct: 248 cgcattcttttctggaaggtcttccaaacttacaggacctgggcaaacgaacattggt 307
          |||

Query: 241 gaagatggtgaggaaatgctgcttctgatctggcacttgagctggatggcgcaagaat 300
          |||
Sbjct: 308 gaagatggtgaggaaatgctgcttctgatctggcacttgagctggatggcgcaagaat 367
          |||

Query: 301 ttgctgaggcaattgggttatgccgatagcgttcatgattacgtcagccgcatatgatg 360
          |||
Sbjct: 368 ttgctgaggcaattgggttatgccgatagcgttcatgattacgtcagccgcatatgatg 427
          |||

Query: 361 atagaaatTTTgctgatgaagaaggccatatcgactggctggaaacggaacttgatctg 420
          |||
Sbjct: 428 atagaaatTTTgctgatgaagaaggccatatcgactggctggaaacggaacttgatctg 487
          |||

Query: 421 attcagaagatgggctgcaaaattatctgcaagcacagatccgcaagaaggttga 477
          |||
Sbjct: 488 attcagaagatgggctgcaaaattatctgcaagcacagatccgcaagaaggttga 544
          |||
```

Sequence for pT7.Bfr-E18A/M52L

FASTA Format Results:

```
GATNGNGNGNCGGNTAACAAATTNCCCCTNCTAGNAAATAATTTTGTTTAACTTTAAGNAAGGAGNATATACATATG
AAAGGTGATACTAAAGTTATAAAATTATCTCAACAAACTGTTGGGAAATGCGCTTGTGCGCAATCAATCAGTACTTTC
TCCATGCCCGAATGTTTAAAAACTGGGGTCTCAAACGTCTCAATGATGTGGAGTATCATGAATCCAATTGATGAGCT
GAAACACGCCGATCGTTATATTGAGCGCATTCTTTTTCTGGAAGGCTTCCAAACTTACAGGACCTGGGCAAACCTG
AACATTGGTGAAGATGTTGAGGAAATGCTGCGTTCGATCTGGCACTTGGAGCTGGATGGCGCGAAGAATTTGCGTG
AGGCAATTGGTTATGCCGATAGCGTTCATGATTACGTCAGCCGCGATATGATGATAGAAATTTTGCCTGATGAAGA
AGGCCATATCGACTGGCTGGAAACGGAACTTGATCTGATTTCAGAAAGATGGGCCCTGCAAAATTTATCTGCAAGCACAG
ATCCGCGAAGAAGGTTGAGGATCCGAATTCGAGCTCCGTCGACAAGCTTGGCGCCGCACTCGAGCACCACCACCAC
CACCCTGAGATCCGGCTGCTAACAAAGCCCGAAAGGAAGCTGAGTTGGCTGCTGCCACCCTGAGCAATAACTAG
CATAACCCCTTGGGGCTCTAAACGGGTCTTGAGGGGTTTTTTGCTGAAAGGAGGAACTATATCCGGATTGGCGAA
TGGGACGCGCCCTGTAGCGGCGCATTAAGCGCGGCGGGTGTGGTGGTTACCCGACGCTGACCGCTACACTTGCCC
AGCGCCCTAGCGCCCGCTCCTTTNCCCTTTNCCCTTCTCCNCACGTTCCGCGGCTTTNCCCGTCAAGCTN
TAAATCGGGGCTCCCTTAGGGTNCNGNTTAGTGCCCTNCGNCACCTCNCCCAAAACCTTGATAGGTGATGGTTACC
NANTGGCTTNGCCTGNNGACGTTTTCCCTTTNACGTTGGNACCNGNTTNTTATNGTGGACTCTGTTCAANTGGA
NANCCACCNTTCTGGNTTTNNTT
```

Blast2 Result:

```
Query: 1 atgaaaggtgataactaaagttataaattatctcaacaaactggtgggaaatgagcttgtc 60
          |||
Sbjct: 74 atgaaaggtgataactaaagttataaattatctcaacaaactggtgggaaatgagcttgtc 133
          |||
```

E18A

```
Query: 61 gcaatcaatcagtaactttctccatgcccgaatggttaaaaactggggctctcaaacgtctc 120
          |||
Sbjct: 134 gcaatcaatcagtaactttctccatgcccgaatggttaaaaactggggctctcaaacgtctc 193
          |||
```

M52L

```
Query: 121 aatgatgtggagtatcatgaatccattgatgagatgaaacacgccgatcggtatattgag 180
          |||
Sbjct: 194 aatgatgtggagtatcatgaatccattgatgagctgaaacacgccgatcggtatattgag 253
          |||
```

```
Query: 181 cgcattcttttctggaaggtcttccaaacttacaggacctgggcaaacctgaacattggt 240
          |||
Sbjct: 254 cgcattcttttctggaaggtcttccaaacttacaggacctgggcaaacctgaacattggt 313
          |||
```

```
Query: 241 gaagatggtgaggaaatgctgcttctgatctggcacttgagctggatggcgcaagaat 300
          |||
Sbjct: 314 gaagatggtgaggaaatgctgcttctgatctggcacttgagctggatggcgcaagaat 373
          |||
```

```
Query: 301 ttgctgaggcaattgggttatgccgatagcgttcatgattacgtcagccgcatatgatg 360
          |||
Sbjct: 374 ttgctgaggcaattgggttatgccgatagcgttcatgattacgtcagccgcatatgatg 433
          |||
```

```
Query: 361 atagaaatTTTgctgatgaagaaggccatctgactggctggaaacggaacttgatctg 420
          |||
Sbjct: 434 atagaaatTTTgctgatgaagaaggccatctgactggctggaaacggaacttgatctg 493
          |||
```

```
Query: 421 attcagaagatgggctgcaaaattatctgcaagcacagatccgcaagaaggttga 477
          |||
Sbjct: 494 attcagaagatgggctgcaaaattatctgcaagcacagatccgcaagaaggttga 550
          |||
```


Sequence for pT7.Bfr-E18A/M52L/E94A

FASTA Format Results:

```
GTNAGTGNNNCGNNTAAACAATTNCCCCTCCTAGCCAAATANNNTTTTGTGTCTAACTTTAAGNAAGGGAGGATAT
ACATATGAAAGGTGATACTAAAGTTATAAAATTATCTCAACAAACTGTTGGGAAATGCGCTTGTTCGCACaTCAATC
AGTACTTTCTCCATGCCCGAATGTTTAAAAAAGTGGGGTCTCAAACGTCCTCAATGATGTGGAGTATCATGAATCCAT
TGATGAGCTGAAACACGCCGATCGTTATATTGAGCGCATTCTTTTTCTGGAAGGTCTTCCAAACTTACAGGACCTG
GGCAAAC TGAAACATTGGTGAAGATGTTGAGGAAATGCTGCGTTCTGATCTGGCACTTGCCTGGATGGCGCGAAGA
ATTTGCGTGAGGCAATTGGTTATGCCGATAGCGTTTCATGATTACNTCAGCCGCGATATGATGATAGAAAATTTTGGC
TGATGAAGAAGGCCATATCGACTGGCTGGAAACGGAACTTGATCTGATTANAAGATGGGCCCTGCAAAAATTTCTG
CAAGCACAGATCCGCGAAGAAGGTTGAGGATCCGATTTGAGCTCCGGTCNACAGCTTGCNCCGCNCTCGAGCACC
ACCNCCACCACCCTGAGATCCGGCTGCTAACAAAANCCNGAAAGGAAGCTGATTTGNCTGCTGCCNCCCGGTGAG
CAATAACTAGCNTAACTCCCTTNGGGNCCTCTAACCGGGCTTGAGGGNTTTTTGTGAAANGAGGAACTNTNTC
NCGGATTGNTNANTGGGACCCGCCCTGTAGCGGCCATTAAGCCNCGGCGGTTNTTNGTGNACNCGCANCNTGCC
CGNTACACTTNNCANCCCCCTAGCCCCGNTANNTTNCNTTCTNCCCTTCCCTTCCNGCCNGTTCNCCGCTTTTCN
CGTTAGCTTAANGGGGGCNTCCCTTANGGTNCCATTNANTNNTACCGNACNCCNCCNCAANTTGNNTNGGGGNTG
GTNCNNMNTGGNCNCTCCCNANANAANCGNTTNCNNTTANNTGGNCCNCTTCTTAAAAGTCCCTTNNCCAACNG
ANNACATACCNTTNGGTTNTANTTNTTATAGNGATTNCNANNCNCCCTCTTANAAAANTCTNAAAAA
```

Blast2 Result:

```
Query: 1 atgaaaggtgataactaaagttataaattatctcaacaaactggtgggaaatgagcttgt- 59
|||
Sbjct: 81 atgaaaggtgataactaaagttataaattatctcaacaaactggtgggaaatgagcttgtt 140
```

E18A

```
Query: 60 cgca-atcaatcagtaactttctccatgcccgaatggttaaaaactggggctctcaaacgtc 118
|||
Sbjct: 141 cgcacatcaatcagtaactttctccatgcccgaatggttaaaaactggggctctcaaacgtc 200
```

M52L

```
Query: 119 tcaatgatgtggagtatcatgaatccattgatgagatgaaacacgccgatcggtatattg 178
|||
Sbjct: 201 tcaatgatgtggagtatcatgaatccattgatgagctgaaacacgccgatcggtatattg 260
```

```
Query: 179 agcgcattcttttctggaaggtcttccaaacttacaggacctgggcaaacgaacattg 238
|||
Sbjct: 261 agcgcattcttttctggaaggtcttccaaacttacaggacctgggcaaacgaacattg 320
```

E94A

```
Query: 239 gtgaagatggtgaggaaatgctgcttctgatctggcacttgagctggatggcgcaaga 298
|||
Sbjct: 321 gtgaagatggtgaggaaatgctgcttctgatctggcacttgagctggatggcgcaaga 380
```

```
Query: 299 atttgctgaggcaattggttatgccgatagcgttcatgattacgtcagccgcgatatga 358
|||
Sbjct: 381 atttgctgaggcaattggttatgccgatagcgttcatgattacntcagccgcgatatga 440
```

```
Query: 359 tgatagaaatttgctgatgaagaaggccatatacactggctggaaacggaacttgatc 418
|||
Sbjct: 441 tgatagaaatttgctgatgaagaaggccatatacactggctggaaacggaacttgatc 500
```

```
Query: 419 tgattcagaagatgggctgcaaaaattatctgcaagcacagatccgcgaagaaggttga 477
|||
Sbjct: 501 tgattcanaagatgggctgcaaaaattatctgcaagcacagatccgcgaagaaggttga 559
```


Blast2 Results:

```
Query: 1   atgaaaggtgataactaaagttataaattatctcaacaaactgttgggaaatgagcttgtc 60
          |||
Sbjct: 551 atgaaaggtgataactaaagttataaattatctcaacaaactgttgggaaatgagcttgtc 492

Query: 61   gcaatcaatcagtacttttctccatgcccgaaatgtttaaaaactggggtctcaaacgtctc 120
          |||
Sbjct: 491 gcaatcaatcagtacttttctccatgcccgaaatgtttaaaaactggggtctcaaacgtctc 432

Query: 121  aatgatgtggagtatcatgaatccattgatgagatgaaacacgccgatcgttatattgag 180
          |||
Sbjct: 431 aatgatgtggagtatcatgaatccattgatgagatgaaacacgccgatcgttatattgag 372

Query: 181  cgcattcttttctggaaggtcttccaaacttacaggacctgggcaaaactgaacattggt 240
          |||
Sbjct: 371 cgcattcttttctggaaggtcttccaaacttacaggacctgggcaaaactgaacattggt 312

Query: 241  gaagatgttgaggaaatgctgcttctgatctggcacttgagctggatggcgcaagaat 300
          |||
Sbjct: 311 gaagatgttgaggaaatgctgcttctgatctggcacttgagctggatggcgcaagaat 252

Query: 301  ttgcgtgaggcaattggttatgccgatagcgttcatgattacgtcagccgcgatatgatg 360
          |||
Sbjct: 251 ttgcgtgaggcaattggttatgccgatagcgttcatgattacgtcagccgcgatatgatg 192

Query: 361  atagaaatttgctgatgaagaaggccatatcgactggctggaaacggaacttgatctg 420
          |||
Sbjct: 191 atagaaatttgctgatgaagaaggccatatcgactggctggaaacggaacttgatctg 132

Query: 421  attcagaagatgggcctgcaaaattatctgcaagcacagatccgcgaagaaggt 474
          |||
Sbjct: 131 attcagaagatgggcctgcaaaattatctgcaagcacagatccgcgaagaaggt 78
```

Appendix 5: Mass Spectrometric Results

The protein samples (bFT-WT and all bFT variants) were prepared for electrospray mass spectrometry from heat denaturation and ammonium sulfate precipitation purification steps. The solution used for MS contained 50:50/MeCN:H₂O and 0.2% FA. The calculated mass was determined by mass calculation using the amino acid sequence. This predicted mass was compared to that mass MS, in which graph a) represents the overall calculation mass/charge, graph b) represents high percent intensity of mass/charge, and graph c) is the calculation determined by the selected mass/charge in graph b).

Wild-type bFT

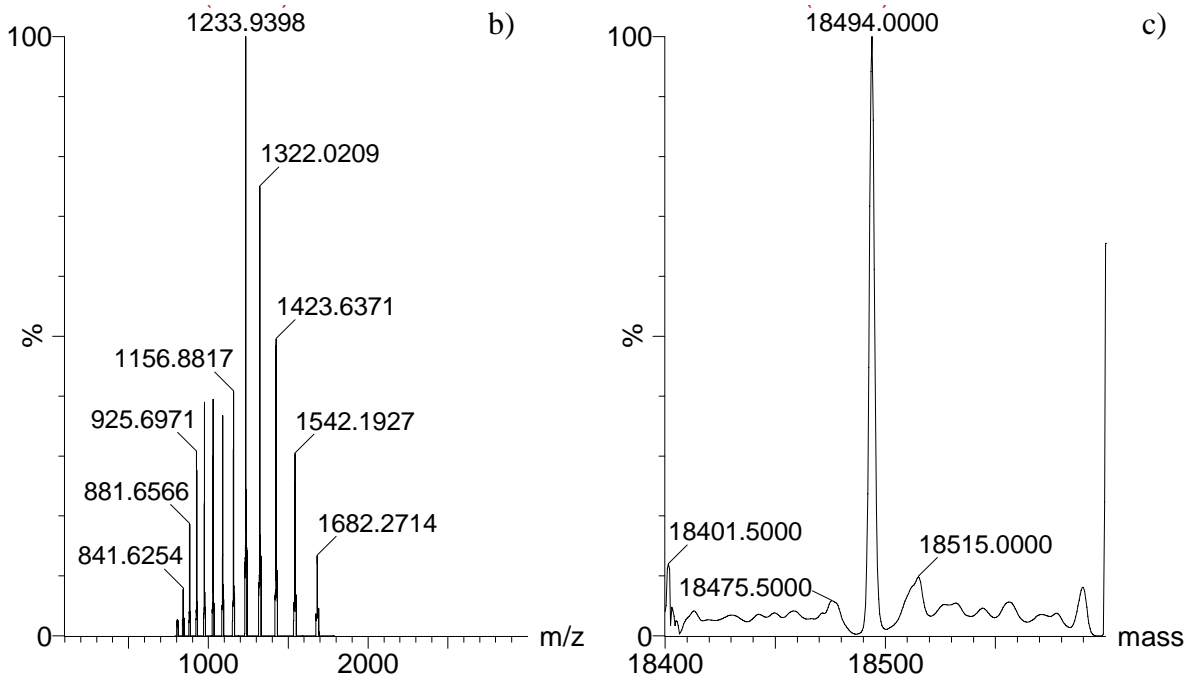
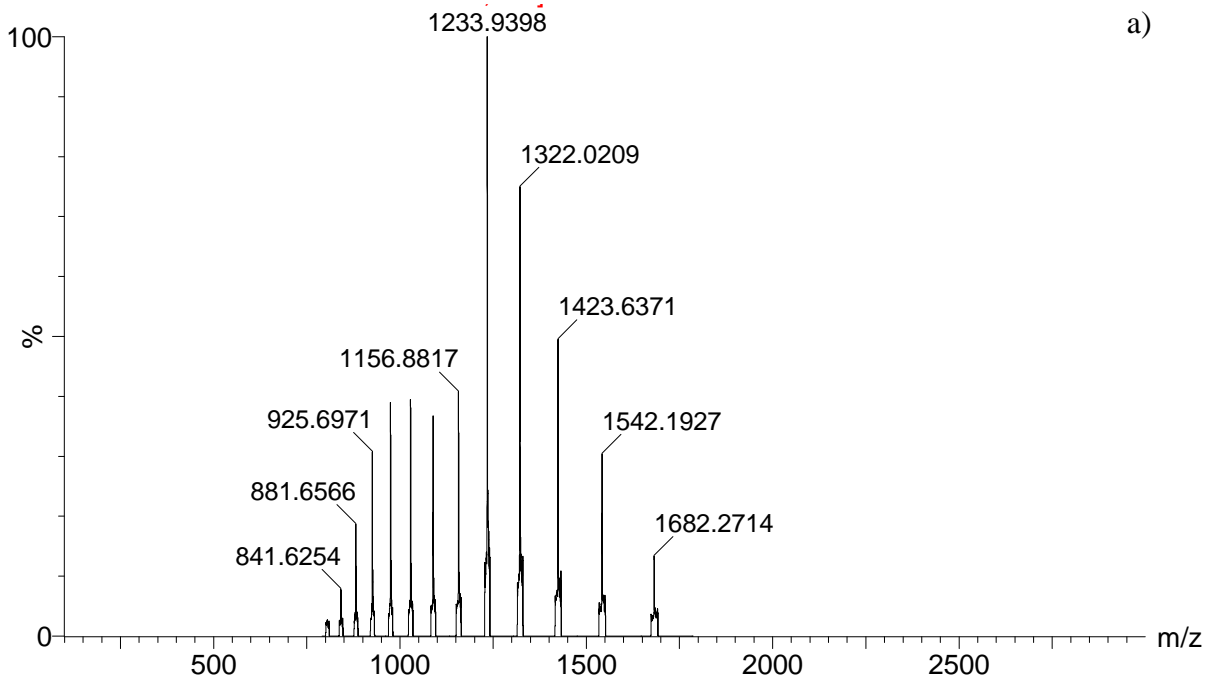


Figure A5.1: The electrospray mass spectrums of wild-type bFT showing the molecular weight of single subunit at 18494.00 Da comparing to the calculated mass of 18495.03 Da.

bFT-E18A

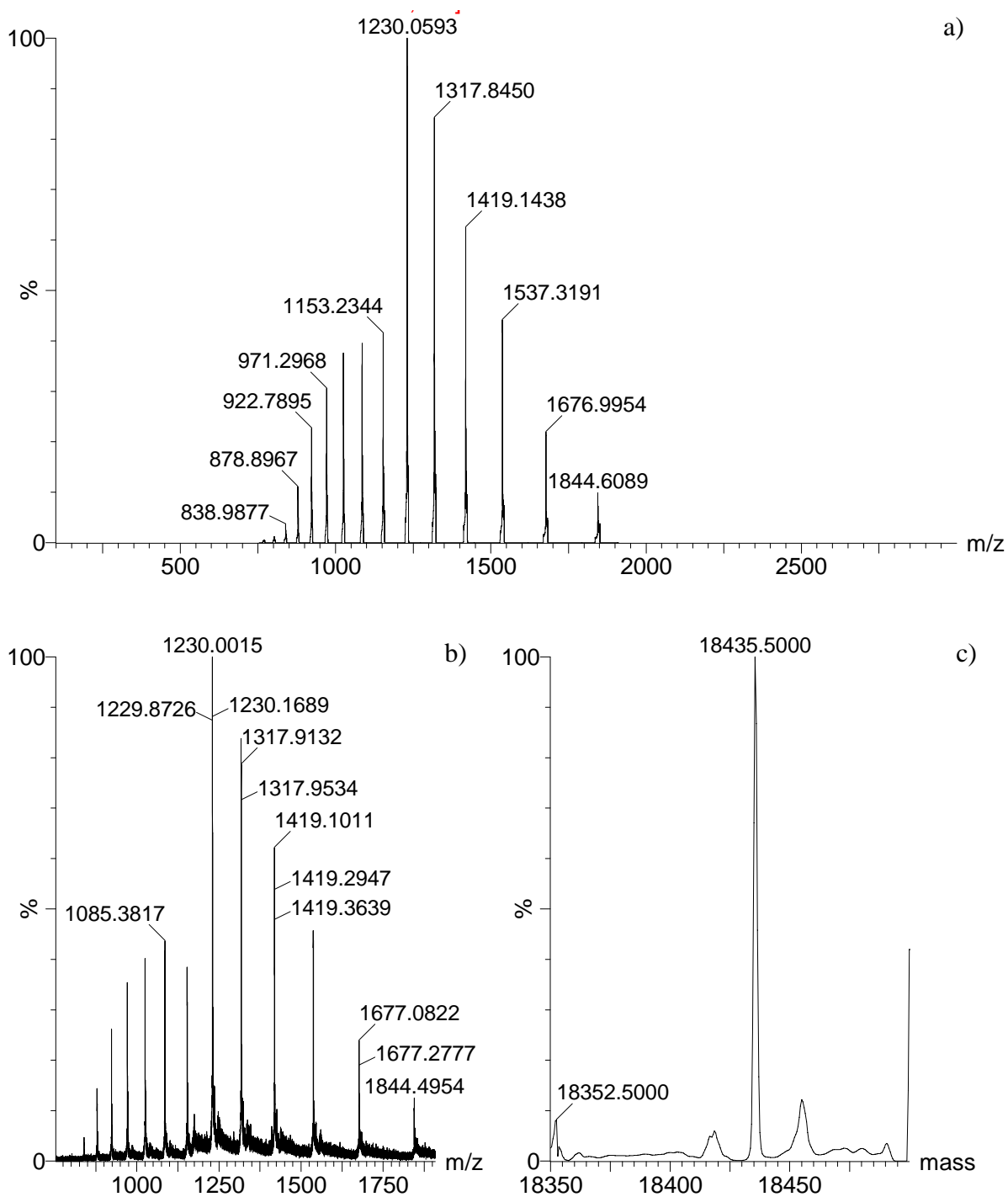


Figure A5.2: The electrospray mass spectrums of bFT-E18A showing the molecular weight of single subunit at 18435.50 Da comparing to the calculated mass of 18436.99 Da.

bFT-M52L

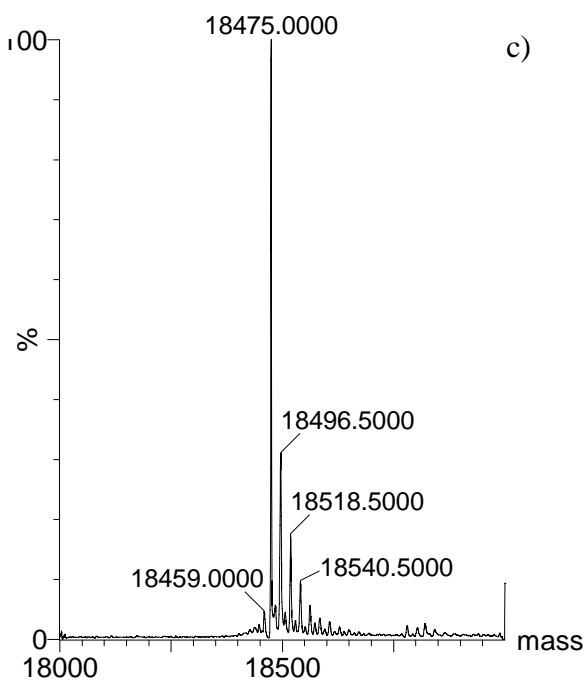
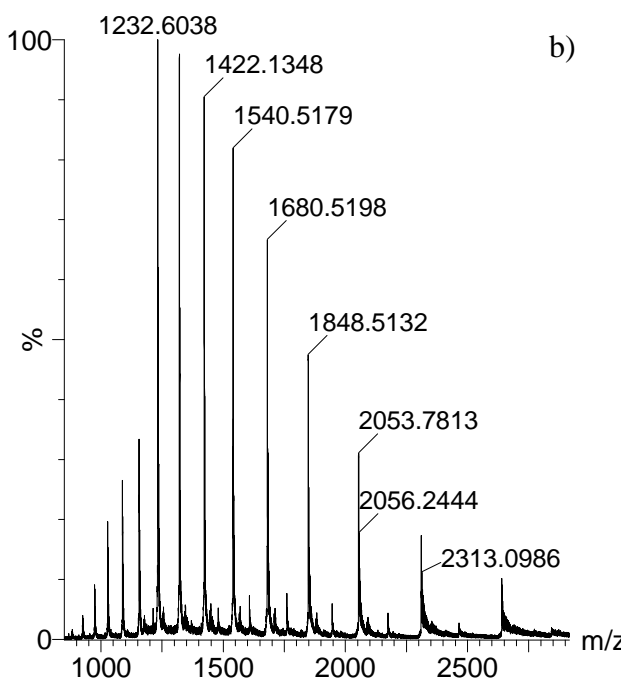
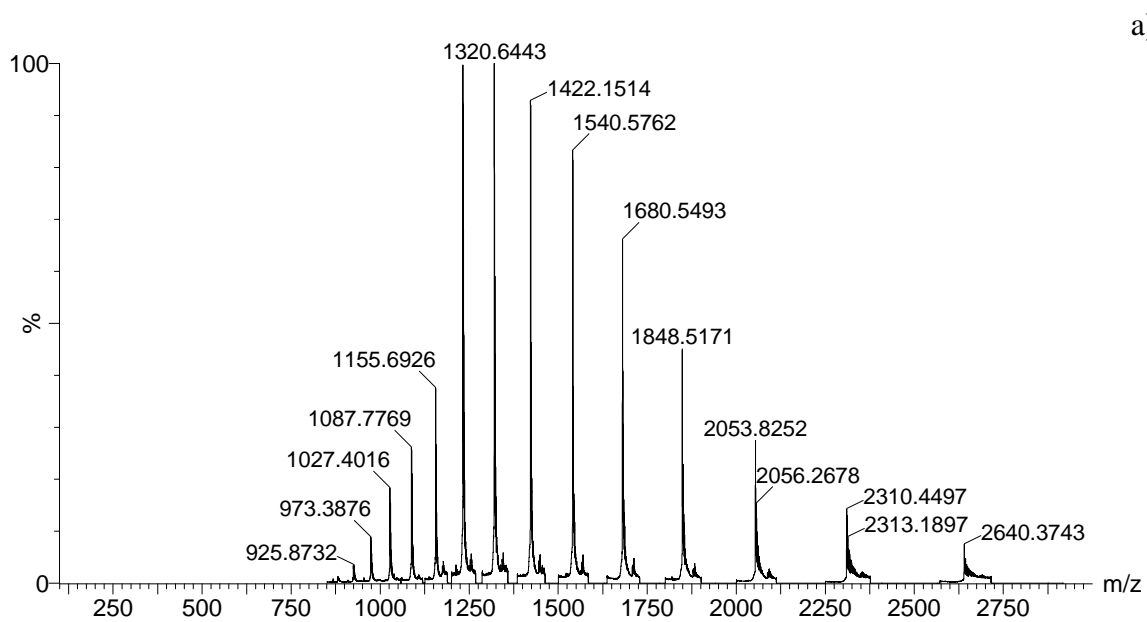


Figure A5.3: The electrospray mass spectrums of bFT-M52L showing the molecular weight of single subunit at 18475.00 Da comparing to the calculated mass of 18476.90 Da.

bFT-E94A

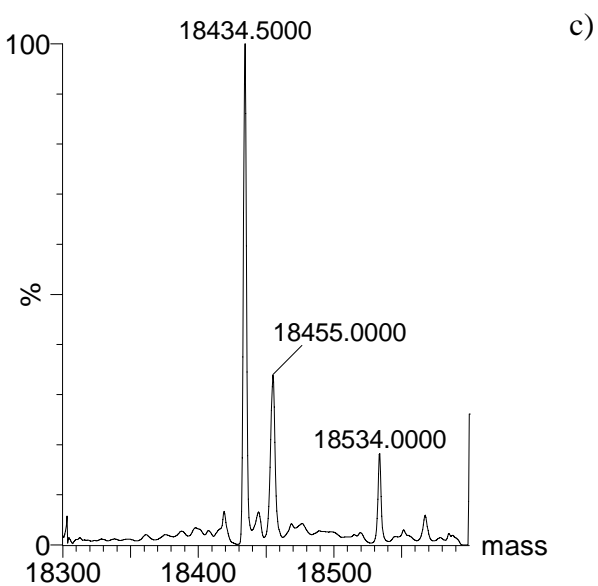
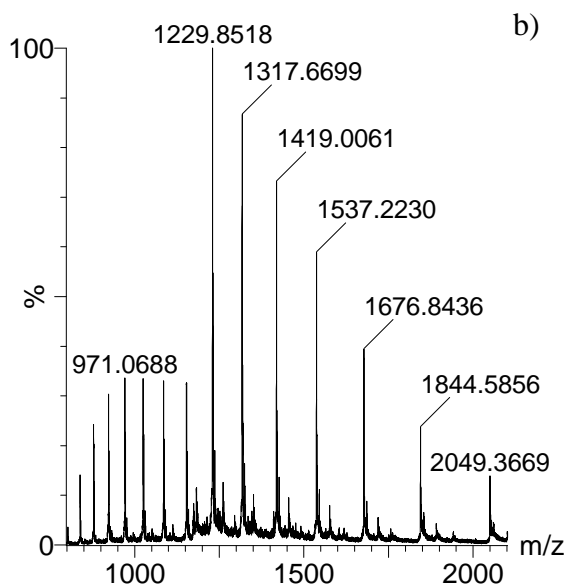
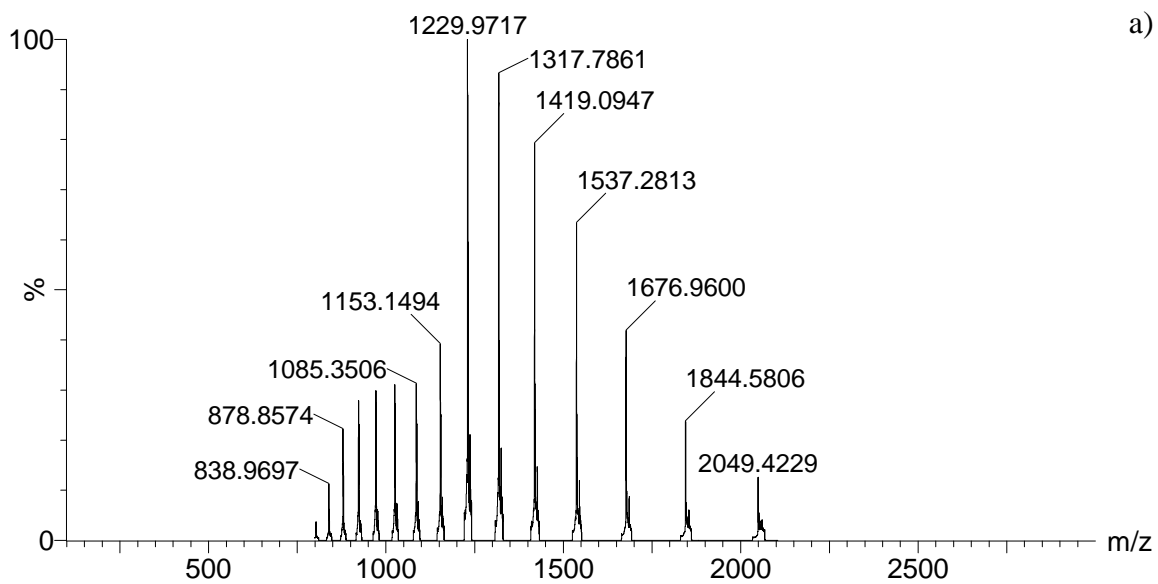


Figure A5.4: The electrospray mass spectrums of bFT-E94A showing the molecular weight of single subunit at 18434.50 Da comparing to the calculated mass of 18436.99 Da.

bFT-E18A/M52L

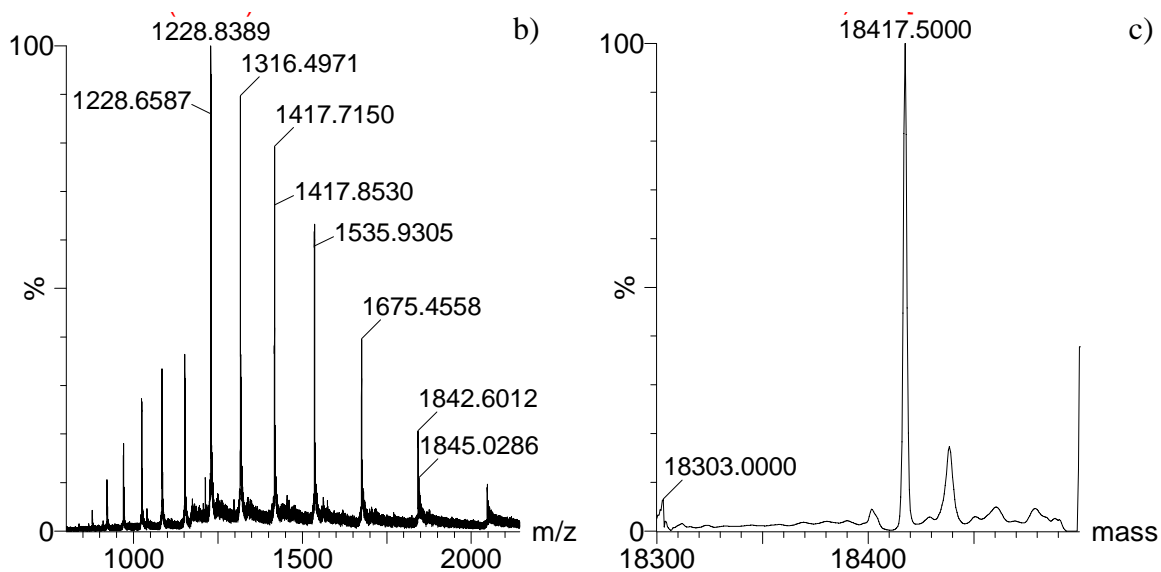
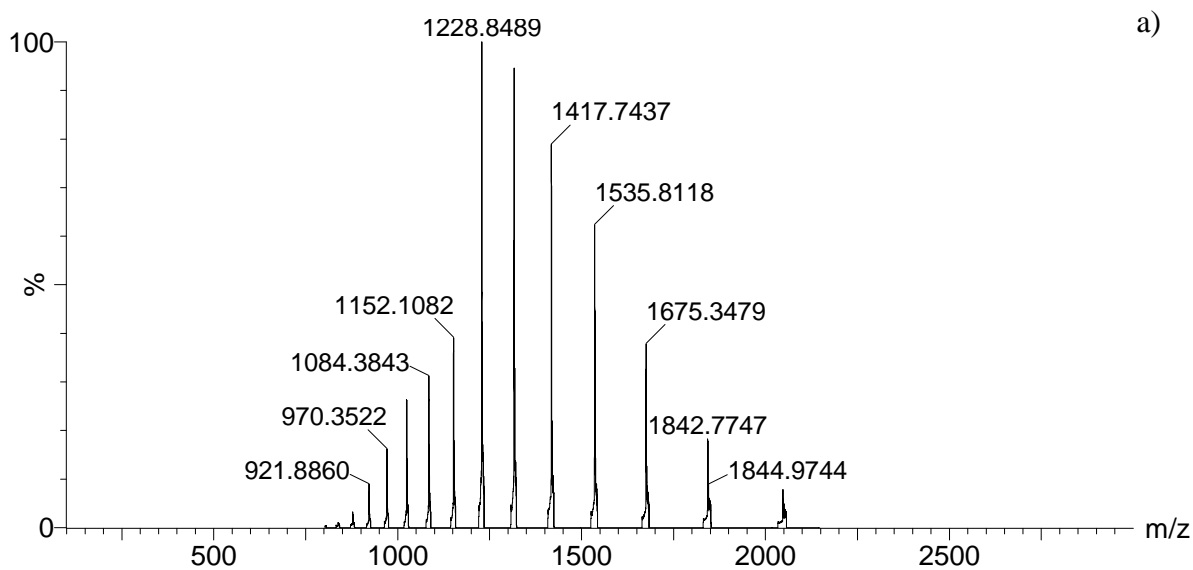


Figure A5.5: The electrospray mass spectrums of bFT-E18A/M52L showing the molecular weight of single subunit at 18417.50 Da comparing to the calculated mass of 18418.90 Da.

bFT-E18A/E94A

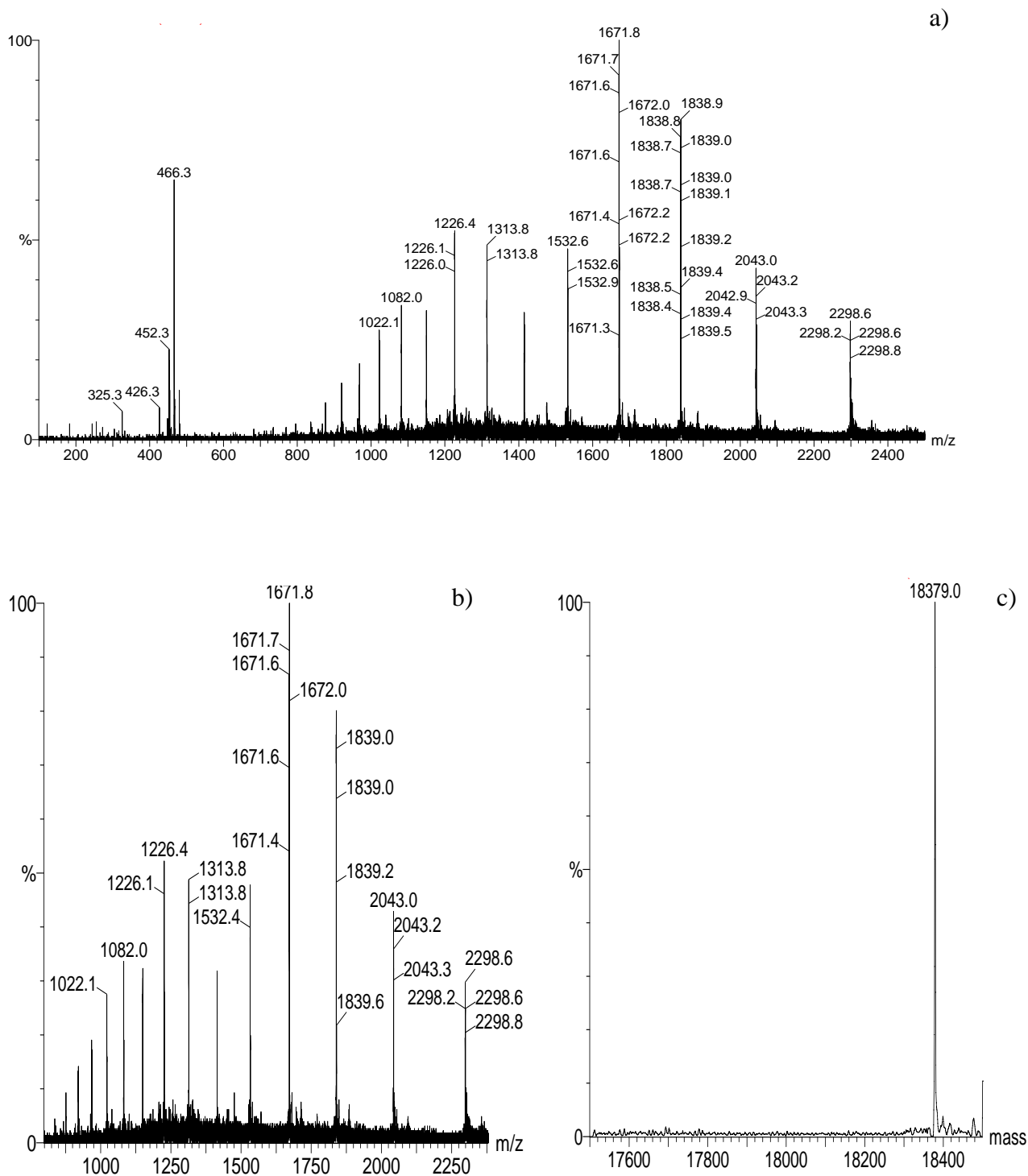


Figure A5.6: The electrospray mass spectrums of *bFT-E18A/E94A* showing the molecular weight of single subunit at 18379.00 Da comparing to the calculated mass of 18378.95 Da.

bFT-M52L/E94A

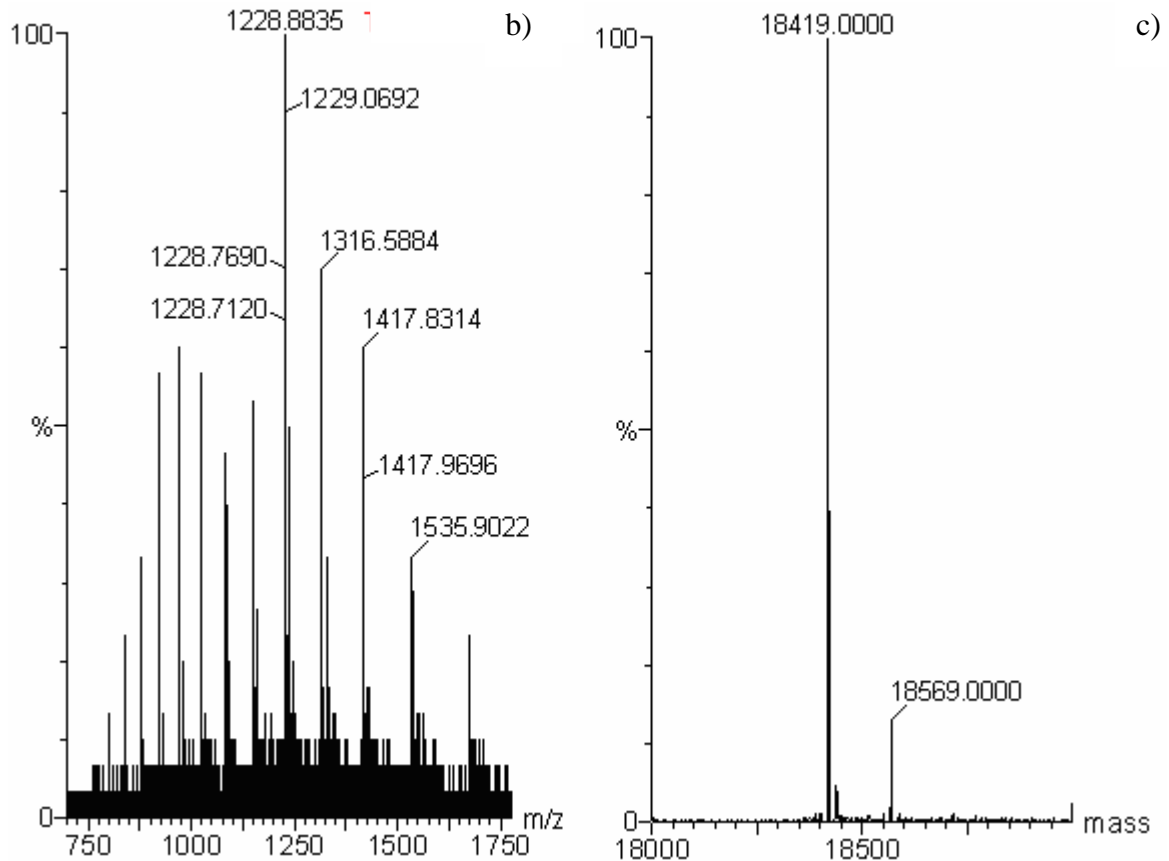
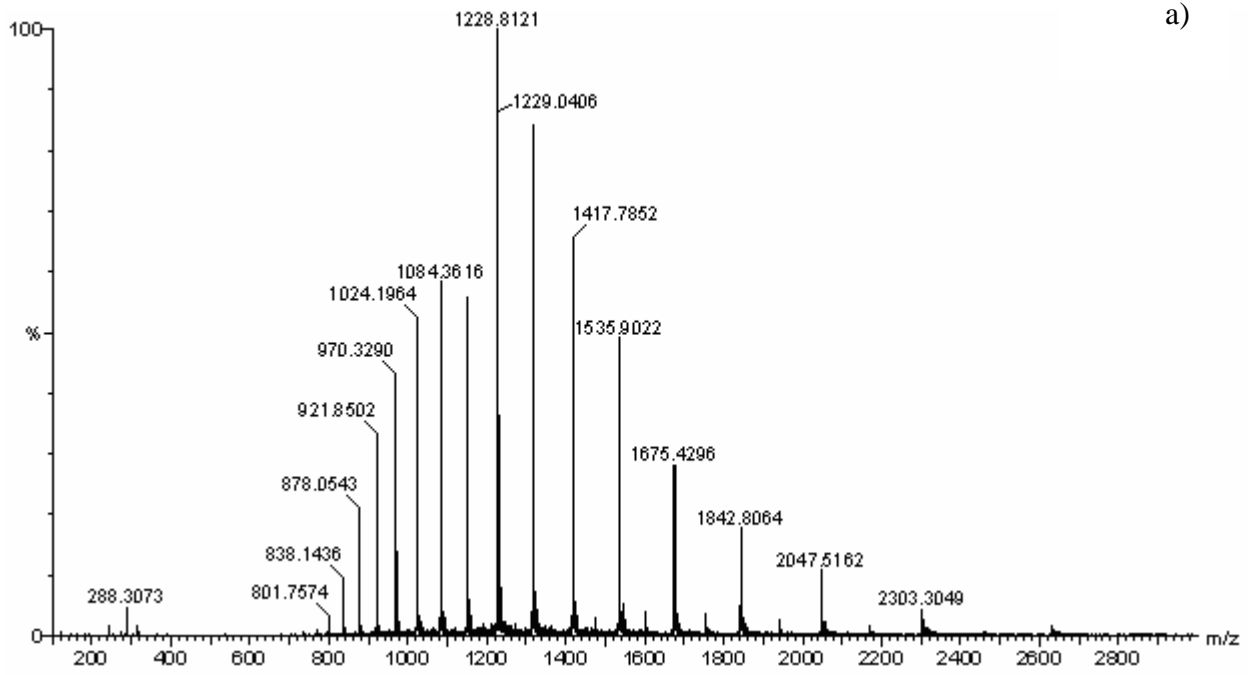


Figure A5.7: The electrospray mass spectrums of bFT-M52L/E94A showing the molecular weight of single subunit at 18419.00 Da comparing to the calculated mass of 18418.96 Da.

bFT-E18A/M52L/E94A

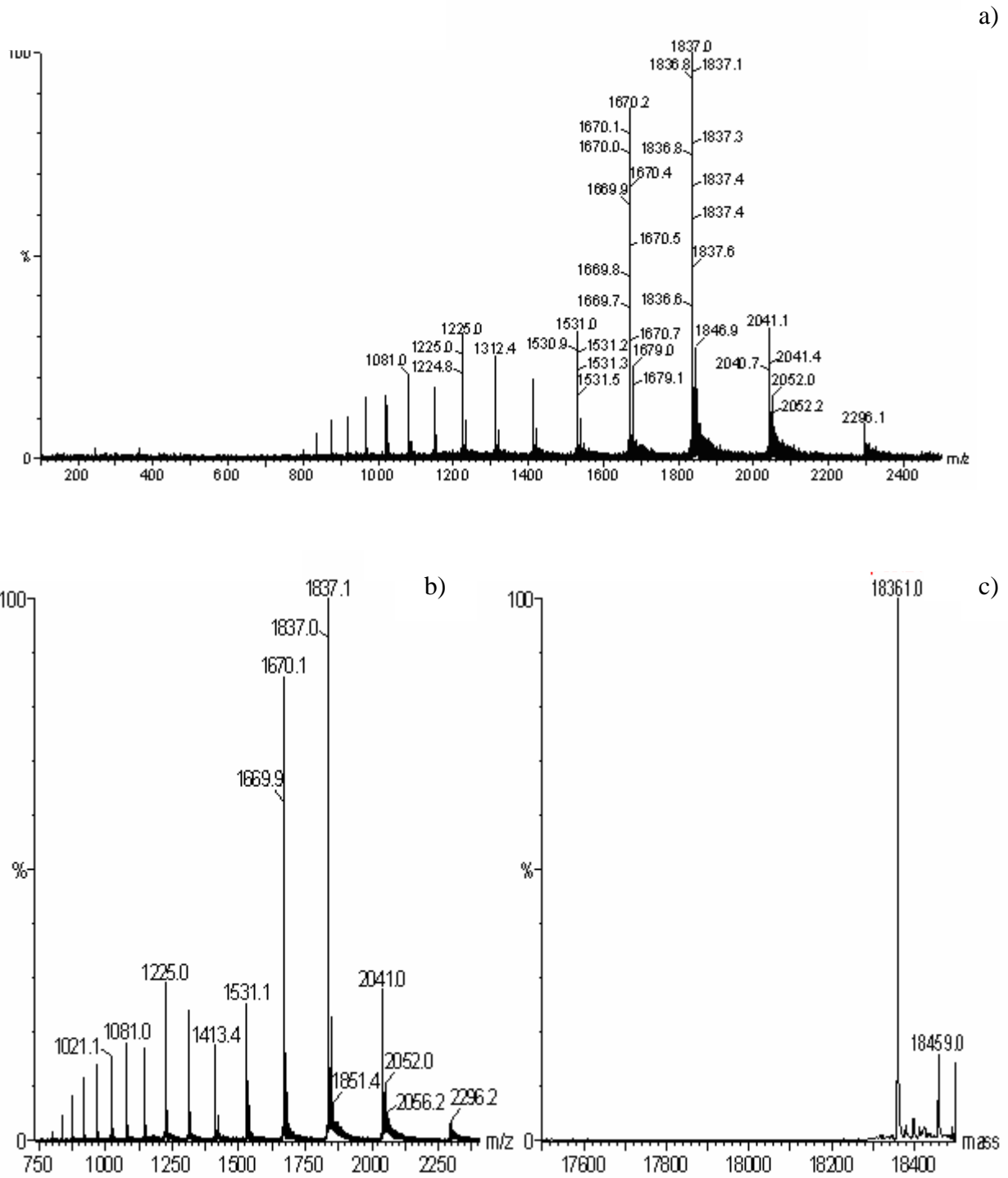


Figure A5.8: The electrospray mass spectrums of bFT-E18A/M52L/E94A showing the molecular weight of single subunit at 18361.00 Da comparing to the calculated mass of 18360.82 Da.

bFT-WT with His₆-tag at the C-terminus

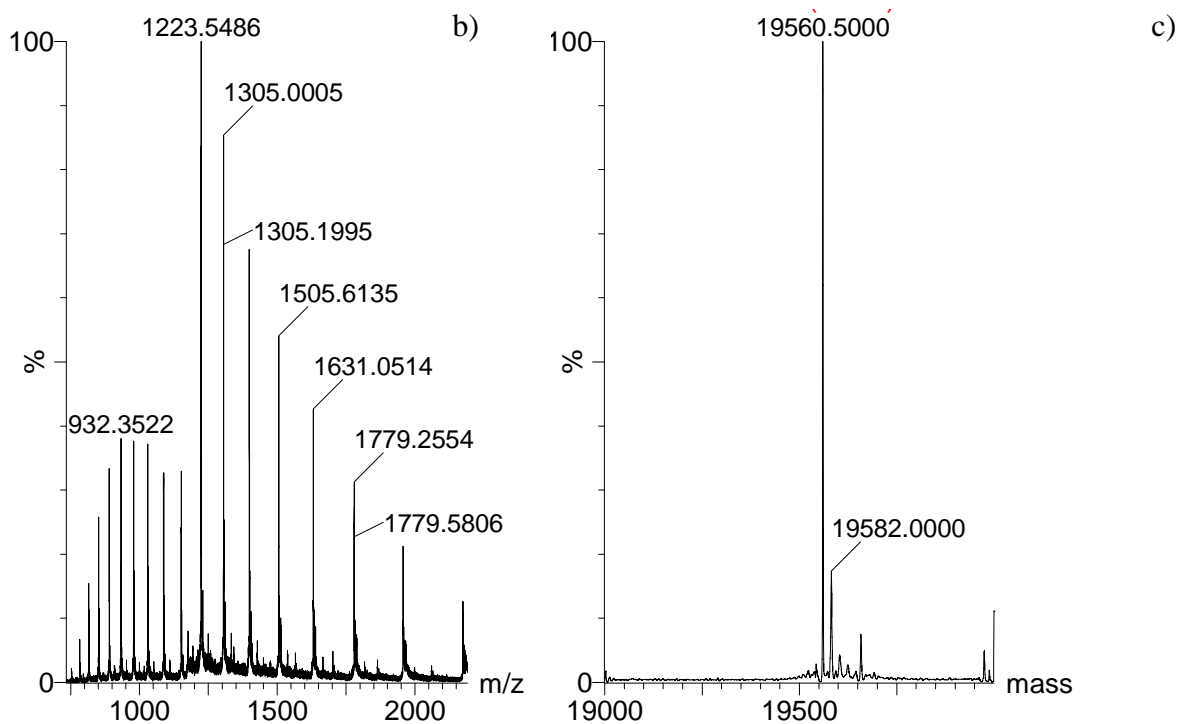
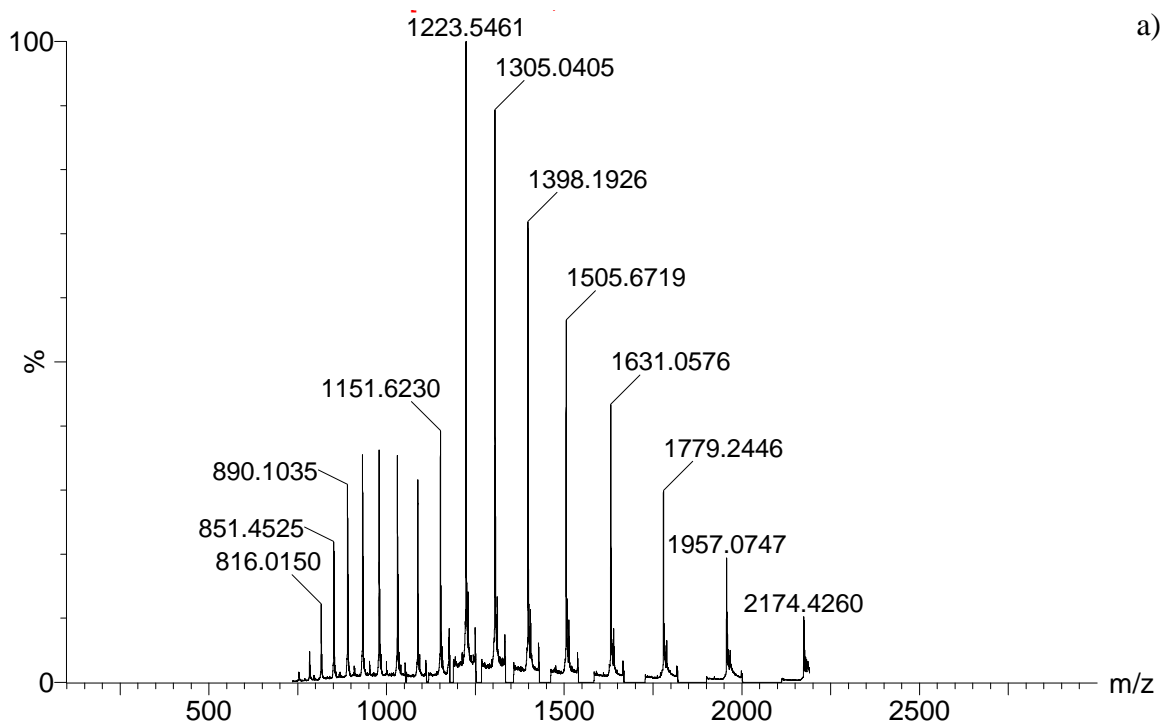


Figure A5.9: The electrospray mass spectrums of bFT-WT with His₆-tag at the C-terminus showing the molecular weight of single subunit at 19560.50 Da comparing to the calculated mass of 19560.10 Da.

Appendix 6: Spectrophotometric Results for Wild Type and Variants of Bacterioferritin

The spectrum of wild-type and bFT variants confirmed the existence of heme-incorporated protein. The absorption peaks at 418, 525, and 560 nm associated with the Soret, β , and α bands of the oxidized heme moiety, respectively, are observed.

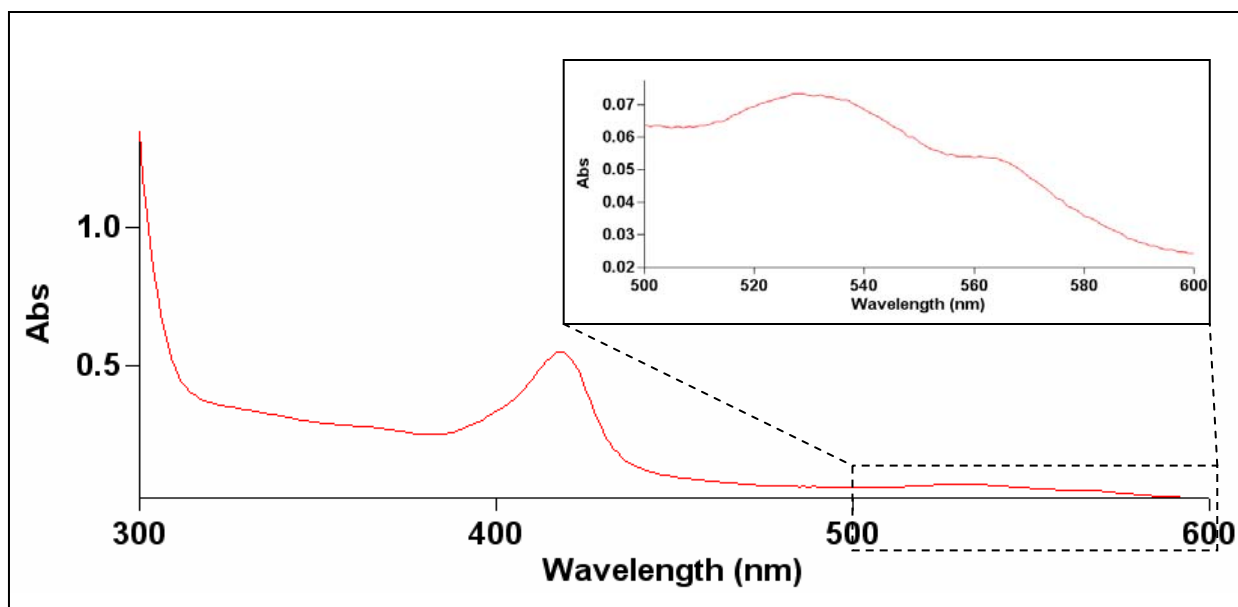


Figure A6.1: A spectroscopic scan of bFT-WT shows the absorption at 418, 525, and 560 nm. The region between 555-600 nm was expanded.

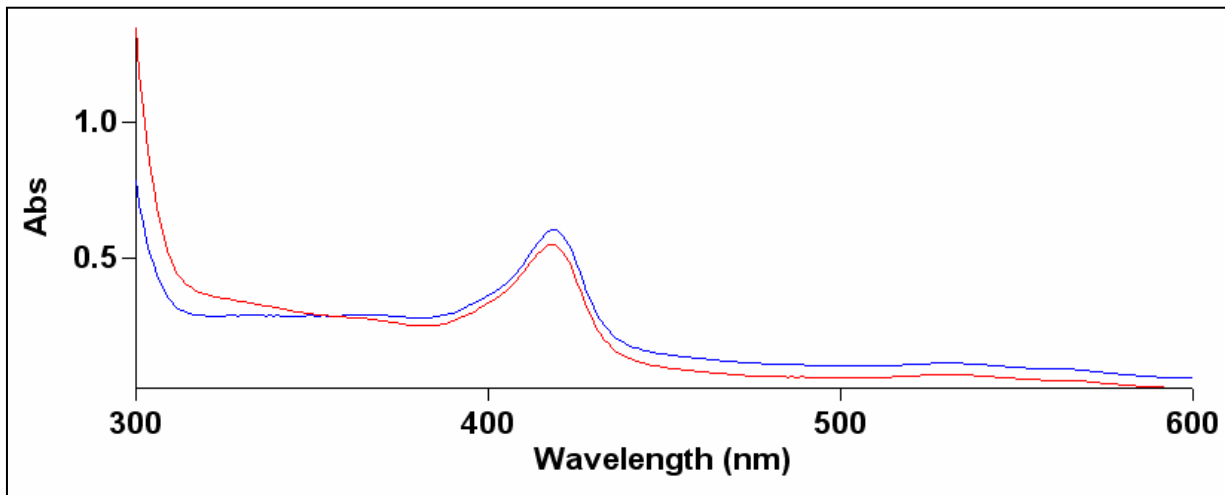


Figure A6.2: A comparison of spectroscopic scans between wild-type bFT (red) compared with that of bFT-E18A (blue).

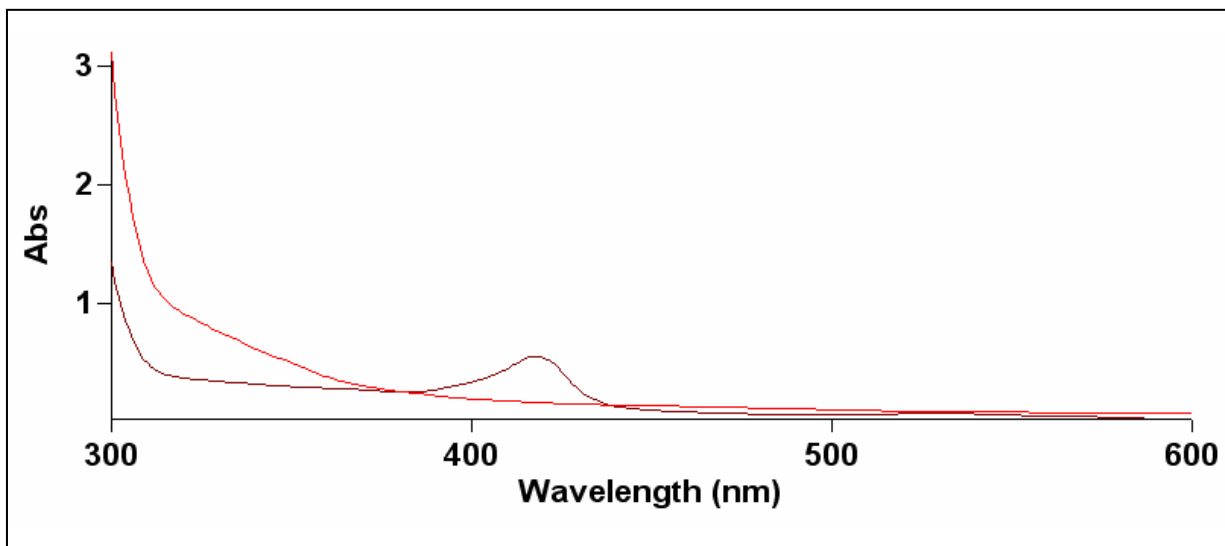


Figure A6.3: A comparison of spectroscopic scans between wild-type bFT (red) compared with that of bFT-M52L (brown).

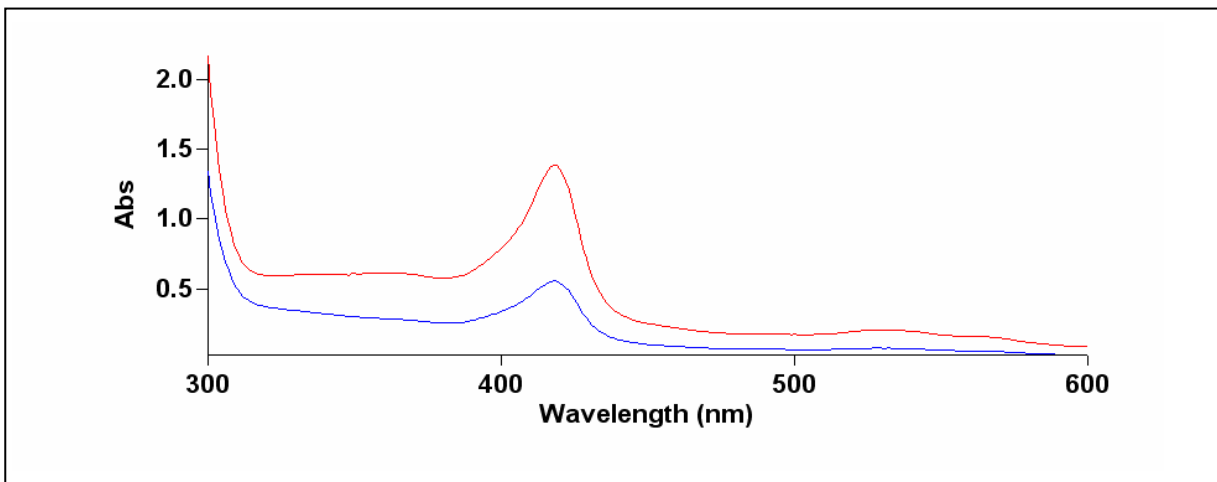


Figure A6.4: A comparison of spectroscopic scans between wild-type bFT (blue) compared with that of bFT-E94A (red).

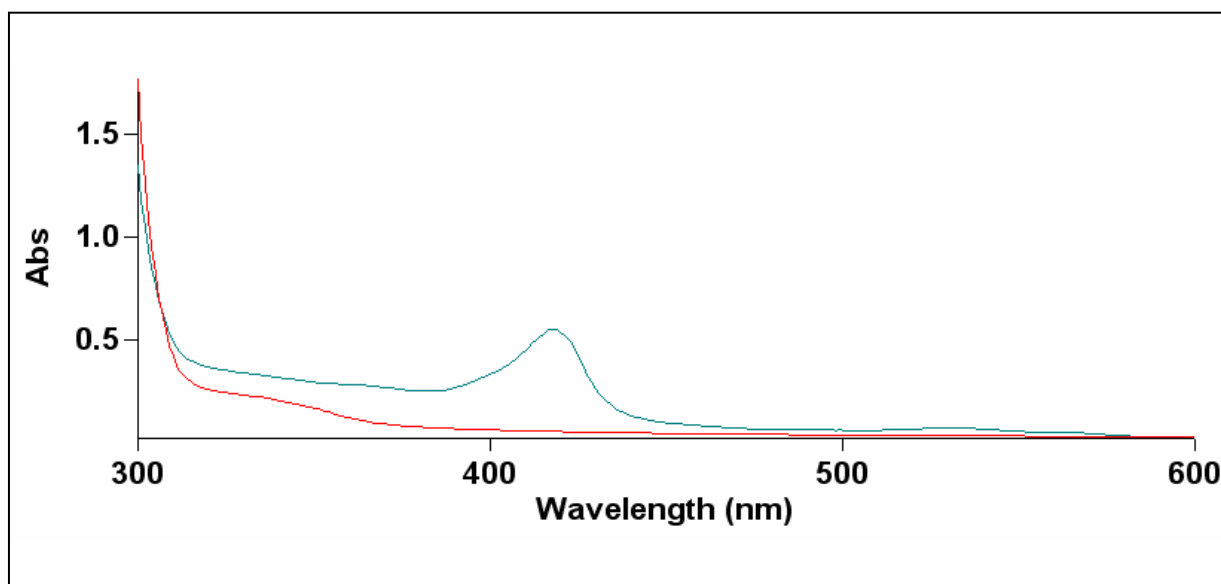


Figure A6.5: A comparison of spectroscopic scans between wild-type bFT (green) compared with that of bFT-E18A/M52L (red).

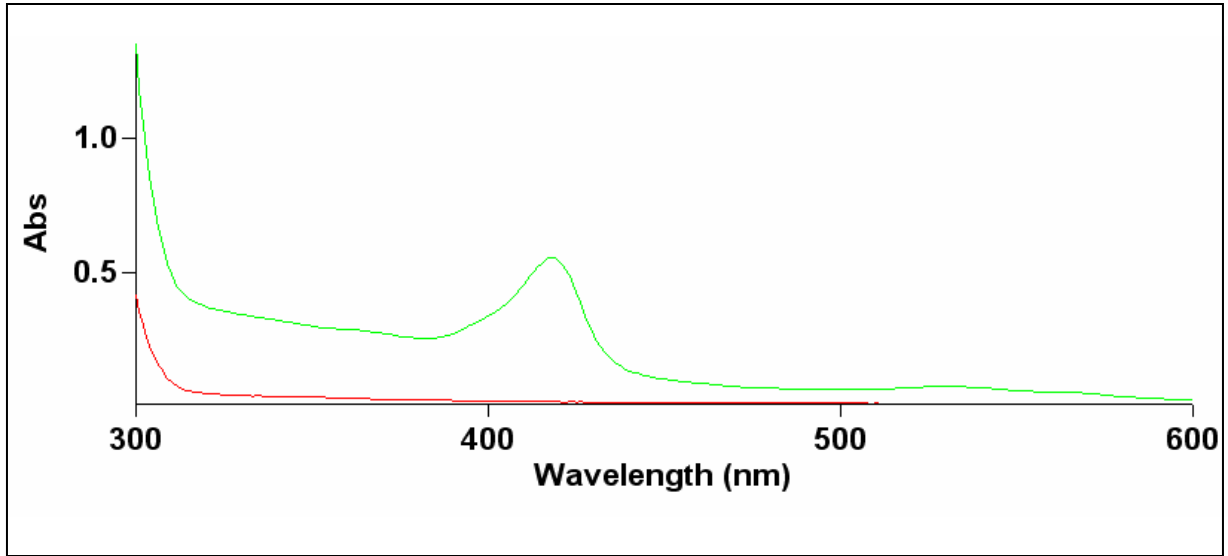


Figure A6.6: A comparison of spectroscopic scans between wild-type bFT (green) compared with that of bFT-M52L/E94A (red).

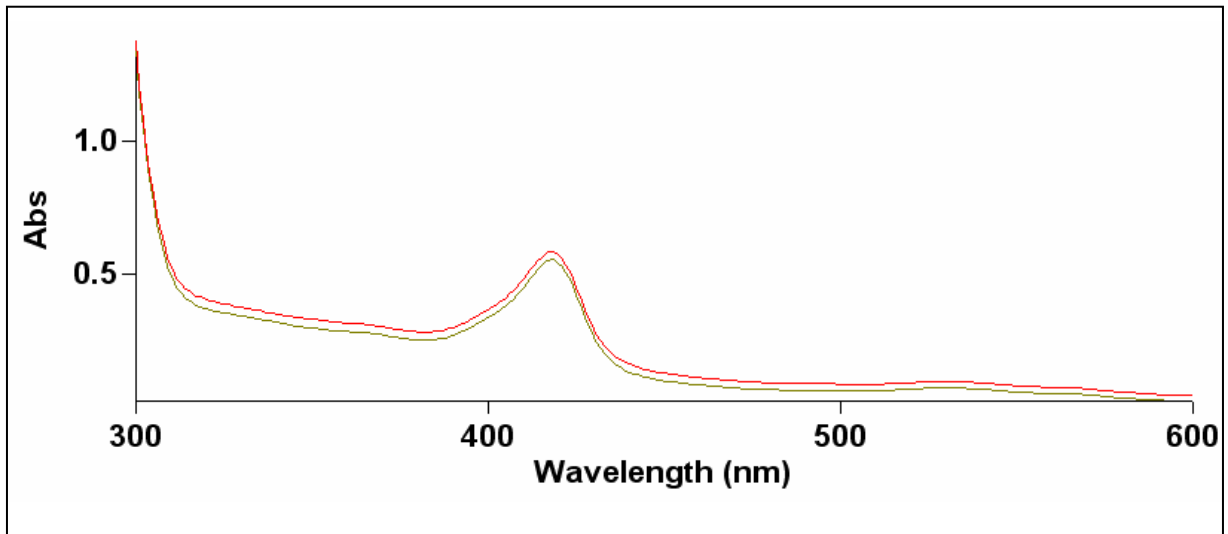


Figure A6.7: A comparison of spectroscopic scans between wild-type bFT (red) compared with that of bFT-E18A/E94A (yellow).

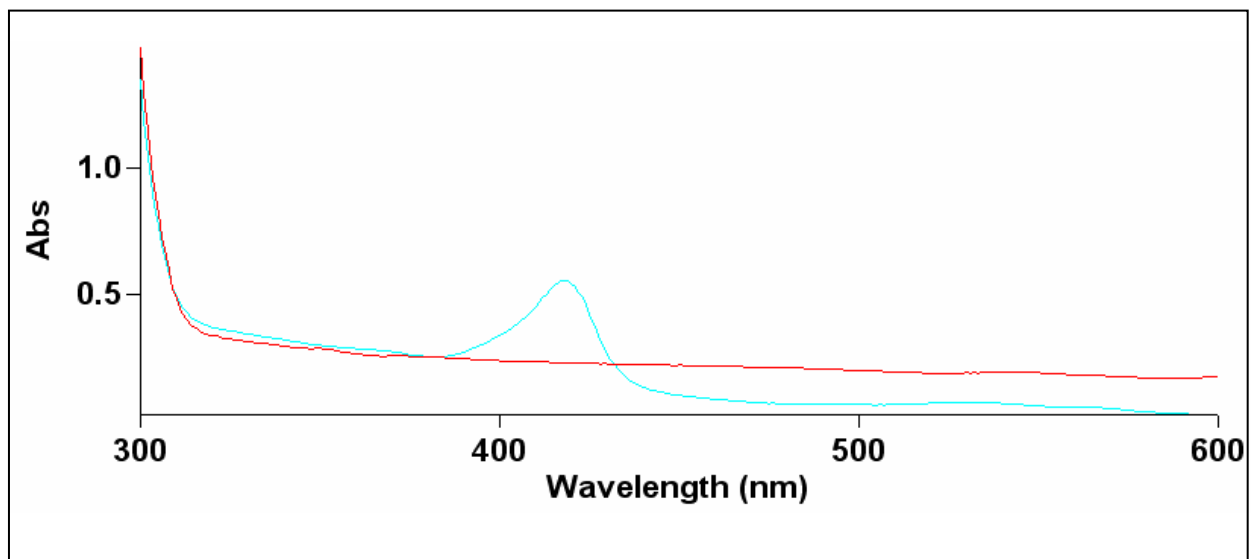


Figure A6.8: A comparison of spectroscopic scans between wild-type bFT (blue) compared with that of bFT-E18A/M52L/E94A (red).

Appendix 7: Gel Filtration Chromatographic Results (Superose 6) of Wild-type and Variants of Bacterioferritin

Bio-Rad gel filtration standard protein plot was done by performing Superose 6 gel filtration chromatography on a set of known mixed proteins, thyroglobulin (679 kDa), γ -globulin (158 kDa), ovalbumin (44 kDa), myoglobin (17 kDa), and vitamin B₁₂ (1.35 kDa) (Figure A7.1). The standard proteins in a solution containing 20 mM Tris-OH (pH 8.0) and 100 mM NaCl was run through a Superose 6 column with 0.5 mL/min flow rate. The eluted volumes of each protein were calculated in terms of K_a (Table A7.1), where K_a is $(V_e - V_0)/(V_t - V_0)$, V_0 is the void volume, V_e is the elution volume, and V_t is the total bed volume. The void volume is 8 mL determined from Blue Dextran eluted volume (Figure A7.2). The total bed volume, which is the volume of the Superose 6 column resin is 24 mL. Then K_a was plotted as a function of $\log(\text{MW})$ (Figure A7.3). Example of calculation for thyroglobulin is $K_a = (12.8 - 8.0)/(24.0 - 8.0) = 0.29688$ (Table A7.1).

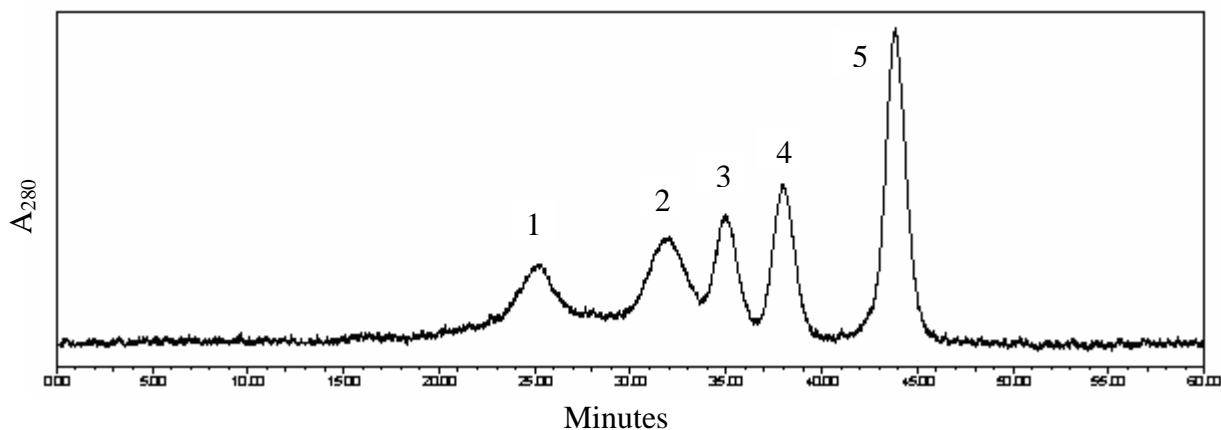


Figure A7.1: The Superose 6 gel filtration chromatogram of Bio-Rad standard protein. Each peak represented a particular protein as stated in Table A7.1.

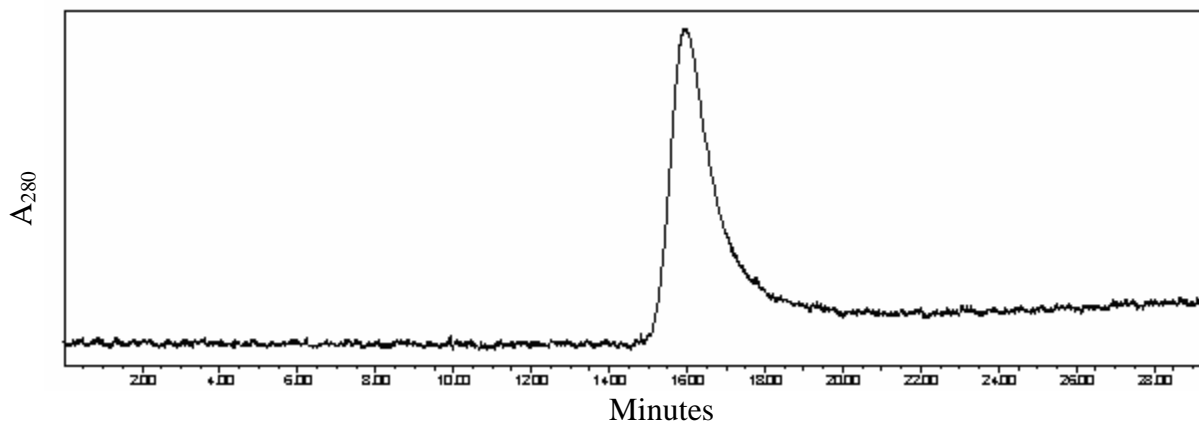


Figure A7.2: The Superose 6 gel filtration chromatogram of Blue Dextran shows the void volume used for the calculation in protein standard curve.

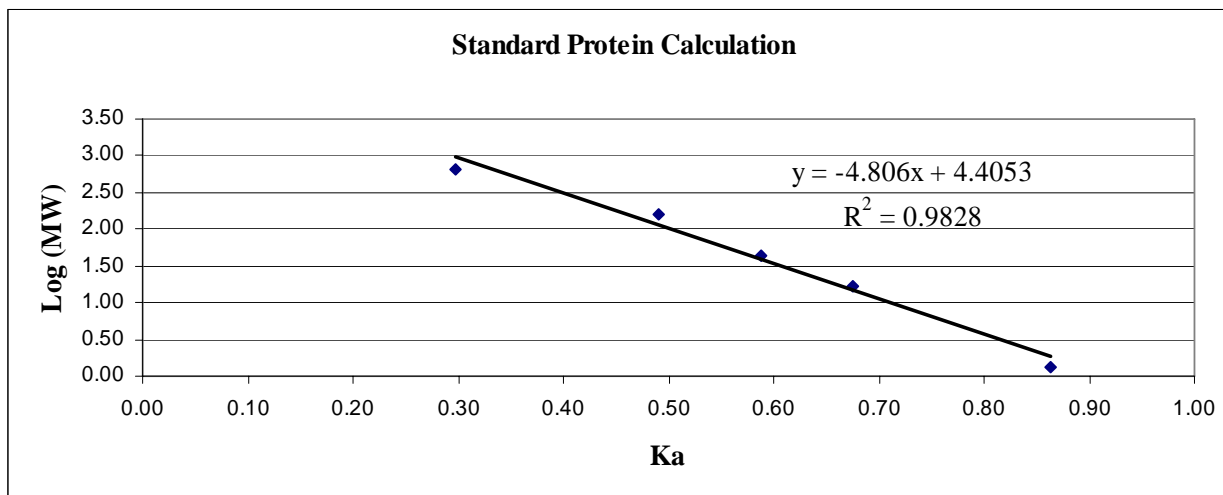


Figure A7.3: Bio-Rad protein standard curve used for molecular weight calculation of protein samples. The data for this plot was shown in Table A7.1.

Table A7.1: The table shows the molecular weight of standard protein and eluted volumes in duplicate, which was used for plotting the standard protein curve.

Standard Protein	MW (kDa)	log (MW)	V _e (trial 1) (mL)	V _e (trial 2) (mL)	Average V _e (mL)	K _a
Blue Dextran (V _o)			8.00	8.00		
Thyroglobulin	670.00	2.826075	12.90	12.60	12.75	0.29688
γ-globulin	158.00	2.198657	16.00	15.70	15.85	0.49063
Ovalbumin	44.00	1.643453	17.50	17.30	17.40	0.58750
Myoglobin	17.00	1.230449	18.80	18.80	18.80	0.67500
Vitamin b-12	1.35	0.130334	21.80	21.80	21.80	0.86250

It was found earlier that the MW of 24-subunit apoFT determined from Superose 6 gel filtration chromatography is less than that of the literature (~450 kDa) (Chapter 3), and it was suggested that the gel filtration chromatography could not be used to determine protein MW (for bFT and apoFT). In order to prove that even though the calculated MW of 24-subunit apoFT determined by Superose 6 gel filtration chromatography is incorrect and the Superose 6 chromatograms can be used to determine a degree of quaternary structures, the Stokes radius of apoFT is determined from the plot of protein standards' Stokes radius versus their elution volumes. In addition, its MW can be calculated using the Stokes-Einstein and Svedberg equations and the plot of MW versus sedimentation coefficient times Stokes radius. The molecular weight, Stokes radius, and sedimentation coefficient of protein standards (thyroglobulin (670 kDa, Stokes radius of 85 Å, sedimentation coefficient of 19S), γ -globulin (158 kDa, 48.1 Å, 6.6S), ovalbumin (45 kDa, 30.5 Å, 3.55S), myoglobin (17 kDa, 21.2 Å, 2S), and vitamin B12 (1.35 kDa, 8.5 Å)) are received from the literature (Qasim and Salahuddin, 1979; Andrews, 1970; Cui *et al.*, 2002; Husain and Sadana, 1974; Siegel and Monty, 1966; Post *et al.*, 2002; Venkatesh and Deshpande, 1999) (Table A7.2), while the experimental average elution volumes are from Table A7.1. The Stokes radius for apoFT is calculated from the linear equation, which is received from the plot of Stokes radius versus elution volumes, $y = -8.5464x + 186.68$, where y is the Stokes radius (Å) and x is the elution volume (mL) (Figure A7.2). Since the experimental elution volume of apoFT is 14.5 mL, its Stokes radius is calculated to be $((-8.5464 \times 14.5) + 186.68) 62.8$ Å. The molecular weight of 24-subunit apoFT can be determined from the Stokes-Einstein and Svedberg equations:

$$M = (6\pi\eta r N s_{20,w})/(1 - \nu\rho),$$

where M is the molecular weight, η is the solvent viscosity, r is the Stokes radius, N is Avogadro's number, $s_{20,w}$ is the sedimentation coefficient, v is the apparent partial specific volume of the protein, and ρ is the density of the solvent (Notides and Williams-Ashman, 1967). From the plot of molecular weight versus the Stokes radius times the sedimentation coefficient, the linear equation $y = 0.4179x$, where y is the molecular weight (kDa) and x is the sedimentation coefficient times Stokes radius ($\text{\AA} \times S$), is used to calculate the MW of 24-subunit apoFT. By using this equation, the calculated Stokes radius (62.8 \AA), and the literature sedimentation coefficient (17S) (Rothen, 1944), it is found that apoFT has a MW of $(0.4179 \times 62.8 \times 17)$ 446 kDa.

Table A7.2: The table shows the molecular weight, the Stokes radius, the average elution volumes, the sedimentation coefficient, and the sedimentation coefficient times Stokes radius of protein standards, which was used for the plots in Figure A7.2 and A7.3.

Standard Protein	MW (kDa)	Stokes radius (\AA)	Average V_e (mL)	Sedimentation coefficient (S)	Sedimentation coefficient \times Stokes radius ($\text{\AA} \times S$)
Thyroglobulin	670	85.0	12.75	19.00	1615.00
γ -globulin	158	48.1	15.85	6.60	317.46
Ovalbumin	44	30.5	17.40	3.55	126.03
Myoglobin	17	21.2	18.80	2.00	42.40
Vitamin b-12	1.35	8.5	21.80		

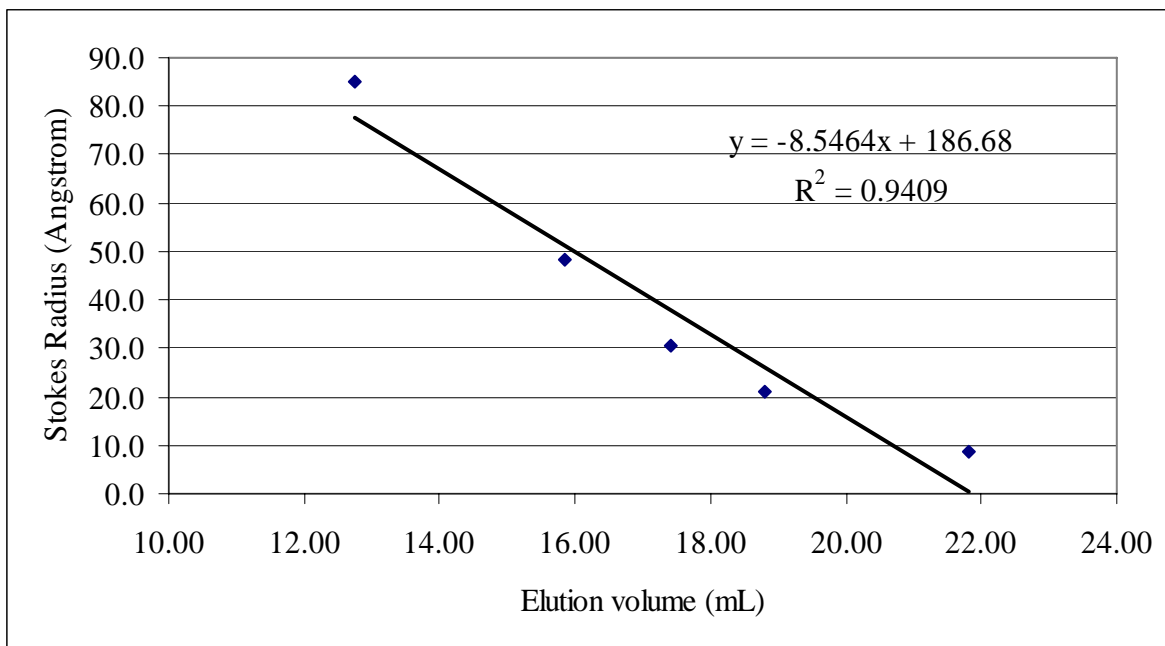


Figure A7.4: The plot of Stokes radius versus elution volumes of protein standards showing the linear equation that is used for the calculation of Stokes radius of apoFT.

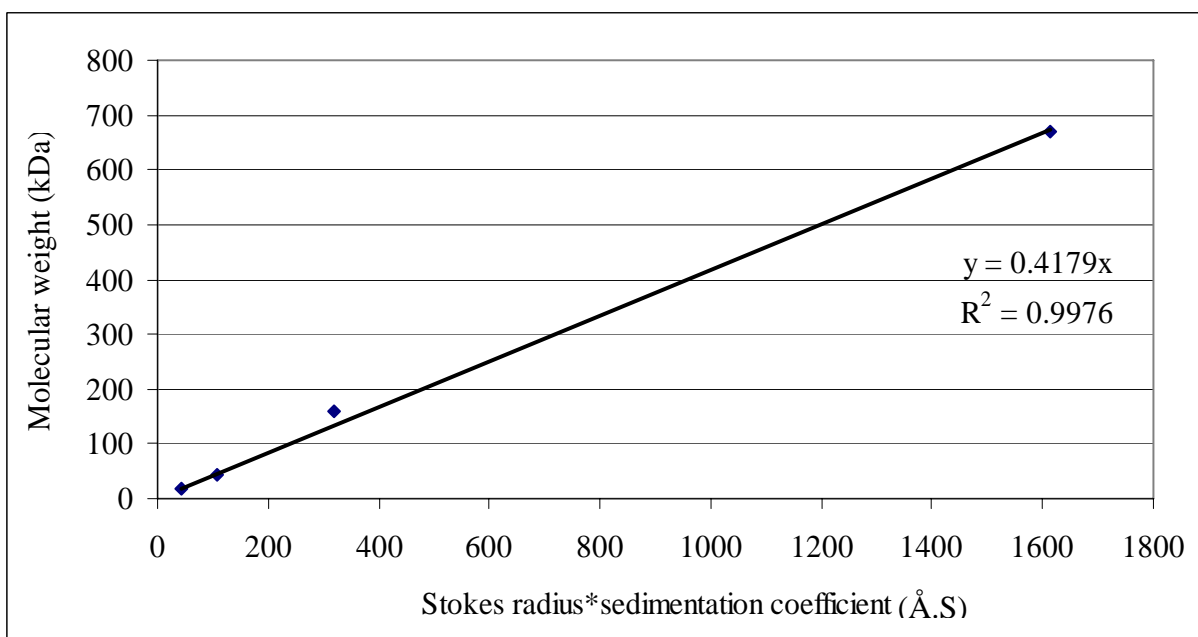


Figure A7.5: The plot of molecular weights versus Stokes radius times sedimentation coefficients of protein standards showing the linear equation that is related to the Stokes-Einstein and Svedberg equations and is used for the calculation of the molecular weight for 24-subunit apoFT.

The samples for gel filtration chromatography (Superose 6) were wild-type bFT and all bFT variants. The samples were prepared from protein purification processes, which included heat denaturation and ammonium sulfate precipitation, followed by filtration and injection into 100 μ L loop of a HPLC. The concentration of sample was 1.35 mg/mL in buffer containing 20 mM Tris-OH (pH 8.0) and 100 mM NaCl running through the Superose 6 column with a 0.5 mL/min flow rate. The following data presents the gel filtration chromatograms (Superose 6) of each protein sample. Each eluted fraction was calculated for its MW by comparing with the protein standards. SDS PAGE was used to confirm the existence of desired monomeric protein. Example of the calculation for peak 1 of bFT-WT is $K_a = (14.6 - 8.0)/(24.0 - 8.0) = 0.4125$ (Figure A7.6). Then logMW (y-value) was found in the standard protein plot (Figure A7.5) by insert K_a value as x-value in the equation $y = -4.806x + 4.4053$, where $\log MW = (-4.806 \times 0.4125) + 4.4053 = 2.4633$, and so MW is 290.6 kDa (Table A7.3).

Gel filtration (Superose 6) of bFT-WT

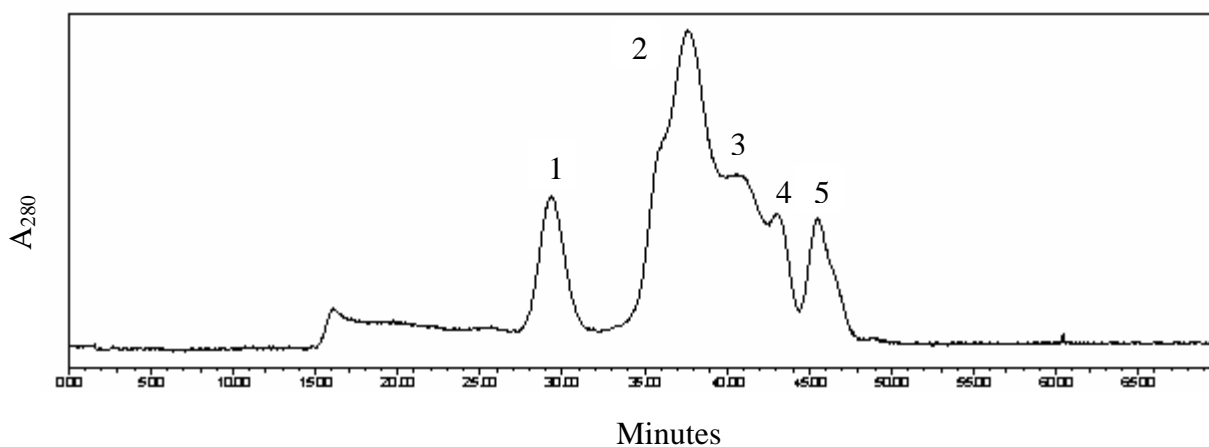


Figure A7.6: The Superose 6 gel filtration chromatogram of bFT-WT shows five eluted peaks.

Table A7.3: The calculated molecular weight of each eluted Superose 6 fraction from bFT-WT

bFT-WT	MW (kDa)	log (MW)	V_e (mL)	K_a
Peak 1 (24-subunit)	290.6	2.4633	14.6	0.4125
Peak 2 (monomer)	17.3	1.2383	18.6	0.6625
Peak 3	5.6	0.7482	20.2	0.7625
Peak 4	2.6	0.4113	21.3	0.8313
Peak 5	1.0	-0.0175	22.7	0.9188

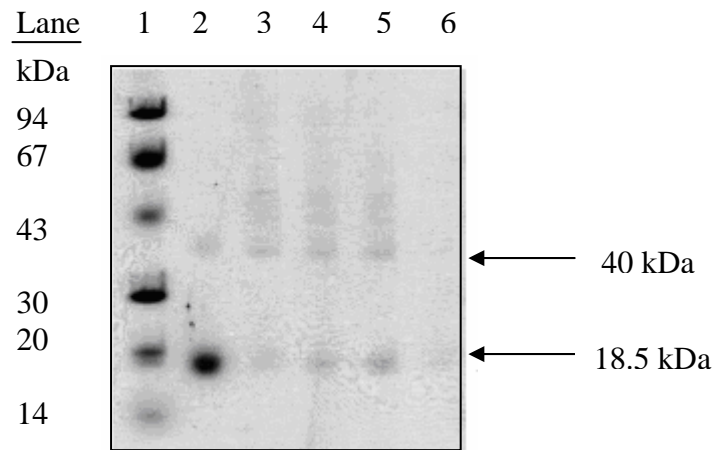


Figure A7.7: The SDS PAGE results of Superose 6 eluted fractions of bFT-WT. The lists below indicate proteins contained in each eluted fraction.

Lane	Sample
1	MWM
2	Eluted peak 1 of bFT-WT
3	Eluted peak 2 of bFT-WT
4	Eluted peak 3 of bFT-WT
5	Eluted peak 4 of bFT-WT
6	Eluted peak 5 of bFT-WT

Gel filtration (Superose 6) of bFT-E18A

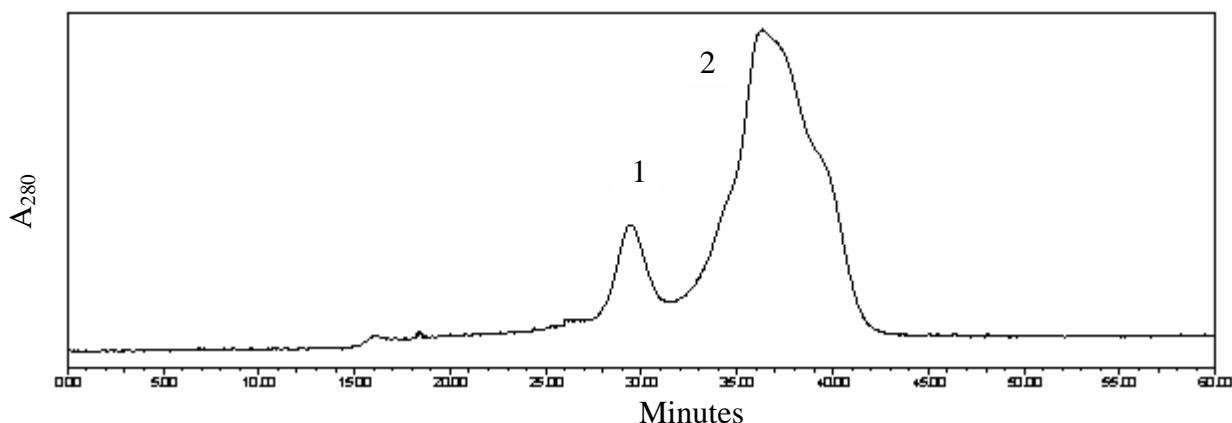


Figure A7.8: The Superose 6 gel filtration chromatogram of bFT-E18A shows two eluted peaks.

Table A7.4: The calculated molecular weight of each eluted Superose 6 fraction of bFT-E18A

bFT-E18A	MW (kDa)	log (MW)	V_e (mL)	K_a
Peak 1 (24-subunit)	290.6	2.4633	14.6	0.4125
Peak 2 (dimer)	26.4	1.4220	18.0	0.6250

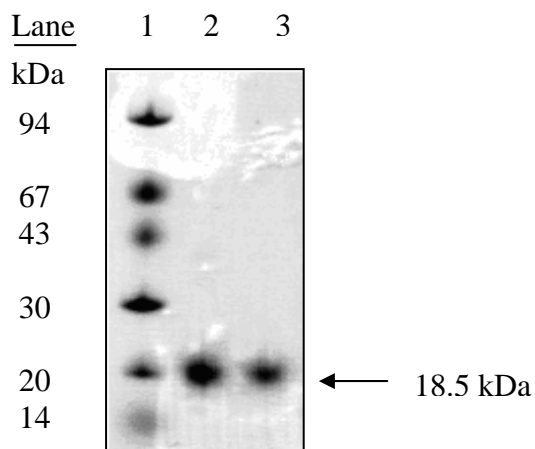


Figure A7.9: The SDS PAGE results of Superose 6 eluted fractions of bFT-E18A. The lists below indicate proteins contained in each eluted fraction.

Lane	Sample
1	MWM
2	Eluted peak 1 of bFT-E18A
3	Eluted peak 2 of bFT-E18A

Gel filtration (Superose 6) of bFT-M52L

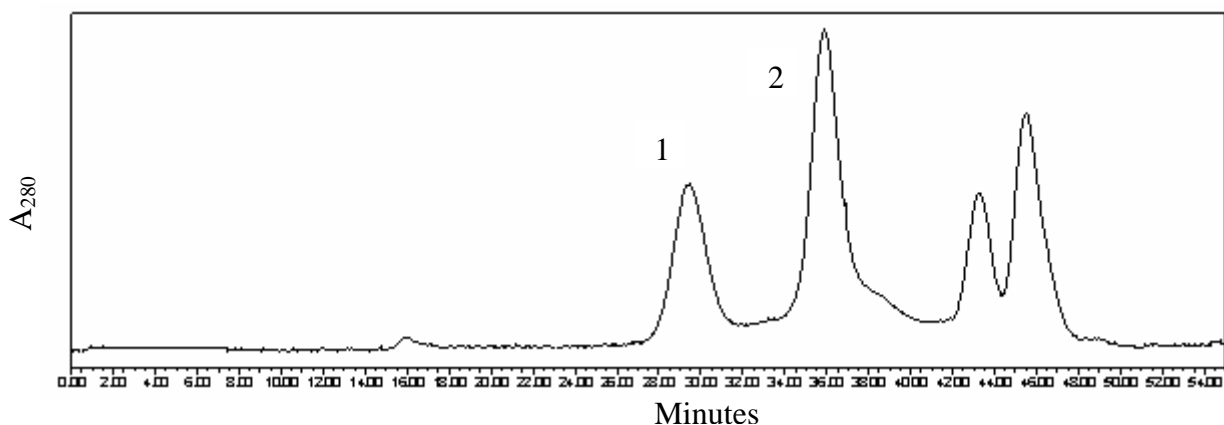


Figure A7.10: The Superose 6 gel filtration chromatogram of bFT-M52L shows two main eluted peaks

Table A7.5: The calculated molecular weight of each eluted Superose 6 fraction of bFT-M52L

bFT-M52L	MW (kDa)	log (MW)	V _e (mL)	K _a
Peak 1 (24-subunit)	264.7	2.4228	14.6	0.4125
Peak 2 (dimer)	23.5	1.3715	18.1	0.6313

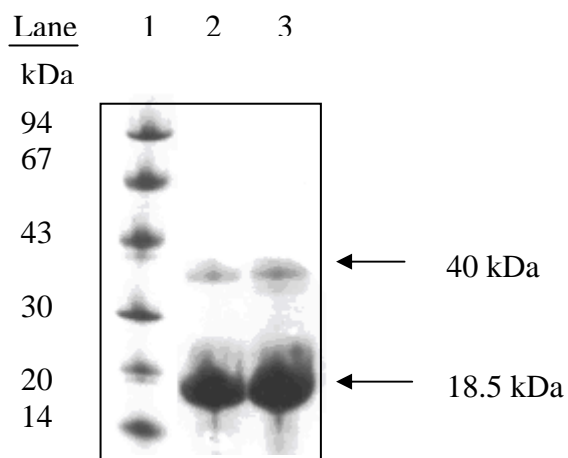


Figure A7.11: The SDS PAGE results of Superose 6 eluted peaks of bFT-M52L. The lists below indicate proteins contained in each eluted fraction.

Lane	Sample
1	MWM
2	Eluted peak 1 of bFT-M52L
3	Eluted peak 2 of bFT-M52L

Gel filtration (Superose 6) of bFT-E94A

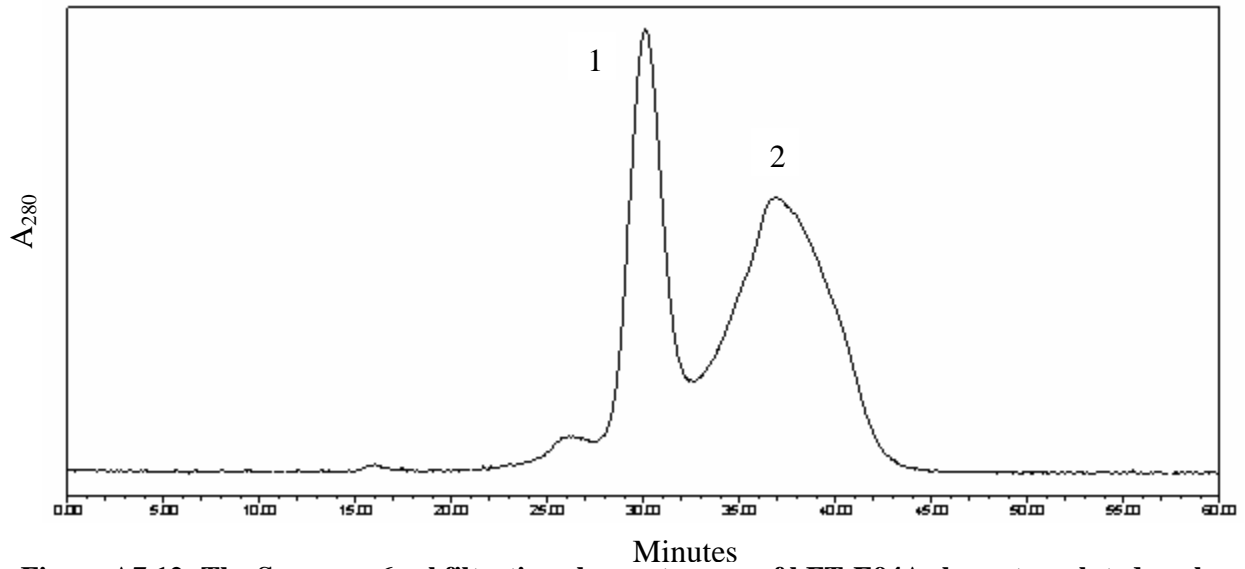


Figure A7.12: The Superose 6 gel filtration chromatogram of bFT-E94A shows two eluted peaks

Table A7.6: The calculated molecular weight of each eluted Superose 6 fraction of bFT-E94A

bFT-E94A	MW (kDa)	log (MW)	V _e (mL)	K _a
Peak 1 (24-subunit)	289.7	2.4620	14.5	0.4063
Peak 2 (monomer)	17.9	1.2519	18.5	0.6563

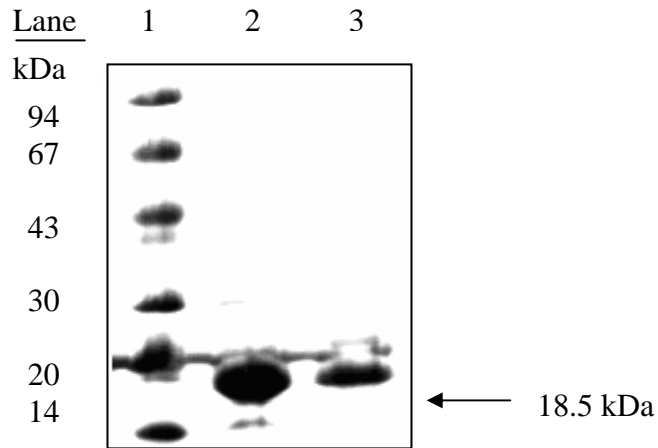


Figure A7.13: The SDS PAGE results of Superose 6 eluted fractions of bFT-E94A. The lists below indicate proteins contained in each eluted fraction.

Lane	Sample
1	MWM
2	Eluted peak 1 of bFT-E94A
3	Eluted peak 2 of bFT-E94A

Gel filtration (Superose 6) of bFT-E18A/M52L

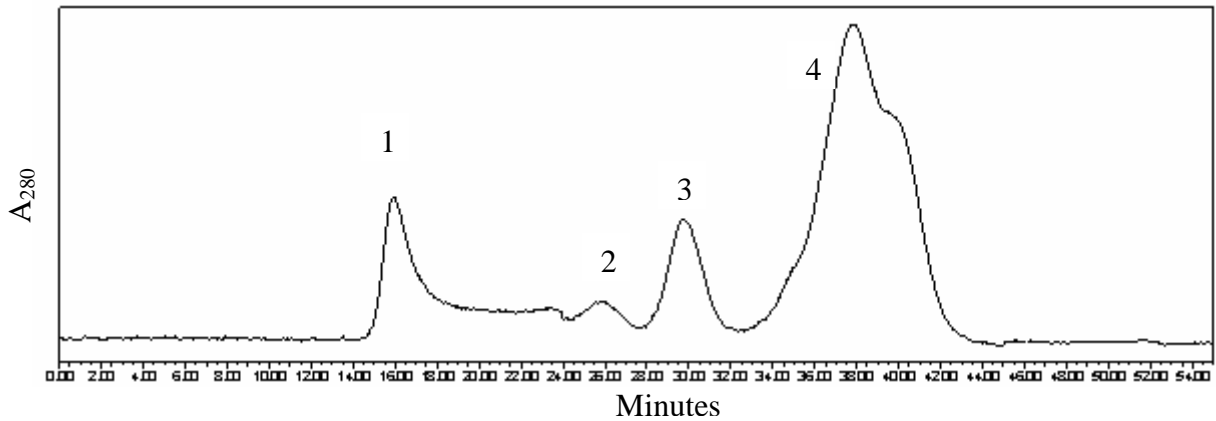


Figure A7.14: The Superose 6 gel filtration chromatogram of bFT-E18A/M52L shows four eluted peaks.

Table A7.7: The molecular weight of each eluted Superose 6 fraction of bFT-E18A/M52L

bFT-E18A/M52L	MW (kDa)	log (MW)	V _e (mL)	K _a
Peak 1 (aggregates)	29199.5	4.4654	7.8	-0.0125
Peak 2 (aggregates)	985.2	2.9935	12.7	0.2938
Peak 3 (24-subunit)	264.7	2.4228	14.6	0.4125
Peak 4 (monomer)	13.5	1.1312	18.9	0.6813

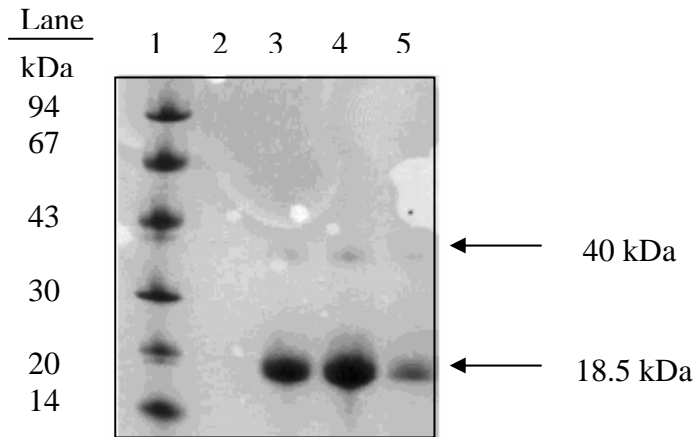


Figure A7.15: The SDS PAGE results of Superose 6 eluted fractions of bFT-E18A/M52L. The lists below indicate proteins contained in each eluted fraction.

Lane 1	Sample	Lane 4	Sample
1	MWM	4	Eluted peak 3 of Bfr-E18A/M52L
2	Eluted peak 1 of Bfr-E18A/M52L	5	Eluted peak 4 of Bfr-E18A/M52L
3	Eluted peak 2 of Bfr-E18A/M52L		

Gel filtration (Superose 6) of bFT-M52L/E94A

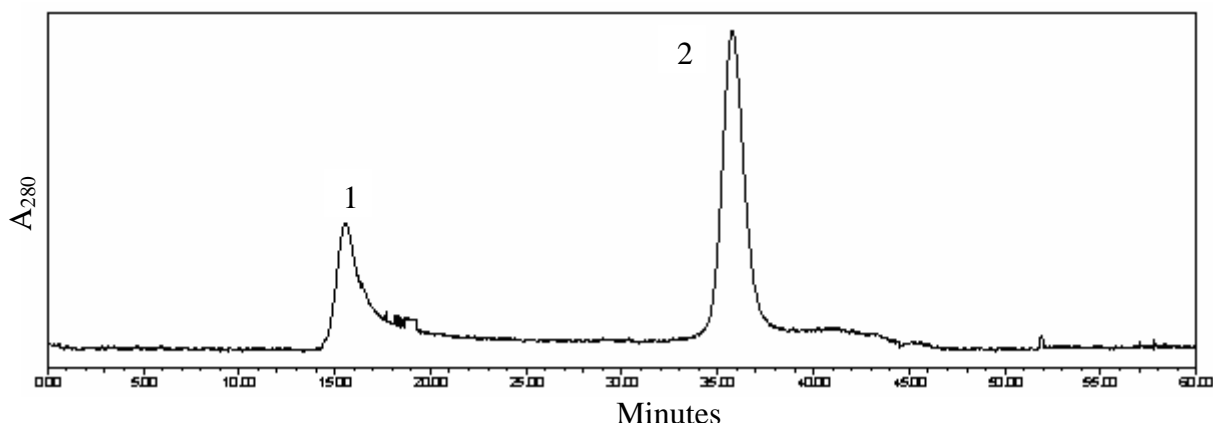


Figure A7.16: The Superose 6 gel filtration chromatogram of bFT-M52L/E94A shows two eluted peaks.

Table A7.8: The calculated molecular weight of each eluted Superose 6 fraction of bFT-M52L/E94A

bFT-M52L/E94A	MW (kDa)	log (MW)	V_e (mL)	K_a
Peak 1 (aggregates)	35152.3	4.5460	7.8	-0.0125
Peak 2 (dimer)	35.0	1.5445	17.6	0.6000

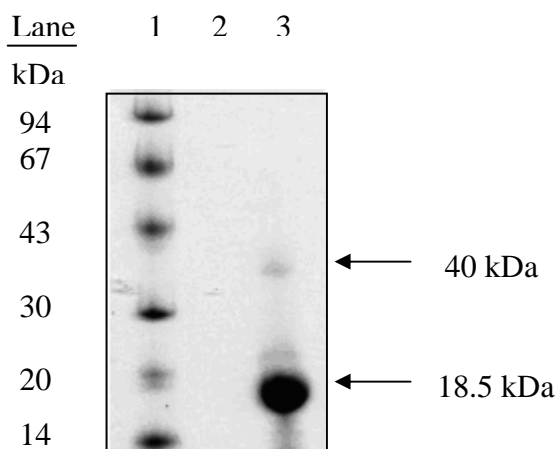


Figure A7.17: The SDS PAGE results of Superose 6 eluted fractions of bFT-M52L/E94A. The lists below indicate proteins contained in each eluted fraction.

Lane	Sample
1	MWM
2	Eluted peak 1 of bFT-M52L/E94A
3	Eluted peak 2 of bFT-M52L/E94A

Gel filtration (Superose 6) of bFT-E18A/E94A

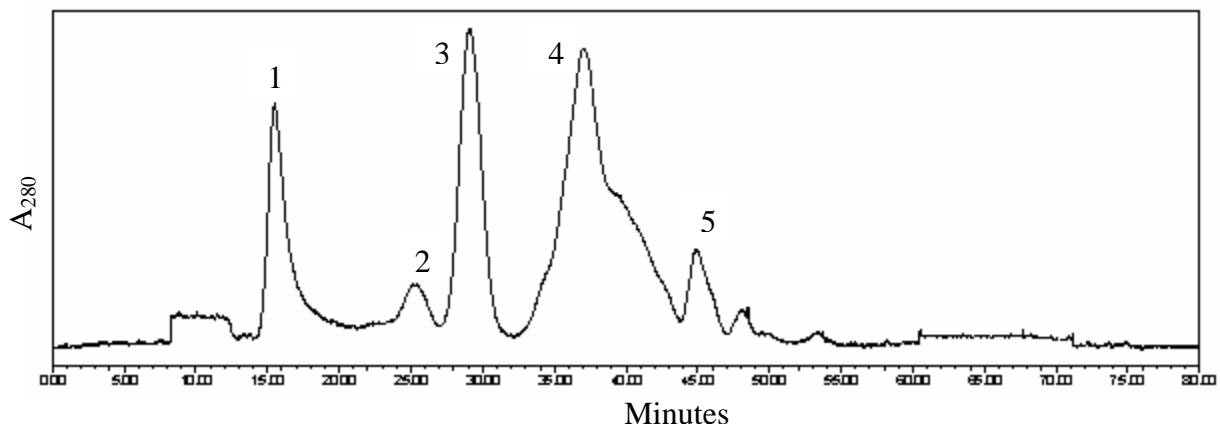


Figure A7.18: The Superose 6 gel filtration chromatogram of bFT-E18A/E94A shows five eluted peaks.

Table A7.9: The calculated molecular weight of each eluted Superose 6 fraction of bFT-E18A/E94A

bFT-E18A/E94A	MW (kDa)	log (MW)	V_e (mL)	K_a
Peak 1 (aggregates)	35152.3	4.5460	7.8	-0.0125
Peak 2 (aggregates)	1109.8	3.0452	12.7	0.2938
Peak 3 (24-subunit)	290.6	2.4633	14.6	0.4125
Peak 4 (monomer)	17.3	1.2383	18.6	0.6625
Peak 5	1.1	0.0438	22.5	0.9063

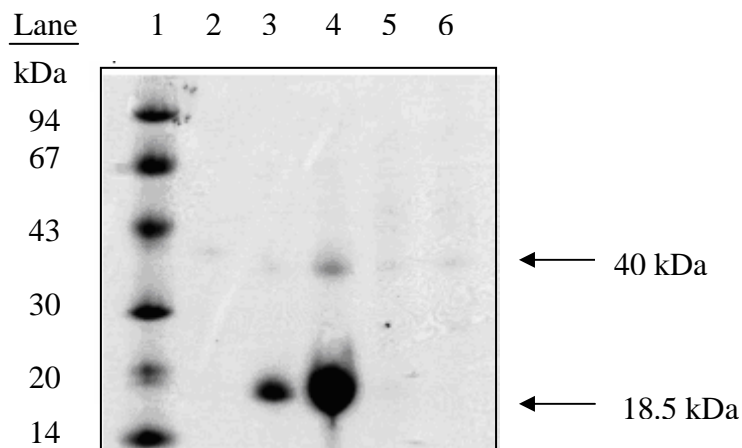


Figure A7.19: The SDS PAGE results of Superose 6 eluted peaks of bFT-E18A/E94A. The lists below indicate proteins contained in each eluted fraction.

Lane	Sample
1	MWM
2	Eluted peak 1 of bFT-E18A/E94A
3	Eluted peak 2 of bFT-E18A/E94A
4	Eluted peak 3 of bFT-E18A/E94A
5	Eluted peak 4 of bFT-E18A/E94A
6	Eluted peak 5 of bFT-E18A/E94A

Gel filtration (Superose 6) of bFT-E18A/M52L/E94A

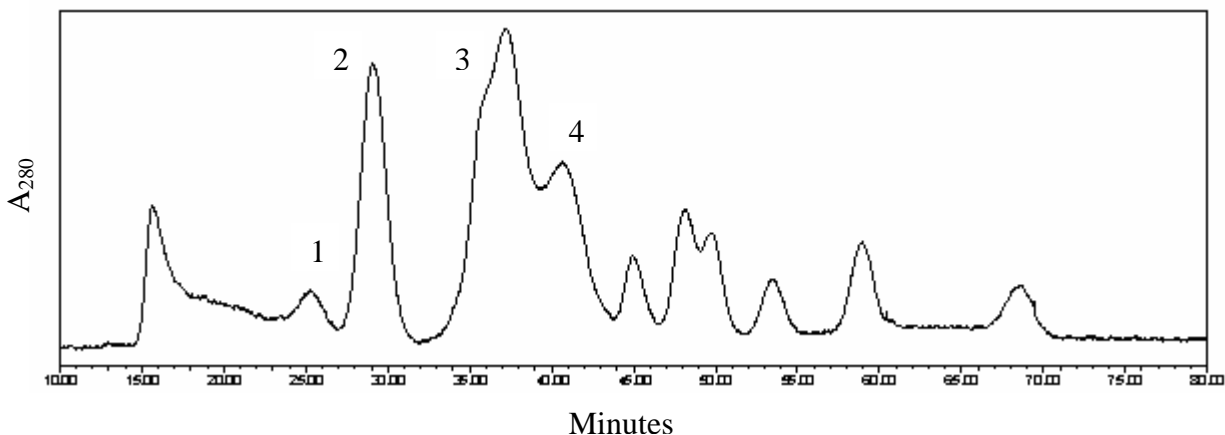


Figure A7.20: The Superose 6 chromatogram of bFT-E18A/M52L/E94A shows four eluted peaks.

Table A7.10: The calculated molecular weight of each eluted Superose 6 fraction of bFT-E18A/M52L/E94A

bFT-E18A/M52L/E94A	MW (kDa)	log (MW)	V_e (mL)	K_a
Peak 1 (aggregates)	1277.9	3.1065	12.5	0.2813
Peak 2 (24-subunit)	334.6	2.5246	14.4	0.4000
Peak 3 (monomer)	18.6	1.2689	18.5	0.6563
Peak 4	4.5	0.6563	20.5	0.7813

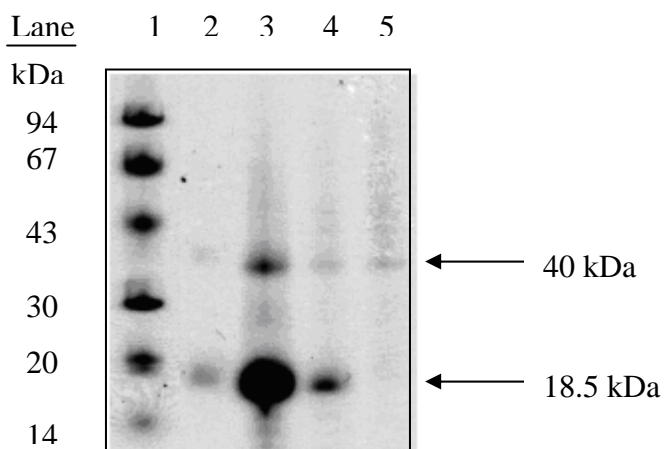


Figure A7.21: The SDS PAGE results of Superose 6 eluted fractions of bFT-E18A/M52L/E94A. The lists below indicate proteins contained in each eluted fraction.

Lane	Sample
1	MWM
2	Eluted peak 1 of bFT-E18A/M52L/E94A
3	Eluted peak 2 of bFT-E18A/M52L/E94A
4	Eluted peak 3 of bFT-E18A/M52L/E94A
5	Eluted peak 4 of bFT-E18A/M52L/E94A

Gel filtration (Superose 6) of bFT with His₆-tag at the C-terminus

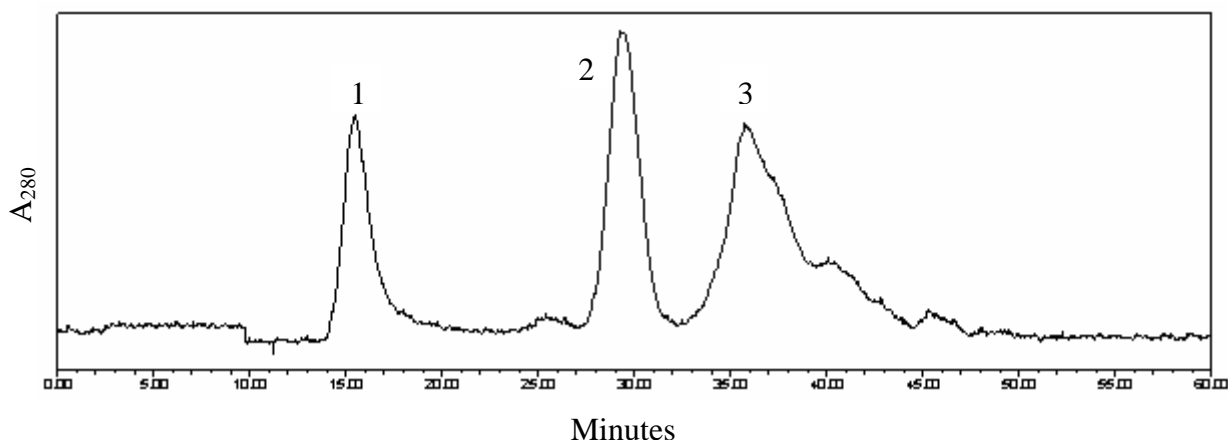


Figure A7.22: The Superose 6 gel filtration chromatogram of bFT with His₆-tag at the C-terminus shows three eluted peaks.

Table A7.11: The calculated molecular weight of each eluted Superose 6 fraction of bFT with His₆-tag at the C-terminus

Bfr with His₆-tag	MW (kDa)	log (MW)	V_e (mL)	K_a
Peak 1 (aggregates)	37723.4	4.5766	7.8	-0.0178
Peak 2 (24-subunit)	300.2	2.4773	14.8	0.4222
Peak 3 (dimer)	32.5	1.5112	18.0	0.6247

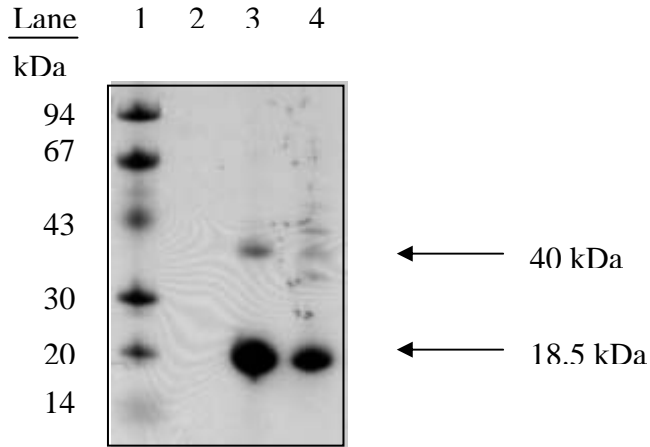


Figure A7.23: The SDS PAGE results of Superose 6 eluted fractions of bFT with His₆-tag at the C-terminus. The lists below indicate proteins contained in each eluted fraction.

Lane	Sample
1	MWM
2	Eluted peak 1 of bFT with His ₆ -tag at the C-terminus
3	Eluted peak 2 of bFT with His ₆ -tag at the C-terminus
4	Eluted peak 3 of bFT with His ₆ -tag at the C-terminus

Appendix 8: Calculation of Extinction Coefficient for Dye Molecules in Pro-Q[®] Sapphire 365 Oligohistidine Gel Strain

A series of different dye stain dilutions were scanned for emission intensity between 400-550 nm (Figure A8.1) and for excitation intensity between 300-400 nm (Figure A8.2). The maximum fluorescence intensities at 440 for the emission scan and at 345 nm for the excitation scan were collected (Table A8.1). Graphs of the emission fluorescence intensities versus dye concentration and the graph of excitation fluorescence intensity versus dye concentration were plotted (Figure A8.3). Since the slope of this trend line corresponds to Beer-Lambert law ($A = \epsilon'BC$), where A is absorption, B is the cuvette path length (1 cm), C is concentration (M), and ϵ' is the fluorescence extinction coefficient ($\text{cm}^{-1}\text{M}^{-1}$), ϵ' for both experiments (excitation scan and emission scan) of Pro-Q[®] sapphire 365 oligohistidine gel stain is calculated to be approximately $\sim 23\,000\text{ cm}^{-1}\text{M}^{-1}$.

Calculations of the extinction coefficient measured by UV-visible spectrophotometer were performed in parallel with the one using fluorescence measurements and are shown as follows. By using the Beer-Lambert law ($A = \epsilon_{345}BC$), the extinction coefficient (ϵ_{345}) is calculated to be approximately $\sim 0.0023 \times 10^7\text{ cm}^{-1}\text{M}^{-1}$ or $23\,000\text{ cm}^{-1}\text{M}^{-1}$.

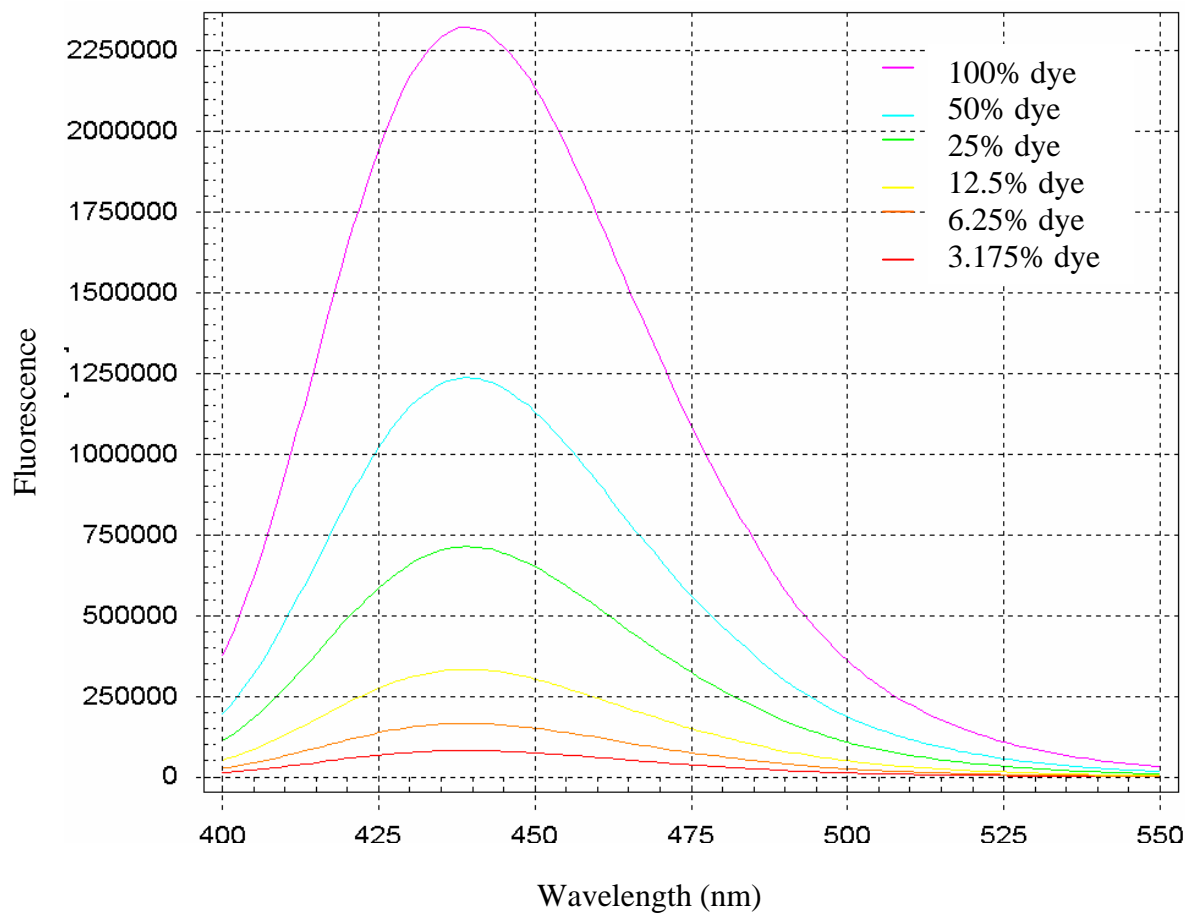


Figure A8.1: The emission spectra scanned between wavelengths 400-550 nm with fixed excitation wavelength at 345 nm of dye series show maximum fluorescent intensity at 440 nm.

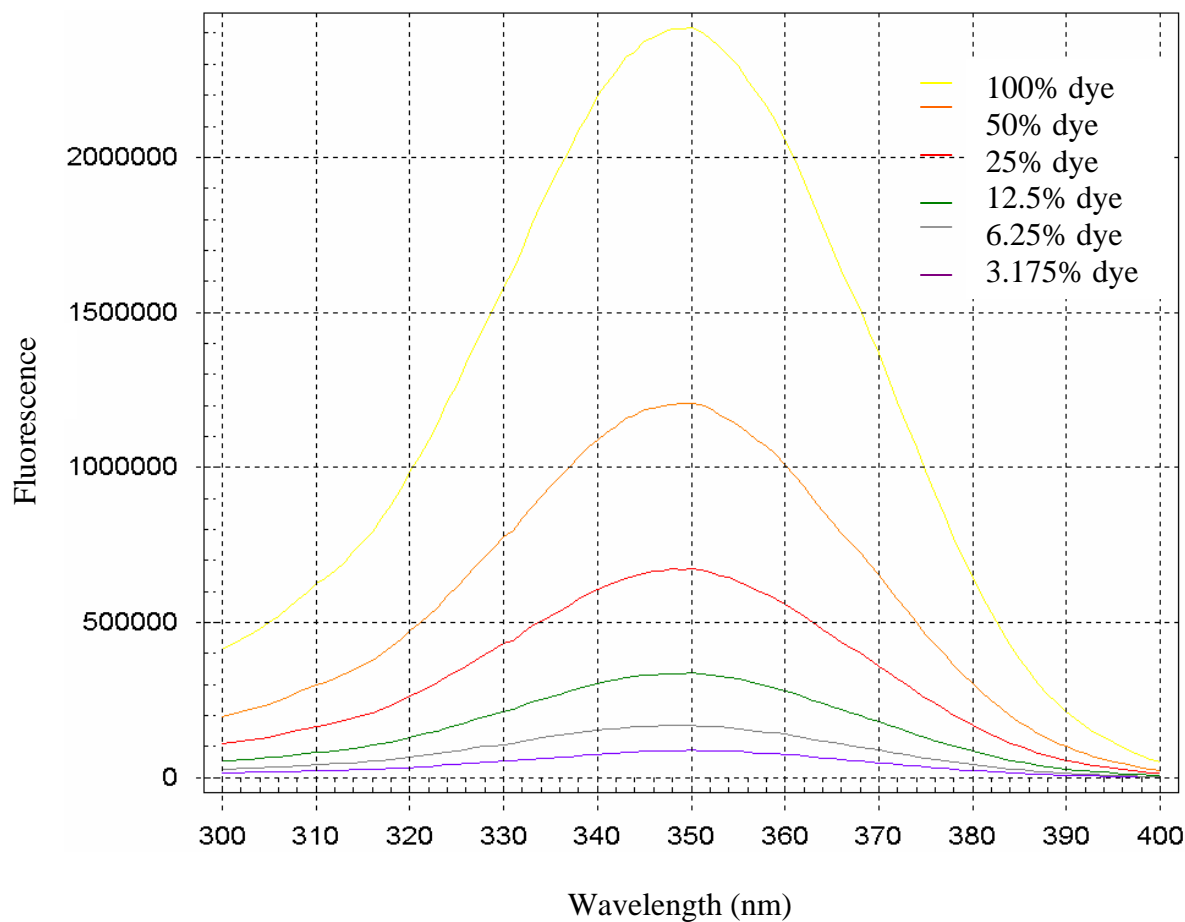


Figure A8.2: The excitation spectra scanned between wavelengths 300-400 nm with fixed emission wavelength at 440 nm of dye series show maximum fluorescent intensity at 345 nm.

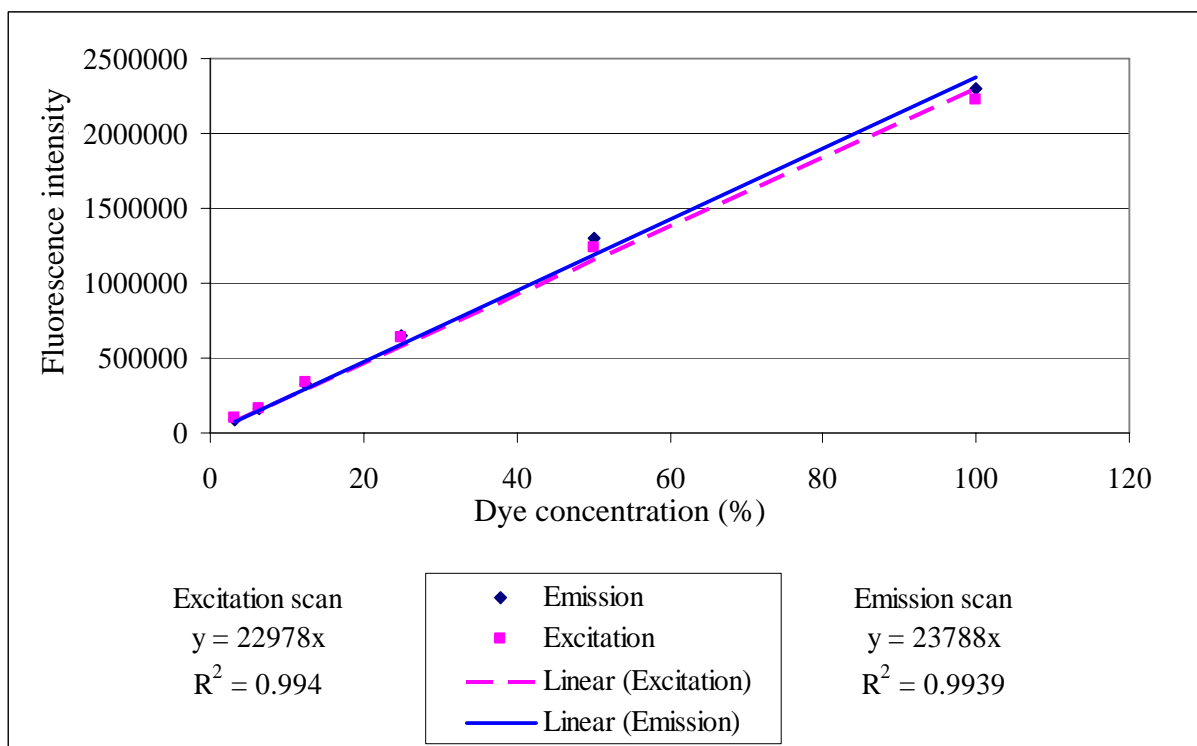


Figure A8.3: The plot of fluorescent intensity of emission wavelength 440 nm and excitation wavelength at 345 nm versus % dye concentration. The slope of the trend lines represents extinction coefficient of Pro-Q[®] sapphire 365 oligohistidine gel stain.

Table A8.1: Collected data for emission intensity and excitation intensity of the series of different dye stain dilutions. These data were used for the plot of fluorescence intensity versus dye concentration as above.

% Dye concentration	Emission intensity 1	Emission intensity 2	Average emission intensity	Excitation intensity 1	Excitation intensity 2	Average excitation intensity
3.175	82115.0	92042.0	87078.5	84296.0	107973.0	96134.5
6.250	165645.0	164724.0	165184.5	165579.0	157802.0	161690.5
12.500	332857.0	309239.0	321048.0	330376.0	333612.0	331994.0
25.000	710203.0	598118.0	654160.5	659272.0	617396.0	638334.0
50.000	1237826.0	1362989.0	1300407.5	1185799.0	1296792.0	1241295.5
100.000	2318869.0	2289270.0	2304069.5	2374601.0	2081612.0	2228106.5

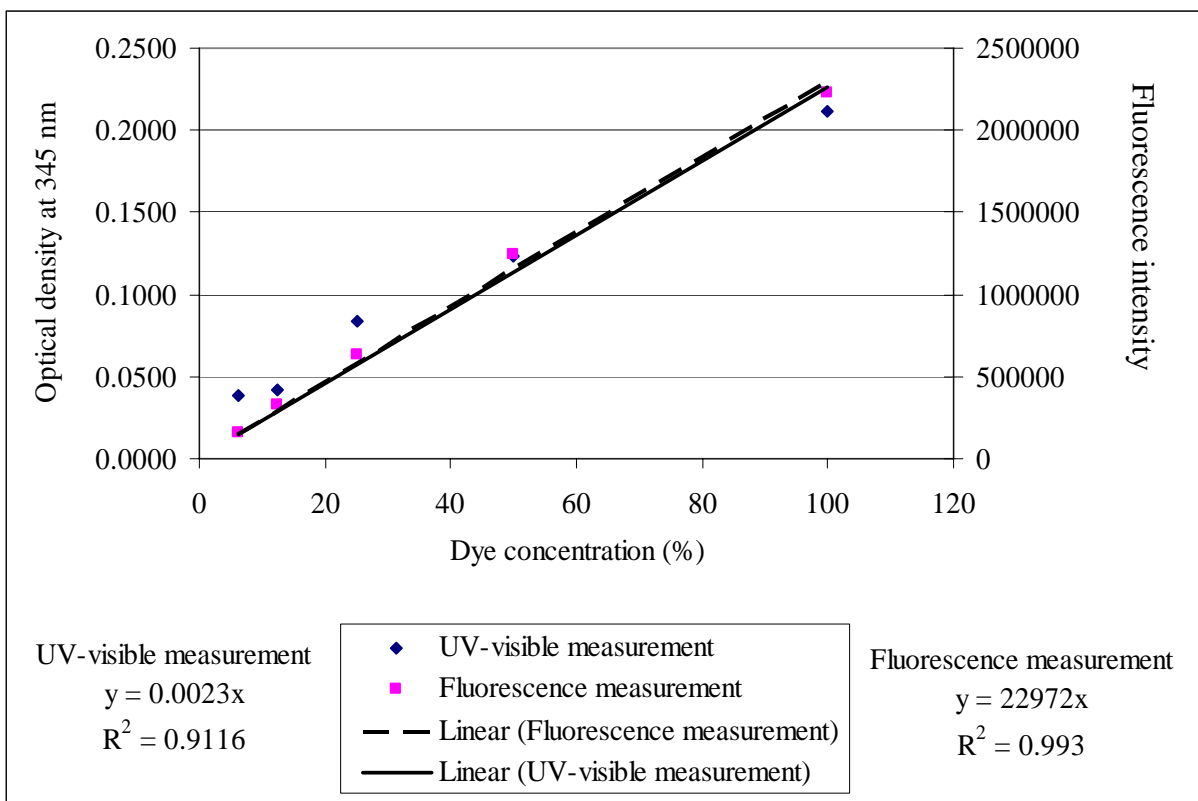


Figure A8.4: The plots of fluorescent intensity of excitation wavelength at 345 nm versus dye concentration compared with that of optical density versus dye concentration showing the slopes of the trend lines that represent extinction coefficient of Pro-Q[®] sapphire 365 oligohistidine gel stain.

Table A8.2: Collected data for optical densities of the series of different dye stain dilutions. These data were used for the plot of optical density versus dye concentration as above.

% Dye concentration	OD ₃₄₅ trial 1	OD ₃₄₅ trial 2	Average OD ₃₄₅
6.25	0.0397	0.0365	0.0381
12.50	0.0413	0.0424	0.0419
25.00	0.0849	0.0824	0.0837
50.00	0.1249	0.1224	0.1237
100.00	0.2027	0.2207	0.2117

Appendix 9: Calculations of Heme Groups Present in Bacterioferritin

The spectrophotometric absorption of bFT-WT, bFT with His₆-tag at the C-terminus, and encapsulated bFT with His₆-tag at the C-terminus at 417 nm corresponds to the absorption of the Soret band of the oxidized heme moiety. The number of heme groups incorporated in each protein sample was calculated using the Beer-Lambert law, $A = \epsilon_{417}BC$, where A is absorption, B is the path length of cuvette (1 cm), C is concentration (M), and ϵ_{417} is the extinction coefficient measured at 417 nm ($M^{-1}cm^{-1}$). The results of the calculation are shown in Table A9.1. An example of bFT-WT heme group calculation is as follows. The protein concentration of 0.42 mg/mL was converted to 97 μ M from the calculation using the MW of bFT, which is 444 kDa. From the Beer-Lambert law, A is 0.0686, B is 1 cm, and ϵ_{417} is 137 000 $M^{-1}cm^{-1}$ per heme per *E. coli* ferricytochrome protein (Yariv *et al.*, 1981). Therefore, the concentration of heme is 50 μ M, and each bFT subunit contains 0.53 heme groups or ~12 heme groups per 24 subunits.

Table A9.1: The table represents the number of heme groups incorporated in various bFT samples

Samples with 0.42 mg/mL protein concentration	OD₄₁₇	Amount of heme groups
Native bFT-WT	0.0686	12
Native bFT with His ₆ -tag at the C-terminus	0.0602	10
bFT with His ₆ -tag at the C-terminus with encapsulated dye	0.0740	12
bFT with His ₆ -tag at the C-terminus after additional 5 hours of dialysis time with encapsulated dye	0.0493	9

Appendix 10: Calculations of Encapsulated Dye inside Protein Cavity

From the Beer-Lambert law, the concentration of dye molecules encapsulated in the protein cavity can be calculated from the equation $A = \epsilon_{345}BC$, where A is absorbance of the dye in Pro-Q[®] sapphire 365 oligohistidine gel stain measured at 345 nm, B is the cuvette path length (1 cm), C is the concentration of dye inserted in the protein core (M), and ϵ_{345} is the experimental extinction coefficient at 345 nm ($23\,000\text{ M}^{-1}\text{cm}^{-1}$) (Appendix 8). With the calculated dye concentration and known concentrations of proteins (measured using Bradford assay), the number of encapsulated dye molecules for each of the protein samples was determined (Table A10.1). An example of a calculation for the amount of dye encapsulated in a combination of 60/40:Histag/WT is as follows. The concentration of protein was measured and shown in section 4.4.3 (Table 4.6), which was 0.672 mg/mL or 1.51 μM (MW of the protein is approximately 444 kDa). The average absorbance measured from duplicated experiments at 345 nm is 0.2044. The concentration of dye is calculated from $C = A/\epsilon B = 8.9\ \mu\text{M}$, where $A = 0.2044$, $B = 1\text{ cm}$, and $\epsilon_{345} = 23\,000\text{ M}^{-1}\text{cm}^{-1}$. Therefore, the number of dye molecules encapsulated inside 1 molecule of protein on average is calculated from the ratio of encapsulated dye concentration and protein concentration (~ 6 molecules). Since there is only 60% Histag in this combination protein, so the maximum dye that can be encapsulated is (24×0.6) ~ 14 dye molecules. The efficiency of this experiment is $\sim 43\%$. The calculations for the amount of dye molecules encapsulated in 100% Histag protein is similar, and it is shown that there are ~ 6 encapsulated dye molecules. The encapsulated dye molecules of this protein are maximized when each subunit binds one molecules of dye, which are 24 dye molecules in total. Therefore, efficiency of this encapsulated protein is 25%.

Table A10.1: The table shows data for the calculation of encapsulated dye molecules in 100% Histag protein and the combination of 60/40:Histag/WT protein.

Encapsulated samples	Protein conc. (μM)	OD₃₄₅ trial 1	OD₃₄₅ trial 2	Average OD₃₄₅	Conc. of encapsulated dye (μM)	Number of encapsulated dye (molecules)
100% Histag protein	0.83	0.1053	0.1360	0.1206	5.2	6
60:40/Histag/WT mixture	1.51	0.2346	0.1742	0.2044	8.9	6

Appendix 11: Metal Analysis of Pro-Q[®] Sapphire 365 Oligohistidine Gel

Stain

The results from metal analysis are shown in Table A11.1. Calculations of the amount of Ni²⁺ in Pro-Q[®] sapphire 365 oligohistidine gel stain are as follows. The average Ni²⁺ concentration from duplicate experiments (ICP-MS) is $(1.48 + 1.37) \div 2 = 1.425$ mg/L. The samples were diluted 5 times before performing metal analysis; therefore, the actual concentration of Ni²⁺ is $1.43 \times 5 = 7.15$ mg/L or 60.7 μ M (molar mass of Ni²⁺ is 58.69 g/mol). Since the concentration of dye molecule in Pro-Q[®] sapphire 365 oligohistidine gel stain was ~ 9.2 μ M, the ratio of Ni²⁺/dye is ~ 6.6 .

The high concentration of Na⁺ is also observed. The average Na⁺ concentration is $(557 + 567) \div 2 = 562$ mg/L. With 5 times dilution, the concentration of Na⁺ becomes (562×5) 2.81 g/L or 120 mM (molar mass of Na⁺ is 23 g/mol).

Table A11.1: ALS Laboratory Group Analytical Report for metal analysis results representing the metal detection in Pro-Q[®] sapphire 365 oligohistidine gel stain and Chelex treated water (a control sample).

Metal analysis	Detection limit (mg/L)	Metal detection in Pro-Q [®] sapphire 365 oligohistidine gel stain (mg/L)	Metal detection in Pro-Q [®] sapphire 365 oligohistidine gel stain (mg/L)	Metal detection in Chelex treated water (mg/L)
		Trial 1	Trial 2	
Aluminum (Al)	0.1	<0.1	<0.1	<0.1
Antimony (Sb)	0.05	<0.05	<0.05	<0.05
Arsenic (As)	0.01	<0.01	<0.01	<0.01
Barium (Ba)	0.1	<0.1	<0.1	<0.1
Beryllium (Be)	0.01	<0.01	<0.01	<0.01
Bismuth (Bi)	0.01	<0.01	<0.01	<0.01
Boron (B)	0.5	<0.5	<0.5	<0.5
Cadmium (Cd)	0.001	<0.001	<0.001	<0.001
Calcium (Ca)	5	<5	<5	<5
Chromium (Cr)	0.01	<0.01	<0.01	<0.01
Cobalt (Co)	0.005	<0.005	<0.005	<0.005
Copper (Cu)	0.01	<0.01	<0.01	<0.01
Iron (Fe)	0.5	<0.5	<0.5	<0.5
Lead (Pb)	0.01	<0.01	<0.01	<0.01
Magnesium (Mg)	5	<5	<5	<5
Manganese (Mn)	0.01	<0.01	<0.01	<0.01
Molybdenum (Mo)	0.01	<0.01	<0.01	<0.01
Nickel (Ni)	0.02	1.48	1.37	<0.02
Phosphorus (P)	0.5	0.6	0.5	<0.5
Potassium (K)	10	<10	<10	<10
Selenium (Se)	0.05	<0.05	<0.05	<0.05
Silicon (Si)	1	<1	<1	<1
Silver (Ag)	0.001	<0.001	<0.001	<0.001
Sodium (Na)	5	557	567	<5
Strontium (Sr)	0.01	<0.01	<0.01	<0.01
Thallium (Tl)	0.003	<0.003	<0.003	<0.003
Tin (Sn)	0.01	<0.01	<0.01	<0.01
Titanium (Ti)	0.02	<0.02	<0.02	<0.02
Tungsten (W)	0.1	<0.1	<0.1	<0.1
Uranium (U)	0.05	<0.05	<0.05	<0.05
Vanadium (V)	0.01	0.02	0.02	0.02
Zinc (Zn)	0.03	<0.03	<0.03	<0.03
Zirconium (Zr)	0.04	<0.04	<0.04	<0.04

Appendix 12: Metal Analysis of Iron Ions Incorporated in 24-Subunit Bacterioferritin

The results from metal analysis are shown in Table A12.1, where the metal detection was found in 24-subunit bFT with His₆-tag at the C-terminus (0.50 mg/mL), which was isolated by Superose 6 gel filtration chromatography.

Table A12.1: ALS Laboratory Group Analytical Report for metal analysis results representing the metal detection in 24-subunit bFT with His₆-tag at the C-terminus (two trials sample) and dialysis buffer (a control sample).

Metal analysis	Detection limit (mg/L)	Metal detection in 24-subunit bFT with His₆-tag at the C-terminus (mg/L)	Metal detection in 24-subunit bFT with His₆-tag at the C-terminus (mg/L)	Metal detection in dialysis buffer (mg/L)
		Trial 1	Trial 2	
Aluminum (Al)	0.1	<0.1	<0.1	<0.1
Antimony (Sb)	0.05	<0.05	<0.05	<0.05
Arsenic (As)	0.01	<0.01	<0.01	<0.01
Barium (Ba)	0.1	<0.1	<0.1	<0.1
Beryllium (Be)	0.01	<0.01	<0.01	<0.01
Bismuth (Bi)	0.01	<0.01	<0.01	<0.01
Boron (B)	0.5	<0.5	<0.5	<0.5
Cadmium (Cd)	0.001	0.002	0.002	0.002
Calcium (Ca)	5	<5	<5	<5
Chromium (Cr)	0.01	<0.01	<0.01	<0.01
Cobalt (Co)	0.005	<0.005	<0.005	<0.005
Copper (Cu)	0.01	<0.01	0.01	<0.01
Iron (Fe)	0.5	<0.5	<0.5	<0.5
Lead (Pb)	0.01	0.04	0.04	0.03
Magnesium (Mg)	5	<5	<5	<5
Manganese (Mn)	0.01	0.02	<0.01	<0.01
Molybdenum (Mo)	0.01	<0.01	<0.01	<0.01
Nickel (Ni)	0.02	<0.02	<0.02	<0.02
Phosphorus (P)	0.5	<0.5	<0.5	<0.5
Potassium (K)	10	20	20	20
Selenium (Se)	0.05	<0.05	<0.05	<0.05
Silicon (Si)	1	<1	<1	<1
Silver (Ag)	0.001	<0.001	<0.001	<0.001
Sodium (Na)	5	15	15	<5
Strontium (Sr)	0.01	0.01	<0.01	<0.01
Thallium (Tl)	0.003	<0.003	<0.003	<0.003
Tin (Sn)	0.01	<0.01	<0.01	<0.01
Titanium (Ti)	0.02	<0.02	<0.02	<0.02
Tungsten (W)	0.1	<0.1	<0.1	<0.1
Uranium (U)	0.05	<0.05	<0.05	<0.05
Vanadium (V)	0.01	<0.01	<0.01	<0.01
Zinc (Zn)	0.03	0.19	0.2	<0.03
Zirconium (Zr)	0.04	<0.04	<0.04	<0.04
Sulfur (S)	10	20	20	<10